

Generation and Reactions of Organic Radical Cations in Zeolites

Hermenegildo García^{*,†} and Heinz D. Roth^{*,‡,§}

Departamento de Química/Instituto de Tecnología Química UPV-CSIC, Universidad Politécnica de Valencia, Camino de Vera s/n, Apartado 22012, E-46071-Valencia, Spain, and Department of Chemistry and Chemical Biology, Rutgers University, Wright-Rieman Laboratories, New Brunswick, New Jersey 08854-8087

Received September 21, 2001

Contents

I. Introduction	3948	V.C Spontaneous Radical Cation Conversions in Zeolites	3976
II. Zeolites as Hosts	3949	V.C.1 Intra-Zeolite Reactions not Involving a Second Guest	3976
II.A Chemical Composition, Crystal Structure, Characterization	3949	V.C.2 Ion–Ion or Ion–Molecule Reactions in Zeolites	3976
II.B Nature of the Active Sites	3951	V.C.3 Spontaneous Deprotonation of Radical Cations	3977
II.B.1 Redox Reactivity and Acidity	3951	VI. Generation of Radical Cations by Radiolysis in Zeolites	3978
II.B.2 Influence of Oxygen	3952	VI.A Radical Cations of Linear and Branched Alkanes	3978
II.C Characterization of Zeolite Active Sites Exemplified	3953	VI.B Radical Cations of Cycloalkanes	3979
III. Adsorption Procedures	3954	VI.C Radical Cations of Strained Ring Substrates	3980
IV. Experimental Techniques to Study Radical Cations in Zeolites	3955	VI.D Radical Cations of Alkenes	3980
IV.A Optical Absorption Spectroscopy	3955	VI.E Radical Cations of C ₇ H ₈ -Isomers	3981
IV.B IR and Raman Spectroscopy	3956	VI.F Radiolysis of Ethyne	3982
IV.C Magnetic Resonance Methods	3956	VI.G Radiolysis of Polynuclear Aromatics	3982
V. Spontaneous Generation of Radical Cations in Zeolites	3957	VII. Photochemical Generation of Radical Cations in Zeolites	3983
V.A Spontaneous Radical Cation Formation Exemplified	3957	VII.A Zeolites as Inert Media: ET between Donor and Acceptor Guests	3983
V.A.1 Radical Cations from Alkenes	3957	VII.A.1 2,4,6-Triphenylpyrylium Ion as Electron Acceptor	3984
V.A.2 Radical Cations from Alkynes	3959	VII.A.2 Cyanoaromatics and Nitrogen Heterocycles as Acceptors	3986
V.A.3 Adsorption of Alkanes and Cycloalkanes	3959	VII.A.3 Acetophenone as Acceptor vs Aliphatic Amines	3986
V.A.4 Radical Cations from Cycloalkenes	3960	VII.B Zeolites as Single Electron Acceptors: Photoionization inside Zeolites	3987
V.A.5 Adsorption of Benzene and Derivatives	3961	VII.B.1 Photochemistry of Aromatics in Zeolites	3987
V.A.6 Radical Cations of α,ω -Diphenylpolyenes and Aryl Olefins	3963	VII.B.2 Photoionization of meso-Tetraphenylporphyrin	3988
V.A.7 Radical Cations of Polynuclear Aromatics	3964	VII.B.3 Photochemistry of Squaraines	3989
V.A.8 Radical Cations of Nitrogen-Containing Substrates	3965	VII.B.4 Photochemistry of Aryl- and Diarylethylenes	3989
V.A.9 Radical Cations of Sulfur and Selenium-Containing Substrates	3967	VII.B.5 Photochemistry of Bibenzyl Systems	3991
V.A.10 Radical Cations of Organic Polymers Embedded in Zeolites	3970	VII.B.6 Decarboxylation of Carboxylic Acids	3991
V.A.11 Fullerene	3971	VII.C Viologens in Zeolites – Inert Media or Electron Acceptors	3991
V.B Competition between Protonation and Oxidation	3971	VII.C.1 ET between Aromatic Donors and Viologen Acceptors	3991
V.B.1 Protonation vs Oxidation of Aromatic/Unsaturated Hydrocarbons	3971	VII.C.2 ET from Zeolites to Viologen Acceptors	3992
V.B.2 Protonation vs Oxidation of <i>N,N'</i> -Diphenylhydrazine	3974	VII.C.3 Ruthenium Bipyridyl as Electron Donor	3993
V.B.3 The Nature of the Blue Species Generated upon Adsorption of 1,1-Diarylethenes onto Acid Zeolites	3974	VII.D Oxygen as Electron Acceptor: Visible Light Irradiation of Hydrocarbon \times O ₂ CT Complexes inside Large-Pore Zeolites	3995
		VIII. Electrochemical Generation of Radical Cations in Zeolites	3997
		IX. Radical Anions within Zeolites	3998

* To whom correspondence should be addressed.

[†] Universidad Politécnica de Valencia.

[‡] Rutgers University.

[§] Profesor Visitante IBERDROLA de Ciencias y Tecnología, Instituto de Tecnología Química UPV-CSIC, Universidad Politécnica de Valencia.

X. Organic Radical Cations Generated in Inorganic Solids Related to Zeolites	4000
XI. Concluding Remarks and Perspective	4001
XII. Acknowledgments	4002
XIII. References	4002

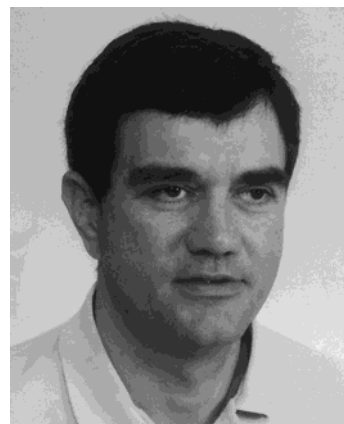
I. Introduction

The structures and catalytic properties of zeolites have been intensively investigated as prototypes of acidic industrial catalysts.^{1–12} Zeolites were first introduced as catalysts for large-scale gas-phase reactions in petrochemistry.^{10–12} Compared to conventional liquid acids, these materials offer significant advantages for processes such as cracking, aromatization, aromatic isomerization, or disproportionation. They are thermally stable, and offer convenient reactor design; they are easy to separate from the reaction products, and can be regenerated after suffering deactivation; and they offer shape selectivity and control of the reaction outcome. The promising results of gas-phase reactions in zeolites triggered intense research aimed at developing the potential of zeolites for general acid-catalyzed organic reactions in the liquid phase under batch conditions. During the past two decades, an ever-increasing volume of research has been carried out promoting the use of zeolites as solid catalysts for organic reactions in the liquid phase, e.g., in the production of fine chemicals under environmentally benign conditions.^{5–9} As a result of these studies, heterogeneous catalysis of organic reactions by zeolites can be considered a mature field.

One of the most intriguing properties of acid zeolites is their ability to generate spontaneously organic radical cations upon adsorption of organic electron donors (Section V). Additional radical cations can be generated by action of radiation (Section VI) or light (Section VII). The rigid microporous solids serve as excellent matrices, stabilizing otherwise reactive or unstable radical cations. The restricted mobility within zeolite pores limits the tendency of free radicals or radical cations to dimerize and prevents access of reagents that typically would cause their decay in solution. Accordingly, radical cations have increased lifetimes and can be studied by conventional spectroscopic techniques. In special cases, the limiting geometry of the zeolite pores may selectively incorporate substrates with suitable geometries or restrict the shape of sequestered intermediates generated in the zeolites.

Early work in this area was carried out to probe the activities of active solids, such as silica, alumina, and natural or synthetic zeolites. More recently, the radical cations sequestered in zeolites have attracted interest in their own right. The reactions of primary radical cations and their conversions into well-defined secondary intermediates or products have been attracting ever-growing interest (Section V.C).

We will consider first the composition and geometry of zeolite hosts (Section II), the nature of the active sites (Section IIB), adsorption procedures (Section III), and experimental techniques for characterizing intermediates sequestered in zeolites (Section IV). Having established the properties of the



Hermenegildo García (Herme) was born in Canals (Spain) in June 1957 and studied Chemistry at the Universidad de Valencia. He graduated in 1979 and received a Ph.D. in preparative organic photochemistry under the guidance of Prof. Miguel A. Miranda in 1983. He joined Universidad Politécnica de Valencia (UPV) where, in 1991, he was appointed a member of the newly founded Instituto de Tecnología Química, jointly sponsored by the Spanish National Research Council (CSIC) and UPV. In 1996, he was promoted to *catedrático* (Professor). He was a visiting scientist at the University of Reading, U.K., in 1987 with Prof. Andrew Gilbert, and in J.C. (Tito) Scaiano's Laser Flash Photolysis group at the University of Ottawa (1992–1993, 12 months; 1995, six months; 2000, three months). He is author or co-author of over 200 papers, dealing mostly with the application of zeolites as hosts for organic guests and as solid catalysts and holds three international patents. His current research interests are in supramolecular photochemistry and photocatalysis, development of photoactive nanoscopic materials, and heterogeneous catalysis.



Heinz D. Roth was born in the Lower Rhine region of Germany and studied chemistry at the Universities of Karlsruhe and Köln, where he received a Dr. rer. nat. degree (Emmanuel Vogel, synthesis of 1,6-methanocyclodecapentaene). After two years as a postdoctoral fellow in William Doering's laboratory at Yale University (thermal reorganization of Feist's ester), he joined the Organic Chemistry Research and Development Department of (AT&T) Bell Laboratories, where he was named Distinguished Member of Technical Staff. In 1988, he joined Rutgers University, New Brunswick, NJ, as Professor of Chemistry. His research interests include mechanisms of light-induced and thermal reactions; structure and reactivity of short-lived reaction intermediates, especially radical ions, free radicals, and carbenes; electron donor–acceptor interactions and photo-induced electron transfer; and the history of science, with an emphasis on photochemistry.

host(s), we will discuss the generation of radical cations in zeolites, beginning with the spontaneous generation upon incorporation (Section V). In this section, we will also mention competing reactions caused by the Brønsted acid sites of the zeolite (Section V.B). Conversions of primary radical cations within zeolites, occurring either spontaneously, or following thermal or photochemical activation will be

discussed separately (Section V.C). Finally, we will treat the radiolytic, photochemical, and electrochemical generation of radical cations in zeolites in three separate sections. Scarce reports on the characterization of radical anions within zeolites are also included in this review (Section IX). Finally a noncomprehensive section with radical cation generation in solids related to zeolites has also been included.

The review goes back to the early incorporation studies probing the activities of natural as well as synthetic zeolites in the early 1970s and covers the literature until mid-2000.

II. Zeolites as Hosts

Numerous original research articles and several reviews deal with the synthesis, modification, and characterization of zeolites.¹⁻⁴ In fact, material science related to zeolites has experienced a very rapid growth in recent years owing to the importance of zeolites as catalysts in the production of fine chemicals⁵⁻⁹ and in the petrochemical industry.¹⁰⁻¹² For the purpose of this review, it appears pertinent to summarize briefly the main features of zeolite structure and composition that make these materials so appropriate as hosts to generate and stabilize organic radical cations.

II.A Chemical Composition, Crystal Structure, Characterization

Zeolites are crystalline aluminosilicates whose lattice consists of a network of SiO_4^{4-} and AlO_4^{4-} tetrahedra with Si or Al atoms at the centers and oxygen atoms in each corner.¹³⁻¹⁷ The tetrahedra share the corners or edges; thus, the number of oxygens is twice that of Si plus Al atoms. In contrast to amorphous silica or silica-alumina, which lack long-range ordering, zeolites are crystalline; their tetrahedra are spatially arranged in strictly regular fashion. The building blocks are repeated in the three principal directions of the unit cell. The chemical composition and some general properties of zeolites are summarized in Figure 1.

The Si/Al ratio of a zeolite unit cell may be varied within a certain range without affecting its crystal structure. The ionic radii of the two elements are very similar, allowing the isomorphous substitution of Si by

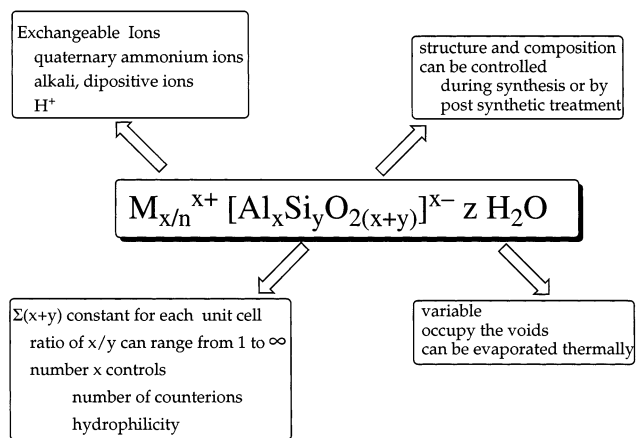


Figure 1. Chemical composition of zeolites.

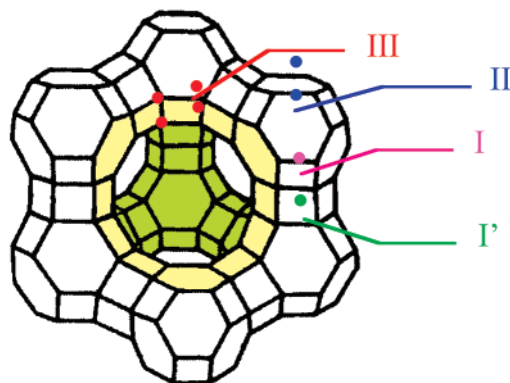


Figure 2. Faujasite supercavities (α -cages) constructed of sodalite cages and hexagonal prism subunits; the charge-compensating cations occupy different crystallographic positions, designated by Roman numerals.

Al within the tetrahedron units. While the ratio of Si/Al may vary, the sum of Si+Al atoms remains constant.

A network of SiO_4^{4-} tetrahedra is neutral; each AlO_4^{5-} tetrahedron introduces one negative charge in the lattice. The negative charges are balanced by an appropriate number of cations, usually mono- or dipositive, inorganic or organic. Typical cations include alkali metal and quaternary ammonium ions. The latter are usually introduced as templates during the zeolite synthesis to shape the geometry of the lattice during hydrothermal crystallization.

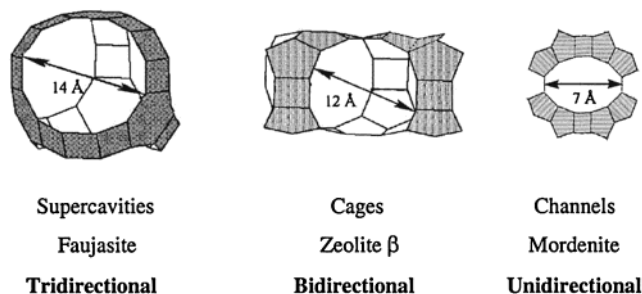
The location of the cations within the zeolite voids and their mobility have been studied by neutron diffraction and multinuclear solid-state NMR studies. In special cases, the type and site of the cation is known exactly. For example, the cations of X and Y faujasites may occupy three different locations (Figure 2).

The Si/Al ratio significantly influences the zeolite properties; it may vary from Si/Al = 1 (faujasite X) to Si/Al = ∞ (silicalite). The Al content of an aluminosilicate determines the number of cations in the framework, and such properties as the thermal and chemical stability or the polarity of the internal surfaces. Typically, zeolites with a high Al content (X zeolite) are thermally and chemically less stable, so that dehydration at high temperature may cause partial dealumination by water being desorbed with a decrease of crystallinity ("self-steaming").¹⁸ The polarity of the internal voids is governed by the Al content; it is highly relevant to the ability of zeolites to generate and stabilize organic radical cations. This parameter controls the population and density of cations in the micropores and affects the electron density on the oxygens. Strong electrostatic fields experienced by an organic guest inside zeolite voids¹⁹⁻²¹ have been invoked to explain the remarkable ability of zeolites to stabilize otherwise elusive positively charged organic intermediates as well as charge-transfer complexes.^{22,23}

The hydrophilicity/hydrophobicity of zeolites is related to the polarity of the pores. Zeolites without framework Al are the most hydrophobic.^{24,25} All zeolites contain variable amounts of water in the intracrystalline voids, either strongly bound to the solid or more loosely bound by hydrogen bridges. The

Table 1. Classification of Zeolites According to Pore Dimensions^a

designation	pore diameter [Å]	comp of pore opening	example	guest molecules
small	3–5	8 O	Erionite	O ₂ , H ₂ O
medium	5–6	10 O	ZSM-5	C ₆ H ₆ , C ₆ H ₅ X, <i>p</i> -C ₆ H ₄ X ₂
large	6–9	12 O 18 O	β, Y, Ω UTD-1, VPI-5	
extra large	> 20		MCM-41 mesoporous solids	supra- molecular chemistry

^a Ref 29.**Figure 3.** Topologies of the internal voids of zeolites (based on ref 31).

amount of water adsorbed in a zeolite increases with its Al content.²⁶

All water has to be removed before guest molecules can be accommodated in the zeolite pores; residual water, even very low concentrations, affects the cation–guest interaction significantly. Unfortunately, there are intrinsic difficulties in determining the water content under real experimental conditions. This uncertainty may explain occasional difficulties to reproduce results. The chemical composition of synthetic zeolites can be controlled either during synthesis (by varying the composition of the mother gels)^{27,28} or by postsynthetic modifications. Both methods require careful control of experimental conditions.

As for the crystal structure of zeolites, the long-range ordering of the primary tetrahedra defines nondeformable channels and cavities of strictly uniform dimensions on the molecular (nanometer) scale. They can host organic guest molecules of dimensions smaller than the apertures of the pores. Over 300 known zeolites are classified in the Atlas of Zeolites according to the symmetry of the unit cell.^{30,31} For researchers interested in the host–guest chemistry of zeolites, a classification according to the dimensions of their micropores is more convenient (Table 1).²⁹ The apertures are formed by a cyclic array of oxygens alternating with Si or Al; their number determines the diameter of the pore. Zeolites with increasing pore sizes can accept increasingly larger molecules; zeolites are useful for supramolecular chemistry.

Besides the pore dimensions, the topology of the internal voids is very important for the incorporation of guest molecules (Figure 3). In this regard, zeolites can be divided into tri-, bi- and monodirectional

Table 2. Characteristic Properties of Selected Aluminosilicates^a

	BET area ^b m ² × g ⁻¹	average pore size Å	pore volume mL × g ⁻¹
clay	46	35.7	0.08
pillared clay	250	13.4	0.18
ZSM-5	375	5.5	0.11
mordenite	400	7.4	0.16
zeolite Y	550	12.7	0.32
MCM-41	750	30	0.59

^a Refs 17 and 33–36. ^b According to the Brunauer–Emmett–Teller algorithm.³⁸

materials. Faujasites X and Y are typical tridirectional zeolites; their internal space consists of almost spherical cages (“supercavities”), 13 Å in diameter, interconnected tetrahedrally through four smaller round openings of 7.4 Å diameter.³¹ ZSM-5 is a bidirectional zeolite; its structure is formed by two systems of oval channels, one straight (5.2 × 5.7 Å), the other sinusoidal (5.3 × 5.6 Å), crossing each other at right angles.³¹ Mordenite can be considered a monodirectional zeolite; its channels (12-oxygen opening) are parallel and arranged like a honeycomb.³¹

The topology of the zeolite host is crucial for the diffusion of the guest through the interior; it controls the maximum uptake achievable. Zeolites with tridirectional structures are more accessible and allow diffusion readily, whereas diffusion in monodirectional zeolites is seriously restricted.³²

It is also of interest whether the guest is adsorbed on the internal or the external surface. In general, adsorption of a guest from the vapor phase at elevated temperatures is more favorable than from solution at room temperature, due to the interference of solvent molecules. The relative polarities of solute, solvent, and zeolite play a significant role in the adsorption (cf., Section III). The surface area of zeolites per unit weight are among the highest for any solid; the internal surface area is much larger than the external one. Representative values are given in Table 2.

The ability of zeolites to include organic guests inside the intracrystalline voids is an example of supramolecular chemistry. The host provides a rigid environment containing active sites accessible to the guest. The special role of the zeolite in the resulting supramolecular chemistry has been described by terms such as *molecular sieves*,¹⁷ *microscopic reactor*,³³ *molecular pocket*,³⁴ or *reaction cavity*.^{35,36}

Zeolites are among the most extensively characterized solids. Since the 1960s, a powerful array of experimental techniques has been developed to determine many textural, physical, and chemical parameters of zeolites, including high-resolution electron microscopy,^{39–41} atomic absorption spectroscopy, powder X-ray diffraction,³¹ and spectroscopic techniques,⁴² such as IR⁴³ and multinuclear solid-state NMR,⁴⁴ MAS NMR (²⁹Si and ²⁷Al),⁴⁵ and X-ray photoelectron spectroscopy (XPS).^{42,46} As a result, the characteristics of zeolite batches can be quantified, laying the foundation for reproducible results. Detailed descriptions of these techniques are available in the literature.¹

Highly reactive tricoordinated Al has been proposed as the site of Lewis acidity;⁴⁷ however, attempts to detect the corresponding NMR signal have met with failure. Therefore, it is generally accepted that Lewis sites correspond to extraframework-Al (EFAI).^{48,49}

II.B Nature of the Active Sites

The composition and structure of the centers responsible for the electron acceptor ability of zeolites are still subject to controversy and debate. Understanding the nature of these sites may provide control over their population and strength and make it possible to "tune" zeolites to produce optimal yields of radical cations. These features have obvious implications in the area of catalysis, especially for cracking and refining in the petrochemical industry.^{10–12,50}

There is limited experimental information to identify the active sites. Direct ESR evidence for the fate of the electron transferred to the zeolite in the oxidation step is available only in rare and special cases.⁵¹ Typically, the captured electrons are ESR silent, suggesting that they may be highly delocalized. This finding is not limited to zeolites; other solid electron acceptors show similar behavior; for example, only the organic radical cation can be observed by ESR after one-electron oxidation by AlCl_3 .⁵²

Initially, the activity of zeolites was ascribed to impurities, such as Fe.^{53–55} Although the nature of Fe^{III} centers in zeolites are well understood,^{56,57} they can hardly serve to explain the activity of synthetic samples prepared from pure Fe-free components. Alternatively, lattice defects and disruptions in the crystal structure, including tricoordinated Al,⁵⁸ or incompletely coordinated or unusually terminated lattice atoms, $\equiv\text{Si}^\cdot$ and $\equiv\text{Si}-\text{O}^\cdot$ were considered as active sites.^{59–62} Any explanation invoking anomalies, either impurities or lattice defects, rather than intrinsic properties of the zeolite fail to account for the high ion yields,⁶³ which require densities of active sites as high as one per cage.

II.B.1 Redox Reactivity and Acidity

A more widely accepted explanation links the redox reactivity of zeolites to their acidity,^{58,64–67} in analogy to the formation of radical cations from aromatics or heterocycles by liquid or solid Brønsted or Lewis acids.⁵² Zeolites are solid acids approaching the acidity of superacids;⁶⁸ their application as industrial catalysts is mainly that of heterogeneous acids.⁶⁹ In fact, several early studies of organic radical cations on amorphous silica–alumina were undertaken to elucidate the acid properties of these solids.^{70,71} It is pertinent to summarize the nature and structure of the Brønsted and Lewis acid centers in zeolites.

Protons contained within the zeolite lattice are Brønsted sites.^{69,72,73} The H^+ forms of zeolites can be prepared from alkali ion containing forms by ion exchange with concentrated hydrochloric acid at elevated temperatures. A milder method employs exchange of alkali ions by NH_4^+ ; thermal decomposition eliminates NH_3 , leaving H^+ in the framework. The protons of acidic zeolites are covalently bonded

to the oxygen closest to a negatively charged aluminum, forming oxonium species. The bridging $\equiv\text{Si}(\text{OH})-\text{Al}\equiv$ hydroxy groups can be monitored by IR spectroscopy ($3800\text{--}3400\text{ cm}^{-1}$).

Zeolites encompass sites with a wide range of acidities,⁷⁴ whose distribution depends on their chemical composition and crystal structure. The acidity has been formulated as a function of the mean Sanderson electronegativity of the framework.^{75,76} The acidity of hydroxy groups in the framework decreases as the number of Al centers in the second coordination sphere increases.⁷⁷

An alternative explanation for the increased activity/reactivity invokes the so-called confinement theory.^{78–83} This model assumes that molecules in a restricted environment can be perturbed by strong Coulombic fields (electrostatic activation), causing confined guest molecules to be more basic and to have reduced ionization potentials compared to molecules in a vacuum. In addition, the limited space available may distort and "compress" the frontier molecular orbitals (FMOs), giving rise to electronic activation.^{78–81} Spectroscopic evidence in support of molecular confinement was gained recently by studying the electronic 0,0 transitions for anthracene and naphthalene in a series of pure silica zeolites (identical composition, no Coulomb effects), differing only in the pore size: the 0,0 bands showed gradual shifts toward longer wavelengths with decreasing pore size.^{82,83}

Zeolites also contain Lewis sites;⁶⁹ these were attributed to tricoordinated Al centers. However, this type of Al has not been detected by ^{27}Al MAS NMR (vide supra). Instead, samples exhibiting Lewis acidity have octahedrally coordinated Al centers, suggesting that extraframework Al species (EFAI), generated during steaming or calcination of hydrated zeolites, are responsible for the Lewis acidity.

The acidity of zeolites can be determined by temperature programmed adsorption/desorption methods using probe molecules such as NH_3 or CO .⁴² The pyridine adsorption/desorption method specifically probes acid sites in solids by IR;⁸⁴ characteristic absorption bands for protonated pyridinium ion (1550 cm^{-1}) and for a Lewis adduct (1450 cm^{-1}) allow the separate determination of Brønsted and Lewis sites in a single measurement. Pyridine vapor is adsorbed onto dehydrated zeolite at room temperature and desorbed at increasing temperatures (e.g., in the range $250 > T > 400\text{ }^\circ\text{C}$) at reduced pressure ($\sim 10^{-2}$ Pa) over a period of several hours (cf., Figure 4). The amount of pyridine desorbed at different temperatures indicates the strength of the sites. Molar absorptivity coefficients of the pyridine Brønsted and Lewis bands are known and allow IR intensities to be converted to concentrations of acid sites ($\mu\text{mol per gram of solid}$).⁸⁵ Zeolites probed under similar conditions can be rated on a quantitative acidity scale. Acid sites on the external surface of pentasil zeolites can be probed by adsorbing a bulky base, such as 2,4-di-*tert*-butylpyridine.⁸⁶

There is a continuing debate whether Brønsted^{51,69,87} or Lewis^{53,88–90} sites are responsible for the electron acceptor ability of zeolites. Shih proposed

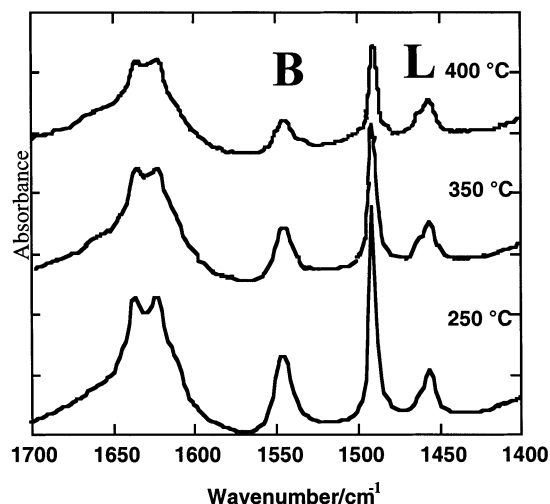
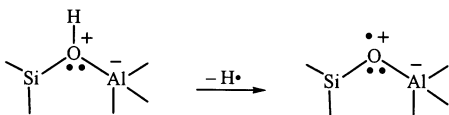
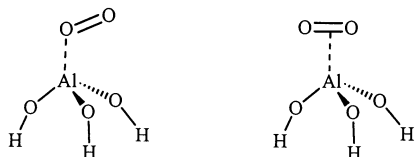


Figure 4. IR spectra (aromatic region) of pyridine-loaded HY zeolite assaying abundance and strength of Brønsted (B) and Lewis (L) acid sites after annealing between 250 and 400 °C; pyridine in B sites is increasingly desorbed, whereas pyridine in L sites is mostly retained (H. García, V. Fornés, unpublished results).

Scheme 1



Scheme 2. Model Clusters for Calculating the Electron Acceptor Ability of O₂ Adsorbed onto Zeolite Lewis Acid Sites^a

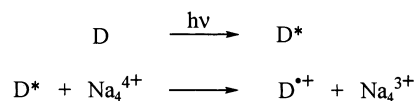


^a The "sigma" cluster (left) was predicted to be more stable than the ("pi") cluster.⁸⁹

positive holes on oxygens bridging Si and Al as the electron acceptor sites in the zeolite.⁹¹ Such holes may originate by loss of hydrogen atoms from Brønsted acid sites (Scheme 1). Indeed, Ozin and Godber were able to correlate the disappearance of Brønsted sites (3647 cm⁻¹) with the appearance of a broad water band (~3350 cm⁻¹) upon incorporating ferrocene into zeolite Y.⁵¹ They proposed homolytic dehydroxylation of the framework as part of the oxidation process.

On the other hand, *ab initio* quantum chemical calculations of simple cluster models at the Hartree–Fock level using a 3-21G basis set estimated the electron affinities of two simple cluster models, in which molecular oxygen is coordinated to a tricoordinated Al (Lewis site) through either a nonbonding or a π orbital (Scheme 2). Although the estimated electron affinity of the more stable σ -complex is rather high (2.225 eV), this cluster was considered a possible electron acceptor center.⁸⁹ Because the basis set used in these calculations was somewhat limited, and calculation resources have become more affordable in the decade since this study, it may be useful to extend the calculations to more sophisticated

Scheme 3



models with an increased basis set and higher levels of electron correlation.

This discussion is not always based on complete experimental data, because a complete profile of Brønsted and Lewis acid sites rarely has been reported for the many cases in which radical cations have been formed. This relationship could be probed by preparing and characterizing a series of zeolite samples with different populations of Brønsted and Lewis sites and determining quantitatively their ability to form radical cations, ideally for a series of molecules with a range of redox potentials (Section II.C). Nevertheless, a consensus appears to have been reached about the inability of Al-free zeolites (silicalite) to generate radical cations;⁹² for example, Ramamurthy et al. showed that an increasing Al content enhanced the electron acceptor ability.⁹³

The distribution of oxidation potentials in zeolite active sites is another point on which only limited information is available. Ramamurthy et al. assigned an upper limit to the redox potential of the active sites in Na-ZSM-5 (1.65 V),⁹³ whereas Caldararu et al. studied the distribution of sites in the H⁺-forms of X and Y faujasites quantitatively by ESR.⁹⁴ The analogy with other types of catalysts (hydrogenation, acidity) suggests that zeolites most likely contain not a single, uniform type of oxidation site, but a distribution of sites with a range of oxidizing abilities (redox potentials). The distribution should depend on factors such as the framework Si/Al ratio as well as the crystal structure of the zeolite.

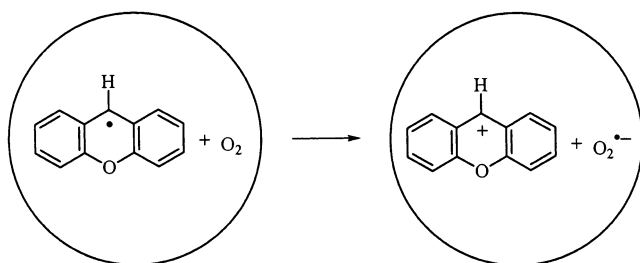
The existence of variable redox potentials of zeolite active sites, depending on the crystal structure of the zeolite, are supported by divergent results observed upon incorporation of benzene (IP 9.24 eV) into different zeolites. Benzene radical cation is readily formed in dealuminated mordenites or pentasil zeolites, but was not detected in tridirectional, large-pore Y zeolite.^{63,95–100}

In addition to active sites in the zeolite lattice, Yu et al. proposed the charge-balancing cations as electron acceptors in photoinduced processes (Scheme 3).^{101–103} Ion clusters, e.g., Na₄³⁺, were proposed as intermediates in the photoinduced radical cation generation in Na-faujasite. The cluster ions have short lifetimes, typically in the microsecond range. The existence of M_n⁽ⁿ⁻¹⁾⁺ clusters sets limitations for the nature of the electron acceptor sites in zeolites. This would indicate that there are no electron sinks more stable than strongly reducing alkali atoms. Such clusters of alkali metal atoms have been established inside zeolites based on their ESR spectra,¹⁰⁴ in the context of zeolites behaving as solid superbases.^{105,106}

II.B.2 Influence of Oxygen

Molecular oxygen could play a central role in the one-electron oxidation process.^{53,62,87,89,107,108} It has been suggested that the active sites may be created

Scheme 4



by oxygen during the thermal dehydration of the zeolites.⁹¹ This would explain the well-documented influence of oxygen present during the thermal pretreatment on the number of spins that can be measured for some zeolites.

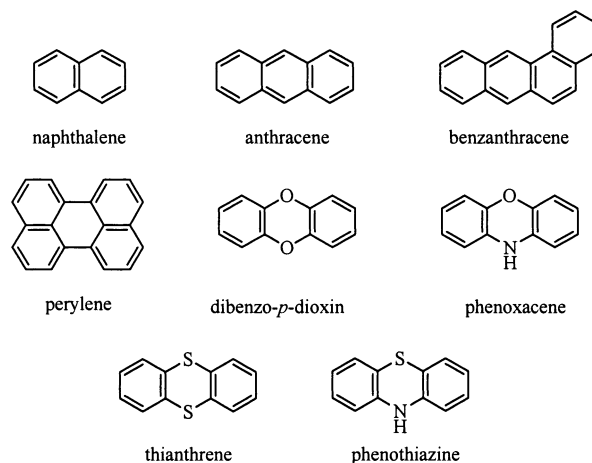
Rigorous exclusion of oxygen during all stages of zeolite synthesis, calcination, and dehydration has not been reported (and perhaps not been achieved). The fact that organic radical cations can be generated after activation of zeolites under argon seems to indicate that oxygen is not necessary for the process.^{51,53,67} However, an increase in the radical cation yield in the presence of oxygen has been noted in several cases.^{51,53,67} The generation of radical cations by conventional acid media also proceeds in the absence of oxygen, but the efficiency is enhanced in its presence.^{109–111} Interestingly, highly reactive oxygen atoms, generated by decomposition of N_2O , do not increase the activity of ZSM-5.¹¹² Another possibility that would reconcile many experimental observations sees O_2 as regenerating active sites exhausted after an electron-transfer step. In this scenario, oxygen would serve as the final electron sink and render the overall process catalytic; it would not be necessary for a limited degree of oxidation, but would increase the turnover at the active sites.

The zeolite framework plays a crucial role in this oxidation. In this context, we mention the recent conversion of xanthyl radical to xanthylum cation by oxygen inside the cavities of alkali exchanged Y zeolites (Scheme 4).¹¹³ Time-resolved diffuse-reflectance laser flash photolysis showed instantaneous formation of xanthyl radical after the laser pulse. Subsequently, the delayed formation of xanthylum cation was observed due to one-electron oxidation of the radical. This process takes place on the microsecond time scale in the presence of oxygen; the growth of xanthylum cation can be followed conveniently by laser flash spectroscopy. The oxidation occurs with Li^+ or Na^+ as counterions, but not with Cs^+ .

II.C Characterization of Zeolite Active Sites Exemplified

Because of the importance of using well-characterized zeolites, we discuss in some detail three studies probing the distribution of active sites in zeolites and their range of oxidative strength. In an early study, Goupil et al. used benzene and a series of condensed aromatic hydrocarbons with different oxidation potentials (E_{ox} /ionization potentials, IP) and molecular sizes to probe the concentration of active sites in various zeolites.¹¹⁴ The number of spins generated

Scheme 5. Aromatic/Heteroaromatic Probes for the Activity of Zeolites



were correlated with the arene IP or, perhaps more appropriately, with their E_{ox} . Perylene and benzantracene were used to “titrate” the external sites; they have low IP and E_{ox} , but are too bulky to enter into the micropores. The number of external sites in Cr^{III} containing zeolites ($\sim 5 \times 10^{17}$ spin g^{-1}) was independent of the Cr^{III} concentration inside the pores. Activation under air generated a higher spin count (5×10^{17} spin g^{-1}) than activation under nitrogen (3.9×10^{17} spin g^{-1}); the presence of a reducing gas (H_2) eliminated the external sites almost completely.

Because benzene (IP 9.24 eV; E_{ox} 2.3 V) failed to react with Cr^{III} containing zeolites, it could be used as an “inert” solvent for the adsorption of naphthalene (IP 8.3 eV; E_{ox} 1.54 V) or anthracene (IP 7.74 eV; E_{ox} 1.09 V), which “titrate” the total (external plus internal) sites present. Some samples oxidized perylene (IP 7.2 eV; E_{ox} 1.0 V) and benzantracene (IP 7.6 eV; E_{ox} 1.18 V), whereas naphthalene and anthracene showed no activity, indicating a redox potential, $1.0 < E_{ox} < 1.09$ V ($7.6 < IP < 7.74$ eV), for the external sites of these zeolites.¹¹⁴ Of course, this study does not address the chemical nature of the active sites.

Caldararu et al. determined the “activity” distribution of acceptor sites in X and Y zeolites by quantitative ESR measurements.⁹⁴ The population of sites and their oxidative strength was “titrated” with four condensed (hetero-) aromatics of different oxidation potentials and of molecular diameters sufficiently small (~ 6 Å) to allow diffusion into the faujasite pores. A large polycyclic arene (perylene) was chosen to probe the oxidizing sites on the external surface. Silica–alumina and γ -alumina, two amorphous solids of known ability to generate aromatic radical cations, were included for comparison (Table 3).

The radical cations of the probe molecules were recognized by their hyperfine splittings. They were stable under the reaction conditions; the ESR intensity remained constant after an initial build-up; the results were reproducible within $\pm 10\%$ (Table 3). This work parallels earlier studies on silica–aluminas using electron donors with a range of oxidation potentials, in which the size of the probe molecules was not considered.¹¹⁵

Table 3. Number of Active Sites (by Quantitative ESR Measurements) for Selected Zeolites as a Function of the Electron Donor Probe^a

zeolite	HY			SiO ₂ -Al ₂ O ₃	γ -Al ₂ O ₃
	HX	HY	steamed		
Si/Al ratio	1.6	3.0		6.0	
BET area (m ² × g ⁻¹)	358	527	309	237	215
probe	IP (eV)	spin count (10 ¹⁸ spins × g ⁻¹)			
dioxin	7.87		3.0	1.0	
phenoxacene	7.76	very weak	66	36	3.6
anthracene	7.56	0.4	2.2	9.6	2.2
phenothiazine	7.23	26	176	102	60
perylene	6.92	3	8		8
total vs strong acceptor sites		66	80	11	27
internal vs external sites		9	22		~1

^a Ref 94.

The data showed that acid HY zeolites contain more oxidizing sites than silica-alumina or γ -alumina; both solids had a distribution of acceptor sites with varying oxidizing strength. The ratio of sites occupied by phenothiazine (IP = 7.23 eV) and anthracene (IP = 7.56 eV) indicate the (narrow) range of oxidative strength. Steaming of Y zeolite in water vapor (known to cause framework dealumination) reduced the total number of oxidizing sites, but increased the population of the strongest sites. This behavior parallels the influence of steaming on the strength distribution of acid sites in zeolites.^{69,116} The ratio of phenothiazine to perylene radical cation (lowest IP; shortest diameter, 7.7 Å > 7.4 Å, diameter of pore opening) gives an estimate of internal vs external electron acceptor sites. Additional studies continuing this excellent approach to evaluate strength and distribution of internal vs external oxidizing sites for "steamed" HY, would add valuable information.

The third study used the thianthrenium radical cation, Th⁺,^{109,117,118} to correlate the Brønsted/Lewis acidity and topology of zeolites with their ability to generate radical cations. In solution, Th⁺ is generated readily upon dissolving Th ($E_{ox} = 1.47$ V vs NHE)¹¹⁹ in Brønsted or Lewis acids, forms moderately stable salts with nonnucleophilic counterions (BF₄⁻),^{109,120} and has a characteristic UV-Vis spectrum (λ_{max} 270, 290, 550 nm; cf., Th, λ_{max} 260 nm).

The adsorption procedure proved to be crucial for the incorporation of Th into a series of zeolites (H⁺ or alkali ion forms (Table 4)).^{67,114} Incorporation from organic solvents had distinct disadvantages; attempts to adsorb Th from isoctane solution onto offretite or medium pore zeolites failed to yield significant incorporation (thermogravimetry, DR spectroscopy), although sizable ESR signals were observed. These results again illustrate the high sensitivity of the ESR method.

In contrast, adsorption from the vapor phase at 200 °C under Ar led to well resolved DR and IR spectra of Th⁺, even in medium-pore zeolites and mesoporous MCM-41 aluminosilicate.⁶⁷ The role of the incorporation procedure was rationalized as due to a combination of factors, such as a higher kinetic energy of Th,

Table 4. Ability of Selected Acid Zeolites to Oxidize Thianthrene^a

zeolite	characteristics		incorporation procedure	ability to oxidize Th
	Si/Al	acid sites ^b		
NaY	2.4	neutral	solution	
CsY ^c	2.4	basic	solution	
HY ^d	2.4	B + L	solution	✓
HY-NaCl ^e		mostly L	solution	
HYD	15	B + L	solution	✓
HYD-W ^f		mostly B	solution	✓
HBeta	13	B + L	solution	✓
silicalite ^g	∞	neutral	vapor phase	
HZSM-5	17.5	B + L	vapor phase	✓
MCM-22	13.6	B + L	vapor phase	✓
MCM-41	11.3	weak acid sites	vapor phase	✓

^a Ref 67. ^b B = Brønsted, L = Lewis. ^c 70% Cs⁺ exchange. ^d Exclusively H⁺. ^e From HY by complete Na⁺ exchange. ^f From HYD by (NH₄)₂SiF₆ washings. ^g No Al.

enhanced lattice vibrations, and reduced restrictions to diffusion in the absence of solvent. The nonplanar structure of Th was recognized as a major obstacle to incorporation.¹²¹

The location of Th⁺ in the internal voids follows from two lines of evidence: ZSM-5 samples of similar micropore volume and BET surface area but different particle size (different ratio of external to internal surface area) generated equal yields of Th⁺; XPS analysis of a silicalite sample containing Th⁺ showed no C or S on or near the surface; these were detected only after intensive Ar⁺ ion sputtering had destroyed the outer layers of the silicalite particles.⁹²

Quantitative ESR measurements of a series of H⁺ and NH₄⁺ zeolites with a range of Si/Al ratios showed spin counts (5 × 10¹⁹ spin g⁻¹) 3 orders of magnitude higher than those measured for Na⁺-ZSM-5. These results support several conclusions: (i) ZSM-5 generates Th⁺ more efficiently than zeolite Beta, even though Beta adsorbs more Th than ZSM-5; (ii) the active sites generating Th⁺ need not be strongly acidic (NH₄⁺ and H⁺ forms generated similar spin counts); (iii) the population of oxidizing sites increased with the Al content of the zeolite; and (iv) the yield of Th⁺ is up to one tenth that of the total number of acid sites.⁹²

The chemical nature of the sites responsible for the electron acceptor ability was probed by samples, which had been submitted to alkali ion exchange to remove Brønsted acid sites or dealuminated by washing with ammonium hexafluorosilicate to remove Lewis acid sites. The samples were characterized by pyridine adsorption/desorption and tested for the presence of Th⁺. The results link the oxidative ability of the tested zeolites to the presence of Brønsted acid sites: zeolites containing Brønsted acid sites generate Th⁺ even in the absence of Lewis acid sites, whereas those without Brønsted sites failed to generate Th⁺ even if they contained Lewis acid sites (Table 4).^{37,122} Given the fact that the nature of the electron acceptor sites in zeolites is not yet fully understood, further studies probing the link between acid sites and electron acceptor ability are still necessary.

III. Adsorption Procedures

The procedure used to adsorb the substrate onto the zeolite is crucial for radical cation formation and

may affect the species generated. We mention briefly the principal methods of incorporation; in cases, where the incorporation method affects the resulting species, the incorporation method will be specified.

Most commonly, organic substrates are adsorbed onto thermally dehydrated zeolites from inert solvents. Adsorption is favored when the solvent polarity is significantly different from that of the zeolite, and the solute is of similar polarity as the zeolite. For that reason, any residual water molecules are highly detrimental to guest uptake. Details of the zeolite activation (temperature, atmosphere) may be relevant for reproducible results. The adsorption of solvent competes with that of the substrate.^{123–130} Nonpolar hydrocarbons or halogenated solvents are generally more suitable than protic or highly polar ones. Low boiling solvents are more easily removed. Guest molecules can be incorporated at room temperature; however, elevated temperatures may result in higher loadings.

The dimensions of the solvent molecule relative to the zeolite pores may affect the incorporation. For example, isooctane is size-excluded from ZSM-5, allowing organic guests ready diffusion into ZSM-5 at room temperature.¹³¹ However, at elevated temperatures (100 °C; reflux) isooctane can partially penetrate the openings of ZSM-5 channels.¹³² After treatment under these conditions, residual isooctane was detected by IR and MAS ¹³C NMR spectroscopy. Desorption of the residual by vacuum degassing required temperatures above 300 °C, suggesting that the methyl groups are “hooked” into the zeolite pores. Solvents with smaller kinetic diameters (benzene) can be incorporated or used to extract organic material from interior zeolite surfaces.¹³¹

For guests of sufficient vapor pressure, adsorption from the vapor phase is a clean and efficient alternative, well suited for low boiling liquids (viz., pyridine, “IR titration” of acidity) and for solids that sublime, including most condensed polycyclic aromatics. The intended guest can be heated to increase its vapor pressure. Vapor phase adsorption has the advantage of enhanced intra-zeolite diffusion in the absence of solvent and at elevated temperatures. Substrates that cannot be incorporated from solution were successfully incorporated from the vapor phase, for example, C₆₀ fullerene (kinetic diameter 7.9 Å) into NaY (windows diameter 7.4 Å) at temperatures of 500–750 °C (Figure 5).¹³³ Partial loss of crystallinity is to be expected when heating NaY at temperatures about 650 °C.

A variation of this method, chemical vapor deposition, employs a volatile derivative to deposit a nonvolatile solid onto a zeolite, e.g., to include metal clusters into zeolites.^{134,135} Laser ablation of solid surfaces is a variation of this technique, depositing thin films onto zeolite surfaces.

Occasionally, solid-state adsorption is achieved by mixing a solid guest with dehydrated zeolites without solvent or heating. For example, alkali metal clusters were included into the supercages of Y zeolites by mixing the two solids.¹⁰⁵ This method is simpler and cleaner than alternative methods (treatment of alkali-exchanged Y zeolite with organometallic reagents)¹⁰⁶

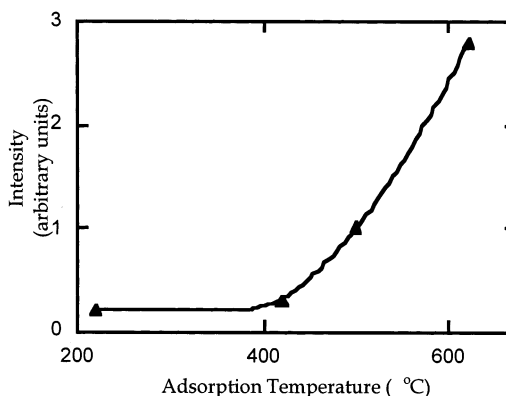
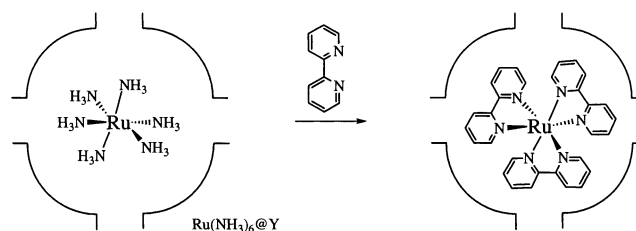


Figure 5. Effect of adsorption temperature on the number of radical cations generated by adsorption of C₆₀ on NaY zeolite. Reprinted with permission from ref 136. Copyright 1997 Chemical Society of Japan.

Scheme 6. Ship-in-a-Bottle Synthesis of Ru(bpy)₃²⁺ by NH₃-to-bpy Ligand Exchange after Incorporating Ru(NH₃)₆³⁺ into Y Zeolite Supercages^a



^a Ref 141.

and results in a higher final uptake of metal;¹⁰⁵ however, it requires much longer times and a suitable procedure to remove the excess of guest molecules.

Finally, for tridirectional zeolites containing large cavities accessible only through small openings, organic guests can be assembled in the large cavity (*ship-in-a-bottle synthesis*),^{137–139} producing bulky assemblies immobilized inside the zeolite. Initially used by Herron et al. to assemble organometallic oxidation catalysts inside Y zeolite supercages,^{137,138,140} this method was applied also to form tris(2,2'-bipyridyl)ruthenium(II) complex [Ru(bpy)₃²⁺] inside zeolite Y by adsorption of hexaammoniaruthenium(III) and subsequent treatment with 2,2'-bipyridine (bpy).¹⁴¹ The resulting Ru(bpy)₃²⁺ has a diameter of 12 Å, much larger than the pore opening (Scheme 6).

Inorganic assemblies, such as nanoclusters of TiO₂, were prepared by similar procedures inside zeolites: adsorption of monomeric (TiO₂)²⁺ and subsequent oligomerization generated TiO₂/zeolite composites,^{142–144} which serve as heterogeneous electron-transfer photocatalysts.^{145,146} Treatment of the same zeolites with colloidal TiO₂ sols did not lead to significant incorporation of TiO₂.¹⁴²

IV. Experimental Techniques to Study Radical Cations in Zeolites

IV.A. Optical Absorption Spectroscopy

Zeolites contain no chromophores above 180 nm;¹⁴⁷ UV/vis spectra of zeolite samples above ~240 nm

represent exclusively the adsorbed guest. Still, zeolites are not transparent; they appear as “white”, opaque solids because the particles reflect and scatter light. In special cases, zeolite wafers prepared from particles of appropriate size permit recording of UV/vis transmission spectra.¹⁴⁸

Absorption spectra of organic radical cations generally are shifted significantly relative to the parent molecules.¹⁴⁹ For example, simple conjugated dienes absorb near 220 nm, whereas their radical cations absorb above 550 nm. The open-shell configuration of radical cations allows electronic transitions not present in the precursor. The new bands may appear in the visible (many radical cations are highly colored) or even the far-IR region.¹⁴⁹

Optical spectroscopy is a powerful tool to probe organic radical cations. A special modification, diffuse reflectance spectroscopy,¹⁵⁰ allows recording optical spectra of organic guests in “opaque” zeolite powders. The scattered light reflected by the solid surface corresponds to the intensity reflected by a pure white surface (BaSO₄) minus that absorbed by the chromophore. The low intensity of scattered light requires special techniques (e.g., integrating spheres) to collect all reflected light. Diffuse reflectance plots matching the optical spectrum in transmission are obtained by subtracting the reflectance (R) from a “white” standard, and converting it into a function, $F(R)$, usually according to the Kubelka–Munk expression,¹⁵¹

$$F(R) = (1 - R)^2/2R \quad (1)$$

For $R \ll 1$, the function is conveniently simplified to

$$F(R) = 1/R \quad (2)$$

For short-lived intermediates time-resolved laser flash diffuse-reflectance is available from picosecond to microsecond resolution.^{152–154}

Emission spectroscopy also can be applied to study opaque solids. Given excitation at $\lambda > 240$ nm, the luminescence is characteristic of the organic guest. Conventional fluorimeters can be adapted for solid samples by simple front-face attachments preventing reflected excitation light from reaching the detector. Luminescence has been widely applied to probe the effect of the environment on organic guests in diverse heterogeneous media,¹⁵⁵ but as yet to few organic radical cations. This is mainly because radical cations absorb in the visible extending into the far-IR region. The corresponding emission falls into a spectral range where conventional monochromators and gratings no longer work. Emerging technologies and improved components may make radical cation emission studies feasible in the foreseeable future. Additionally, the emission quantum yields of radical cations may be low as a result of the small energy gap.

IV.B IR and Raman Spectroscopy

Compressed zeolite wafers are sufficiently transparent in the IR region for conventional IR transmission measurements. They can be obtained similar to KBr disks for IR spectra of organic solids. Moisture has to be excluded rigorously, often requiring thermal

pretreatment under high vacuum ($\approx 10^{-2}$ Pa). Although zeolites have strong lattice absorptions, they have spectral windows in the range 3400 to 1200 cm^{-1} , making accessible a most informative region to probe for organic functional groups. The paucity of IR data for radical cations to date may be due to the strong IR absorptions of residual solvents used to incorporate substrates, which interfere with the spectra of the solutes.

As mentioned earlier (Section II.B), IR spectroscopy is very useful for assessing the abundance, nature, and strength of acid sites.⁶⁹ In addition, internal and external silanol OH groups and acidic bridging hydroxyls ($\equiv\text{Si}(\text{OH})\text{Al}\equiv$) can be differentiated in the 3800–3400 cm^{-1} region in dehydrated zeolite wafers.¹⁵⁶ Changes occurring with the formation of oxidized species can identify the groups underlying the electron acceptor ability of zeolites.

Transient IR spectroscopy, extended recently to the microsecond time scale,¹⁵⁴ is available to study radical cations too short-lived for conventional IR spectroscopy. However, it has not yet been applied to the study of organic radical cations within zeolite matrices.

Raman spectroscopy also reveals vibrational/rotational transitions.⁴³ This technique is complementary to IR, as it detects IR-silent transitions of symmetrical entities (no change in dipole moment). Because most zeolites lack intense Raman absorptions, Raman spectra can be recorded simply in quartz capillaries or glass cells, instead of the ionic salt windows employed in IR spectroscopy. The handling of zeolite samples for Raman spectroscopy is simple; moisture does not pose a problem because water is Raman-silent. Further, since Raman spectroscopy measures scattered light, the zeolites need not be compressed into disks. Although Raman spectroscopy has so far found limited application in the characterization of organic species embedded within zeolites, it appears destined to become increasingly important, particularly with the advent of compact, affordable Raman spectrometers for routine operation. Among the work on organic radical cations within zeolites reported so far, we mention the transient Raman spectra of methyl viologen radical cations, studied by several groups.^{141,157}

IV.C Magnetic Resonance Methods

Among NMR techniques, ¹³C NMR spectroscopy has provided significant information about the detailed nature of zeolites,⁴⁵ but is not suitable to study (paramagnetic) radical cations. In contrast, electron spin resonance (ESR) provides detailed information about radical ions in zeolites. Irradiation with a frequency satisfying the resonance condition (eq 3) stimulates transitions between magnetic levels,

$$h\nu = g\mu H_0 \quad (3)$$

where h is the Planck constant, g is a parameter characteristic for the radical under scrutiny, μ is the Bohr magneton, and H_0 is the spectrometer field strength.

The (hyperfine) interaction of an unpaired electron with nearby magnetic nuclei gives rise to a pattern of signals that may be characteristic for the radical ion. The splitting identifies the magnitude of the interaction; the number of signals and their relative intensities reflect the number of equivalent nuclei so coupled. The splitting pattern provides the key to the spin density distribution in the radical ion.^{158,159} ESR spectroscopy has been exceedingly useful to identify and characterize many radical cations.

The application of ESR spectroscopy is limited to species with lifetimes greater than a few milliseconds. Generation of free radicals by flash photolysis allows time-resolved (TR) ESR spectroscopy.¹⁶⁰ These experiments may yield radical ions with substantial deviations from equilibrium populations, giving rise to significantly enhanced spectra in absorption, emission, or in a combination of both modes; however, the splitting pattern of the intermediate remains unaffected. Thus, the enhanced intensities facilitate the detection of short-lived radicals at low concentrations. The effects underlying these spectra, first noted in 1963,¹⁶¹ are known as chemically induced dynamic electron polarization (CIDEP).^{162,163} TR-ESR experiments require sophisticated instrumentation; they involve the repetitive generation of radical ions by short laser pulses and the subsequent time-resolved recording of the transients.^{164–168}

A related technique, fluorescence detected magnetic resonance (FDMR), offers improved time resolution ($10^{-7} > \tau > 10^{-9}$ s), and its sensitivity exceeds that of standard ESR by several orders of magnitude. FDMR was first applied in the study of matrix-isolated phosphorescent triplet states;¹⁶⁹ the technique is useful for probing ESR spectra of short-lived radical ion pairs, if they form products in electronically excited states that decay by radiative pathways.^{170–173} Strong ESR signals can be observed particularly, if intersystem crossing is induced principally by the applied magnetic field on a time scale $(gH_1)^{-1}$ compatible with the pair lifetime. FDMR can be applied to radical ion pairs produced by pulse radiolysis in nonpolar solvents. Typically, per-deuterated aromatic electron acceptors (anthracene-*d*₁₀) are employed to minimize the spectrum due to the radical anion.

V. Spontaneous Generation of Radical Cations in Zeolites

In contrast to the wide use of acid zeolites as heterogeneous catalysts,^{6,174–177} there are relatively few reports describing the use of zeolites to promote electron-transfer reactions on a preparative scale. However, for some vapor-phase reactions catalyzed by acid zeolites radical cations have been proposed as alternative intermediates instead of the more conventional carbenium ions.^{178,179} Examples include the methanol-to-gasoline conversion catalyzed by HZSM-5,¹⁸⁰ the isomerization and disproportionation of alkylbenzenes on H-mordenite,¹⁸¹ or the *ortho*-to-*para* isomerization of dihalobenzenes by transition metal ion exchanged zeolites.¹⁸² Aromatic radical cations have been invoked in the deactivation (coke formation) of noble metal-exchanged Y zeolites dur-

ing the vapor-phase deep oxidation of benzene.¹⁸³

A plethora of organic radical cations can be generated in zeolites, either spontaneously upon inclusion of their precursors or by action of light, anodic oxidation, or radiation.^{93,99,184–203} The rigid microporous solids serve as excellent matrices, stabilizing otherwise reactive or unstable radical cations,^{67,92} due to the combined contributions of the intense electrostatic fields inside the zeolite and from topological restrictions that prevent access of external reagents. Following early work aimed to probe the activities of active solids, the role of their physicochemical parameters in radical cation generation was evaluated. Finally, the sequestered radical cations and their controlled conversion into secondary species attracted interest. Reactive zeolites with larger channels or supercages allow major reorganizations, dimerizations, or ion–molecule reactions.

The ability of zeolites to generate radical cations is most likely related to the presence of acid sites (Section II.B); accordingly, zeolites containing Brønsted acid sites may generate carbenium ions. The competition between radical cation and carbenium ion formation was studied using diverse substrates and zeolite hosts (Section V.B). Some radical cations sequestered in zeolites are converted by spontaneous reactions with active sites of the host (Section V.C). Deprotonation is frequently observed; more deep-seated conversions may also occur. Radical cations can be converted also by the action of heat or light. For substrates with oxidation potentials too high for spontaneous oxidation or for “guests” sequestered in less active zeolites, radical cations may be generated by radiolysis (Section VI), photolysis (Section VII), or anodic oxidation (Section VIII).

V.A Spontaneous Radical Cation Formation Exemplified

This section deals with the generation of organic radical cations by adsorption onto zeolites without additional activation. Radical cations have been obtained from a wide range of substrates, including alkenes, cycloalkanes, alkynes, and even selected alkanes. Their discussion is arranged according to substrate type. Sequestered in the zeolite, the resulting radical cations can be remarkably persistent with lifetimes ranging from minutes to years, so that they can be studied conveniently by the full range of spectroscopic techniques (cf., Section IV).

V.A.1 Radical Cations from Alkenes

Thirty years ago, Corio and Shih first observed a radical cation after incorporating an alkene (**1**) into the channels of a synthetic mordenite.²⁰⁴ They reported the ESR spectrum of 2,3-dimethylbut-2-ene radical cation (**1**^{•+}).²⁰⁴ A well-resolved 13-line spectrum ($A = 17.5$ G, four CH₃ groups; nine lines discernible) showed little change over the temperature range $77 < T < 300$ K, suggesting a small internal rotational barrier for the four methyl groups (Figure 6). Deviations of individual line intensities from the binomial distribution were ascribed to line width effects and frequency shifts.

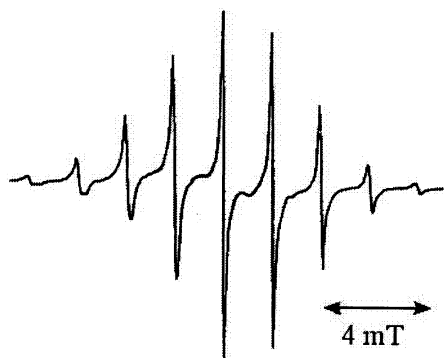
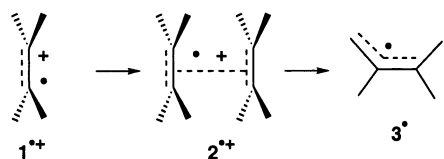
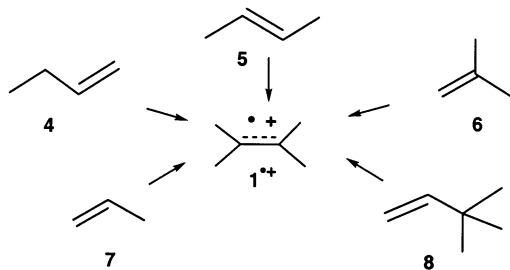


Figure 6. ESR spectrum of 2,3-dimethylbut-2-ene radical cation, $1^{\bullet+}$; 9 lines are discernible; two pairs of outer signals fall within the noise. Adapted from ref 201. Copyright 1998 Elsevier Science.

Ichikawa and colleagues observed 2,3-dimethylbut-2-ene radical cation ($1^{\bullet+}$; C6) and its π -dimer ($2^{\bullet+}$) “as byproducts of acid-catalyzed reactions” of but-1-ene (4), but-2-ene (5), and 2-methylpropene (6).²⁰⁵ The radical cation, $1^{\bullet+}$, forms the dimer radical cation, $2^{\bullet+}$, by reaction with neutral 1; $2^{\bullet+}$ is converted to the neutral 2,3-dimethylbutenyl radical (3^{\bullet}), apparently by proton transfer to the alkene.



These results suggest acid-catalyzed isomerization, dimerization, and fragmentation of the C_4 -monoolefins, generating 1, which is then oxidized on a suitable site in the zeolite. Quenching the loaded zeolite in water and extraction of the reaction products showed only minor quantities (<1%) of 1. This is clear evidence that the ESR method may show a bias for detection of the most stable radical cation, in this case, $1^{\bullet+}$.



Rhodes observed $1^{\bullet+}$ and $2^{\bullet+}$ upon adsorption of propene (7; C3) onto H-mordenite.¹⁸⁹ The radical cation, $1^{\bullet+}$, was also formed when 3,3-dimethyl-1-butene (8) was adsorbed. Interestingly, the 3,3-dimethyl-1-butene radical cation ($8^{\bullet+}$) is stable to rearrangement in Freon matrices. This led the author to suggest rapid H^+ catalyzed conversion of 8 to 1, before the one-electron oxidation.

Roduner and co-workers found that adsorption of 2,5-dimethyl-2,4-hexadiene (9) on activated H-mordenite leads to the radical cation ($9^{\bullet+}$), readily identified by two strongly coupled sets of six equivalent protons ($A = 1.31$ mT; $A = 1.06$ mT) and two protons of $A =$

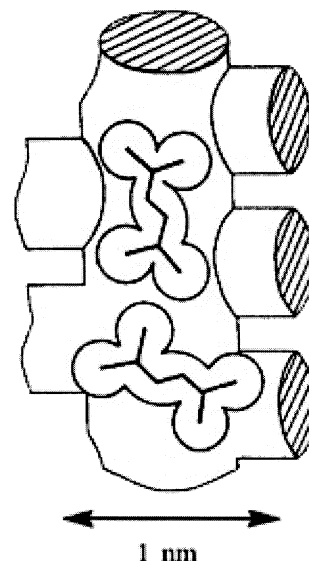
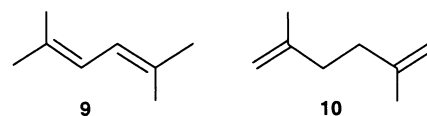


Figure 7. Visualization of 2,5-dimethyl-2,4-hexadiene radical cation, $9^{\bullet+}$, rigidly packed inside the straight channels of ZSM-5. Adapted from ref 207. Copyright 1992 The Royal Society of Chemistry.

0.25 mT at a line width of 0.12 mT.²⁰⁶ These parameters agree closely with those reported for the radical cation in dichloromethane, convincing evidence for the identity of the species in the zeolite.

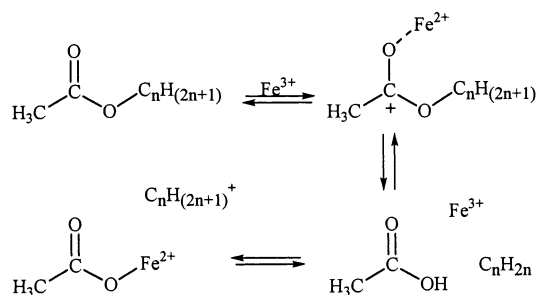


Incorporation of 9 into H-ZSM-5 produced a multiplet with lower resolution; still, at least 11 lines ($A = 1.18$ mT) were observed, corresponding essentially to the envelope of the spectrum in H-Mor. The comparably low resolution was ascribed to the more rigid packing of $9^{\bullet+}$ in the HZSM-5 matrix (Figure 7).

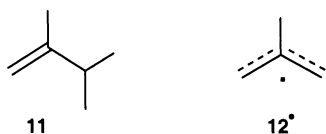
The same radical cation, $9^{\bullet+}$, was also formed upon incorporating 2,5-dimethylhexa-1,5-diene (10) into H-mordenite; its formation can be readily explained by rearrangement on the zeolite.²⁰⁷ Somewhat more difficult to explain is the formation of $9^{\bullet+}$ from 1, as it requires a complex sequence of dimerization, rearrangement, and fragmentation.²⁰⁶ Moreover, these results are different from those of Ichikawa et al. who obtained $1^{\bullet+}$ in this reaction.²⁰⁵ One explanation for the obvious discrepancy between these results lies in differences in the experimental conditions, such as the composition of the zeolites and the distribution of active sites. The divergent results illustrate the importance of using well-characterized zeolites to achieve reproducible results.

No less surprising is the observation of ESR spectra essentially identical to that of $9^{\bullet+}$ upon incorporation of 2-methylpropene (6; C₄) or 2,3-dimethyl-1-butene (8; C₆) into H-mordenite. The formation of $9^{\bullet+}$ from 6 can be rationalized by a series of simple steps, such as deprotonation of radical cation, $6^{\bullet+}$, coupling of the 2-methylpropenyl radicals, 12^{\bullet} thus formed, and oxidation. In contrast, the mechanism leading from 11 to $9^{\bullet+}$ is less straightforward, as it requires loss

Scheme 7



of a C₂ fragment before dimerization or loss of a C₄ unit after dimerization. In either case, highly specific dimerization/fragmentation pathways of significant complexity are indicated.



Dehydrated H-mordenite, especially Fe^{III} containing samples, converts alkyl acetates to alkenes and acetic acid.²⁰⁸ The activity of H-mordenite increased up to 4-fold upon introduction of 10.5% Fe^{III}. A wide range of alkyl acetates, particularly the *tert*-butyl derivative, generated 2,3-dimethyl-2-butene radical cation or its dimer radical cation; only ethyl acetate failed to undergo this reaction. The results can be explained by electron transfer from the alkyl acetates directly to Fe^{III} or, alternatively, to a Brønsted acid site, whose electron acceptor ability is enhanced by Fe^{III}.

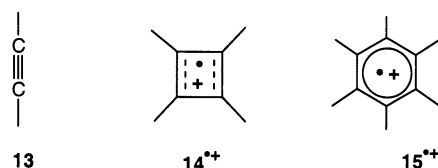
As is frequently the case for zeolite-induced reactions, mechanistic details of this conversion are not known. One pathway involves cleavage of the C–O bond, generating an alkyl carbocation and an acetyloxy free radical. Deprotonation of the alkyl carbocation would form the alkene (Scheme 7).

An alternative mechanism is suggested by the fact that the net conversion corresponds to a *cis*-elimination. Reactions of this type are carried out typically in the gas phase, at temperatures of ~500°. The overall reaction sequence is complex; following the formation of the alkene radical cation, it must include skeletal rearrangements as well as C–C bond formations and cleavages.²⁰⁸ Regardless of which mechanism is operative, the conversion aptly demonstrates the catalytic power of the zeolite.

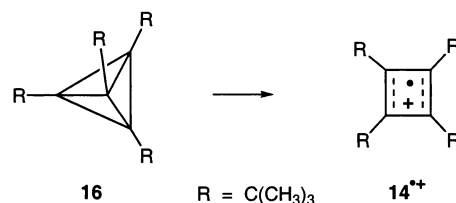
V.A.2 Radical Cations from Alkynes

Adsorption of butyne, (**13**), onto Na-ZSM-5 generated a spectrum ($A = 10.0$ G, 6H) assigned to the radical cation **13**^{•+}.²⁰⁹ Above the boiling point of **13** (27 °C), the spectrum “changed into nine lines with 6.60-G separation” ($g = 2.0029$) similar to the splitting in hexamethylbenzene radical cation (**15**^{•+}). Adsorption of butyne, (**13**), onto H-Mor generated the known spectrum of tetramethylcyclobutadiene radical cation (**14**^{•+}; $A = 9.0$ G, 12 H), apparently via cycloaddition of the monomer radical cation onto butyne.¹⁸⁷ Upon raising the temperature of the zeolite sample to 330 K, a spectrum resembling that of

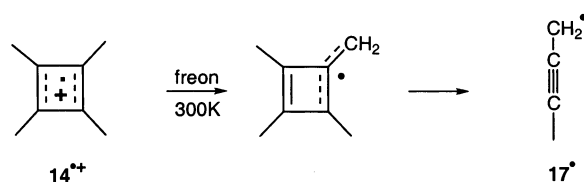
hexamethylbenzene radical cation (**15**^{•+}) was observed ($A = 6.7$ G; 6 equivalent methyl groups). It is tempting to consider a second cycloaddition, of **13** onto **14**^{•+}, and subsequent ring-expansion to **15**^{•+}. This reaction was ruled out because it has no precedence in Freon matrices.



γ -Irradiation of **13** in Freon matrices, at 77 K gave rise to the ESR spectrum of the radical cation, **13**^{•+};^{210–212} upon allowing the matrix to warm (and soften), the ESR spectrum changes to that of **14**^{•+}, documenting the cycloaddition of **13**^{•+} onto **13**. A similar radical cation, **14**^{•+} ($R = t\text{-C}_4\text{H}_9$) was obtained upon oxidation of tetra-*tert*-butyltetrahedrane (**16**; $R = t\text{-C}_4\text{H}_9$).²¹³

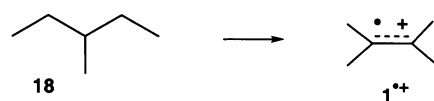


Upon warming of the Freon matrices, **14**^{•+} is converted to methylpropargyl radical (**17**[•]), most likely via deprotonation and fragmentation.²¹⁴ Accordingly, **15**^{•+} must be formed by a different pathway, possibly by acid-catalyzed trimerization of butyne.

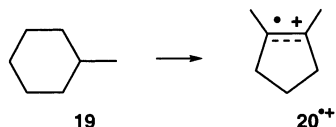


V.A.3 Adsorption of Alkanes and Cycloalkanes

Chen and Fripiat succeeded in generating radical ions from saturated hydrocarbons, 3-methylpentane (**18**), or 1-methylcyclohexane (**19**), by sequestering them into H-mordenite and heating for several hours.¹⁹⁴ The resulting species were identified by their ESR spectra.²¹⁵ Adsorption of **18** and heating to 100 °C for 4 h produced a “nine-line spectrum” ($A = 17.3$ G, $g = 2.003$), which was identified by Roduner and Crockett as that of the (omnipresent) 2,3-dimethylbutene radical cation (**1**^{•+}).²¹⁵



Similarly, the 13-line spectrum ($A = 17$ G, $g = 2.003$) observed after adsorption of **19** was also assigned to a rearranged species, 1,2-dimethylcyclopentene radical cation (**20**⁺; $A = 16.7$ G, 2 CH₃, $A = 34.2$ G, 4H).²¹⁵ An isotropic simulation with the hfcs of authentic **20**⁺²¹⁶ is in excellent agreement with the experimental spectrum.

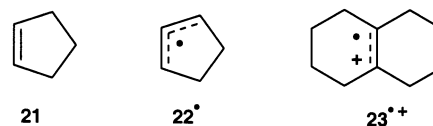


The conversion of **19** to **20**⁺ was rationalized by protonation of the tertiary carbon of **19**, followed by elimination of H₂; both reactions have ample precedence (occasionally, protonation is followed by loss of low alkanes). The resulting carbocations may undergo extensive isomerizations; ultimately, loss of a proton may generate cycloalkenes (viz., **20**), which are converted to the corresponding radical cations by interaction with acid sites.

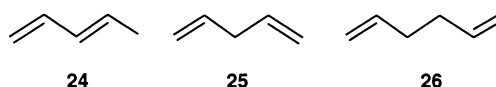
V.A.4 Radical Cations from Cycloalkenes

Corio and Shi also were the first to incorporate a cycloalkene into mordenite.²⁰⁴ Upon sequestering cyclopentene (**21**) into the zeolite, they observed a spectrum which they considered as a quintet of triplets ($A = 37.0$ G, 4 H; $A = 14.5$ G, 2H) and ascribed to the cyclopentene radical cation (**21**⁺). The line shape analysis of the spectrum and its temperature dependence was explained by rapid rotation about the (pseudo-) 5-fold axis with a barrier, $\Delta E = 1.4$ kcal/mol.²⁰⁴ Upon warming of the sample to 310 K, the ESR spectrum underwent significant changes to a different quintet of triplets ($A = 25.2$ G, 4 H; $A = 14.5$ G, 2H). This conversion was ascribed to an ion–molecule reaction, proton transfer from the radical cation to neutral cyclopentene, generating cyclopentenyl free radical, **22**.⁸⁷ Although this assignment appears plausible, the actual chemistry is considerably more complicated.

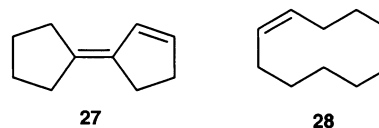
Fifteen years later, Rhodes reinvestigated the chemistry of **21** on mordenite and noted that the low-temperature spectrum is actually a quintet of quintets.¹⁸⁶ In addition, the authentic ESR spectrum of **21**⁺ ($A = 50.3$ G, 2 H; $A = 48.5$ G, 2 H; $A = 8.6$ G, 2H),^{167,217} observed since the original work, proved incompatible with the spectrum observed in the mordenite. On the other hand, the ESR spectrum of bicyclo[4.4.0]dec-(1,6)-ene (octalin) radical cation, **23**⁺, ($A = 37.0$ G, 4 H_{ax}; $A = 14.5$ G, 4 H_{eq}), generated by γ -radiolysis of **23** in CFCl₃,²¹⁸ shows excellent agreement with the spectrum obtained from **21** in mordenite. Accordingly, the spectrum obtained from **21** was identified as that of **23**⁺. Concerning the mechanism of the conversion of **21** to **23**⁺, Rhodes argued that **21** is converted to **23** prior to oxidation. The cyclopentene radical cation may add to the neutral parent, forming a cyclobutane type radical cation; ring-opening to a “localized” cyclodecadiene and formation of a 1,6-transannular bond yield a 1,4-bifunctional species, which can be converted to **23**⁺ by a sequence of deprotonations/protonations.



A number of additional substrates, including *E*- and *Z*-penta-1,3-dienes (*E*- and *Z*-**24**), penta-1,4-diene (**25**), and hexa-1,5-diene (**26**), form the same radical cation, **23**⁺, in a series of deep-seated reorganizations. The authors used comparative studies of the series of dienes in Freon matrices to propose Brønsted acid catalysis as the key to the molecular transformations.¹⁸⁸ It is perhaps easier to understand the conversion of the pentadienes, **24** and **25**, to **23**⁺ than that of a hexadiene, **26**.

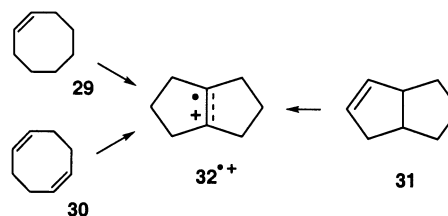


Additional insight was provided by Crockett and Roduner; at higher temperature, the ESR spectrum of **23**⁺ is slowly converted to that of a new species, 3-cyclopentylidenecyclopentene radical cation, **27**⁺ (originally ascribed by Shih to **22**⁺).¹⁹¹ The new assignment was confirmed by the development of an identical ESR spectrum upon incorporating **27** into mordenite.¹⁹¹ The radical cation, **23**⁺, was also obtained upon incorporating cyclodecene, **28**, into H-mordenite.

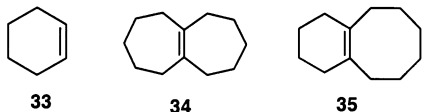


Interestingly, the fate of **23**⁺ depends on the precursors from which it is generated. For this reason, the second radical cation, **27**⁺, derived from **21** at higher temperature, cannot be a product of **23**⁺. Apparently, **23**⁺ and **27**⁺ are formed by competing mechanisms on the zeolite. The (more rapid) formation of **23**⁺ may proceed via a metathesis reaction to cyclodecadiene, followed by ring closure and hydrogen migration. The subsequent slower formation of **27**⁺ was rationalized via a cationic mechanism: addition of cyclopentyl carbocation to cyclopentene, followed by proton loss and dehydrogenation, giving rise to **27**. Because of its low oxidation potential, the diene, **27**, should readily reduce **23**⁺.¹⁹¹ The conversion of **23**⁺ into **27**⁺ is an example of a bimolecular ion–molecule reaction in a zeolite.

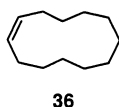
A central role for a dominating radical cation was observed also for C-8 hydrocarbons: cyclooctene, **29**, cycloocta-1,5-diene, **30**, and bicyclo[3.3.0]oct-2-ene, **31**; all give rise to bicyclo[3.3.0]octa-(1,5)-ene radical cation, **32**⁺.¹⁹¹



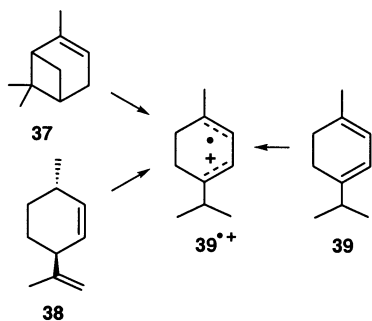
In connection with this study, Crockett and Roduner incorporated a series of cycloalkenes into H-mordenite.¹⁹¹ In analogy to **21**, cyclohexene (**33**) undergoes dimerization and ring enlargement reactions. The formation of bicyclo[5.5.0]- or bicyclo[6.4.0]-dodecene radical cation, **34**⁺ or **35**⁺, respectively, from **33** appears more plausible than the earlier reported formation of **23**⁺ from **26**.



Interestingly, the larger cycloalkenes, cyclooctene (**29**), cyclodecene (**28**; vide supra), and cyclododecene (**36**) undergo transannular ring closure, generating the radical cations of symmetrical bicyclo[n.n.0]-alkenes. The formation of transannular alkene radical cations, viz., **23**⁺ and **32**⁺, from **28** or **29**, respectively, requires dehydrogenation, either by transfer of molecular hydrogen to the zeolite or alternating one-electron oxidation and deprotonation.¹⁹¹



Terpenes readily isomerize upon contact with zeolites;²¹⁹ the mechanisms, once again, may be relatively complex. Crockett and Roduner observed identical ESR spectra from three different terpenes, α -pinene (**37**), *trans*-iso-limonene (**38**), and α -terpinene (**39**), establishing once again a central role for a single dominating radical cation. The observed spectrum is complex, featuring 10 nuclei with hfcs between 1.96 and 0.43 mT; the smallest coupling still exceeds the line width by at least a factor of 2. The spectrum was identified as the radical cation of α -terpinene, **39**⁺.²²⁰



The conversion of **38** to **39**⁺ is readily explained, either by formation of the radical cation, **38**⁺, followed by repeated deprotonation and protonation, or by acid catalyzed rearrangement to **39**, followed by oxidation. On the other hand, the conversion of **37** to **39**⁺ requires cleavage of the allylic-tertiary cyclobutane bond and a series of deprotonations and protonations. The sequence of these steps poses an interesting problem, but only limited mechanistic information is available. The authors were able to eliminate Brønsted acid catalysis, because no D was

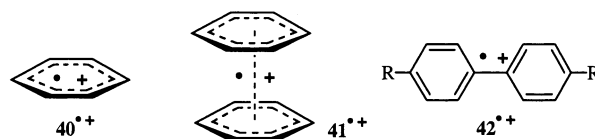
incorporated into **39**⁺ when the reaction was carried out in D-mordenite.²²⁰

V.A.5 Adsorption of Benzene and Derivatives

The adsorption of benzene (**40**) onto various zeolites under a wide range of reaction conditions has been studied in detail; at least four different species have been characterized. UV-Vis irradiation (> 2.8 eV) of benzene adsorbed on ZSM-5 generated a radical pair spectrum, consisting of two doublets with splittings of 8 and 24 mT. Upon heating of the sample, this spectrum decayed and was replaced (irreversibly) by that of benzene (monomer) radical cation, **40**⁺.²²¹ At 173 K, this species showed an essentially isotropic septet with $g = 2.0026$ and $A_H = 0.45$ mT.¹¹² A UV/vis band at 670 nm was considered characteristic for **40**⁺.⁵³ Appropriate zeolites can oxidize benzene directly; thus, adsorption of **40** onto activated H-ZSM-5 at ambient temperatures generated a highly resolved ESR spectrum of **40**⁺.⁶⁴ The monomer radical cation and its hexadeuterio isotopomer were also generated by radiolysis at cryogenic temperatures and studied in detail (vide infra).²²²

On the basis of ESR evidence, **40**⁺ was also proposed as the key intermediate in the polycondensation of benzene on ZSM-5 at temperatures below ~125 °C.²²³ The observation of **40**⁺ challenges the "classic" electrophilic substitution mechanism for aromatic substitution. Similarly, substituent effects observed for the vapor-phase nitration of aromatics with dinitrogen tetroxide over Beta zeolite correlate better with the ionization potential of the aromatics than with the Hammett coefficients. This result casts doubts on the involvement of the conventional electrophilic aromatic substitution mechanism and suggests radical cations as possible key intermediates.^{224,225}

Under different conditions, two additional species were observed, a dimer radical cation (**41**⁺; $A_H = 0.22$ mT), first observed by Corio and Shih,²⁰⁴ and biphenyl radical cation (**42**⁺). The spectrum of **42**⁺ was not recognized by Corio and Shih; its identity was assigned by Kurita et al., based on a simulation with $A_o = 3.37$ G, $A_m = 0.52$ G, $A_p = 6.74$ G.²²⁶



The powder ESR and ENDOR spectra of authentic **42**⁺ generated upon adsorption of **42** on H-ZSM-5 or silica gel have an anisotropic g -tensor. The hyperfine couplings of the *para* and *ortho* protons support a nearly planar structure, with a twist angle of 10° between the phenyl rings. Simulation of the ENDOR spectra identified the principal hyperfine tensors of the *para* and *ortho* protons.²²⁷

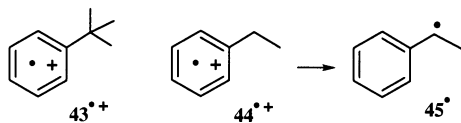
Exposure of activated NH₄-mordenite to benzene vapor at room temperature generated a well-resolved ESR spectrum¹⁰⁸ with the known splitting of the benzene dimer radical cation (**41**⁺).²²⁸

The signal intensity of $41^{+\bullet}$ increased substantially (~ 5 -fold) when O_2 was introduced into the ESR sample, even more significantly (> 25 fold) when the zeolite was pretreated with O_2 at elevated temperatures. Introduction of SO_2 caused a similar increase of radical cation concentration and, in addition, generated the ESR spectrum of $SO_2^{\bullet-}$ ($g_{xx} = 2.0012$; $g_{yy} = 2.0025$; $g_{zz} = 2.0071$). These experiments suggest that the catalyst affects the electron transfer from benzene dimers (or aggregates); the authors considered tricoordinated Al atoms as the reactive centers, and argued that their activity is enhanced by an inductive effect due to O_2 or SO_2 .

Several methyl-substituted benzene derivatives were studied under similar conditions, giving rise to the full range of intermediates. For example, durene (1,2,4,5-tetramethylbenzene) gave rise to an essentially isotropic spectrum ($A = 10.8$ G, 12 H), clearly due to the monomer radical cation, tetramethyl- $40^{+\bullet}$, as the hfc is very close to that of an authentic sample. Similarly, a 13-line spectrum obtained from 1,2,3,4,5-pentamethylbenzene and a 19-line spectrum ($A = 6.6$ G) obtained with hexamethylbenzene support monomer radical cations.²⁰⁴ Interestingly, the 13-line ESR spectrum of pentamethyl- $40^{+\bullet}$ was interspersed with weaker signals exactly midway between the 13 lines, compatible with the presence of a dimer radical cation in addition to pentamethyl- $40^{+\bullet}$.²⁰⁴ In contrast, the identity of a dimer radical cation derived from *p*-xylene is questionable, because the cited evidence, "methyl hf coupling constants of 3.8 G (six equivalent protons)" does not appear to support the assignment.²²⁶

On the other hand, toluene was converted to *p,p'*-dimethylbiphenyl radical cation ($42^{+\bullet}$, $R = CH_3$), and *o*-xylene formed 3,4,3',4'-tetramethylbiphenyl radical cation.²²⁶ The formation of biphenyl radical cations was formulated via *p,p'*-coupling followed by transfer of 2 H to a catalytic site, converting an active oxygen site, "cat-O", to "cat H_2O ".

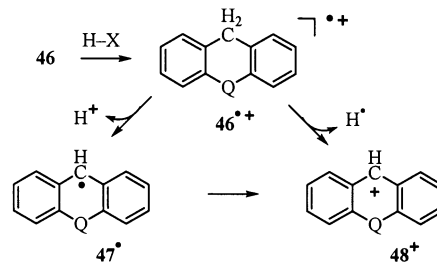
The reactions of a series of alkylbenzenes were studied in the temperature range -120 to 170 °C.⁹⁹ Significant differences were observed depending on the nature of the alkyl group. *n*-Propyl-, *n*-butyl-, and *iso*-propylbenzene undergo dealkylation, an observation compatible with a classical ionic mechanism involving protonation followed by loss of the alkyl group. However, *tert*-butylbenzene, **43**, takes a most interesting alternative course, forming the radical cation, $43^{+\bullet}$. This result casts doubt on the classical mechanism, at least at room temperature, and suggests one-electron oxidation instead. In light of this result, the formation of 1-phenylethyl radical, 45^\bullet , may be formulated as one-electron oxidation ($44^{+\bullet}$), followed by deprotonation (vide infra).⁹⁹



Radical cations of alkyl aromatics are readily deprotonated in solution.²²⁹ The resulting benzylic radicals may react by coupling or oxygenation²²⁹ or, because of their low oxidation potentials, be oxidized

to benzyl cations. Thermochemical calculations indicated that hydrogen atom loss at the benzylic position may become competitive, depending on the stability of the carbocation,²³⁰ but no firm experimental evidence supporting direct formation of benzylic carbocations was observed in solution.

In contrast, adsorption of xanthene (**46**, $Q = O$) or dibenzotropyliidene (**46**, $Q = CH=CH$) on acid zeolites caused spontaneous generation of the xanthyl and dibenzotropylium cations ($48^{+\bullet}$).⁶⁶ Their formation was formulated via loss of hydrogen atoms from alkylaromatic radical cations ($46^{+\bullet}$) because the zeolites showed parallel activity for the generation of aromatic cations and radical cations. Although details of how the zeolite acid sites generate $46^{+\bullet}$ were not addressed, and the fate of the electron not revealed, it is worth noting that pure Brønsted acids (trifluoroacetic acid) also generate $48^{+\bullet}$ from **46**. This observation again points out that zeolites share the ability to generate radical cations with conventional (liquid) Brønsted and Lewis acids; what sets zeolites apart is their ability to increase the lifetime of these species and control their reactivity.



Interestingly, fluorene (**46**, $Q = -$) behaved strikingly different. The fluorenyl cation ($48^{+\bullet}$, $Q = -$) is much less stable than the aromatic (6π -) xanthyl and dibenzotropylium cations ($48^{+\bullet}$, $Q = O$, $CH=CH$) because of the antiaromatic (4π -) cyclopentadienyl moiety.²³¹ Accordingly, the lifetime of fluorene radical cation ($48^{+\bullet}$, $Q = -$; λ_{max} 630 nm) is increased; its DR spectrum on H-mordenite or ZSM-5 is identical with an authentic solution spectrum.²³²

The series of Y zeolite samples employed for the generation of xanthyl cation was analyzed by the pyridine adsorption/desorption method to correlate their Brønsted and Lewis population (Figure 8) with their ability to generate xanthyl cation. The activity of a Y zeolite sample with only Brønsted sites (exhaustive washings with hexafluorosilicate solutions to remove oligomeric polyoxo(hydroxy)aluminates) to generate xanthyl cation was undiminished. This result clearly shows that Brønsted acid sites can generate radical cations.

Adsorption of anisole (**49**) onto Cu^{2+} -exchanged montmorillonite afforded two species.²³³ Initially, the radical cation, $49^{+\bullet}$, was formed. This assignment was based on the Raman spectrum, which was similar to that of **49**, but with frequency shifts and changes in relative intensities similar to changes between the spectra of *para*-disubstituted benzenes and their radical cations.^{234,235} After annealing, the Raman spectrum of 4,4'-dimethoxybiphenyl radical cation ($42^{+\bullet}$, $R = OCH_3$) appeared. Similar results were

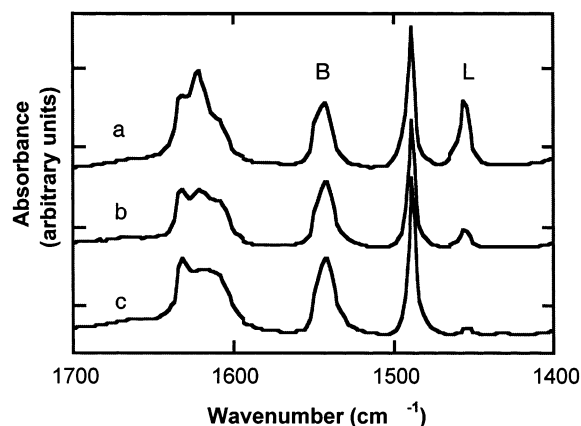


Figure 8. FT-IR spectrum (aromatic region) of pyridine retained on (a) HY (Si/Al 2.6), (b) HYD (Si/Al 5.2), and (c) HYD washed with $(\text{NH}_4)_2\text{SiF}_6$ after adsorption at room temperature and subsequent annealing (300 °C; 10^{-2} Pa; 1 h). The intensities of Brönsted sites (B) are comparable whereas those of Lewis sites (L) are significantly depleted, especially after washing with $(\text{NH}_4)_2\text{SiF}_6$. Reprinted with permission from ref 66. Copyright 1995 American Chemical Society.

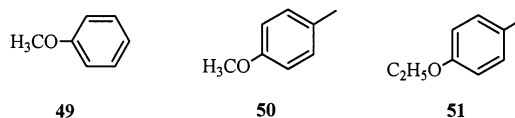
observed for the adsorption of **49** on Cu^{2+} -hectorite, based in this case, on IR data and product studies.²³⁶

Transition-metal exchanged montmorillonites formed radical cations upon adsorption of benzene and derivatives.^{233,234,236–240} Adsorption of 4,4'-dimethoxybiphenyl (**42**, $\text{R} = \text{OCH}_3$) onto Cu^{2+} -exchanged montmorillonite yielded the radical cation, **42**^{•+}, $\text{R} = \text{OCH}_3$, identified by the UV/Vis spectrum previously observed upon g-radiolysis in a Freon matrix (77 K),²³³ and characterized also by Raman and UV/Vis spectroscopy. Upon exposure to moisture, **42**^{•+}, $\text{R} = \text{OCH}_3$, decayed to a species, identified as 4,4'-dimethoxybiphenyl cation (DMeOB^+) based on the significant amount of copper ions remaining as Cu^+ .²³³ The actual structure of the putative " DMeOB^+ " (structure not drawn in the original article) is in question (a cationic " DMeOB^+ " requires loss or gain of a hydrogen atom or another neutral radical from **42**^{•+}, $\text{R} = \text{OCH}_3$).

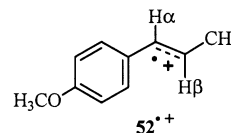
Adsorption of additional benzene derivatives ($\text{X} = \text{Cl}, \text{F}, \text{OH}$) onto Cu^{2+} , Fe^{3+} , or Ru^{2+} -exchanged montmorillonites²³³ also gave rise to biphenyl radical cations. These species were identified specifically by the presence of an inter-ring C–C stretching Raman band near 1300 cm^{-1} and by a UV/Vis band near 600 nm (580–670 nm); both features are considered characteristic for substituted biphenyl radical cations. Only montmorillonites exchanged with metal ions of sufficient oxidation potentials produced aromatic radical cations and promoted their subsequent reactions; Pd^{2+} -montmorillonite showed limited activity, whereas Cr^{3+} and Ca^{2+} -montmorillonites failed to generate radical cations.²³³

Several phenol ethers gave rise to well-resolved ESR spectra upon inclusion in ZSM-5.¹⁹⁸ The spectrum obtained from *p*-methylanisole (**50**) featured a quartet of quartets ($A = 15.0, 3.9 \text{ G}$; $g = 2.0040$), in good agreement with the known spectrum of **50**^{•+} ($A_{\text{CH}_3} = 15.25 \text{ G}$, $A_{\text{OCH}_3} = 4.3 \text{ G}$; $g = 2.0032$), obtained by Ce^{IV} oxidation in a flow system.²⁴¹ Minor discrepancies could be due to matrix effects. Similarly,

p-methylethoxybenzene (**51**) produced a quartet of triplets ($A_{3\text{H}} = 15.0 \text{ G}$, $A_{2\text{H}} = 4.7 \text{ G}$; $g = 2.0042$), respectively, assigned to the corresponding radical cation, **51**^{•+}. The quartet splitting ($A_{\text{CH}_3} = 15.0 \text{ G}$) is similar to that of **50**^{•+}; the lesser splitting ($A_{\text{CH}_2} = 4.7 \text{ G}$) is analogous to the splitting of ethoxybenzene radical cation ($A_{\text{CH}_2} = 5.0 \text{ G}$).²⁴¹ The results support significant spin density on the *p*-carbons of the two radical cations, considerably higher than on the heteroatom.

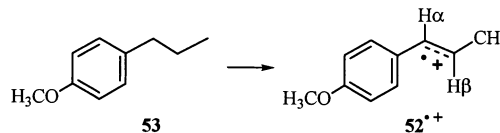


trans-Anethole (**52**), generated a radical cation, **52**^{•+}, with four strongly coupled nuclei ($g = 2.0032 \pm 0.0002$; $A \sim 11 \text{ G}$), assigned to the allylic methyl group and the olefinic β -proton, and at least two nuclei with smaller hfc. The spin density of **52**^{•+} is located mainly in the olefinic side chain. Increased line width up- or downfield from the center suggests that the hyperfine and *g* factor anisotropies are not completely averaged; thus, the motion of the radical ion in the cavities of the zeolite must be restricted.²⁴²



In solution, **52**^{•+} was generated by electron transfer to triplet quinones.^{243–245} CIDNP results support positive hfc for the allylic methyl group and a negative hfc for the β -proton;^{199,245} AM1 calculations support significant hfc for the allylic methyl group (+4.9 G), and the β - (-5.5 G) and α -protons (+2.3 G).²⁴⁵ The hfc measured in Na-ZSM-5 are twice as large²⁴⁶ as any calculated one.²⁴⁵ The electronic spectrum of **52**^{•+} decayed within microseconds following pulse radiolysis, in contrast to a lifetime of several days in the zeolite.

Interestingly, incorporation of *p*-propylanisole (**53**) onto ZSM-5 generated anethol radical cation, **52**^{•+}, identified by its ESR spectrum. This conversion requires a three-electron oxidation plus loss of two protons, possibly alternating.²⁴⁶ Alternatively, the initially formed radical cation may be dehydrogenated at an appropriate active site of the zeolite.



V.A.6 Radical Cations of α,ω -Diphenylpolyenes and Aryl Olefins

In a classic study, Ramamurthy et al. incorporated several *all-trans*- α,ω -diphenylpolyenes, **54**, into (thermally activated) Na-ZSM-5 (Si/Al 22) at ambient temperature from solutions in organic solvents open to air.⁹³ The resulting radical cations, **54**^{•+}, were characterized by ESR and diffuse reflectance spec-

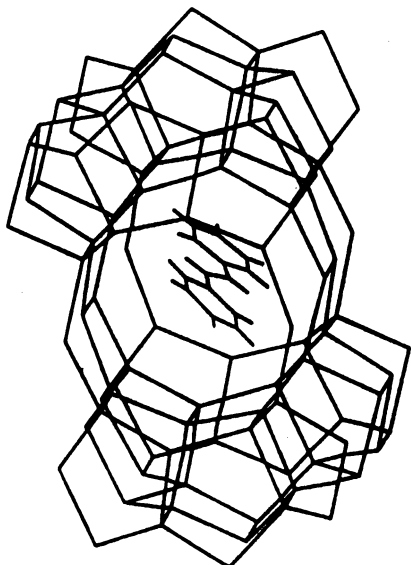
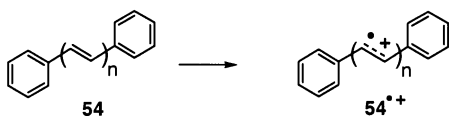


Figure 9. Stick model of stilbene radical cation, 54^+ , $n = 1$, inside the straight channels of ZSM-5. Reprinted with permission from ref 93. Copyright 1991 American Chemical Society.

troscopy.^{93,247,248} The major contribution of this study was the finding that organic radical cations can persist for weeks without significant decay, compared to solution lifetimes in the microsecond range.

All samples showed strong ESR signals ($g = 2.0028$); the radical cations of *trans*-stilbene, 54^+ , $n = 1$, and *trans,trans*-1,4-diphenylbutadiene, 54^+ , $n = 2$, showed well-resolved, essentially isotropic hfc, indicating that these species have sufficient mobility to average out anisotropies. On the other hand, the ESR spectrum of 54^+ , $n = 3$, showed only a broad singlet. The diffuse reflectance UV–Vis spectra of these radical cations in NaZSM-5 matched well those observed under a range of conditions in various other media.



The authors recognized that the remarkable stability of the α,ω -diphenylpolyene radical cations was due to their location inside the zeolite pores. The close match between the geometries of the rod-shaped guest and the narrow ZSM-5 channels (Figure 9) prevents external reagents from approaching the π -system of the polyene.⁹³

Despite the well-known reactivity of organic radical cations toward nucleophiles, the α,ω -diphenylpolyene radical cations survive even when the loaded zeolite is suspended in water or refluxed in methanol. Significantly, radical cations, 54^+ , $n = 1-4$, generated in three-directional large-pore NaBeta (oval cages, $\sim 1.1 \times 0.75$ nm) decay considerably faster. The location of 54^+ , $n = 1-4$, inside ZSM-5 is also supported by the failure to observe radical cations of bulky olefins, such as tetraphenylethylene or 1,1,4,4-tetraphenyl-1,3-butadiene.⁹³

An effective redox potential of 1.65 ± 0.1 V vs SCE was assigned to the zeolite sites, since 4-carbomethoxy-

trans-stilbene failed to show the typical DR UV–Vis spectrum of the radical cation.⁹³ This value is consistent with the failure of naphthalene (**55**, E_{ox} 1.62 V vs SCE) or biphenyl (**42**, E_{ox} 1.80 V vs SCE) to generate radical cations on ZSM-5. This study establishes an upper limit for the effective redox potential of the zeolite without addressing a possible distribution of oxidizing sites with varying redox potentials.

The density of oxidizing sites was estimated by determining the loading at which all absorbed polyene was oxidized. The limiting loading at which no neutral polyene could be detected was 0.005 mg/g of zeolite ($\sim 2 \times 10^{16}$ spin g^{-1}), less than 0.1% of the total polyene loading capacity in NaZSM-5. Significantly higher site densities were found for the H^+ -form of ZSM-5.⁹²

In an attempt to probe the nature of the oxidizing sites, a series of ZSM-5 with different Si/Al ratios was evaluated; they showed an increasing population of oxidizing sites with increasing Al content.⁹³ The estimate of radical cations generated was apparently close to the previously reported population of Lewis acid sites for similar batches of H-ZSM-5. This similarity led the authors to suggest Lewis sites as the oxidizing sites; Brønsted sites were excluded as oxidative sites because the authors assumed that Na-ZSM-5 did not contain such sites. However, their ZSM-5 samples were prepared with tetrapropylammonium ion as template agent; calcination of this as-synthesized zeolite necessarily generates some Brønsted sites; the acid sites were not characterized.

Sequestered in ZSM-5, radical cations 54^+ , $n = 3, 4$, exhibited weak room-temperature emission in the 850–1100 and 900–1150 nm region, respectively. At 77 K, this luminescence showed vibrational structure (~ 1490 and 1170 cm^{-1} for 54^+ , $n = 3$; 1450 and 1170 cm^{-1} for 54^+ , $n = 4$). The weakness of the emission did not permit lifetime measurements. The close coincidence of the absorption and emission spectra and their mirror symmetry suggests that the emission is originating from the lowest spin-allowed, doublet–doublet transition. This assignment is supported by the absence of heavy atom effects in Tl^+ -exchanged ZSM-5. Interestingly, the radical cations that show hyperfine coupling in the ESR, 54^+ , $n = 1, 2$, do not emit, suggesting a connection between mobility in the zeolite and the efficient deactivation of excited states by radiationless decay.

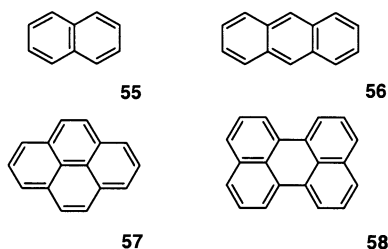
The coloration indicative of radical cation formation upon inclusion of *trans*-stilbene, **54**, $n = 1$, on some commercial silicalite batches²⁴⁹ can only be explained by the presence of Al impurities. Silicalite is an all-silica pentasil zeolite with the same structure of ZSM-5. Because it is Al-free, it is devoid of both acid sites and oxidizing capability; pure silicalite samples fail to generate organic radical cations.

V.A.7 Radical Cations of Polynuclear Aromatics

The interactions of various polynuclear aromatic hydrocarbons with a range of zeolites also have been investigated. Naphthalene, **55**, was the target of several studies; however, no spontaneous generation of 55^+ upon adsorption onto zeolites has been reported as yet; this is probably due to the high

oxidation potential of **55** (1.62 V vs SCE). To clarify this point, it might be interesting to incorporate **55** into strongly acidic zeolites, where benzene radical cations as well as dimer radical cations have been detected (vide supra).

The molecular shape is an important factor in dimer radical cation formation. Aromatics such as anthracene (**56**), biphenyl (**42**), or *trans*-stilbene (**54**⁺, $n = 1$) failed to form dimer radical cations.^{250,251} However, a charge resonance (CR) band at 1450 nm was interpreted as evidence that pyrene (**57**) forms a dimer radical cation.²⁵⁰



Incorporation of **56**, **57**, or perylene (**58**) into mordenite or zeolite Y generated the corresponding radical cations. These species were identified by their complex banded spectra, **56**⁺, $\lambda_{\max} = 719$ nm, **57**⁺, $\lambda_{\max} = 662, 793$ nm, **58**⁺, $\lambda_{\max} = 735$ nm. The stability of radical cations in zeolites is affected by how well they fit into the cavities or channels, whereas the rate of accumulation reflects the diffusion in the intracrystalline phase and the size of the guest. Interestingly, the larger **58** (C₂₀) was incorporated faster than the smaller **57** (C₁₄). This was explained by the fact that **58** is less rigid and, therefore, may diffuse ("squeeze") more easily through the windows of the supercage.²⁵²

V.A.8 Radical Cations of Nitrogen-Containing Substrates

Various nitrogen-containing compounds are efficient electron donors; their incorporation into appropriate activated zeolites may lead to interesting radical cations. However, to date only a limited number of amines and diamino compounds have been investigated under these conditions. For example, tertiary, secondary, and primary aromatic amines, as well as hydrazine and derivatives (benzidines), undergo one-electron oxidation, forming radical cations. Some of these species are deprotonated, either spontaneously or after warming (heating) the samples, generating free radicals.

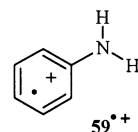
Adsorption of aniline (**59**) into H-Mor generated the radical cation, **59**⁺ ($g = 2.003$; $A = 15.6$ G, 2H; $A = 4.5$ G, ^{14}N).⁸⁸ Upon admitting molecular oxygen into the samples, the ESR spectra change significantly: the signal intensity of **59**⁺ increases, and the spectrum of superoxide ion, O₂^{•−}, is observed ($g_{zz} = 2.040$; $g_{xx} = 2.010$; $g_{yy} = 2.003$; $A_{zz} = 6.3$ G, $I = 5/2$; $A_{xx} = 4.7$ G) in addition to **59**⁺. This spectrum supports an interaction between O₂^{•−} and either a single ²⁷Al center or several Al atoms of a Brønsted site. In faujasite, the ESR signals of **59**⁺ appeared only after the introduction of oxygen; apparently, the faujasite sites are of lower activity. Interestingly, the spectrum of O₂^{•−} in faujasite shows a weaker hyperfine splitting

Table 5. Radical Ion Yield upon Adsorption of Aniline onto Two H-Zeolites in the Presence and Absence of Oxygen^a

zeolite	radical concentration (spins \times g ^{−1})		
	no O ₂	O ₂ (10 mmol \times g ^{−1})	air
H-mordenite	1.6×10^{18}	4.2×10^{18}	5.3×10^{18}
H-Y ^b	^c	1.4×10^{16}	3.7×10^{18}

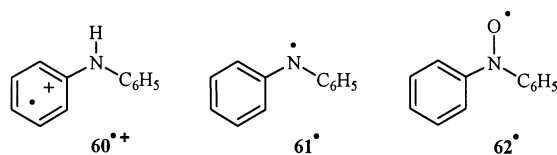
^a Data from ref 88. ^b The radical concentration is time-dependent; the indicated values correspond to the maximum concentration reached. ^c Very weak featureless signal.

($A_{zz} = 5.4$ G) than in H-Mor, suggesting a possible relationship between the splitting and the strength of the electron acceptor site.⁸⁸



The quantities of radical cations generated in the presence or absence of oxygen are summarized in Table 5. These results suggest that coadsorption of oxygen, though not a prerequisite for radical ion generation, enhances the efficiency of aniline oxidation in mordenite significantly. For HY, on the other hand, the assistance of oxygen may be a prerequisite to form radical cations. Certainly, molecular oxygen near a Lewis acid site is a stronger electron acceptor than either of the components separately.

The adsorption of diphenylamine (**60**) onto alumina or silica–alumina was studied since the 1960s in an attempt to understand the nature of active sites on amorphous silica, silica–alumina, synthetic A and Y, and transition metal doped zeolites.²⁵³ The incorporation of **60** gave rise to different intermediates and products. Pure alumina produced diphenylaminyl radicals (**61**[•]) via loss of an electron and a proton, possibly to oxide ion centers characteristic for these materials. Upon standing of the sample, the aminyl radicals formed (stable) diphenylnitroxyl radicals (**62**[•]). On H-Y zeolite, **60** formed the corresponding radical cation, **60**⁺;⁷¹ it was characterized on Na-Y by a weak, broad ESR spectrum ($g = 2.002$, fwhh = 14 G; 9×10^{15} spins g^{−1}).²⁵³



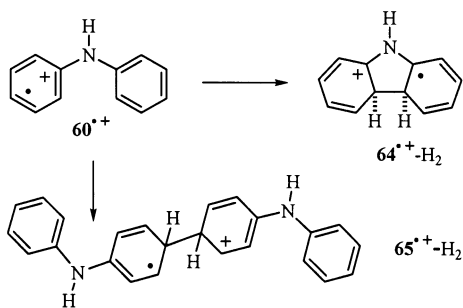
Introduction of polar liquids caused formation of *N,N*-diphenylbenzidine (**63**). The reaction was formulated via *p,p'*-coupling of two radical ions; an alternative pathway, addition of a radical ion to neutral diphenylamine, cannot be eliminated.⁷¹

The oxidation of **60** to **62**[•] in a series of alkali-exchanged X faujasites was followed by ESR.²⁵⁴ KX is a more favorable host for this oxidation than either Li⁺ and Na⁺ or Rb⁺ and Cs⁺-exchanged X. A weak ESR triplet led the authors to propose O₂ preactivation by simultaneous interaction with the zeolite Lewis sites and the hydrogen atom of **60**, followed

by a concerted rearrangement to **62** \cdot and hydroxyl radical.²⁵⁴ No evidence for **60** \cdot^+ was observed in agreement with the fact that alkali-exchanged X zeolites are basic rather than acid solids. Similar experiments with aniline failed to give any evidence for the corresponding nitroxyl radical. In the absence of more conclusive evidence, the concerted mechanism postulated for the formation of **62** \cdot awaits further confirmation.

Analysis of the ESR spectra of diphenylnitroxyl, **62** \cdot and other nitroxyls (TEMPO and derivatives) revealed the rotational mobility of neutral radicals adsorbed in the interior of alkali metal ion exchanged X faujasites.^{254,255}

The radical cations of **60**, carbazole, **64**, and ben-zidine, **63**, were generated upon adsorption into the acid forms of ZSM-5, mordenite, and Y faujasite.²⁵⁶ The corresponding radical cations are interrelated by intra- or intermolecular coupling reactions. Thus, an (intramolecular) *o,o'*-addition-cyclization of the two aryl functions of **60** \cdot^+ would form an extended π -system, containing two cyclohexadienyl moieties; subsequent deprotonation and oxidation may generate **64** or **64** \cdot^+ .



Reactions of this type have been observed in solution for several diphenyl- and triphenylamine radical cations. Alternatively, intermolecular coupling at the *p*-position may link **60** \cdot^+ to **60** or connect two **60** \cdot^+ species, forming **63** \cdot^+ or **63** \cdot^{2+} .²²⁶ Reactions of this type have precedence in several arene radical cations (Section V.A.5).

Upon incorporation into HZSM-5 (loading 30 mg g⁻¹), **60** was converted completely into **60** \cdot^+ or **61** \cdot as shown by complete replacement of the intense IR bands of **60** (1510, 1460 cm⁻¹) by a new band (1470 cm⁻¹), assigned to **60** \cdot^+ . Neutral Na⁺-ZSM-5 samples, obtained by exhaustive ion exchange using concentrated Na₂CO₃, failed to generate **60** \cdot^+ (by DR-UV). This sample exemplifies the high sensitivity of ESR compared to DR-UV spectroscopy: the EPR spectrum still showed a signal, albeit of an intensity 3 orders of magnitude weaker than recorded for acid ZSM-5.²⁵⁶

Exposure to air changed the **60** \cdot^+ samples, depending on the pore dimensions of the zeolite host. In the restrictive channels of ZSM-5, **60** \cdot^+ was converted to **61** \cdot (DR-UV/Vis; Figure 10). The optical spectrum of **61** \cdot in ZSM-5 (λ_{\max} 450, 690 nm) is similar to the transient spectrum in solution, although the absorption maxima in ZSM-5 were significantly shifted relative to those in acetonitrile (λ_{\max} 400, 730 nm). These shifts may reflect different polarities of the

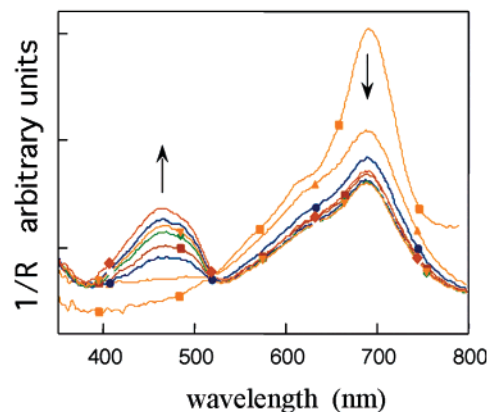


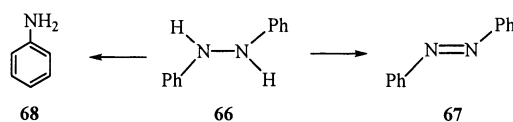
Figure 10. Diffuse reflectance spectra of **60** \cdot^+ in HZSM-5 as a function of time after incorporation. The plot shows increasing absorbance at 465 nm concomitant with the decay of the 690 nm band. H. D. Roth, H. Garcia, enhanced from ref 256. Reproduced by permission of The Royal Society of Chemistry on behalf of The Owner Societies.

media and/or the influence of hydrogen bonds with the zeolite silanol groups.

On alumina,²⁵⁷ the aminyl radical, **61** \cdot , was readily converted to the nitroxyl radical, **62** \cdot . In the case of ZSM-5, formation of **62** \cdot is clearly ruled out; the *g*-factor observed in ZSM-5 (*g* = 2.0026) is typical for nitrogen-centered radicals and much too low for a nitroxyl (*g* = 2.0048).²⁵⁸ The ZSM-5 samples maintained distinct optical and ESR spectra for extended periods of time (> 4 years). Reexamination of "aged" samples showed no further evolution, indicating a remarkable persistence of the radical cations and radicals in the zeolite. The fact that the channel dimensions of ZSM-5 closely match the aromatic ring precludes any reaction of **61** \cdot ; particularly the electrocyclic ring closure to **64** \cdot^+ requires considerably more space around **61** \cdot than is available inside ZSM-5.

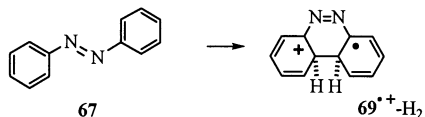
In contrast, the larger pores of zeolite Y allow **60** \cdot^+ sufficient mobility to undergo intramolecular cyclization, generating **64** \cdot^+ (DR-UV/Vis, IR). After adsorption of **60**, a sample of NaY showed a DR band at ~600 nm and its IR spectrum coincided with one obtained by incorporation of **64** in HY.

As noted above, acid zeolites, are proton donors as well as electron acceptors; however, the concurrent involvement of these intermediates has not been documented often. One such case involves adsorption of *N,N*-diphenylhydrazine (**66**) on HZSM-5, yielding azobenzene (**67**) and aniline (**59**).²⁵⁹ The products were explained by competing pathways, initiated by ET to or protonation by zeolite active sites; details will be discussed in Section V.B.



However, we note briefly that the benzidine rearrangement that would form **59**, typically observed for **66** in acid large-pore zeolites,²⁶⁰ is frustrated in the narrow channels of ZSM-5, since the required folded conformation cannot be accommodated. Similarly,

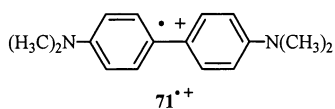
azobenzene (**67**) failed to undergo further conversions, such as cyclization with dehydrogenation, analogous to the cyclization of **60** yielding **64**⁺ in zeolite Y (vide supra). On the other hand, the conversion of **67** to benzocinnolin, **68** does not occur spontaneously upon incorporation into acid zeolites; it required photoactivation and is known to involve the protonated azobenzene (vide infra).²⁶⁰



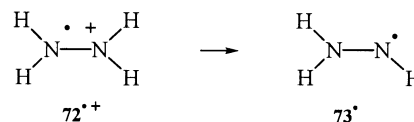
In 1964, Stamires and Turkevitch observed the ESR spectra of several radical cations after incorporating amines into Na-Y and H-Y.²⁶¹ For example, the adsorption of triphenylamine, **70**, from an *n*-heptane solution resulted in a triplet ($g = 2.0027$; $A = 14$ G, ^{14}N), ascribed to the radical cation, **70**⁺. Interestingly, absorption from the gas phase initially produced a broad singlet; however, subsequent introduction of *n*-heptane caused the triplet to appear. Perhaps deposition from the gas phase forms substrate clusters, which are diluted upon introducing the solvent.

Similarly, tris-(*p*-bromophenyl)amine (**70**, *p*-Br) also was converted to its radical cation on HY zeolite.^{199,262} Molecular modeling (KERMIT)²⁶² showed that **70** and *p*-Br-**70** are too large to enter the zeolite Y cavities; at most one *p*-bromophenyl ring could penetrate through the 0.74 nm pore opening. Therefore, *p*-Br-**70**⁺ can be formed only on the external surface. Nevertheless, remarkable loadings (~80 mg of *p*-Br-**70**/g of HY) can be deposited on dealuminated HY (Si/Al 17). With an estimated molecular surface of ~133 Å² for *p*-Br-**70** and an external surface area of ~150 m² × g⁻¹ for HY, the loading corresponds to less than monolayer coverage of the external crystallite surface plus the mesoporous surface.

Incorporation of *N,N*-tetramethylbenzidine (**71**) into Na-Y generated weak, broad spectra (**71**⁺; $g = 2.004$, fwhh = 14 G; 1.7×10^{17} spins/g).²⁶³



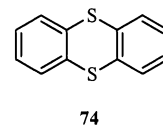
Hydrazine (**72**) failed to generate a radical cation spontaneously on zeolites; however, irradiation ($T = -40$ °C) of this diamine adsorbed on a zeolite molecular sieve produced the corresponding radical cation (**72**⁺); the assignment is based on the observation of a stable 13-line spectrum with an average spacing of 14.2 G. The combination of 2 ^{14}N ($I = 1$) and 4 ^1H nuclei ($I = 1/2$) may result in as many as 25 lines. The observation of 13 lines requires that one hfc (^{14}N) is twice as large as the other splitting (^1H). This assignment is born out by solution results.^{264–267} Upon heating of the sample to 90 °C, **72**⁺ was deprotonated, forming the hydrazyl radical, **73**[·].²⁶⁸



V.A.9 Radical Cations of Sulfur and Selenium-Containing Substrates

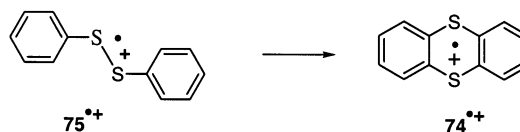
Various substrates containing sulfur (or selenium) as heteroatoms also are good electron donors; their incorporation into appropriate activated zeolites generates radical cations, either with only minor changes in bonding and without changes in connectivity or with significant structural changes.

Adsorption of thianthrene (**74**) within a series of acid zeolites with medium, large, and extra large pore size led to the generation of the corresponding radical cation, **74**⁺.⁶⁷ The intermediate was characterized by a range of techniques, including UV/vis diffuse reflectance, ESR, and IR spectroscopies. Smaller concentrations of **64**⁺ of **74**⁺ were measured when incorporation was carried out from isooctane solution; significantly better yields resulted from vapor phase incorporation at 475 K. In the case of Y and β hosts, dimeric aggregates, [**74**···**74**]⁺, were observed.⁶⁷ The quantitative assessment of the yields of **74**⁺ in the wide range of zeolites was used to characterize the population and strength of the active sites (Section II.C).⁶⁷



The ESR intensities of **74**⁺ samples in solution or in zeolites showed different temperature dependences. The signal intensity in H₂SO₄ decreased with temperature, whereas the contrary is observed for **74**⁺-containing zeolites, which approximately obeyed the Curie law.⁹² These results show that the zeolite framework effectively isolates the individual **74**⁺ entities, preventing the aggregation of entities, which causes the diamagnetic coupling observed in solution.¹¹⁷

Incorporation of diphenyl disulfide (**75**) into pentasil zeolite (NaZSM5) resulted in a superposition of two ESR spectra, two orthorhombic powder patterns with $g_{11} = 2.0136$, $g_{22} = 2.0081$ and $g_{33} = 2.0024$ ($g_{\text{avg}} = 2.0080$) and $g_{11} = 2.0263$, $g_{22} = 2.0090$ and $g_{33} = 2.0022$ ($g_{\text{avg}} = 2.0125$).¹²¹ The isotropic g factor identified the first spectrum as thianthrenium ion (**74**⁺; $g_{\text{iso}} = 2.0084$).¹¹⁸ The minor g -factor difference could be due to host-guest interactions in the zeolite. The second species, with g factor characteristic for a free radical (ion) with spin on sulfur, was assigned to the “extended” radical cation of the precursor **75**⁺, which had proved elusive, because in solution it rapidly rearranges to **74**⁺.



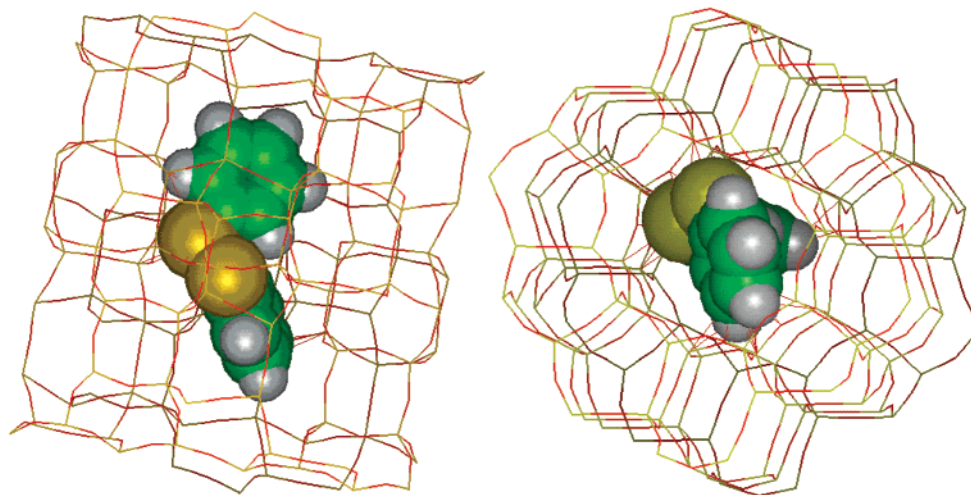


Figure 11. Molecular modeling: two views of the docking of $75^{+\bullet}$ inside the straight channels of ZSM-5. H. Garcia, H. D. Roth, enhanced from ref 272. Copyright 1999 The Royal Society of Chemistry.

While radical cations of sulfur aromatics, viz., $74^{+\bullet}$, are generated readily in concentrated sulfuric acid,⁵² attempts to generate $75^{+\bullet}$ in concentrated H_2SO_4 or with other Brønsted or Lewis acids resulted in $74^{+\bullet}$ as the only detectable radical cation.¹³⁹ Thiophenol likewise generated $74^{+\bullet}$, presumably via $75^{+\bullet}$. Apparently, $75^{+\bullet}$ is highly reactive in solution and rapidly converts to $74^{+\bullet}$, regardless of whether it is generated by chemical,²⁶⁹ photochemical,²⁷⁰ or electrochemical oxidation.²⁷¹ The observation of $75^{+\bullet}$ in ZSM-5 suggests that the narrow zeolite pores stabilize the “extended” radical cation and prevent its cyclization-dehydrogenation to $74^{+\bullet}$ (Figure 11).¹²¹

The nature of the “extended” radical cation, $75^{+\bullet}$, was confirmed by additional spectroscopic probes. The DR spectrum resulting from adsorption of 75 onto H-ZSM-5, “NaZSM-5”, or H-mordenite showed an intense peak at 240 nm and a broad low-intensity band ($\lambda = 1100$ nm) not present in the optical spectra of $74^{+\bullet}$.²⁷² The FT-IR spectrum (aromatic region) of self-supported blue zeolite wafers containing $75^{+\bullet}$ compared to 75 in KBr showed essentially complete conversion to $75^{+\bullet}$ at loadings of up to ~ 3 wt % (Figure 12).

The Na-ZSM-5 samples used in these studies contained Brønsted and Lewis acid sites according to the pyridine adsorption/desorption method. Thoroughly neutralized NaZSM-5/NaCl samples (two consecutive exchanges with buffered aqueous 1 M NaCl solution, pH 8.5) failed to oxidize 75 . This result clearly links the oxidizing ability of NaZSM-5 to residual acidity.²⁷²

Upon heating of the sample in ZSM-5 progressively to 200 °C, $75^{+\bullet}$ was cleanly converted to $74^{+\bullet}$. The sample changed from light blue to deep purple as the characteristic 540-nm band of $74^{+\bullet}$ developed. The IR spectrum also showed a band (1518 cm^{-1}) characteristic for $74^{+\bullet}$. The conversion of $75^{+\bullet}$ to $74^{+\bullet}$ was confirmed also by product studies; upon refluxing a dichloromethane solution of 75 in the presence of HZSM-5, 74 was the sole reaction product together with unreacted 75 .²⁷²

In contrast to the easy conversion $75^{+\bullet}$ to $74^{+\bullet}$, the radical cation of higher congener, diaryldiselenide

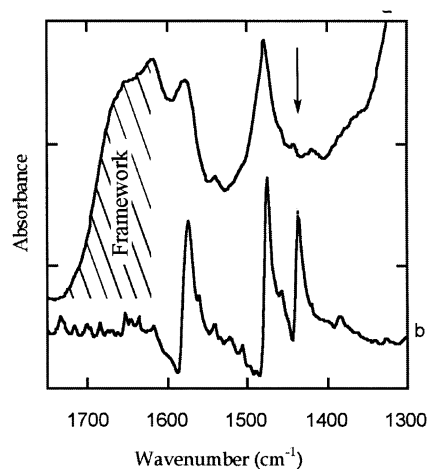


Figure 12. FT-IR spectra (aromatic region) of 75 in a KBr disk (bottom) and of $75^{+\bullet}$ on HZSM-5 (top) after annealing (100 °C; 10^{-2} Pa; 1 h). The spectra illustrate significant conversion of 75 into $75^{+\bullet}$. H. Garcia, H. D. Roth, enhanced from ref 272. Copyright 1999 The Royal Society of Chemistry.

(ArSe–SeAr; Ar: C_6H_5 , $p\text{-Cl-C}_6H_4$) failed to cyclize to selenanthrenium radical cation.²⁷³ Thus, the previously unknown ArSe–SeAr $^{+\bullet}$ radical cations were generated by adsorbing diaryldiselenides onto H-ZSM-5 and characterized by their DR UV–Vis (λ_{max} 520, 550, ~ 950 nm) and ESR spectra. The g factor of ArSe–SeAr $^{+\bullet}$ is larger and more anisotropic than that of ArS–SAr $^{+\bullet}$, consistent with the significantly larger spin–orbit coupling of Se vs S.

2-Phenyl-1,3-dithiane (**76**) was converted to 1,2-dithiolane radical cation ($77^{+\bullet}$) upon incorporation into ZSM-5. The resulting species was identified by its ESR spectrum, which was identical to that of an authentic sample.²⁷⁴ The spectrum had an orthorhombic powder pattern ($g_1 = 2.0293$, $g_2 = 2.0193$, $g_3 = 2.0030$); each g component showed a 1:4:6:4:1 pattern ($a_1 = 10.5$ G, $a_2 = 9.3$ G and $a_3 = 9.2$ G) due to interaction with four equivalent 1H nuclei (Figure 13). The average g value, $g_{\text{avg}} = 2.0172$, was in reasonable agreement with the isotropic g value, $g_{\text{iso}} = 2.0183$, of $77^{+\bullet}$ in solution.^{275,276} The average hfc in the zeolite, $a_{\text{avg}} = 9.7$ G, also agreed well with the

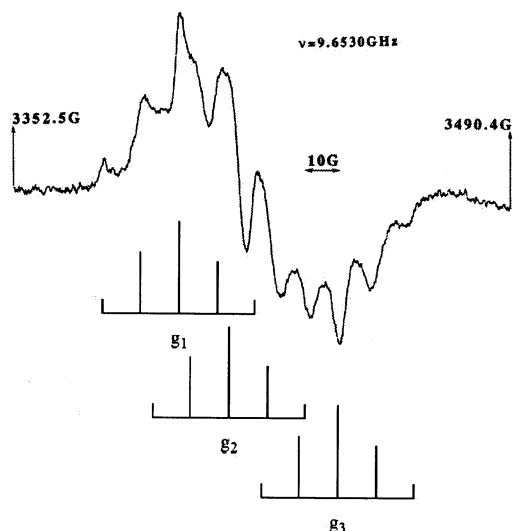


Figure 13. ESR spectrum of 77^{+} sequestered inside ZSM-5. Reprinted with permission from ref 274. Copyright 1998 The Royal Society of Chemistry.

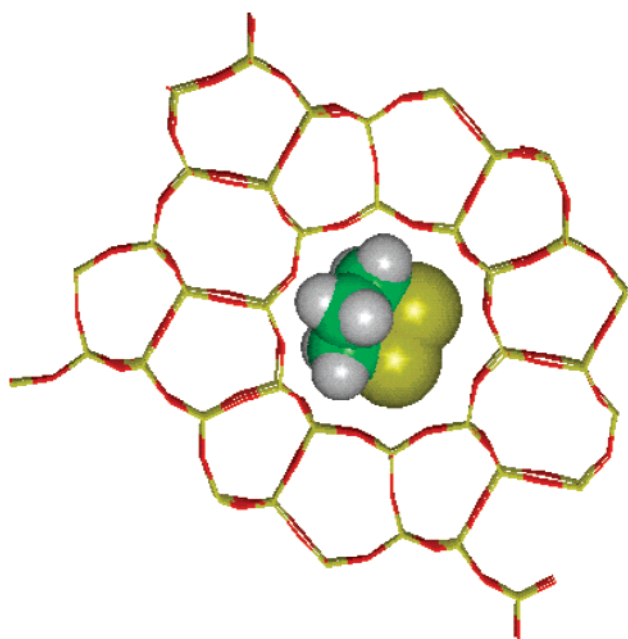
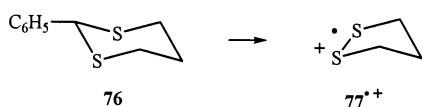


Figure 14. Molecular modeling of 77^{+} sequestered inside ZSM-5. L. Fernandez, H. D. Roth, enhanced from ref 272. Copyright 1999 The Royal Society of Chemistry.

isotropic hfc, $a_{\text{iso}} = 9.75$ G, of 77^{+} in solution.^{275,276}

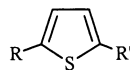


The generation of 77^{+} (cf., Figure 14) by oxidative ring contraction of **76** has precedence in solution; chemical or electrochemical oxidation of **76** leads to the debenzylated, ring-contracted species, 77^{+} ;²⁷⁷ anodic oxidation of dithioacetals is used to remove the dithiane protecting group of carbonyl compounds. The ring-contraction of 76^{+} requires formation of an S–S bond and loss of the benzyl group; it is formulated typically via a disulfide dication.²⁷⁷

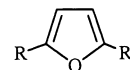
The dynamic behavior of 77^{+} inside the zeolite is unusual. The g factor anisotropy of 77^{+} at room

temperature indicates that this species is not tumbling or rotating fast on the ESR time-scale. On the other hand, the conformational reorientations (“flickering”) of the methylene group (C_4) is uninhibited, based on the equivalence of the pseudoaxial and -equatorial α -protons at C_3 and C_5 . This implies that one or both sulfur centers bearing spin and charge are held rigidly in a potential well or have (a) preferred orientation(s) in the zeolite network, whereas the mobility of the trimethylene segment remains unaffected. This behavior of 77^{+} is radically different from that in solution where the flickering can be arrested without introducing g factor anisotropy.^{275,276}

Partially Cu(II) exchanged Na-ZSM-5 or Na-Y zeolites generated radical cations of electron-rich heterocycles, such as thiophene (**78**), furan (**81**), and their 2-methyl or 2,5-dimethyl derivatives.²⁷⁸ Depending on the size of the reaction cavity compared to the diameter of the substrate and on the substitution pattern, monomer, dimer, or oligomer radical cations were observed.²⁷⁸ Thus, 2,5-dimethylfuran (**83**) gave rise to the monomer radical cation (83^{+} ; triplet of septets, $A = 17.0, 3.5$ G) when adsorbed onto Cu,Na-ZSM-5 from the vapor phase. Under similar conditions, 2-methylfuran (**82**) produced the radical cation of a π -dimer [$(82 \cdots 82)^{+}$, $A = 9.8$ G, 6H, $A = 8.5$ G, 2H; $A = 3.5$ G, 4H]. The relative orientation of the two rings is unknown; the dimer may not have a preferred conformer. ESR spectra obtained upon adsorption of **79**, **82**, or **83** onto Cu,Na-Y, also were attributed to (π -) dimeric radical cations. Last, incorporation of (**78**) and (**81**) into Cu,Na-Y generated oligomer radical cations. In contrast to the π -dimers mentioned above, the oligomers are most likely formed with dehydrogenation (vide infra).



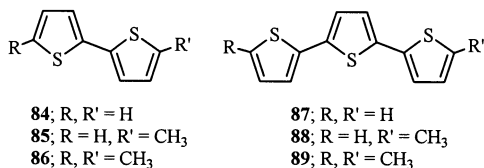
78; R, R' = H
79; R = H, R' = CH₃
80; R, R' = CH₃



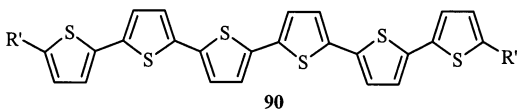
81; R, R' = H
82; R = H, R' = CH₃
83; R, R' = CH₃

Coadsorption of **79** or **82** with benzene (in a ratio of 1 to 10) on Cu,Na-ZSM-5 demonstrated the slow diffusion of substrate molecules through solvent-filled zeolite channels. ESR spectra initially showed only monomer radical cations, 79^{+} or 82^{+} , but upon standing, these were converted, slowly but completely, to dimer radical cations, apparently due to ion–molecule reactions.²⁷⁸

The incorporation of thiophene and thiophene oligomers into zeolites goes back to the pioneering studies of Enzel and Bein.²⁷⁹ The oxidation of a series of α, α' -fused thiophene oligomers in zeolites was studied in attempt to prepare isolated conducting polymer strands.^{247,279–282} Inclusion of **78**, **84**, and **87** into Na-ZSM-5 or Na- β generated broad ESR spectra ($g = 2.0028$) without discernible hfc, supporting the formation of oligothiophene radical cations, e.g., 84^{+} or 87^{+} . The DR spectrum of terthiophene radical cation, 87^{+} in zeolites, showed a band at 530 nm in good agreement with the absorption spectrum observed during electron-transfer reaction of **87** by flash photolysis.²⁸³



Upon standing or mild heating, **87**⁺ and **88**⁺ were oxidized to dications, **87**²⁺ and **88**²⁺ ($\lambda_{\max} \sim 835$ nm) or, by coupling to a second species with dehydrogenation, to sexithiophene dication, **90**²⁺ ($\lambda_{\max} = 1020$ nm). The identification of the 835 nm peak as due to the terthiophene dication rests on the observation that it is formed even at very low loading levels. In contrast, the 1020 nm band required elevated loading levels and increased with increased loading level, suggesting formation by an intermolecular reaction.



The increased absorption wavelength supports extended conjugation; it is compatible with α, α' -coupling and loss of molecular hydrogen, by direct dehydrogenation or by alternating deprotonations and oxidations. The α, α' -coupling is enforced by the geometry of the zeolite: the free volume available in the straight channels fails to accommodate β, β' -coupling. The preference for α, α' -coupling is also supported by two additional facts: (a) in contrast to **87**⁺ and **88**⁺, no longer wavelength band is observed for the α, ω -dimethyl derivative, **89**⁺, whose α -coupling is blocked by the methyl groups; (b) some β, β' -dimers are known and, predictably, they show minimal conjugation. Finally, the analogous incorporation of bithiophene, **84**, yields a radical cation, **84**⁺, which rapidly forms the (trimeric) sexithiophene dication, **90**²⁺.

V.A.10 Radical Cations of Organic Polymers Embedded in Zeolites

The formation of conducting polymers, e.g., polypyrrole, polythiophene, or polypyrrole,^{284–286} embedded within inorganic oxides or clays has attracted much attention.^{234,239,240,287–290} The importance of polarons in the controlled polymerizations within the constrained voids of porous hosts has not been widely recognized.²⁹¹ We will discuss some systems where spontaneous doping of the conducting polymer was observed in zeolites. The first conducting polymer inside a zeolite was obtained by polymerization of pyrrole in Fe³⁺ and Cu²⁺ exchanged Y zeolite.²⁹² Polymers of pyrrole, aniline, and thiophene within Cu²⁺ and Fe³⁺ exchanged zeolite Y and mordenite were also reported.^{279,293–295} Furans and thiophenes were chemically oxidized in Cu²⁺ exchanged ZSM-5 and zeolite Y, yielding radical cation characterized by ESR.²⁹⁶

Polyacetylene was obtained by direct polymerization of acetylene on the exterior surface of small-pore zeolites²⁹⁷ or inside H⁺- or transition metal exchanged ZSM-5, mordenite, Beta, Y and mesoporous MCM-41.^{298–303} The hybrid polyacetylene/zeolite samples

were characterized by analytical and spectroscopic techniques, including electron microscopy, DR, IR, Raman, MAS ¹³C NMR, XPS combined with Ar⁺ sputtering and ESR spectroscopy. Ni²⁺ and Zn²⁺ ions were highly active centers for the polymerization, far exceeding H⁺-exchanged zeolites.³⁰³ Pure Brønsted zeolites tend to form shorter oligomers or conjugated carbocations by protonation of the C=C double bonds. Polymerization at ~ 300 °C generated samples whose free volume was completely filled with polyacetylene (> 40 wt % carbon content).

An ESR study of Ni²⁺-exchanged zeolites showed a polaron signal due to the organic polymer superimposed on an extremely broad signal assigned to NiO clusters, in agreement with a conducting material (NiO) detected in a SQUID experiment.³⁰⁴ The aggregation of Ni²⁺ forming these clusters depends strongly on the polymerization temperature. Hybrids essentially free of NiO clusters are obtained when the polymerization is carried out at ≤ 250 °C and when the initial intense exothermic burst is carefully controlled.³⁰⁵ The organic polarons approximately follow the Curie law (intensity $\propto 1/T$).

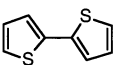
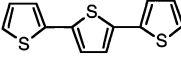
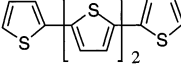
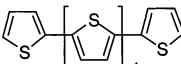
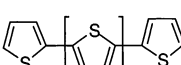
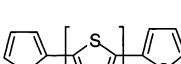
The potential of zeolites to grow organic conducting polymers under controlled conditions is illustrated by the case of thiophene oligomers inside ZSM-5.²⁸³ In solution, oxidation of thiophene rapidly generates polythiophene chains by coupling in the α -position. The evolution of optical spectra as a function of polythiophene chain length is difficult to follow because the short-chain oligomers are highly reactive and rapidly polymerize further. Oligo- and polythiophenes can form two different charged species, polarons and bipolarons, each with distinctive spectroscopic features. The optical transitions of each state can be assigned only if the oligomerization is conducted in a medium, such as a zeolite, that slows the polymerization to a convenient time scale.

The oxidation potential of thiophene is too high to be oxidized by NaZSM-5 ($E_{\text{ox}} \sim 1.6$ V vs SCE). Therefore, thiophene polymerization was approached by reacting preformed oligomers, which behave like thiophene but have lower oxidation potentials, as the number of thiophene units increases. Coupling of the oligomers inside ZSM-5 exclusively occurs in the α position (vide supra).

A series of radical cations (polarons) and dications (bipolarons) were formed via a series of single electron abstraction, dimerization, or trimerization. Oligomerization inside ZSM-5 was notably slower than in solution; the oligomeric polarons and bipolarons could be characterized by conventional spectroscopy. The rate of oligomerization retarded dramatically with increasing chain length, due to the reduced diffusion coefficients in zeolites. The largest oligothiophene formed at room temperature contained nine thiophene units. Thiophene oligomer radical cations embedded in NaZSM-5 or NaBeta are persistent in air for months without significant degradation.

The electronic transitions of the neutral oligomers and their polarons and bipolarons show systematic variations with the number of thiophene units, in agreement with quantum chemical band theories for conducting polymers. The increasing ease of oxidation

Table 6. Electronic Absorption Bands from Thiophene Oligomers ($n \leq 9$) into NaZSM-5^a

Oligomer	State	λ_{\max} (nm)
	neutral	300
	polaron	407
	neutral	354
	polaron	522
	bipolaron	833
	neutral	390
	polaron	614
	bipolaron	636, 1046
	neutral	434
	polaron	775
	bipolaron	600, 1019
	bipolaron	661, 1383
	bipolaron	761, 1450

^a These species are too short-lived in solution (from ref 283).

with increasing chain length, oligomers beyond six thiophene units, showed bipolarons free of polarons (Table 6). No details are available about thiophene oligomerization in solution.

Extrapolation of the data in Table 6 to a polythiophene of infinite chain length and its polaron and bipolaron yielded values for the band gap ($17\,400 \pm 200 \text{ cm}^{-1}$) and bipolaron transitions (775 and 2000 nm) in excellent agreement with experimental values. For the controversial polaron transition for infinite chain length, the predicted λ_{\max} (1350 nm) based on the study of oligomers in ZSM-5 gives also a reasonable value based on the comparison with polypyrrole. These values demonstrate that the zeolite-embedded thiophene oligomers are excellent short-chain models for doped polythiophene.

V.A.11 Fullerene

[60]Fullerene readily undergoes one-electron reduction; the radical anion, $C_{60}^{\bullet-}$, is a stable species under a variety of conditions. In contrast, the radical cation, $C_{60}^{\bullet+}$, is unstable in solution.³⁰⁶ Although $C_{60}^{\bullet+}$ was detected as a transient species following pulse radiolysis, an ESR spectrum was not observed. Both radical anion and radical cation can be generated upon incorporation into appropriate zeolites. Adsorption of [60]fullerene onto Na-X generated the radical anion ($g = 1.9995$); the radical cation was obtained upon heating a solid mixture of an Fe^{3+} -exchanged zeolite Y and [60]fullerene in a sealed ESR tube at 420 °C for 12 h.¹³⁶ The ESR spectrum showed an isotropic signal ($g = 2.0027 \pm 0.0002$), clearly different from those of $C_{60}^{\bullet-}$ ($g = 2.000$) or triplet C_{60} ($g = 2.0014$). Upon addition of perylene (**58**; $E^0_{(D/D^+)} = 1.04 \text{ V vs SCE}$), the $C_{60}^{\bullet+}$ signal was replaced by the spectrum of **58**^{•+} ($g = 2.0027$, $A_1 = 3.0 \text{ G}$, $A_2 = 0.6 \text{ G}$, $A_3 = 3.8 \text{ G}$). Addition of tetramethyltin ($E^0_{(D/D^+)} = 1.56 \text{ V vs SCE}$) caused a decrease of the signal, in accord with electron transfer from the adsorbate to $C_{60}^{\bullet+}$ ($E^0_{(D/D^+)} = 1.57 \text{ V vs SCE}$).

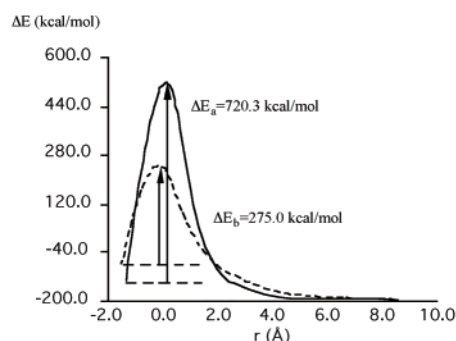
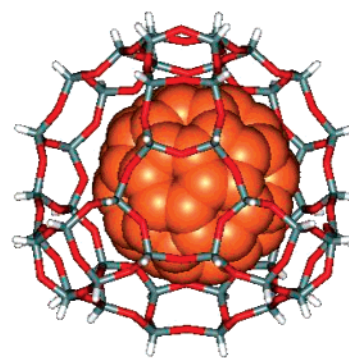


Figure 15. Top: molecular model of C_{60} in zeolite Y (H. García, unpublished); bottom: calculated energy barrier for C_{60} crossing through a ring simulating the faujasite pore opening at 400 °C (case a) and 700 °C (case b); (cf. ref 307).

The signal intensity of $C_{60}^{\bullet+}$ increased dramatically with the level of Fe^{3+} ion in the zeolite; this result supports electron transfer from C_{60} to Fe^{3+} inside the zeolite supercages. The $C_{60}^{\bullet+}$ intensity also increased with the adsorption temperature. Because the molecular diameter of C_{60} (7.9 Å) is slightly larger than that of the Y zeolite supercage (7.4 Å; Figure 15), its diffusion through the micropores is very limited. An increase in temperature facilitates the diffusion by increasing the kinetic energy of the adsorbate and the vibration frequency of the lattice (Figure 15, bottom). The location of C_{60} in zeolite Y has been determined by high-resolution electron microscopy.³⁰⁷

V.B. Competition between Protonation and Oxidation

The ability of zeolites to generate radical cations is related to the presence of acid sites. Therefore, adsorption onto acid zeolites may convert organic compounds into carbocations and radical cations concurrently. Several studies using a range of substrates and zeolite hosts address this competition, including a series of aromatic and unsaturated compounds and *N,N*-diphenylhydrazine. Of special interest is the persistent “blue species” (λ_{\max} 605 nm) formed from 1,1-diphenylethylene on silica–alumina. The history of this species aptly demonstrates the problems of assigning intermediates sequestered in zeolites on the basis of weak ESR signals; for this reason, it is discussed in detail below.

V.B.1 Protonation vs Oxidation of Aromatic/Unsaturated Hydrocarbons

A series of hydrocarbons, **54**^{•+}, $n = 3$, anthracene (**56**), pyrene (**57**), and perylene (**58**), were incorpo-

Table 7. Distribution of Framework (fr) and Nonframework (NF) Al in Calcined Acid Zeolites (by ^{27}Al MAS NMR) and Yields of Protonated 1,6-Diphenyl-1,3,5-hexatriene (54-H^+ , $n = 3$) and Radical Cation ($54^{+\cdot}$, $n = 3$)^a

zeolite	Si/Al	Al _{fr}	Al _{non-fr}	Al _{non-fr} /Al _{fr}	$54^{+\cdot}$	54-H^+
H,Na-ZSM-5	25	3	0.7	0.23	0.43	0.40
Na-ZSM-5/ex	26	3	0.6	0.20	0.37	0.18
H-Mor	9	3.6	1.2	0.33	0.33	0.33
H-Y	2.95	30.4	18.2	0.59	0.11	0.35
H-Y-de-Al	2.8	36.4	19.2	0.53	0.37	0.36

^a From ref 310.

rated in ZSM-5, mordenite, and Y zeolites which had been characterized by NMR.²⁵² Calcination of NH_4^+ - or H^+ -zeolites at 550 °C causes partial framework dealumination.^{18,73,308,309} The expelled framework Al remains in the channels as oligo- or polymeric aluminum oxides, which are considered to be Lewis acid sites. Nonframework Al is octahedral (^{27}Al NMR ~ 0 ppm), whereas framework Al is tetrahedral (~ 50 ppm); their ratio can be determined by ^{27}Al MAS NMR.⁴⁵ The Al distribution after calcination was scrutinized for its correlation with the electron acceptor ability of the zeolites (Table 7).²⁵²

Of the probe molecules, only **54**, $n = 3$, has a molecular size and shape appropriate for incorporation into medium pore ZSM-5.²⁵² The DR UV–Vis spectra after adsorption of the hexatriene onto ZSM-5 showed the presence of unreacted hexatriene (λ_{max} 346, 360, 380 nm), its known radical cation (λ_{max} 540, 605, 764, and 811 nm)⁹³ and an additional species (λ_{max} 480 nm) identified as the carbocation arising from protonation at C-1 (Table 7). The new species is not affected by dry oxygen, but decays upon exposure to laboratory air, regenerating **54**, $n = 3$. On the other hand, the radical cation $54^{+\cdot}$, $n = 3$, is more persistent than the carbocation.

A “Na-ZSM-5/ex” sample, prepared from H,Na-ZSM-5 by two consecutive ion exchanges (0.2 M aqueous NaCl), has reduced populations of Brønsted and Lewis sites (^{27}Al MAS NMR). The exchanged sample lost much of its ability to protonate **54**, $n = 3$, whereas the yield of $54^{+\cdot}$ decreased to a lesser extent (Table 7). The small decrease in the yield of $54^{+\cdot}$ was ascribed to loss of some nonframework Al in the exchange. Interestingly, neutral Na-ZSM-5 without acid sites, obtained by a synthesis without tetrapropylammonium templating agent, has a significantly lower capacity to adsorb **54**, $n = 3$, due the presence of Na^+ in the channels; it failed to generate either $54^{+\cdot}$ or 54-H^+ .

Adsorption of **54**, $n = 3$, in Na^+ or H^+ -mordenite and other Y zeolites generated radical cation and carbocation in variable proportions depending on the framework and nonframework Al content of the zeolites (Table 7). Brønsted acid sites were considered responsible for the protonation, whereas nonframework Al was thought to generate radical cations.²⁵²

Variable ratios of carbocations and radical cations were observed also upon adsorption of anthracene (**56**) and pyrene (**57**) on H-mordenite and H-Y zeolites, and of perylene (**58**) on H-Y. The resulting species were characterized by their optical spectra. This study represents a serious attempt to probe the

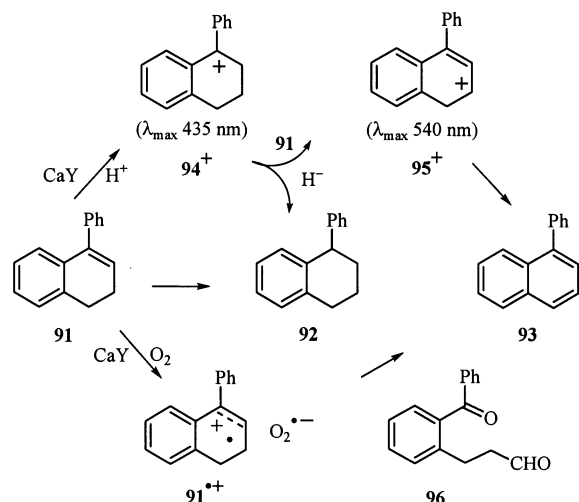
generation of organic radical cations in a series of zeolites whose acid properties were characterized by MAS NMR. However, application of this methodology to calibrate Brønsted and Lewis sites suffers from two inherent limitations.¹⁷⁴ The low sensitivity of solid-state NMR causes relatively large uncertainties. Thus, Na^+ -mordenite samples “free of nonframework Al” according to NMR generated $54^{+\cdot}$, which the authors ascribed to undetected amounts of nonframework Al. Alternative methods to assess the Brønsted and Lewis zeolite acidity (pyridine adsorption/desorption) are notably more sensitive (vide supra).⁶⁹ Second, ^{27}Al NMR spectroscopy does not differentiate between protonated framework Al (Brønsted acid sites) and sites neutralized by Na^+ ions. Thus, H,Na-ZSM-5 subjected to two consecutive H^+ -to- Na^+ ion exchanges ($\text{NaCl}/\text{H}_2\text{O}$) should be devoid of Brønsted acid. However, the resulting Na-ZSM-5/ex protonated **54**, still forming the corresponding carbocation, something that does not fit with the ^{27}Al NMR spectrum showing no nonframework Al. ^{27}Al NMR also failed to reveal the strength distribution of framework and nonframework Al, particularly for Y zeolites. This information is vital when addressing the relative protonation vs electron acceptor ability of zeolites.

The stability of cations and radical cations were affected by the nature of the probe molecule and by the size of the cavities. Molecules fitting tightly into the cavities (**54**, $n = 3$, in ZSM-5) are protected by the framework; no further changes occur (vide supra). When the cavities are larger than the guest, the species undergo further evolution; the larger the zeolite pores, the faster the changes. For **54**, $n = 3$, in mordenite, carbocation and radical cation decay slowly; in acid Y zeolites, only weak DR UV–Vis spectra for carbocation and radical cation are observed.

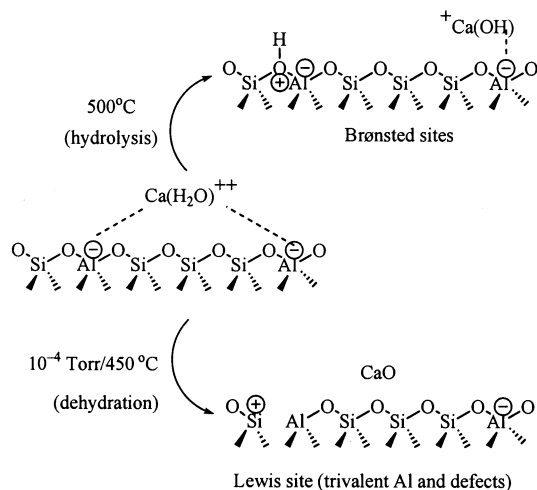
Some carbocations had significantly shorter lifetimes than radical cations. For example, the carbocation derived from **54**, $n = 3$, decays faster than the protonated form of arenes; this explains why it was not observed in earlier work on ZSM-5.⁹³ It was assumed that the carbocations decay by reverting to their neutral precursors.³¹¹ Alternative (more likely) possibilities, e.g., trapping by water or other nucleophiles, including $\equiv\text{Si-OH}$ silanol groups of the zeolite walls, were not considered even though the influence of ambient moisture on the lifetime and decay of the carbocations was noted.

Thermally activated CaY has been reported to function as proton donor as well as electron acceptor. Adsorption of 1-phenyl-3,4-dihydronaphthalene, **91**, at a loading of 1 molecule per supercage gave rise to equal yields of 1-phenyltetralin, **92**, and 1-phenyl-naphthalene, **93**.³¹² During the reaction, the DR spectrum showed two bands (435, 540 nm), assigned to cations **94**⁺ and **95**⁺. The products were rationalized via protonation and intermolecular hydride transfer (from **91** to **92** and **93**) as the key steps (Scheme 8). Experiments with D-exchanged zeolite led to incorporation of only one D into **92**. This result confirmed that the zeolite worked as a true catalyst, and not as a stoichiometric reagent.

Scheme 8



Scheme 9

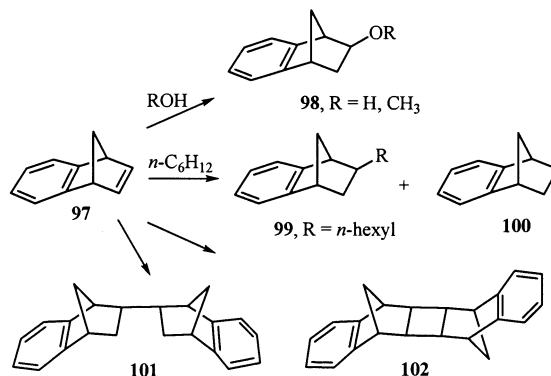


At much lower loading (<1 molecule per 100 supercages) **93** was the major product (~92%) along with low yields of a ring-cleaved dicarbonyl product, **96**, (~3%). A strong, structureless ESR signal (g 2.0019) during the reaction was attributed to the radical cation, **91**⁺. Activation of CaY under nitrogen instead of air reduced the yield of **93** by an order of magnitude. The products were rationalized via ET, forming **91**⁺ and superoxide ion, $O_2^{\bullet-}$, favored by the strong electrostatic fields inside the zeolite. The radical ion pair could react by internal hydrogen or proton transfer to $O_2^{\bullet-}$ or by cycloaddition resulting in oxidative cleavage of the C=C bond. The hydrogenation of styrene derivatives on CaY zeolite is not unusual; the oxidative cleavage yielding **96** is without precedence.

As mentioned in Section II, the activation procedure can affect intermediates and product distribution significantly.^{313,314} Thus, dehydration of CaY zeolite in a preheated oven (~500 °C, air, 10 h) generated large quantities of Brønsted acid sites by hydrolysis of solvated $Ca(H_2O)_n^{2+}$ ions within Y. The resulting sample, promoted H^+ -catalyzed reduction of arylalkenes or rearrangement, both rationalized via carbocations (Scheme 9).^{308,309,312}

Alternative procedures of dehydration yield much lower populations of Brønsted acid sites without

Scheme 10



affecting Lewis acid sites. For example, CaY degassed under reduced pressure (5×10^{-4} Torr), slowly heated to 450 °C, and maintained at this temperature for 10 h has very low Brønsted acid counts (Scheme 10).^{308,309} This sample only converted *cis*-stilbene to the (more stable) *trans* isomer.

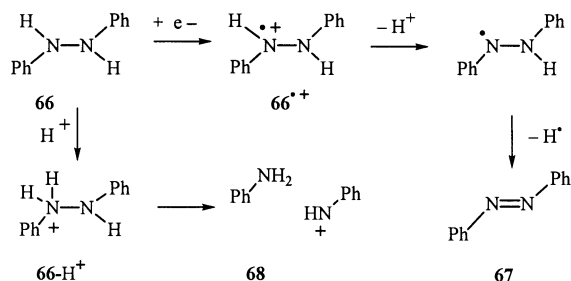
Radical cations formed by addition of stilbenes to activated CaY persist for days. The ESR signals of these species were broad and featureless; therefore, the species were identified by their DR-UV/Vis spectra. The formation of radical cations is favored by thermal treatment, which reduces the population of Brønsted acid relative to Lewis sites. This led to the conclusion that Brønsted acid sites are not responsible for the electron acceptor ability of the CaY zeolite.³¹²

However, a later detailed 1H and ^{31}P NMR and $^1H/^{27}Al$ double resonance study by the same authors, monitoring the 1H decoupled ^{31}P MAS NMR spectrum at -150 °C, failed to detect significant concentrations of Lewis acid sites with trimethylphosphine $[P(CH_3)_3]$ as a basic probe.³¹⁵ The failure to observe the characteristic ^{31}P signal of $P(CH_3)_3$ bound to EFAl Lewis sites (near -50 ppm) was common to all CaY samples regardless of activation procedure. Because only Brønsted sites were detected, the hypothesis that Lewis acid sites are responsible for the generation of radical cations on CaY needs to be revisited. These apparent discrepancies illustrate the fact that some results are reproduced only with difficulty. In view of this, and given the significant role of the activation procedure, it might appear desirable to determine the actual Brønsted and Lewis populations by control experiments in each experiment, but this extreme measure is hardly practical.

The interaction of *cis*-stilbene with H-mordenite or HZSM-5 also appears to involve both H^+ and electron transfer. The dark, one-way *cis*-*trans* isomerization was ascribed to protonation-deprotonation; subsequent dimer formation was assigned to the reaction of *trans*-stilbene with its radical cation.³¹⁶

In this context, we also mention some reactions of benzonorbornadiene, **97**, with alkaline earth-exchanged Y faujasites. Typically, the tight fit of organic radical cations in ZSM-5 prevents the access of potential reagents; the resulting lack of reactivity limits the chemical utility of medium pore zeolites as initiators of ET promoted reactions. Thus, product studies using these zeolites as ET catalysts are rare.

Scheme 11. Suggested Mechanism for the Formation of the Blue Species



Large pore zeolites, on the other hand, are better suited to promote ET or H^+ transfer reactions, because they allow reagents access to radical cations.

Thus, thermally dehydrated, alkaline earth- (except Ba^{2+} -) exchanged Y faujasites induced rapid chemical reactions of **97** at room temperature. The product distribution depends on the nature of the solvent, the presence of residual water, and the loading level (Scheme 10).³¹⁷ The large quantity of **97** converted per gram of zeolite (>150 mg/g) argues against an earlier suggestion⁹³ that lattice defects are responsible for the oxidizing ability of zeolites.

The radical cation was proposed as the key intermediate because of a broad, structureless ESR signal. The resulting ether and alcohol, **98**, $\text{R} = \text{H}, \text{CH}_3$, tend to support this mechanism, although the stereochemistry was not identified. Another argument in support of $\mathbf{97}^{\cdot+}$, the supposed ability of CaY to generate persistent radical cations of aryl alkenes,^{317,318} was later amended, and the assignment changed to a dimeric allylic carbocation.³¹⁵ Thus, given the high sensitivity of ESR and the absence of quantitative information, it would be of interest to revisit the postulated intermediate. The predominant pathway, reduction of the $\text{C}=\text{C}$ double bond yielding benzenobornene, **100**, is not a typical radical cation reaction.

V.B.2 Protonation vs Oxidation of *N,N'*-Diphenylhydrazine

As noted earlier,²⁵² acid zeolites are proton donors as well as electron acceptors and may generate carbenium ions and radical cations. However, the concurrent involvement of these intermediates has not been documented very often. One such case involves adsorption of *N,N*-diphenylhydrazine, **66**, on HZSM-5, yielding azobenzene (**67**) and aniline (**59**).²⁵⁹ The mass balance after solid-liquid extraction was incomplete ($\sim 75\%$), indicating that some organic material was retained in the solid; the IR spectrum of the extracted solid corresponded to that of **59**.

The two products are related formally as disproportionation products; however, their yields did not show the required balance (excess **67**). Accordingly, two competing pathways were invoked to rationalize the results. Aniline was rationalized via protonation of **66**, yielding $\mathbf{66-H}^+$, and N–N bond cleavage, whereas **67** was explained via electron transfer ($\mathbf{66}^{\cdot+}$, and deprotonation plus loss of a hydrogen). A transient broad DR spectrum (λ_{max} 800 nm) in the initial reaction stages, assigned to $\mathbf{66}^{\cdot+}$, supports this interpretation (Scheme 11). Related dehydrogenations

generating alkenes or their radical cations in zeolites have been observed in hydrocarbon systems.^{198,242}

V.B.3 The Nature of the Blue Species Generated upon Adsorption of 1,1-Diarylethenes onto Acid Zeolites

In a seminal study, Rooney and Pink showed that adsorption of electron-rich aromatic compounds onto silica–alumina generated the respective radical cations by electron transfer from the organic substrate to the solid.^{70,319} Many later studies corroborated the ability of silica–alumina and other inorganic surfaces to generate significant populations of radical cations from organic substrates with different functional groups.

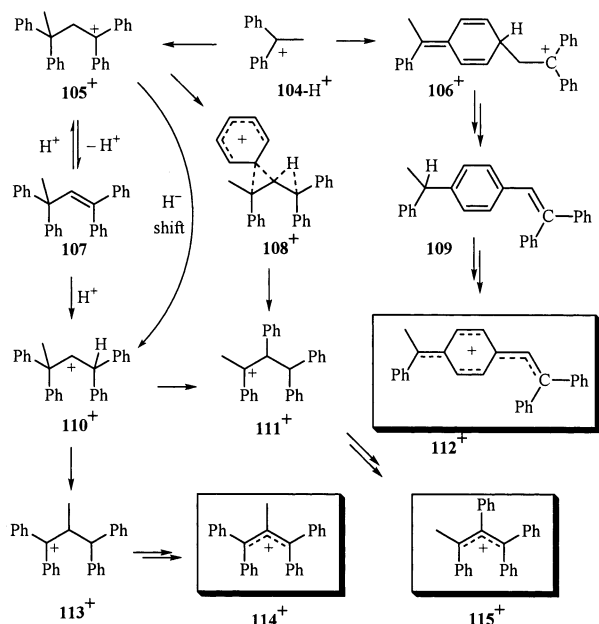
Rooney and Pink also added 1,1-diphenylethylene, **103**, to silica–alumina and found a persistent blue species (λ_{max} 605 nm) and assigned it to hydrated $\mathbf{103}^{\cdot+}$, based on a weak, featureless ESR signal and the analogy to other aromatic compounds.³¹⁹ This blue species attracted much attention but proved to be enigmatic.^{257,320–330} ESR integration showed an insignificant spin population, casting doubt on its assignment to a radical cation; the concentration dependence suggested some type of dimer.^{320,321} Alternative structures, such as a π -complex between **103** and a Lewis acid site or a carbenium ion were also proposed over the years.^{331–336}

Shortly after Rooney and Pink's work the first synthetic zeolites were reported.¹³ It was logical to extend the earlier work to probe whether synthetic HY zeolites could generate radical cations. For the first study of spontaneous radical cation formation on HY, Stamires and Turkevich selected triphenylamine (**70**) and **103**.²⁶¹ With the benefit of hindsight, these choices were unfortunate: **103** gave rise to the blue species (again assigned to $\mathbf{103}^{\cdot+}$); **70** probed only the external surface because it is too large to pass through the 0.74 nm pore opening.¹⁹³

Pulse radiolysis studies produced "authentic" UV–Vis spectra of $\mathbf{103}^{\cdot+}$ (λ_{max} 550 nm) and a dimer radical cation, $[\mathbf{103}\cdots\mathbf{103}]^{\cdot+}$, (λ_{max} 520 nm),^{337,338} both different from the maximum of the "blue species". However, nanosecond laser flash studies of *p*-substituted derivatives revealed that $\mathbf{103}^{\cdot+}$ is highly reactive in solution and unlikely to be detected in pulse radiolysis. This study ruled out $\mathbf{103}^{\cdot+}$ as responsible for the 605-nm band and assigned a dimer, $[\mathbf{103}\cdots\mathbf{103}]^{\cdot+}$, as the species observed in pulse radiolysis.³³⁹ Of course, if $\mathbf{103}^{\cdot+}$ dimerizes rapidly, it will not be persistent in large pore zeolites.

A species of λ_{max} 615 nm was reported also upon adsorption of **103** onto a 88% Ca^{2+} -exchanged Y zeolite (and again erroneously assigned to $\mathbf{103}^{\cdot+}$),^{312,318} based on the qualitative observation of a "strong ESR signal with a *g* value of 2.00235";³⁴⁰ this result directly contradicts the report of insignificant spin populations.^{320,321} Oxygen was deemed essential for the generation of the blue species; **103** only produced "a very light green color" on CaY activated under nitrogen.³¹⁰ Interestingly, the blue color (λ_{max} 620 nm) of bis-(*p*-dimethylamino)-**103** faded upon degassing and was regenerated upon introduction of air; this process was reversible for at least six cycles.³¹² The influence of air on bis(*p*-dimethylamino)-**103** is unique;

Scheme 12



it was attributed to its very low oxidation potential (0.66 V vs SCE),³¹² enabling molecular oxygen to serve as electron acceptor in this special case. Of course, O₂ can hardly account for the oxidation of diarylethenes with higher oxidation potentials. The authors later assigned the blue species in CaY as due to a dimeric allylic carbocation.^{315,339} The role of oxygen, however, does not fit the revised structure.

A study of the blue species sequestered in H-Y and H-Beta, quantified the number of spins;³³² although the signal was "moderately strong", it showed only 10¹⁵ spins × g⁻¹. For a dimer (360 Da), this corresponds to only 10⁻⁴ mg × g⁻¹, a very minor fraction of the organic material remaining (~30 mg × g⁻¹; combustion analysis) after exhaustive extraction.³³² Clearly, the ESR spectrum is not related to the optical spectrum. The high sensitivity of ESR may detect minor quantities of intermediates unrelated to the major species present.

Product studies following adsorption of **103** on silica-alumina (25%) and other zeolites revealed similar product distributions for various solid supports, consisting of variable amounts of the olefinic dimer **107** and a cyclized dimer containing an indene function as well as minor quantities of benzophenone.³³⁹

In situ IR spectra support diamagnetic **103** dimers (formed via acid-catalysis) as the predominant species in zeolite Y. ¹³C NMR spectra of acid solutions containing the blue species also identified dimeric species as major components (Scheme 12; Figure 16). The good resolution of the spectra is incompatible with significant concentrations of paramagnetic species. Semiempirical (ROHF) calculations using the ZINDO method support 1,1,3,3-tetraphenyl-1-butylium, **105**, as the blue species, but allylic cation structures could not be ruled out.

In summary, the data suggest that the color of the solids are likely due to minor quantities of a delocalized carbocation with a strong UV-Vis band;³⁴¹ conjugated cations, **112**⁺, **114**⁺, and **115**⁺, are com-

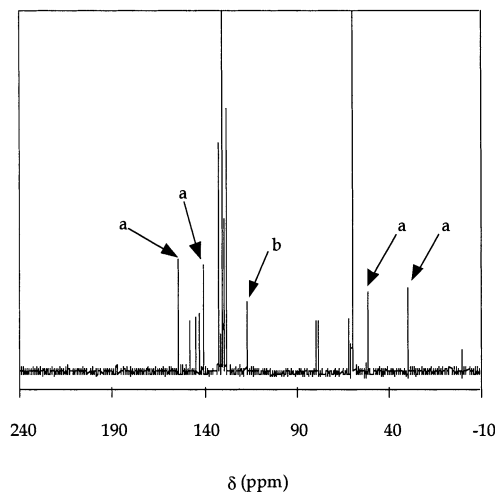


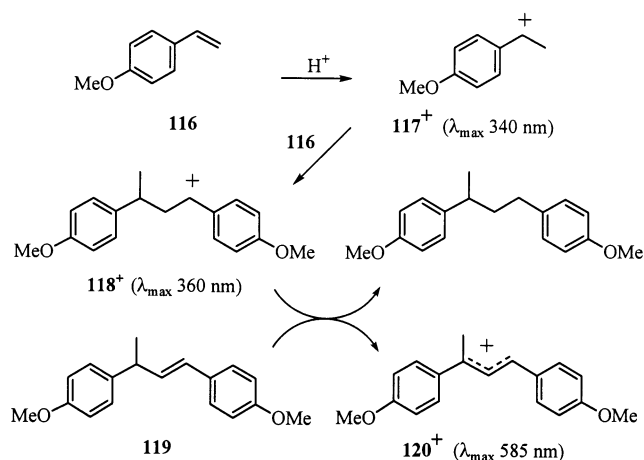
Figure 16. ¹³C NMR spectrum obtained by dissolving 1,1-diphenylethylene (**103**) in dimethyl sulfate/sulfuric acid. The UV-Vis spectrum of this solution coincides with that of the "blue species". Characteristic peaks of unreacted **103** (a) and of dimer **112**⁺ (b) are labeled. Reprinted with permission from ref 332. Copyright 1997 Elsevier Science.

patible with these spectra.^{315,319} Because the structural information of UV-Vis spectra is limited, alternative conjugated carbocations may also be compatible with the 605-nm band. Formation of the allylic carbocations, **114**⁺ and **115**⁺, requires at least one energetically unfavorable step, viz., the rearrangement, **105**⁺ to **110**⁺, a series of questionable shifts (**105**⁺ to **111**⁺), or an *anti*-Markovnikov protonation (**107** to **110**⁺). Perhaps Rooney's proposal, assigning the blue species to the highly delocalized **112**⁺, is most reasonable, involving the bimolecular reaction, *para*-attack of a phenyl ring of **104**⁺ on the terminal C=C carbon of **103** (Scheme 12).³⁴²

Adsorption of some styrenes also led to the erroneous identification of an intermediate as a radical cation. Adsorption of styrenes with electron donating or withdrawing substituents onto ZSM-5 and ZSM-11 zeolites generated various colors in the solids.³⁴³ Because Na⁺-zeolites were inactive, the color formation was ascribed to Brønsted acid sites, and the species identified as radical cations, based on an ESR signal and the fact that organic radical cations often are highly colored. A value of ~10¹⁸ spins g⁻¹ (1.6 × 10⁻⁶ mol g⁻¹) was estimated for 4-vinylanisole, **116**, on silicalite, corresponding to 0.23 mg of **116**⁺/g of zeolite; lower concentrations (~10¹⁷ spins g⁻¹) were measured for other samples.³⁴³ Later work, combining product studies, laser flash generation of styrene radical cations within zeolites, comparison of DR spectra with authentic radical cation spectra in solution, and comparison of in situ IR spectra with calculated IR spectra led to the consensus that a dimeric allylic carbenium ion, e.g., **120**⁺, is responsible for the color (Scheme 13), possibly arising by hydride transfer, e.g., from **119** to **118**⁺, between two acid-catalyzed "primary" dimer species.³⁴⁴⁻³⁴⁷

While this mechanism may be feasible in large-pore zeolites, it cannot be considered for ZSM-5: the narrow channels will frustrate any mechanism requiring an exchange between the central sections of two dimeric species; a hydride transfer from **119** to

Scheme 13



118⁺ is highly unlikely. An alternative pathway, involving sequential oxidations and deprotonations, is more likely and has precedence in ZSM-5.³⁴²

The examples discussed in this section illustrate cases where much effort has been devoted to identifying deeply colored species, which actually represented minor percentages of the organic material adsorbed. The high extinction coefficients of these intermediates give a misleading impression of their concentration. Quantitative EPR spectroscopy appears appropriate in these cases.

V.C Spontaneous Radical Cation Conversions in Zeolites

As mentioned above, the primary radical cations generated in zeolites species may undergo secondary conversions on a time scale comparable to that of their generation. Some of these have been discussed in the previous Section (V.A). They are compiled here in a brief overview; we first review conversions due to zeolite active sites, followed by reactions involving a second guest molecule or species, which occur especially in zeolites with large supercages. Finally, we mention a few neutral radicals formed by intra-zeolite reactions (Section V.C.3).

V.C.1 Intra-Zeolite Reactions not Involving a Second Guest

The simplest and perhaps most frequently encountered reaction of newly formed radical cations in zeolites is deprotonation. Protons attached near a positive charge generally have significantly increased acidities. This trend is enhanced in the zeolite environment, particularly in acid–base active zeolites. As a result, several types of radical cations are rapidly deprotonated in zeolites. In addition to N or O acids (anilines, phenols, oximes), which frequently are deprotonated (Section V.C.3), substrates containing allylic or benzylic protons also undergo this reaction.

Some free radicals generated by deprotonation are readily oxidized to cations (Section V.A.5). Some cations may be deprotonated a second time, generating styrene or butadiene derivatives.²⁴⁶ The resulting alkenes are more easily oxidized than the original substrates, generating delocalized radical cations.²⁴⁶

The overall conversions amount to three-electron oxidation with loss of two protons or, alternatively, loss of molecular hydrogen from a radical cation (Section V.A.5). Conversely, phenyl-substituted alkenes or stilbenes were reduced (hydrogenated) to phenylalkanes and diphenylethanes, respectively, on CaY zeolite.³¹² These conversions suggest protonation as well as reduction of the substrate on appropriate zeolite sites (cf. Section V.B.1).

Some strained ring hydrocarbons undergo ring opening with deprotonation, possibly via radical cations as primary, short-lived intermediates. For example, cyclopropane or vinylcyclopropane systems generate allyl or pentadienyl free radicals, respectively (Section V.C.3). Similarly, a localized ring-opened free radical species was obtained from an oxacyclopropane system, possibly with deprotonation (Section VI.C).

In some cases, strained ring systems undergo ring opening with an apparent hydrogen migration. For example, arylcyclopropanes are converted to *trans*-arylpropene radical cations; this cyclopropane-to-propene conversion appears to proceed by at least two different pathways, including protonation.³⁴⁸

Conversely, some aromatic ring systems undergo ring-closure via *o,o'*-coupling (Section V.A.9). The ring-closure generates extended bifunctional systems, containing one or two cyclohexadienyl moieties; further oxidation and deprotonation may give rise to systems with two aromatic rings; a third oxidation step may generate the corresponding radical cation. The overall reaction again amounts to three-electron oxidation with loss of two protons or loss of molecular hydrogen from a radical cation.

Radical cations prone to fragmentation typically are not stabilized inside zeolites. Thus, photolysis of bicumyl in NaY generated cumyl cations by cleavage of the doubly benzylic bond between the cumyl moieties (Section VII.B).³⁴⁹ The fragmentation is a general case of the opening of strained ring compounds mentioned above.

Similarly, radical cations containing activated C–O bonds may undergo elimination. Thus, dehydrated H-mordenites, especially Fe^{III} containing samples, convert a wide range of alkyl acetates to alkenes and acetic acid (Section V.A.1). This Fe^{III} catalyzed reaction is analogous to a well-established pyrolytic reaction.

Upon incorporation into ZSM-5 2-phenyl-1,3-dithiane (**76**) was converted into 1,2-dithiolane radical cation (**77⁺**) without evidence for an intervening species.³⁵⁰ The interesting ring-contraction requires formation of an S–S bond and loss of the benzyl moiety (Section V.A.9).

V.C.2 Ion–Ion or Ion–Molecule Reactions in Zeolites

Incorporation into the internal voids of zeolites can protect radical cations from external reagents, particularly when the fit between host and guest is tight. Large supercages, on the other hand, often fail to protect the incorporated species. For example, radical cations of substrates with relatively high oxidation potentials can be replaced by a different species upon introducing an adsorbate of lower oxidation potential.

For example, the radical cations of octalin, **23**⁺, or of the benzene π -dimer, **41**, were replaced by 2,5-dimethylhexa-2,4-diene radical cation, **9**⁺, upon addition of **9** (Section V.A.5). Similarly, the radical cation of fullerene was replaced, upon introducing perylene, by the perylene radical cation (Section V.A.11). These exchange reactions occur only at low loading levels, as an excess of the first substrate apparently may block access to the internal cavities. Similarly, the slow conversion of methylthiophene or methylfuran radical cations, **79**⁺ or **82**⁺, to the corresponding π -dimer radical cations during coadsorption with excess benzene was ascribed to slow diffusion through solvent-filled zeolite channels (Section V.A.9). This finding may indicate that the radical cations are accessible, in principle, and that they are not firmly connected to a "complexing" site in the zeolite. This conclusion is independently supported by the sharp spectra of some radical cations in some appropriate zeolites (cf., Figure 6).^{207,351}

Radical cations of benzene derivatives may couple to activated aromatic moieties. This reaction is an intermolecular version of the cyclization reaction discussed above; the intermolecular addition typically occurs in the (more readily accessible) *p*-position. Subsequent oxidation and deprotonation gives rise to biphenyl derivatives; a third oxidation step generates their radical cations. The overall reaction amounts to a three-electron oxidation with loss of two protons or loss of molecular hydrogen from a radical cation (Section V.A.5). If the para position is occupied, π -dimer radical cations may be formed instead (vide infra).

Thiophene or oligothiophene radical cations couple to a second radical cation or to a neutral molecule. Subsequent dehydrogenation or similar stepwise processes may yield radical cations or dication with extended π -systems (Section V.A.9,10).

In zeolites with sufficiently large cavities, radical cations of aromatic hydrocarbons (Section V.A.5) or olefins (Section V.A.1) may form sandwich dimer radical cations by reaction with the neutral parent molecule. The π -dimer radical cations of tetramethylethylene or benzene have been encountered frequently in addition to those of furan or thiophene and derivatives (Sections V.A.1, V.A.9).

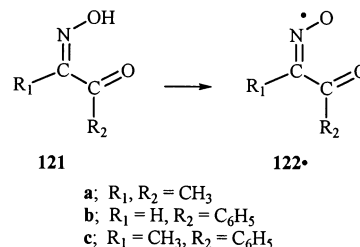
In some cases, S- or N-centered radical cations may form σ -dimer radical cations by adding to the corresponding center of the parent molecule (Sections V.A.9 and VII.A.3). The radical cation of ethyne generated on NaZSM-5 by radiolysis, formed benzene radical cation, in a sequence of ion-molecule reactions amounting to trimerization (Section VI.F).

Some radical cations are oxygenated by interaction with extraneous reagents such as molecular oxygen or water, or by reaction with reactive oxygen sites or oxygen species generated in the zeolite. Thus, benzene radical cation was converted by molecular oxygen to dihydroxybenzene radical cation.⁵³ "Atomic oxygen", produced by decomposition of N₂O on Fe-containing ZSM-5, converted adsorbed benzene to phenol radical cation instead of the monomer or π -dimer radical cations.¹¹² An oxygen containing product formed upon exposure of **54**⁺, *n* = 3, to air

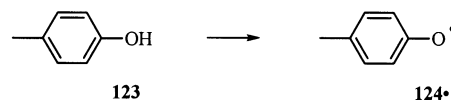
was tentatively identified as an endo-peroxide.²⁵² Another oxygenation reaction, the formation of the nitroxide free radical, **62**[•], during the incorporation of diphenylamine, **60**, most likely proceeds via the aminyl, **61**[•] (Section V.A.8).

V.C.3 Spontaneous Deprotonation of Radical Cations

Incorporation of acetyl or benzoyl oximes into ZSM-5 generated iminoxyl radicals via deprotonation.^{352,353} Butane-2,3-dione-monoxime, **121a**, and 1-phenylpropa-1,2-dione-2-oxime, **121c**, gave rise to ESR powder spectra indicative of a free radical with axially symmetric *g* and hyperfine tensors; the *g*_{||} and *g*_⊥ components were split into 1:1:1 triplets due to the hfc of a ¹⁴N nucleus (*I* = 1; e.g., **121a**, *A*_{||} = 45.7 G; *A*_⊥ = 26.7 G); the central portion of the spectrum showed a three-proton hfc (*I* = 1/2; e.g., **121a**, *A*_{iso} = 1.9 G). The data are compatible with iminoxyl radicals, **122**[•]a,c, with lifetimes of ~2–3 days, compared to ~10 min in benzene. Benzoyliminoxyl radical (**122b**[•]) obtained from phenylglyoxaloxime (**121b**) showed an additional splitting due to the azomethine hydrogen (*A*_{||} = 8.8 G; *A*_⊥ = 2.9 G). These data support a radical, **122b**[•], whose principal axes, *A*_{N,||} and *A*_{H,||}, of ¹⁴N and ¹H dipolar hyperfine couplings are located nearly perpendicular to each other. These findings unambiguously identify iminoxyl **122b**[•] as the *Z*-isomer.³⁵³



In contrast to phenol ethers, which readily form radical cations (Section V.A.5), simple phenols gave rise to phenoxyl radicals. Incorporation of *p*-methylphenol (**123**) into NaZSM-5 zeolite generated *p*-methylphenoxyl (**124**[•]; *g* = 2.0042; *A* = 14.6 G, 3H; fwhh = 2.1 G). The ESR spectrum was complicated by powder-like features at the low and high field end. The well resolved 1:3:3:1 quartet and comparison with a solution spectrum (*A*_b = 11.95 G, 3H; *A*_{2,6} = 6.0 G, 2H) identified the species as **124**[•].^{354–358} However, the zeolite spectrum failed to show the strong coupling of the *o*-protons; in fact, an ESR spectrum obtained from **123-d**₄ differed only by its reduced line width (*A*_{CH₃} = 14.4 G; fwhh = 1.3 G). These results were rationalized (tentatively) by a distortion of **124**[•] in the zeolite, although there is no specific evidence for any particular site with which it may interact.¹⁹⁸



In addition to "simple" deprotonations of O or N acids, some substrates show more complex reaction sequences. For example, incorporation of *p*-propyl-

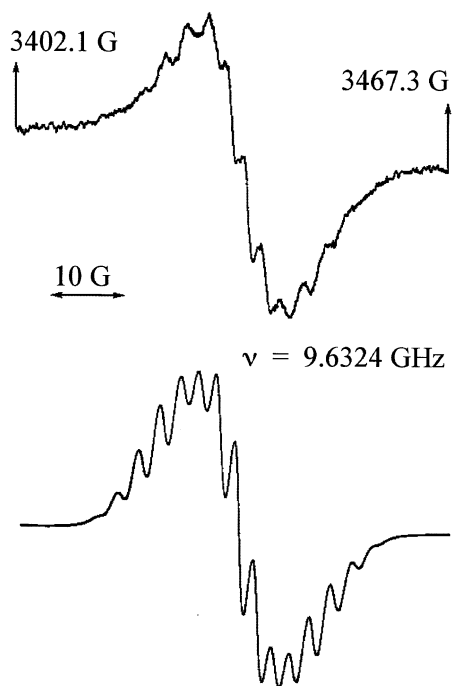


Figure 17. Top: X-band ESR spectrum obtained by incorporation of *trans*-1,2-diphenylcyclopropane *t*-**125** into pentasil zeolite; the spectrum was identified as that of *exo,exo*-**129** \cdot . Bottom: Second-order simulated spectrum of *exo,exo*-**129** \cdot . Reprinted with permission from ref 360. Copyright 2000 Wiley-VCH Verlag GmbH.

anisole (**53**) onto ZSM-5 generated anethol radical cation, **52** $^{+\cdot}$, identified by its ESR spectrum (Section V.A.5).²⁴⁶

Incorporation of *trans*-1,2-diphenylcyclopropane (**125**) into ZSM-5 resulted in ring opening with deprotonation. The radical cation, **125** $^{+\cdot}$, is known to have significant spin density on the benzylic carbons and large hfc's for the benzylic and geminal ^1H nuclei.³⁵⁹ The ESR spectrum in the zeolite showed only one pair of ^1H nuclei with significant coupling ($A = 11.5$ G, 2H; $A = 3.0$ G, 6H; Figure 17); it is incompatible with the presence of **125** $^{+\cdot}$.³⁶⁰

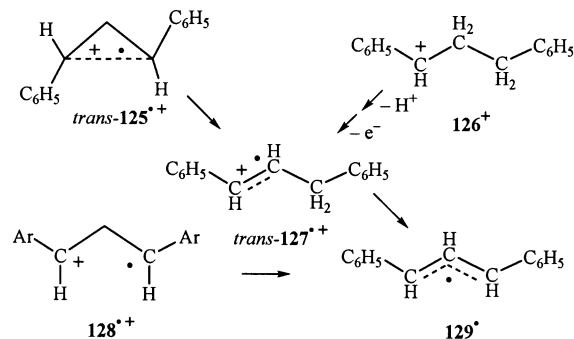
Isotopic labeling of the geminal protons (**125**-*3-d*₂) produced an essentially identical ESR spectrum. The observed hfc's are similar to the *endo*- ^1H nuclei of *exo,exo*-bisarylallyl radicals ($A_{\text{endo}} = 10.2$ G; $A_{\text{o,p}} = 2.9$ G).³⁶¹ Accordingly, the spectrum was assigned to *exo,exo*-1,3-diphenylallyl radical, **129** \cdot ; its formation requires oxidation, ring opening, and loss of a proton; the details of this mechanism could not be assigned.

A mechanism involving distortion and deprotonation of **125** $^{+\cdot}$ in the direction toward **129** \cdot is an interesting possibility; an apparent "conrotatory" distortion of **129** \cdot provides a direct pathway to *exo,exo*-**129** \cdot and is readily accommodated in the zeolite channels. The allylic radical, **129** \cdot , was also generated from *trans*-1,3-diphenylpropene, **127** (Scheme 14).³⁶⁰

VI. Generation of Radical Cations by Radiolysis in Zeolites

Radical cations are also generated efficiently upon γ -radiolysis of appropriate "guests" sequestered in zeolites. In this experiment, a "hole" and a free electron are generated in the zeolite, and the guest

Scheme 14

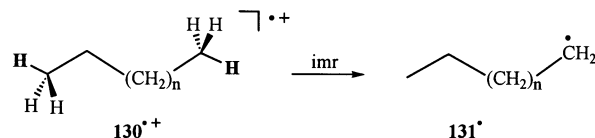


transfers an electron to the "hole". Given the redox as well as acid–base active nature of zeolites, it is not obvious whether the original substrate or a rearranged product is oxidized by interaction with the newly created "hole." In fact, many alkenes undergo significant reactions before the onset of radiolysis.

VI.A Radical Cations of Linear and Branched Alkanes

A pioneering study of alkane radical cations generated by radiolysis of *n*-hexane and *n*-octane was carried out by Toriyama, Nunome, and Iwasaki. Following a series of detailed and elegant studies of alkane radical cations in SF_6 and chlorofluorocarbon matrices,³⁶² they extended their work to pentasil zeolite (ZSM-5).³⁶³ Since the oxidation potentials of the alkanes lie well above the range where oxidation by the zeolite can be expected, it is unambiguous that neutral hydrocarbon molecules interact with the holes generated in the zeolite upon radiolysis. Indeed, incorporation of alkanes into Na- or H-ZSM-5 does not give rise to any absorption above 260 nm.

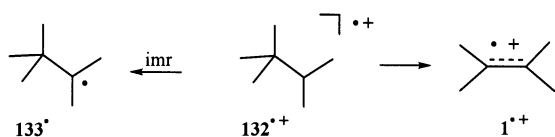
The results are quite interesting. At low alkane concentration (loading: 0.5 wt %), only the characteristic triplets of the radical cations, **130** $^{+\cdot}$ ($n = 3, 5$), are observed (*n*-hexane, $A = 39$ G, 2H; *n*-octane, $A = 29$ G, 2H). This coupling has been assigned to the in-plane protons at the chain ends. A comparison of these spectra with those obtained in chlorofluorocarbons indicates that the alkanes are present in their fully extended conformation only.



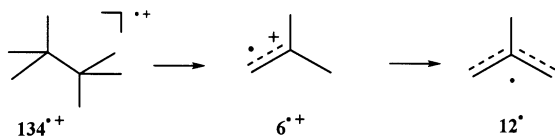
Radiolysis at higher substrate loadings (3.0 wt %) yielded different spectra, which were assigned to the corresponding primary alkyl radicals, **131** \cdot ($n = 3, 5$). Because the appearance of the new species was concentration dependent, their formation was ascribed to an ion molecule reaction (imr), such as transfer of a proton to the neutral alkane. This assignment implies that the radical cations, **130** $^{+\cdot}$ ($n = 3, 5$), are strong acids in the zeolite.

Significant applications of γ -radiolysis to studying radical cations in zeolites have emanated from the radiation group at Argonne National Laboratories.³⁵¹

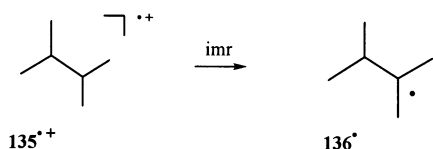
For example, Barnabas et al. studied the fate of highly branched alkanes, 2,2,3-trimethylbutane, **132**, and 2,2,3,3-tetramethylbutane **134**, upon γ -radiolysis in ZSM-5 (counterion not specified).³⁶⁴ Radiolysis of **132** in ZSM-5 at 77 K yielded a six-line spectrum characteristic for **132^{•+}** ($A = 31$ G, 5H).²¹² Upon raising the temperature, in the range 120–200 K, the well-known 2,3-dimethyl-2-butene radical cation, **1^{•+}**, was observed ($A = 17$ G, nine lines observed, 12H). Its formation was ascribed to “thermal elimination of methane”, a reaction similar to the above-mentioned elimination of H₂.²¹⁵ At temperatures above 200 K, a seven-line pattern ($A = 22.5$ G, 6H) appeared, which was ascribed to 2,3,3-trimethyl-2-butyl radical, **133[•]**, apparently due to deprotonation of **132^{•+}**. Because the appearance of this species increased with substrate loading, its formation was ascribed as an ion molecule reaction (imr), similar to the formation of **131[•]** from **130^{•+}**.



γ -Radiolysis of tetramethylbutane (**134**) in pentasil zeolite generated a “seven-line” spectrum ($A = 31$ G, 6H; outer lines not distinct),³⁶⁴ identified as that of **134^{•+}**,^{212,364} the splitting is caused by a single (in-plane) proton per methyl group. An additional weak quartet ($A = 22$ G) indicated methyl radical, likely formed by fragmentation of **134^{•+}**. At 125 K, a new spectrum appeared ($A = 14.9$ G, 2H; $A = 13.8$ G, 2H; $A = 3.3$ G, 3H); it was assigned to 2-methylpropenyl radical, **12[•]**. This species was explained by rapid deprotonation of 2-methylpropene radical cation (**6^{•+}**, not observed). Assigned by the authors to “scission of the central C–C bond” of **134^{•+}**,³⁵¹ this reaction amounts to “elimination” of 2-methylpropane (C₄H₁₀), similar to the loss of CH₄³⁶⁴ and H₂²¹⁵ mentioned above.



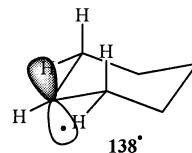
γ -Radiolysis of 2,3-dimethylbutane, **135**, in pentasil zeolite at 4 K forms the corresponding radical cation (**135^{•+}**; a broad quintet, $A = 37$ G); in analogy to radical cations **130^{•+}** and **134^{•+}**, the quintet is caused by coupling of a single proton per methyl group. In addition, 2,3-dimethyl-2-butyl free radical (**136[•]**), recognized as a septet ($A = 23.4$ G) of doublets ($A = 5.5$ G), is formed to a lesser extent.³⁶⁵



VI.B Radical Cations of Cycloalkanes

Irradiation of cyclohexane, **137**, on Na-ZSM-5 at 77 K generated the cyclohexyl free radical, **138[•]**.³⁶⁵

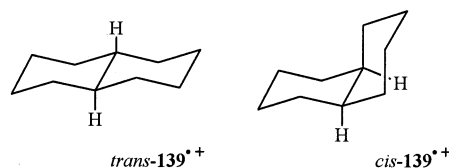
The clear difference between two sets of β -protons in the ESR spectrum ($A = 22$ G, 1H_a; $A = 40$ G, 2H_{ax}; $A = 5$ G, 2H_{eq}) indicates that **138[•]** is conformationally rigid at 77 K. The cyclohexane radical cation, **137^{•+}**, is a possible intermediate, but no evidence for this species was observed.



The formation of **138^{•+}** was ascribed to “spontaneous” proton transfer to the zeolite matrix, in contrast to various previous deprotonations assigned by the authors to ion molecule reactions. Spontaneous proton transfer to zeolites has precedence in the formation of iminoxyl radicals from oximes.^{352,353}

Two bicycloalkane isomers, *cis*- and *trans*-decalin (bicyclo[4.4.0]decane; *cis*-, *trans*-**139**), have been the focus of investigation by both radiolysis³⁶⁶ and photolysis.³⁶⁷ Interestingly, the hyperfine pattern of the *trans* radical cation (*trans*-**139^{•+}**) had shown significant matrix dependence in halocarbon matrices.³⁶⁸ Barnabas and Trifunac studied the radiolysis of *cis*- and *trans*-**139** in a number of synthetic zeolites. The results are most interesting. Depending on the nature of the zeolite host and the temperature, the authors found variations of hyperfine coupling of a magnitude supporting the stabilization of two different “electronic states” (structure types) for both *cis*- and *trans*-radical cations.³⁶⁹ In some zeolites, a single structure was observed, whereas in others both structures were found.

For example, the authors found the structure corresponding to the ²A₁ state of *cis*-**139^{•+}** ($A_{4H} = 49.5$ G in silicalite, 45 K; $A_{4H} = 50$ G in ZSM-34) or a structure corresponding to the ²A₂ state, predicted to be higher in energy by (vacuum) calculations ($A_{4H} = 28.1$ G in silicalite, 95 K; $A_{4H} = 30.2$ G in offretite). For *trans*-**139^{•+}**, they observed radical cation structures corresponding to the (lower-energy) ²Ag state, ($A_{4H} = 50.5$ G in silicalite; $A_{4H} = 51.5$ G in ZSM 34) and the higher-energy ²Bg state ($A_{4H} = 28.5$ G in Na-Y; $A_{4H} = 29.8$ G in Na-W-5), respectively. The spectra show five-line patterns due to coupling of four equatorial protons, either those at the α -carbons (adjacent to the transannular bond; ²A₁, ²Ag), or those at the β -carbons, one C–C bond further removed (²A₂, ²Bg).

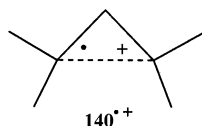


Perhaps even more unusual is the assignment that, in offretite, a fast equilibrium between structures corresponding to the ²A₁ and ²A₂ states of *cis*-**139^{•+}** exists, which results in a nine-line spectrum ($A = 30$ G). Finally, a deprotonated neutral radical was reported in the case of *cis*-**139**; its formation was

ascribed to ion–molecule reactions. This assignment, based in essence on two weak lines, may require confirmation under more favorable conditions.

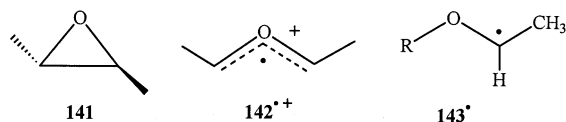
VI.C Radical Cations of Strained Ring Substrates

Qin and Trifunac studied the radiolysis of several strained-ring compounds in zeolite Na-Y. For example, radiolysis of 1,1,2,2-tetramethylcyclopropane, **140**, produced an ESR spectrum that could be simulated with the known hyperfine coupling parameters of a radical cation, $140^{\bullet+}$, with one lengthened cyclopropane bond ($A = 18.7$ G, 2H; $A = 14.9$ G, 12H).³⁷⁰ The structure of this radical cation was originally established on the basis of CIDNP results (in solution)³⁵⁹ and confirmed by ESR studies in chlorofluorocarbon matrices.³⁷¹

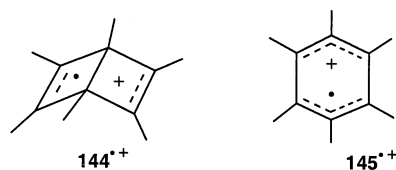


In the zeolite, $140^{\bullet+}$ was not deprotonated; apparently, the radical cation is well isolated from other molecules, because its bulky shape does not permit ready migration in the channels, precluding ion molecule reactions.

Radiolysis of *trans*-2,3-dimethyl-1-oxacyclopropane (**141**) in zeolite Na-Y resulted in the known quintet spectrum ($A = 22.5$ G) of a localized, ring-opened free radical species, 143^{\bullet} . The splitting is due to the interaction of the electron spin with one α -proton and the three β -protons of one methyl group. Since no additional splitting is observed, the nature of the remaining moiety attached to the ESR active pendant is unknown and subject to speculation. The species is stable in the range $77 < T < 200$ K.³⁷⁰ In contrast, radiolysis of **141** in chlorofluorocarbon matrices produced, in addition, a delocalized, ring-opened radical cation, $142^{\bullet+}$.³⁷²

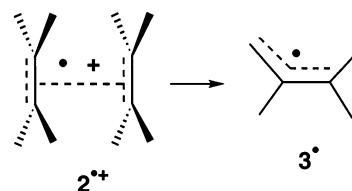


Radiolysis of hexamethyl-Dewar-benzene, **144**, in zeolite Na-X resulted in a spectrum with hyperfine splittings due to four equivalent methyl groups ($A = 10.5$ G, 12 H; nine lines are observed).³⁷⁰ Similar spectra observed upon radiolysis of **65** in chlorofluorocarbon matrices^{104,185,241,373} or deposition on O_2^+ SbF_6^- ³⁷⁴ were ascribed to the hexamethyl-Dewar-benzene radical cation, $144^{\bullet+}$.^{104,185,241,373,374} Of course, the ESR spectra only indicate the presence of four equivalent or nearly equivalent methyl groups, but do not provide specific evidence for the bonding in the central six-atom fragment. Thus, an “elongated” structure, $145^{\bullet+}$, predicted by ab initio methods for $C_6H_6^{\bullet+}$,³⁷⁵ and identified in Freon matrices,³⁷⁴ would have an ESR spectrum essentially identical to that observed in the zeolite.



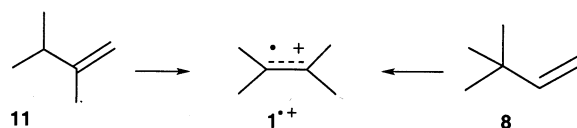
VI.D Radical Cations of Alkenes

Radiolysis of 2,3-dimethylbutene, **1**, in various zeolite hosts resulted in the formation of several different radical species. In zeolite Na-Y only the monomer radical cation, $1^{\bullet+}$, was observed^{351,370} (which was also produced without radiation).^{189,204} In contrast, the neutral 2,3-dimethylbutenyl radical, **3**[•], was formed in zeolite Na-X, apparently by proton transfer to the alkene (in a π -dimer radical cation). In Na-ZSM-5, the π -dimer, $2^{\bullet+}$, and, possibly, higher aggregates were reported in addition to $1^{\bullet+}$ and **3**[•].³⁷⁶ The monomer radical cation showed a well-resolved spectrum in silicalite (9 of 13 lines are clearly detected). The more complex spectrum of the dimer radical cation is clearly observed in silicalite, but the spectra in pentasil zeolites have a much greater line width, apparently due to interaction with the zeolite host and the resulting reduced mobility.



The observed difference between zeolites X and Y are quite interesting.³⁵¹ The topologies of these zeolites are identical; they differ only in their Si:Al ratios. Zeolites Na-X (Si/Al = 1.23) and Na-Y (Si/Al = 2.3) contain 9 and 5 sodium ions per cage, respectively. The deprotonation of $1^{\bullet+}$ generating **3**[•] was ascribed to an ion–molecule reaction; its advent in zeolite Na-X was explained as a consequence of an enhanced mobility of radical cations due to “larger electrostatic and steric factors”.

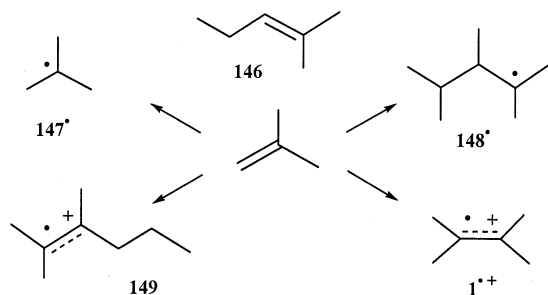
Radiolysis of 2,3-dimethyl-1-butene, **11**, or the 3,3-isomer, **8**, in ZSM-5 generated the spectrum of 2,3-dimethyl-1-butene radical cation, $1^{\bullet+}$, without a preceding radical cation.³⁷⁷ Although no paramagnetic species were detected in the zeolite before radiolysis, acid-catalyzed rearrangement of the alkenes cannot be excluded; in fact, they are very likely.^{370,378}



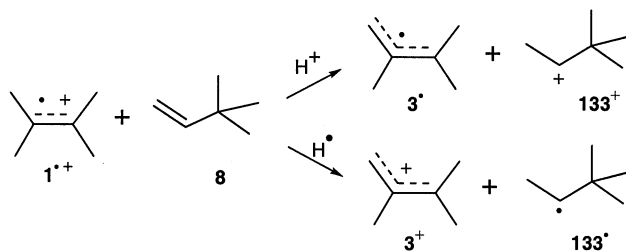
Piocos et al. studied the radiolysis of 2-methylpent-2-ene, **146**, after equilibration on acidic zeolites and on (catalytically inactive) Na-ZSM-5. On Na-ZSM-5, only the radical cation, $146^{\bullet+}$, was formed, whereas the reaction on H-ZSM-5 produced a rearranged radical cation, the familiar $1^{\bullet+}$, and the spectrum of

an unidentified species, "a multiplet with an even number of broader lines and slightly smaller spacing".³⁷⁸

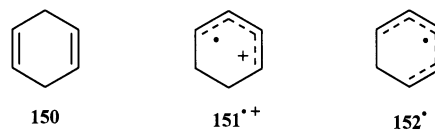
An analogous study of 2-methylpropene, **6**, adsorbed on H-ZSM-5 showed a gradual conversion to C₆, C₈, and larger products by a combination of oligomerization, isomerization, and fragmentations typical for Brønsted acid-catalyzed processes. Radiolysis of the resulting mixture generated two free radicals, 2-methyl-2-propyl (*tert*-butyl, **147**[•]) and 2,3,4-trimethyl-2-pentyl, **148**[•], and two radical cations, the ever-present **1**^{•+}, and 2,3-dimethyl-hex-2-ene radical cation, **70**^{•+}.³⁷⁸ As an aside, we recall that, on H-Mor, **6** gave rise to the dimethylhexadiene radical cation, **9**^{•+}, without requiring irradiation.²⁰⁶



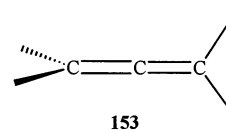
The conversion of radical cations to neutral radicals by ion molecule reactions (net deprotonation) may proceed by two pathways, either proton transfer from the radical cation to the neutral parent or hydrogen transfer from the substrate to the radical cation. Typically, the two mechanisms are indistinguishable because a reaction between a radical cation and its parent produces identical products regardless of the mechanism. The formation of **3**[•] from **1**^{•+} by an ion molecule reaction in the radiolysis of **8** led the authors to argue in favor of H⁺ transfer.³⁷⁷ However, in view of the significant (Brønsted) acid-catalyzed reactions established by Picos et al.,³⁷⁸ rearrangement of **8** prior to radiolysis cannot be excluded, indeed, must be expected. The rearrangement renders the competing mechanisms, once again, indistinguishable.



Cycloalkene radical cations generated by γ -radiation in cryogenic matrices also undergo rapid isomerization. For example, irradiation of cyclohexa-1,4-diene (**150**) produced the well-known^{379,380} ESR spectrum of cyclohexa-1,3-diene radical cation (**151**^{•+});³⁷⁷ only the more stable conjugated species is observed. Upon annealing the sample at 120 K, the spectrum changes to that of cyclohexadienyl (**152**[•]),¹⁶¹ formed in an apparent ion–molecule reaction.³⁷⁰



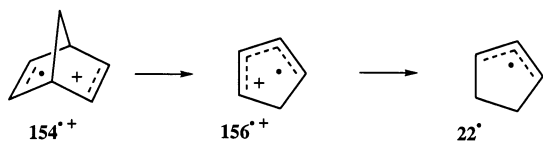
Radiolysis of 2,4-dimethylpenta-2,3-diene, **153** (tetramethylallene), in zeolite Na-Y gave rise to an ESR spectrum showing nine equally spaced signals (of 13 expected) with a Lorentzian line width of 6.0 G; **153**^{•+} is stable in the zeolite matrix (no ion–molecule reactions). The signal intensities deviate from the binomial pattern expected for a 12-proton system; the spectrum can be simulated by assuming hyperfine anisotropy, $A_{||} = 15.2$ G and $A_{\perp} = 14.0$ G.³⁸¹ This explanation requires that the motion of **153**^{•+} in zeolite Na-Y is restricted on the ESR time scale, not an unreasonable assumption in the restrictive zeolite environment.



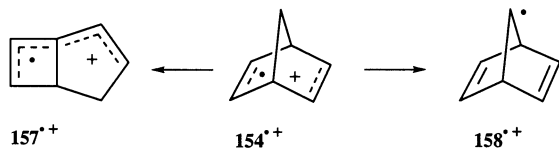
Interestingly, the corresponding isotropic hyperfine coupling ($A = 14.4$ G; in NaY) is significantly larger than coupling constants determined in chlorofluorocarbon ($A = 8.1$ G) or hydrocarbon matrices ($A = 11.3$ G). This finding may indicate significantly different twist angles for the allene radical cation in the different matrices; the wide range of the variation is unusual, indeed. AM1-UHF calculations show that the hyperfine coupling constants of **153**^{•+} increase monotonically with the twist angle, Θ . In view of the significant progress in ab initio methodologies and computing power during the past decade, a reinvestigation of this system appears desirable.

V.I.E Radical Cations of C₇H₈–Isomers

Barnabas, Trifunac, and co-workers investigated the fate of a series of C₇H₈ hydrocarbons: norbornadiene (**154**), quadricyclane (**155**), bicyclo[3.2.0]hepta-2,5-diene (**157**), and cycloheptatriene (**159**). First, γ -radiation of **154** or **155** in Na-ZSM-5 generated the same paramagnetic species ($A = 8.0$ G, 4H; $A = 3.0$ G, 2H);³⁸² these parameters are close to those of authentic **154**^{•+}.^{383,384} No evidence for the elusive radical cation, **155**^{•+}, was observed. Upon annealing at 200 K, the spectrum changed to one, whose splitting pattern ($A = 12.7$ G, 2H; $A = 2.7$ G, 2H)³⁸² identified the new species as cyclopentadiene radical cation, **156**^{•+}.^{167,379} The formation of **156**^{•+} from **157**^{•+} amounts to a retro-Diels–Alder cleavage, a symmetry forbidden process according to Bauld and co-workers.³⁸⁵ The authors explained the formation of **156**^{•+} by postulating "certain polar zeolite sites that stabilize higher electronic states of the radical cation".³⁸⁵ Alternatively, the high charge density in the zeolite pores may lower the activation barrier for the fragmentation. Finally, further heating to 260 K produced yet another spectrum ($A = 24$ G, 4H; $A = 14$ G, 2H),³⁸² identifying the newly generated species as cyclopentenyl free radical, **22**[•], which had been observed previously in matrix studies of **156**^{•+}.^{167,379}

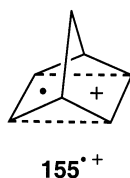


The radical cation, **154⁺**, arises also by radiolysis of **154** and **155** on silicalite, again without any evidence for **155⁺**; however, the fate of **154⁺** upon warming the sample is different. Annealing the sample at ~ 100 K caused limited conversion to an isomeric radical cation, **157⁺**. At higher temperatures, the norbornadien-7-yl radical, **158[•]**, was formed, presumably by an ion–molecule reaction.



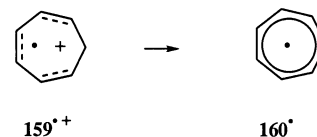
This interesting conversion involves transfer of a proton two C–C bonds removed from the nearest carbon with spin density, typically, protons adjacent to carbons of high spin density; they are acidic and have sizable positive hfc's. The bridge protons of **154⁺** are activated by homo-hyperconjugation, giving them significant hyperfine coupling and causing them to be acidic.^{375,383,384}

A third paper from the same laboratory provided additional details, e.g., more precise measurement of the hyperfine coupling constants, including the splitting of the tertiary hydrogens. Significantly, this paper claimed the first direct observation of the elusive radical cation, **155⁺**,³⁸⁶ a difference spectrum between two ESR traces recorded at 5 and 77 K was ascribed to **155⁺** because it was simulated approximately with hfc's calculated by ab initio methods. This claim is erroneous; the hfc's used for the simulation were calculated at the MP2 level of theory, which seriously overestimates spin densities and negative hyperfine coupling constants.^{375,387} The correct hyperfine pattern of **155⁺** was established in a CIDEP experiment by Ishiguro et al.;³⁸⁸ it was confirmed by measuring the spectrum of a bridge-monodeuterated derivative.³⁸⁸ More recently, the Argonne group was able to reproduce the ESR data of Ishiguro et al. in a zeolite.²⁰²



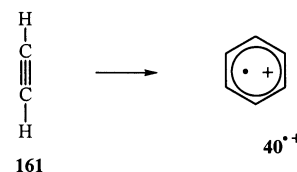
Radiolysis of cycloheptatriene, **159**, adsorbed on Na-ZSM-5 gave rise to the radical cation, **159⁺**, and its deprotonation product, the free radical, **160[•]**.³⁶⁵ The spectrum of **159⁺** is a triplet ($A_7 = 51.6$ G) of quintets ($A_{1,3,4,6} = 5.7$ G); this species is formed exclusively or preferentially in Al-poor zeolites. Upon annealing at $T > 200$ K, **159⁺** is converted to **160[•]** ($A = 4$ G, 7H). With increasing Al content, increasing fractions of the free radical, **160[•]**, were observed. Of

particular interest is the observation that the ratio of **159⁺** to **160[•]** increased with increasing substrate loading. This is the reverse of the dependence expected if an ion molecule reaction were responsible for the observed deprotonation.



VI.F Radiolysis of Ethyne

Radiolysis of ethyne, **161**, adsorbed on NaZSM-5 generated benzene radical cation, **40⁺**, apparently by ion molecule reactions of the ethyne radical cation. No monomer (C_2) or dimer (C_4) radical cations were observed, as the analogy with butyne may have suggested (Section V.A.2).³⁷⁸ These results are significant, not only because of the apparent “trimerization” of **161**, but also because **161** is the substrate with the highest oxidation potential that has been converted to a radical cation by radiolysis in a zeolite. The results establish a relatively high minimum energy for the oxidation-active sites generated upon radiolysis in the zeolite.

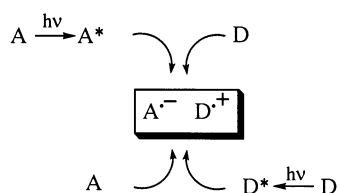


VI.G Radiolysis of Polynuclear Aromatics

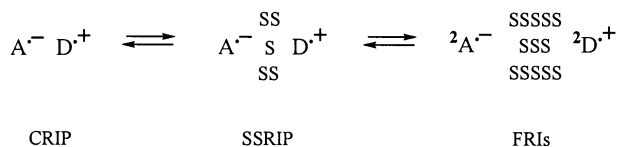
Naphthalene radical cation can be generated by UV- or X-irradiation in ZSM-5. The ESR powder spectrum combined with ENDOR techniques allowed the unambiguous assignment of the g tensor and the hf tensors for the two types of ring protons.³⁸⁹ The electronic spectra of **55⁺** also yielded significant insights. Hashimoto observed loading-dependent nanosecond time-resolved DR spectra following excitation of **55** in faujasite.³⁹⁰ A structured band (680 nm) at low loadings was assigned to the monomer radical cation, whereas a broad band (590 nm) at higher loading was assigned to the dimer radical cation. This assignment is supported by a broad charge resonance (CR) band in the near-IR (~ 1100 nm). The dimer was formed inside the zeolite and was assigned a “twisted” structure with partial overlap of the two π -systems.

Irradiation of **56** in zeolite Y gave rise to a sharp anisotropic powder spectrum, $g = 2.002$, typical for an organic radical species,³⁹¹ without specific identifying features. Exposure of **57** and a chloro-derivative to ionizing radiation on silica/alumina gave rise to an ESR spectrum showing three features. A broad line (fwhh ~ 50 G), $g = 2.0067$, was assigned to a “reactive site” generated in the zeolite; this feature was also observed in the absence of pyrene. A narrower line (fwhh ~ 20 G), $g = 2.0027$, was identified as an anisotropic (powder) spectrum of **57⁺**. Finally, two sharp lines (fwhh = 1.2 G, $A = 508$ G), which vanish upon annealing, are readily ascribed to H^{\cdot} .³⁹²

Scheme 15



Scheme 16



VII. Photochemical Generation of Radical Cations in Zeolites

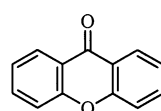
Photoinduced electron transfer (PET) between a donor (D) and an acceptor (A) is a general method for the generation of organic radical ions. Excitation of D or A generates an electronically excited state, D^* or A^* , respectively. Because excited states are more strongly oxidizing as well as reducing than ground states, they readily undergo ET, D^* to A or D to A^* (Scheme 15).

In solution, electron transfer generates either contact radical ion pairs (CRIP) or solvent ("S") separated radical ion pairs (SSRIP). Such pairs can undergo either back electron transfer (BET), a fast *in-cage* reaction regenerating typically the reagent ground states, or diffuse apart forming "free" ions (Scheme 16). The polarity and/or viscosity of the solvent play crucial roles in the forward ET as well as in the balance between BET and forward pathways.

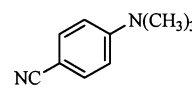
The thermodynamics and kinetics of PET reactions in solution are well understood; comprehensive reviews cover all aspects of these reactions.^{229,393–396} In heterogeneous media, including zeolites, significant advances in PET efficiency and selectivity are still being achieved.³⁹⁷ The highly polar interiors and the strong electrostatic fields (Section II.A) favor PET in zeolites relative to nonpolar solvents; the resulting transients have special features arising from limited diffusion and the protection from external reagents. Because zeolites do not absorb above ~ 240 nm, the organic guests can be excited readily.

The polarities of some zeolites have been calibrated using the xanthone (**162**) triplet state as a probe.^{398,399} These experiments suggest that the interior of NaX, NaY compares to a 70:30 mixture of water–methanol. Other probes (*p*-(dimethylamino)-benzonitrile, **163**, pyrene-1-carbaldehyde, **164**) suggest a dielectric constant of 44 D for NaY supercages.⁴⁰⁰ These data are macroscopic averages, as the distribution of sites within zeolites is nonuniform. A more recent study using pyrene-1-carbaldehyde, Nyle red, and coumarin-500 suggests that the supercages of zeolites X and Y are superpolar in the total absence of water.⁴⁰¹

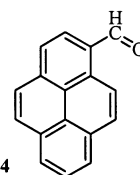
The polarity and acidity/basicity of dehydrated zeolites varies with their composition (Section II.B.2).^{75,76,402} Hydration plays a major role; water



162



163



164

molecules occupy a range of different environments in the pores; those solvating the charge-balancing cations are strongly adsorbed, difficult to evacuate, and easily regained. Residual water can alter the photophysical properties of guests, the lifetime of their transients, or their interaction with quenchers. Hydration of a zeolite can cause relocation of the less polar organic guest toward the external surface.⁴⁰³

In solution, geminate radical ion pairs have lifetimes well below milliseconds; free ions can live orders of magnitude longer. However, in zeolites their lifetimes are dramatically increased.⁴⁰⁴ Kochi and co-workers found that excitation of CT complexes between naphthalene or anthracene and viologens or tropylium ion, respectively, in zeolite Y generated transient spectra of radical cations and radical/radical anions, with microsecond lifetimes. In acetonitrile, the corresponding transients decayed within picoseconds (Table 8). The increase in lifetime in the

Table 8. Lifetimes of Photoinduced Radical Ion Pairs Generated from Selected CT Complexes in Acetonitrile Solution and within NaY Zeolite^a

donor	acceptor	lifetime	
		CH ₃ CN (ps)	zeolite NaY (μs)
naphthalene	methyl viologen	30	6.8
	tropylium	25	3.3
	<i>p</i> -CN- <i>N</i> -methylpyridinium	25	0.11
anthracene	methyl viologen	19	6.4
	tropylium	25	4.2
	<i>p</i> -CN- <i>N</i> -methylpyridinium		3.9
9-methylanthracene	methyl viologen	28	5.6

^aFrom ref 404.

zeolite by 6 orders of magnitude corresponds to a stabilization of the radical cations by ~ 8 kcal \times mol⁻¹.

In special cases, even longer-lived transients may be observed. Photolysis ($\lambda < 310$ nm) of a donor–acceptor diad (1,4-dimethoxynaphthalene linked to a dicyanovinyl acceptor) within Al/MCM-41 gave an ESR signal due to a dicyanovinyl type radical anion, which persisted in the dark (≥ 1 d; Section IX).⁴⁰⁵

VII.A Zeolites as Inert Media: ET between Donor and Acceptor Guests

PET reactions within zeolites fall into three classes; the zeolite may serve as: (i) an inert medium for ET between donor and acceptor; (ii) an electron acceptor toward organic donors; and (iii) an electron donor toward organic acceptors.

Aryl ketones are widely used as energy transfer (EnT) photosensitizers in solution. Within zeolites,

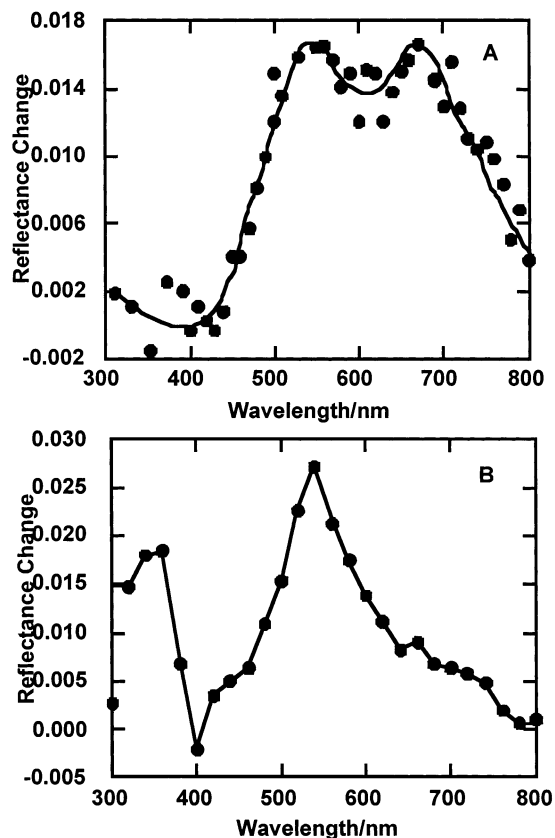


Figure 18. Transient DR spectra of 4-aminobenzophenone in HY (A) and HZSM-5 (B) 0.6 μ s after 266-nm laser excitation. Spectrum B is identical with that from an authentic sample of the chlorohydrate salt of 4-aminobenzophenone. Reprinted with permission from ref 132. Copyright 1996 American Chemical Society.

they serve as EnT as well as ET sensitizers.^{406–408} For example, the 4-aminobenzophenone-sensitized reaction of 1,3-cyclohexadiene (**151**) in H-ZSM-5 forms [2+2] dimers via EnT, but [4+2] dimers via ET;¹³² no acid-catalyzed dimerization was observed;⁴⁰⁹ the distribution of [2+2] versus [4+2] adducts was used to judge the extent of the competing mechanisms.⁴⁰⁹

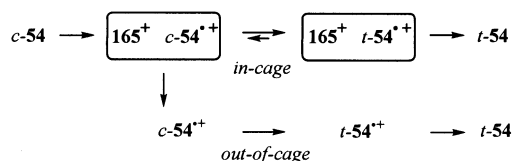
Protonated 4-aminobenzophenone was identified as the actual photosensitizer because it predominates inside H-ZSM-5 (Figure 18).¹³² In agreement with the different distributions of cyclohexadiene dimers derived from competing EnT and ET mechanisms, incorporation of 4-aminobenzophenone into H-Y and H-ZSM-5, respectively, generated two different excited states, as shown by time-resolved diffuse reflectance spectroscopy (Figure 18).

VII.A.1 2,4,6-Triphenylpyrylium Ion as Electron Acceptor

Salts of 2,4,6-triphenylpyrylium ion (**165**⁺) with BF₄⁻ or ClO₄⁻ counterions are good ET photosensitizers in solution.^{406,410} The ion **165**⁺ fits into the zeolite Y supercage (~1.3 nm), but is too large to be incorporated through the openings (~0.74 nm).

However, **165**⁺ can be synthesized in zeolite H-Y by condensation of acetophenone with benzaldehyde on Brønsted acid sites;⁴¹¹ once formed, it remains immobilized inside the cavities. Similar (“mechani-

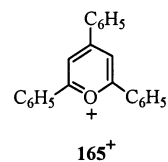
Scheme 17



cal”) immobilization also occurs in supramolecular assemblies such as catenanes and rotaxanes.

Although the H-Y zeolite used for the ship-in-a-bottle synthesis is strongly acidic when it is thermally dehydrated, the strongest acid sites are being replaced (poisoned) by **165**⁺ as it is being formed. Pyridine titration of **165**⁺ within zeolite Y (“**165**⁺@Y”) after the ship-in-a-bottle synthesis reveals a remarkable decrease in the intensity of the bridging ≡Si(OH)–Al≡ acid groups.⁴¹¹ This decrease is a strong argument for the internal location of the resulting **165**⁺.⁴¹¹ On the other hand, fully hydrated **165**⁺@Y should not be strongly acidic at room temperature. No spontaneous generation of organic radical cations upon adsorption of organic compounds on hydrated **165**⁺@Y has ever been observed.

The engaged **165**⁺@Y is a heterogeneous ET photosensitizer for the isomerization of *cis*- to *trans*-stilbene⁴¹¹ or the PET-promoted cyclodimerization of 1,3-cyclohexadiene.⁴¹² These reactions of **165**⁺@Y were compared with homogeneous PET reactions of **165**⁺.



The **165**⁺-photosensitized isomerization of *cis*-stilbene, **c-54** ($n = 1$), to *trans*-stilbene is initiated by ET, generating **c-54**^{•+} ($n = 1$) paired with pyrylium radical (**165**[•]). The isomerization can occur in the geminate pair or, after escape of **c-54**^{•+}, in free ions (Scheme 17). Addition of azulene suppresses the *out-of-cage* pathway in solution, but does not affect the *in-cage* isomerization; thus, the individual contribution of the two pathways can be determined. In solution, isomerization occurs mainly out-of-cage because geminate pairs readily diffuse apart. In zeolite Y, diffusion is retarded, favoring *in-cage* isomerization, although at lower conversion.⁴¹¹ The larger pore size of MCM-41 (2.5 nm)⁴¹³ facilitates diffusion: the **165**⁺-sensitized isomerization in MCM-41 proceeds by *in-cage* and escape pathways with higher overall efficiencies than in solution (Figure 19).⁴¹¹

165⁺ also cyclodimerizes **151** with good efficiencies in MCM-41 or zeolites Y or LaY (Table 9).⁴¹² However, conversion and selectivity are less favorable than with **165**⁺ salts in solution. Dibenzotropylium cation (**48**, Q CH=CH) in ZSM-5 also induced the photodimerization, but with noticeably lower selectivity.⁴¹²

Although sparingly soluble in water, **165**⁺ BF₄⁻ undergoes complete hydrolytic ring opening within minutes, precluding its use in aqueous media. How-

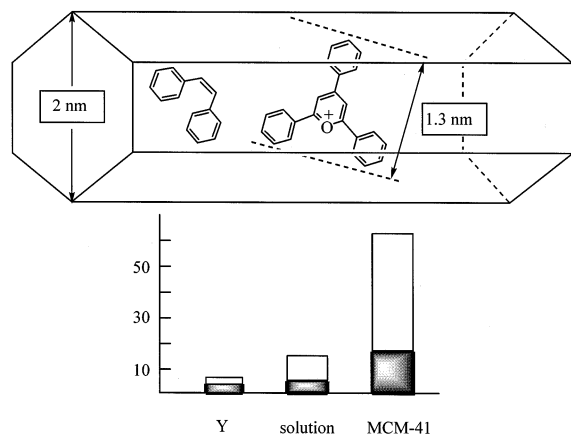


Figure 19. Top: schematic representation of 165^+ and *cis*-54 inside mesoporous MCM-41. Bottom: efficiency of isomerization of *cis*-54 in CH_2Cl_2 sensitized by 165^+ in solution (165^+BF_4^-) and in zeolites Y and MCM-41, divided into *in-cage* (dark) and *out-of-cage* contributions (light) (Adapted from ref 413. Copyright 1994 American Chemical Society).

Table 9. PET Cyclodimerization of 1,3-Cyclohexadiene in Homogeneous Phase (165^+BF_4^-) or by Selected Zeolite-Bound Sensitizers^a

sensitizer	conversion (%)	product distribution (%)		
		[4+2]-endo	[4+2]-exo + [2+2]-anti	[2+2]-syn
165^+BF_4^-	>98	88	12	trace
$165^+ @ \text{Y}$	3	60	34	6
$165^+ @ \text{LaY}$	1	44	48	8
$165^+ @ \text{MCM-41}$	28	68	28	4
48 (CH=CH) ZSM-5	20	32	58	10

^a From ref 412.

ever, 165^+ is persistent in zeolite Y; its DR UV-Vis spectra remained unchanged for months. The stability was explained by molecular modeling: the rigid zeolite lattice impedes nucleophilic attack of H_2O or OH^- on the pyrylium ring, since this would force one phenyl ring out of plane, a change that is apparently precluded in the available space of the Y supercage.

The persistence of $165^+ @ \text{Y}$ in aqueous suspensions allowed the study of its photochemistry in water. Irradiation of $165^+ @ \text{Y}$ generated OH^\bullet radicals via H_2O^+ ,⁴¹⁴ or built up a stationary concentration (2×10^{-2} M) of H_2O_2 . The resulting OH^\bullet radicals were trapped by a wide range of substrates and utilized for the photocatalyzed degradation of pesticides, such as 4-chlorophenoxyacetic acid, **166**,⁴¹⁵ methyl parathion, **167**,⁴¹⁶ propoxur, **168**,⁴¹⁷ and fenvalerate, **169**.⁴¹⁸ Solar irradiation of $165^+ @ \text{Y}$ caused significant degrees of mineralization, comparable to those caused by TiO_2 under similar conditions.

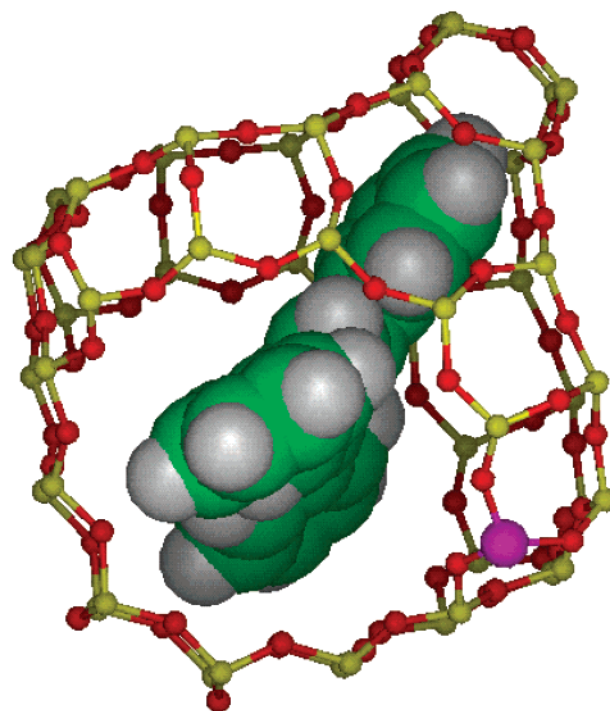
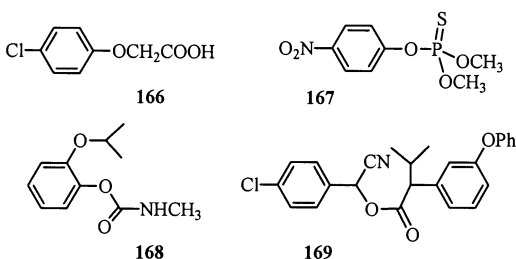


Figure 20. Molecular modeling of the bifunctional photocatalyst, 165^+ in zeolite Y containing a Ti atom (shown purple); 165^+ acts as light harvester, the Ti atom as active site for the hydroperoxide epoxidation. H. Garcia, unpublished; cf. ref 421.

The eventual deactivation of $165^+ @ \text{Y}$ is not due to degradation of 165^+ , but to the blockage of pores by products or adventitious impurities. Therefore, up to 75% of the initial activity can be recovered by solid-liquid extraction of deactivated $165^+ @ \text{Y}$ with CH_2Cl_2 ,⁴¹⁶ making $165^+ @ \text{Y}$ one of the most robust organic photocatalysts.⁴¹⁴

The activity of 165^+ within zeolites can be increased further by combining its ability to generate OH^\bullet and H_2O_2 upon visible light irradiation with the catalytic activity of Ti atoms in the zeolite framework. Ti-containing zeolites are highly active heterogeneous catalysts for the epoxidation of alkenes with H_2O_2 or organic hydroperoxides as oxidizing reagents.^{419,420} A bifunctional photocatalyst, with 165^+ as antenna and framework Ti atoms in zeolite Beta as epoxidation sites (Figure 20), caused dihydroxylation of cyclohexene with water/ O_2 .⁴²¹

The efficiencies and selectivities of homo- (165^+BF_4^-) and heterogeneous ($165^+ @ \text{Y}$) photolyses were compared for the PET rearrangement of bicyclo[2.1.0]pentanes (housanes) to cyclopentenes; both reactions gave similar product distributions. The photolysis with $165^+ @ \text{Y}$ proceeded more slowly and with slightly lower yields than that with 165^+BF_4^- in solution (Table 10).⁴²²

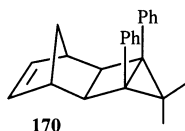
The reduced yields in the zeolite are ascribed to light scattering and the slow diffusion of the substrates through the zeolite lattice. Large housanes, e.g., 4,4-dimethyl-3,5-diphenyl-*endo*-tetracyclo[5.2.1.0.2.6]dec-8-ene (**170**), are size-excluded from zeolite Y and fail to rearrange upon $165^+ @ \text{Y}$ irradiation.

Table 10. Products of the Chemical and Photochemical Electron Transfer Reactions of Housanes in Solution and within Zeolite Cavities^b

Substrate	Sensitizer ^a / Chemical promoter	t (min)	conv (%)	mass balance (%)	Product distribution (%)	
	165 ⁺ BF ₄ ⁻	30	11	1	100	
	165 ⁺ @Y	60	12	90	100	
	TDA	1	100	75	100	
	165 ⁺ BF ₄ ⁻	5	23	26	100	
	165 ⁺ @Y	15	7	41	33	67
	TBA	1	100	89	100	
	DCA/Ph ₂	10	31	60	77	23
	165 ⁺ BF ₄ ⁻	20	36	57	78	22
	165 ⁺ @Y	30	18	40	95	
	TBA	1	100	40	100	

^a TDA: tris(2,4-dibromophenyl)aminium hexa-chloroantimonate; TBA: tris(4-bromophenyl)aminium hexachloroantimonate. ^b From ref 422.

The photoinduced rearrangement of housanes was less efficient than the conversion by catalytic amounts (2–10 mol %) of triarylamminium salts,⁴²² which formed cyclopentenenes with complete conversion and high mass balance via a chain mechanism. The lower efficiency of 165⁺@Y can be ascribed to the retarded diffusion in the micropores, which would render the propagation steps inefficient.



VII.A.2 Cyanoaromatics and Nitrogen Heterocycles as Acceptors

Electron-transfer quenching in zeolites was also studied for various other acceptors. The fluorescence intensity of excited-singlet acceptors (cyanoaromatics, **171**–**173** or ionic *N*-methyl nitrogen heterocycles, **174**, **175**) inside NaX was reduced significantly by arylalkenes, **52**, **116**, and **176**–**178**, whereas the fluorescence lifetimes showed only minor changes.⁴²³

Laser flash photolysis (355 nm) of these sensitizers on NaX containing arylalkenes revealed two competing reactions: ET from an arylalkene in the same supercage, forming radical ion pairs, or photoionization, generating radical cations and trapped electrons. Increased arylalkene loadings favor ET quenching. Strong radical cation signals and half-lives > 10 μs indicate that BET is orders of magnitude slower than in solution (nanosecond half-lives; low cage-escape yields).

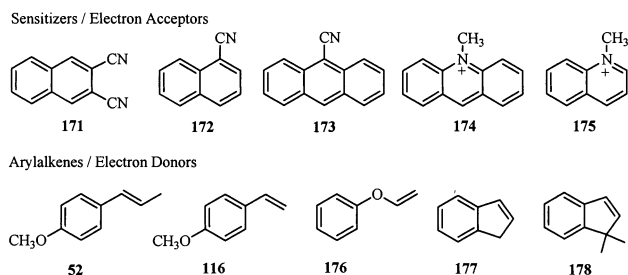
The preparative photochemistry of sensitizer–aryllkene pairs inside NaX yielded mostly cyclobutane [2+2] dimers. The dimers were stable under the reaction conditions; their ratio was independent of the sensitizer. The dimers, and minor yields of oxygenation products for anethole (**52**) or vinylanisole

Table 11. Dimer Ratio in the PET Sensitized Dimerization of Selected Alkenes within NaX Zeolite^a

Conditions	Dimer ratio (%)	
CH ₃ CN, sensitizer	4	96
NaX, 171	66	33
NaX, 172	45	55
NaX, 174	55	45
CH ₃ CN, sensitizer	55	45
NaX, 171	55	45
NaX, 173	65	35
NaX, 174	70	30
NaX, 175	63	37
CH ₃ CN, sensitizer	>95	
NaX, 171	>95	
NaX, 173	>95	
NaX	>95	

^a From ref 423.

(**116**) (Table 11), support arylalkene radical cations as intermediates.⁴²³

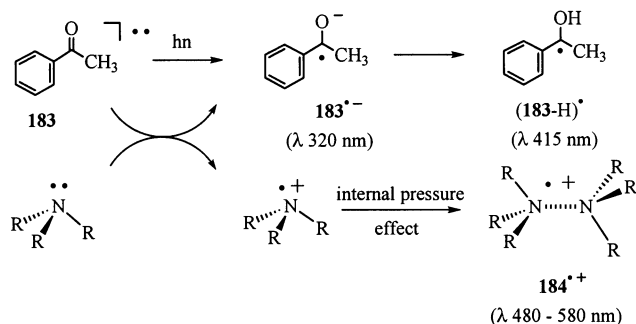


Experiments at different degrees of conversion and loading levels suggested that the dimer reflect the spatial constraints of the zeolite: the rigid supercages favor products of similar molecular shapes, in this case, the cis head-to-head dimers. Triarylmethyl cations also are heterogeneous ET photosensitizers; they dimerize 1,3-cyclohexadiene (**151**) with high selectivity (>80%). The predominant [4+2] dimer supports ET as the major pathway; minor yields of [2+2] dimers suggest some EnT.⁴²⁴

VII.A.3 Acetophenone as Acceptor vs Aliphatic Amines

Irradiating acetophenone, **183**, with aliphatic amines inside NaY generated amine dimer radical cations.⁴²⁵ In solution, only ³**183** (λ_{max} 310 nm) and

Scheme 18



183^{•-} (λ_{max} 445 nm) were detected; aliphatic amine radical cations absorb outside the working range of available photomultipliers. However, dimeric species, formed in a zeolite specific reaction (Scheme 18), are detectable (480–580 nm; Figure 21).⁴²⁶ The confinement and the limited diffusion favor interaction between a radical cation and a neutral amine in the same cavity ("internal pressure effect"). Such effects were invoked also to explain viologen–arene complexes (Section VII.B).^{427,428} The existence of amine dimer radical cations is supported by the formation of hydrazines when irradiating **183**/N(CH₃)₃ in NaY.⁴²⁵ The amine dimer radical cations are σ-dimers. Other (π-) types of dimer radical cations, derived from benzene or 2,3-dimethylbutene, were discussed in Section V.

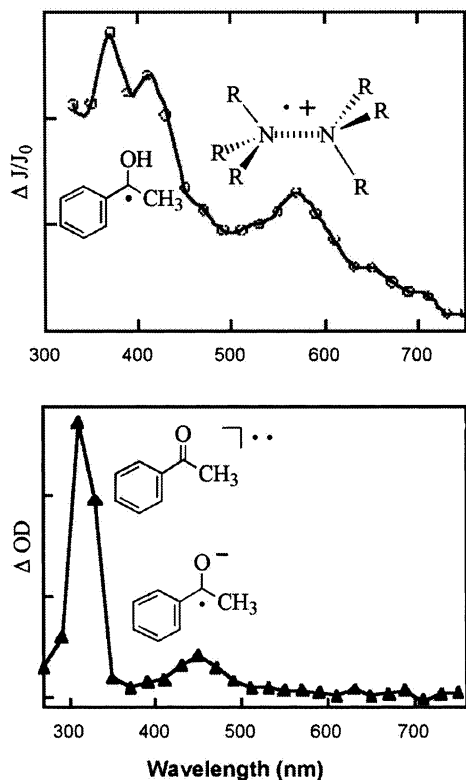
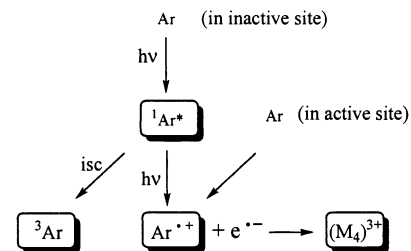


Figure 21. (top) Transient DR spectrum 10 μs after 308 nm excitation of **183**/1,4-diaminobutane in NaY, showing **183-H^{•+}** and the dimer radical cation, **184⁺**; (bottom) UV-Vis spectrum 1 μs after excitation (337 nm) of **183**/N(CH₂CH₃)₃ in CH₃CN-H₂O showing **183^{•-}** and **183^{•+}**. Adapted from ref 425. Copyright 1997 Elsevier Science.

Scheme 19



VII.B Zeolites as Single Electron Acceptors: Photoionization inside Zeolites

Spontaneous radical cation formation (Section V) identifies zeolites as electron acceptors of moderate strength. Photoexcitation of guest molecules facilitates ET from guests for which the oxidative strength of the zeolite is insufficient. In this section, we discuss substrates whose photoreactions proceed, at least in part, by ET to the zeolite.

VII.B.1 Photochemistry of Aromatics in Zeolites

Thomas and co-workers studied the photophysics of aromatics in zeolites.^{429,430} Laser flash photolysis (337 nm) of anthracene (**56**) or pyrene (**57**) in dehydrated, alkali ion-faujasites produced triplet states (**356^{*}**: λ_{max} 420 nm; **357^{*}**: 415 nm), radical cations (**56^{•+}**: λ_{max} 720 nm; **57^{•+}**: 450 nm), and Na₄³⁺ (λ_{max} ~ 550 nm) or Li₄³⁺ clusters (λ_{max} ~ 620 nm) for zeolites X and Y.

Molecular oxygen scavenged triplet states and alkali radical cation clusters, resulting in simpler spectra (Figure 22).¹⁰¹ O₂ also quenched **157^{*}** (*k_q* = 1.32 ± 0.05 × 10⁷ Torr⁻¹ s⁻¹ in zeolite NaX),⁴²⁹ reducing its lifetime (τ ~ 0.3 ns, 300 Torr O₂) to a value much shorter than the laser pulse (10 ns). The dependence of **57^{•+}** yield on O₂ pressure and laser pulse power showed mono- and biphotonic contributions (cf., Scheme 19).⁴²⁹

Aromatic hydrocarbons adsorbed on active sites may undergo single-photon ionization. Although there is no spectroscopic evidence for ground-state CT complexes between aromatics and electron acceptor holes or active sites in the zeolite, their existence cannot be ruled out. Aromatics in non-active sites require a second photon to form radical cations;⁴²⁹

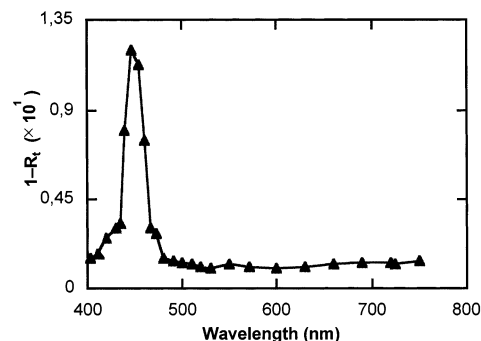


Figure 22. Transient DR spectrum (percent absorption, 1 - R_t) after excitation (337 nm) of **57** in dehydrated NaX (300 Torr O₂), showing **57^{•+}** (450 nm). Triplet **57** and trapped electron are quenched by O₂. Reprinted with permission from ref 101. Copyright 1991 American Chemical Society.

Table 12. Absorption Maxima (λ_{Max}) and Lifetimes for Biphenyl Radical Cation ($42^{+\bullet}$) and Trapped Electrons upon Photolysis of **42 in ZSM-5 Zeolites of Unit Cell Formula $M_6[Al_6Si_{90}O_{192}]^a$**

counterion M^+	biphenyl radical cation, $42^{+\bullet}$		trapped electron	
	wavelength (nm)	lifetime (min)	wavelength (nm)	lifetime (min)
Na^+	370, 670	155	450, 480	17
K^+	370, 670	44	448, 462	4
Cs^+	370, 670	<2	470, 510	131

^a From ref 433.

the biphotonic pathway can be quenched by O_2 . The time elapsed between arene incorporation and laser flash experiment may be relevant for the larger aromatics (pyrene, $0.72 \times 1.3 \text{ nm}^2$), whose migration/relocation inside faujasite micropores (0.74 nm) may require weeks, depending on incorporation and storage conditions.⁴³¹ Laser flash photolysis of naphthalene or *p*-terphenyl in NaX, NaY, or silicalite mainly formed triplet states; radical cations played a secondary role.⁴³²

Likewise, photolysis (248 nm) of biphenyl (**42**) in all-silica, nonacidic Na^+ , K^+ , or Cs^+ -ZSM-5 generated short-lived triplets (λ_{max} 355 nm) and longer-lived radical cations (λ_{max} 380, 660 nm), identified by time-resolved or steady-state DR, Raman and ESR spectra.⁴³³ The triplet state predominated at low laser power and, thus, was assigned to a monophotonic process; radical cation formation was ascribed to a biphotonic process. In all-silica or low framework Al zeolites geminate recombination dominates the deactivation.

The lifetimes of $42^{+\bullet}$ and trapped electron increased dramatically, from minutes to hours, at framework Al content ≥ 6 Al per 96 T atom unit cell (T = Si or Al) with Na^+ or K^+ counterions, decreasing with counterion radius (Table 12). Radical cation and trapped electron decay independently; $42^{+\bullet}$ may decay via ET from the host, creating positive holes in the zeolite. However, no spectroscopic evidence for electron donor sites was obtained.⁴³³

The trapped electrons also showed λ_{max} shifts. Still, their nature remains unclear; ESR spectra failed to support $M_n^{(n-1)+}$ metal clusters (no characteristic fine structure). On the other hand, $M_n^{(n-1)+}$ clusters were detected in faujasites (UV-Vis).⁴³⁴ The different results reflect the lower M^{n+} content per unit weight of highly dealuminated ZSM-5 samples compared to X or Y zeolites. For comparison, radiolysis of bare ZSM-5 with low Al content failed to generate stable electron-hole pairs,^{200,337} but γ -irradiation of Na^+ faujasites (Si/Al ratios 1.8–2.1) generated relatively stable holes; electrons were trapped as $Na_n^{(n-1)+}$ clusters.⁴³⁵

Cyanoaromatics are excellent electron acceptors; their irradiation in zeolites containing electron donors generated radical anions (Section VII.A.2). Interestingly, irradiation of cyanoaromatics in NaX generated radical cations (λ_{max} 380–450 nm) plus electrons, partly trapped as Na_4^{3+} clusters ($\lambda_{\text{max}} \sim 560 \text{ nm}$).⁴²³ The radical cation signals are quite weak relative to Na_4^{3+} . However, residual CH_2Cl_2 (the

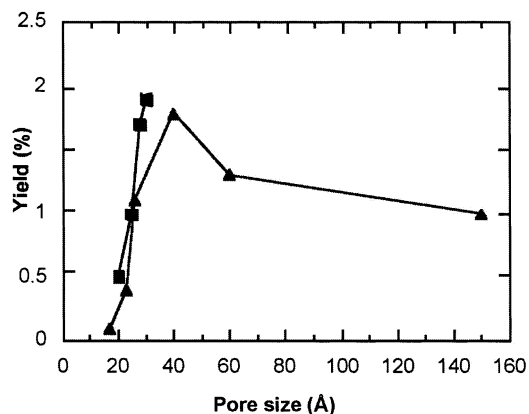


Figure 23. Influence of pore size on the yield of radical cation formation from *meso*-tetraphenylporphyrin (**185**) on porous silica gel (▲) or MCM-41 (■). Reprinted with permission from ref 437. Copyright 1997 American Chemical Society.

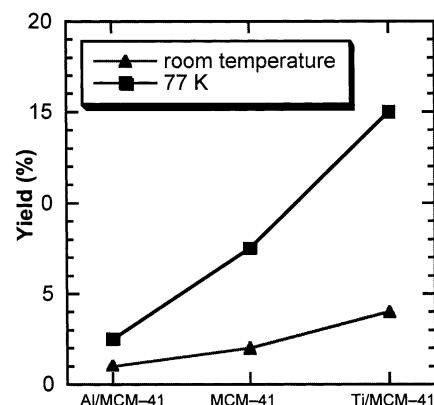


Figure 24. Radical cation yield at room temperature (▲) or 77 K (■) upon irradiation of *meso*-tetraphenylporphyrin (**185**) adsorbed on Al/MCM-41, all-silica MCM-41 and Ti/MCM-41 under equivalent conditions. Reprinted with permission from ref 437. Copyright 1997 American Chemical Society.

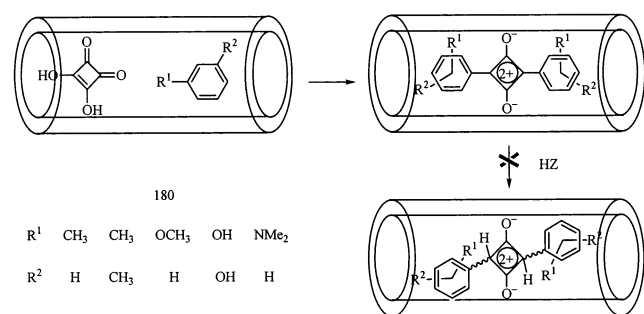
solvent used for incorporation) is an efficient electron scavenger, allowing the cyanoaromatic radical cations to be observed. Radical anions were generated also in acetonitrile at high laser fluencies.⁴³⁶

VII.B.2 Photoionization of *meso*-Tetraphenylporphyrin

Photoionization of *meso*-tetraphenylporphyrin (**185**) free base inside MCM-41, Al/MCM-41, Ti/MCM-41, or porous silica with visible light ($\lambda > 350 \text{ nm}$) at $77 \text{ K} < T < 300 \text{ K}$ gave rise to a persistent porphyrin π -radical cation. The yield (ESR) was highest in in the zeolite with intermediate pores, MCM-41 (33-Å), and decreased for smaller as well as larger pores (Figure 23). The minimum pore size to include the porphyrin was $\sim 23 \text{ Å}$. The decreasing yields of $185^{+\bullet}$ in large pore zeolites were ascribed to faster decay due to higher mobility.⁴³⁷

The yield of $185^{+\bullet}$ increased in the order Al/MCM-41 < MCM-41 < Ti/MCM-41 (Figure 24). The surprisingly low efficiency of the Al-zeolite (Al forms strong acceptor sites) may be due to partial protonation of **185** by the zeolite: the DR spectrum showed, in addition to **185**, a diprotonated species, $185-H_2^{2+}$, which should be difficult to ionize.⁴³⁷ Higher yields of $185^{+\bullet}$ in Ti/MCM-41 were ascribed

Scheme 20



to Ti^{IV} acceptor sites; the easier reduction of Ti^{IV} vs Si^{IV} should lower the decay rate of **185**^{•+}. However, Ti^{III} was not detectable by ESR.

VII.B.3 Photochemistry of Squaraines

The case of squaraines illustrates the utility of zeolites as matrices stabilizing elusive compounds and controlling their photochemistry. These dyes are widely used in photoprinting and photolithography to capture light and create the charge separation reproducing the illuminated image.⁴³⁸ The electron deficiency of the formally dipositive cyclobutenediyl core makes it prone to nucleophilic additions. Therefore, only squaraines with strong electron donor groups (dialkylamino-) in the para- and/or ortho-positions of the aryl substituents had been synthesized.

Acid zeolites as heterogeneous catalyst/hosts made it possible to prepare simple squaraines (**186**, 1,3-ditolyl-, 1,3-di-*m*-xylyl), not accessible previously. 1,3-Ditolyl- and 1,3-*m*-dixylylsquaraines were persistent in mordenite or ZSM-5; the tight fit in the ZSM-5 framework precludes nucleophilic additions to the cyclobutenediyl core (Scheme 20).⁴³⁹ They were characterized in zeolite Y, mordenite, or ZSM-5 by DR UV-Vis, FT-Raman and solid-state ¹³C NMR.

Irradiation of squaraines in solution generated triplet states and radical cations,^{440,441} characterized by UV-Vis spectra and their reactivity toward molecular oxygen; O₂ quenches the triplet state, but does not affect the radical cation. The transient resulting from photolysis of squaraines depends on Al content and crystal structure: in HY (Si/Al 2.6) 1,3-di-*p*-anisylsquaraine gave rise to the radical cation, whereas in H-mordenite (Si/Al 10) the triplet state was formed (Figure 25).⁴³⁹ The difference was attributed to the enhanced electron acceptor ability of zeolites with increasing Al content.⁴³⁹ The transients were identified by comparison of the optical spectra with authentic solution spectra.

VII.B.4 Photochemistry of Aryl- and Diarylethylenes

Laser flash photolysis of *p*-substituted styrenes in NaY generated radical cations (time-resolved DR; Figure 26),^{344,423} as in polar solvents.⁴⁴²⁻⁴⁴⁵ The longer lifetime of radical cations in zeolites shows their ability to control back electron transfer. Inherently less stable radical cations (*p*-H) were stabilized more significantly than more stable ones (*p*-methoxy-, **116**^{•+}). In zeolites styrene radical cations have a narrow range of lifetimes, governed by spacial con-

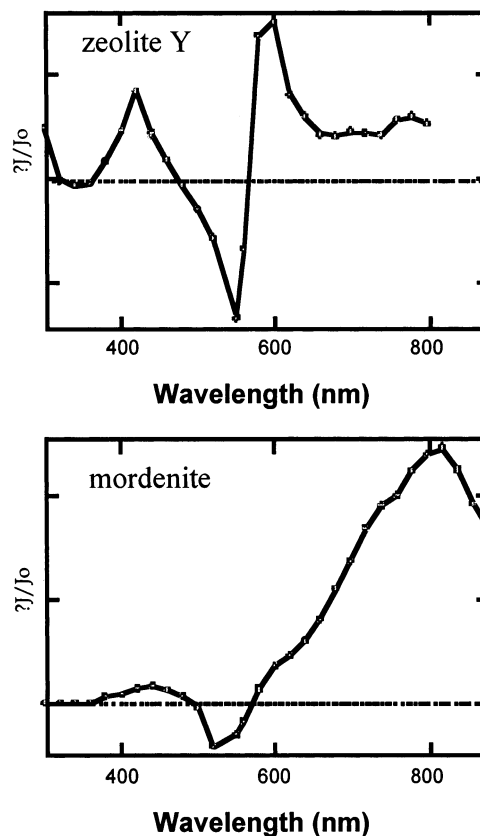


Figure 25. Transient DR spectra (355-nm laser excitation of **186**, R¹ = OCH₃, R² = H) showing radical cation, **186**^{•+}, (Y) or triplet state, ³**186**^{*}, (mordenite). Reprinted with permission from ref 439. Copyright 1997 American Chemical Society.

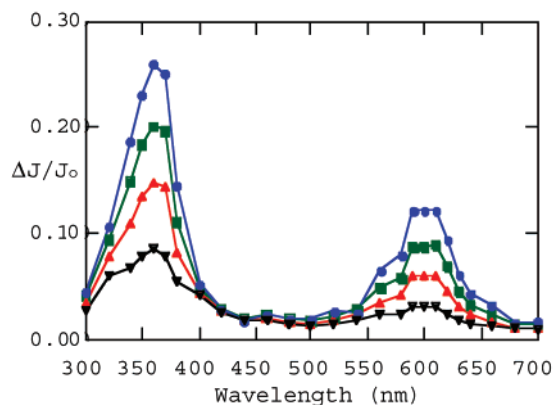
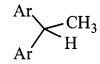
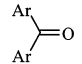
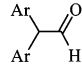


Figure 26. Decay of transient DR spectrum of an O₂ purged sample of 4-methoxystyrene in nonacidic NaY after 266 nm excitation. Enhanced from ref 444. Copyright 1994 American Chemical Society.

straints and slow diffusion, and independent of intrinsic stability, which governs the lifetimes in solution.⁴⁴⁴

The styrene radical cations can be formed only if the substrate remains unaltered by the zeolite. Incorporation of 4-methoxystyrene (**116**) or anethole (**52**) onto some NaY batches produced light colorations,³⁴⁴ ascribed to persistent 1,3-diaryllallyl cations (UV-Vis, Raman) formed via H⁺-catalyzed dimerization by residual acidity in "neutral" Na⁺-zeolite.^{344,446} Naturally, these effects are more pronounced in acid zeolites, especially H-ZSM-5.^{344-346,446}

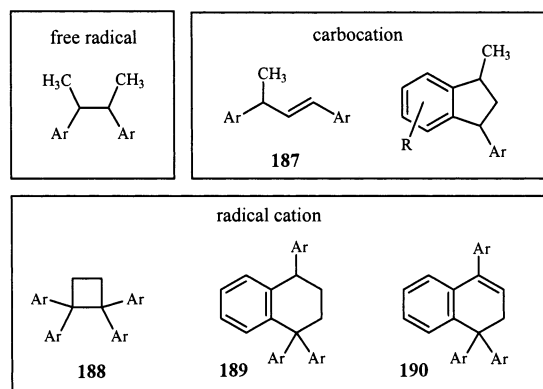
Table 13. Wavelength Dependent Yields upon Irradiation of 103-[(*p*-CH₃O)₂] Adsorbed on/within NaY in Aerated Hexane Slurries^a

Wavelength (nm)	Relative Yields (%)		
			
254	73	15	17
300	33	28	37
350	8	41	49
>400	–	49	51
>520	no reaction		

^aFrom ref 407.

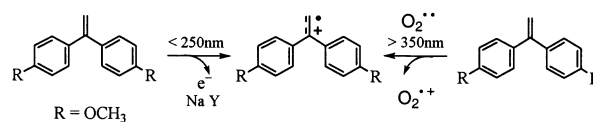
Styrenes or diarylethylenes can dimerize via intermediates, such as carbocations, free radicals, radical cations, and transition metal complexes. The nature of the products may reveal the active intermediate. Irradiation of diarylethylenes within NaY yielded mainly cyclobutane dimers (e.g., **188**),⁴⁴⁷ which may rearrange, subsequently, to aryltetrahydro- or arylidihydronaphthalenes (e.g., **189**, **190**). The results were ascribed to radical cations as key intermediates.

Interestingly, suspensions of *trans*-anethole in the presence of NaX afforded acid-catalyzed acyclic dimers of type **187** (45%) as well as the radical cation-derived *all trans*-cyclobutane dimer (55%; ~50% combined yield).⁴⁴⁸ In contrast, β -methylstyrene, which lacks the electron donating OCH₃ group, failed to dimerize efficiently on NaX (<5% conversion), in either the thermal or photoassisted reaction.⁴⁴⁸



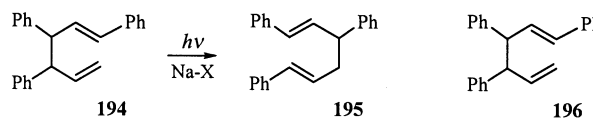
Direct irradiation of bis-(4-methoxyphenyl)ethylene, bis(*p*-CH₃O)-**103**, within NaY zeolite in aerated hexane slurries gave rise to 1,1-bis(4-methoxyphenyl)ethane, **191**, 4,4'-dimethoxybenzophenone, **192**, and 2,2-bis-(4-methoxyphenyl)acetaldehyde, **193**, in yields varying with the excitation wavelength (Table 13).⁴⁰⁷

No products were formed in the absence of oxygen. The radical cation, **103**^{•+}, was considered the key intermediate. However, the significant yields of the reduction product, **191**, suggest involvement of a (1,1-dianisylethyl) carbocation. Wavelength dependent changes in product distribution were ascribed to absorption of short wavelength light by the zeolite framework or longer wavelength light by superoxide

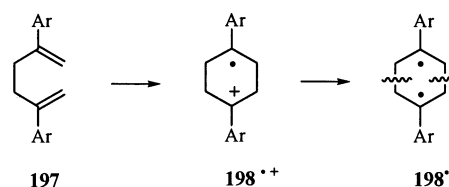
Scheme 21

radical anion (Scheme 21).⁴⁰⁷ This is consistent with the existence of hydrocarbon \cdot O₂ contact CT complexes (vide infra).

Irradiating suspensions of 1,3,4-triphenyl-1,5-hexadiene (**194**) in the presence of NaX caused smooth conversion to 1,3,6-triphenyl-1,5-hexadiene (**195**) (55%).⁴⁴⁹ The *erythro* form was converted considerably more slowly than the *threo*-diastereomer. The reaction required both light and zeolite ("photoassisted" Cope rearrangement); it did not occur upon heating NaX suspensions in CH₂Cl₂ under reflux. On the other hand, neither *meso*- nor D,L-3,4-diphenylhexa-1,5-diene (**196**) undergo the photoassisted zeolite-induced reaction, apparently due to the absence of a styrene moiety, which absorbs at an accessible wavelength.



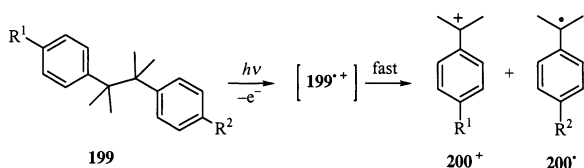
Interestingly, the rearrangement of **194** failed with common chemical/photochemical ET methods (catalytic tris(*p*-bromophenyl)aminium hexachloro-antimonate in CH₂Cl₂ at 0 °C; irradiation of *p*-dicyanobenzene in acetonitrile).⁴⁴⁹ The photoassisted Cope rearrangement of **194** was formulated via the radical cation (**194**^{•+}), formed by ET from the excited state to the zeolite; the subsequent course of the reaction is not clear. On the other hand, the mechanism of the (degenerate) radical cation Cope rearrangement of **197** in polar solvents is known to involve two consecutive intermediates; the radical cation, **197**^{•+}, cyclizes spontaneously to a cyclohexane-1,4-diyl species, **198**^{•+}. The second, ring-opening step occurs in a biradical, **198**^{••}, generated by triplet recombination.^{450–452} Of course, an analogous mechanism in the zeolite is not very likely.



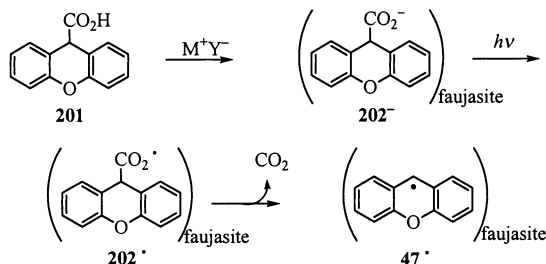
Other photoassisted reactions on zeolites also were ascribed to photoionization of the organic guest. For example, the cyclodimerization of 1,3-cyclohexadiene (**151**) in CH₂Cl₂ and 1-methyl-1,3-cyclohexadiene on NaX afforded only the [4+2] cycloadducts in moderate yields (~30%).⁴⁴⁸ Acyclic dienes lacking the cyclohexadiene chromophore (~240 nm) failed to undergo photocatalyzed cyclodimerization.⁴⁴⁸

Laser flash photolysis of naphthalene or *p*-terphenyl in NaX, NaY, or silicalite formed mainly triplet states and only minor yields of radical cations (vide supra).⁴³² In contrast, the photolysis of *c*- and *t*-

Scheme 22



Scheme 23



stilbene (**54**, $n = 1$) in NaX or on silica gel⁴⁵⁰ gave t -**54**^{•+} (λ_{\max} 475 nm, sharp; \sim 730 nm, broad) as the only detectable transient, formed by a monophotonic process (laser dose dependence).⁴³²

At very low laser intensities, c -**54** formed dihydrophenanthrene ($\lambda_{\max} \sim$ 450 nm) via intramolecular cyclization.⁴⁵³ Significant cis - $trans$ isomerization occurred within the first few laser pulses. Apparently, t -**54**^{•+} is formed by photoionization of minor t -**54** quantities generated by cis - $trans$ isomerization from c -**54**. In fact, irradiation of the c -**54**/tetranitromethane complex in NaX generated a mixture of t - and c -**54**^{•+} (λ_{\max} 510 nm), which failed to isomerize.⁴⁵³

VII.B.5 Photochemistry of Bibenzyl Systems

Radical cations, which readily fragment, are not stabilized inside zeolites. Thus, laser flash photolysis of bicumyl (**199**) or its 4-methoxy- or 4,4'-dimethoxy-derivatives (**199**, R = OCH₃) in NaY generated cumyl cations (**200**⁺) by cleavage of the doubly benzylic bond within nanoseconds (Scheme 22).³⁴⁹ The strong absorption of the cumyl cations (**200**⁺) masks the much weaker absorption of the complementary radicals (**200**[•]) and makes them difficult to observe.

The formation of 4-methoxycumyl cation (**200**⁺, R¹ = OCH₃) and chloranil (tetrachlorobenzoquinone) semiquinone anion upon PET to chloranil supports the proposed mechanism. The failure to observe the bicumyl radical cation, **199**^{•+}, is consistent with its rapid fragmentation in solution ($k_{fr} \sim 10^8$ s⁻¹).⁴⁵⁴

VII.B.6 Decarboxylation of Carboxylic Acids

Photolysis of phenylacetic⁴⁵⁵ or xanthene-9-carboxylic acids (**201**)¹¹³ in alkali cation-exchanged zeolite Y causes ET to the zeolite. This reaction does not involve a radical cation, but the acyloxy radical (**202**[•]). The IR spectrum showed two C=O frequencies corresponding to carboxylic acid and carboxylate base (**202**⁻) in the zeolite; the electron-rich carboxylate group serves as electron donor.¹¹³ ET from the anion (**202**⁻) to the zeolite generated **202**[•], which rapidly decarboxylated to the benzylic radical **47**[•] (Q=O; λ_{\max} 340 nm; Scheme 23).

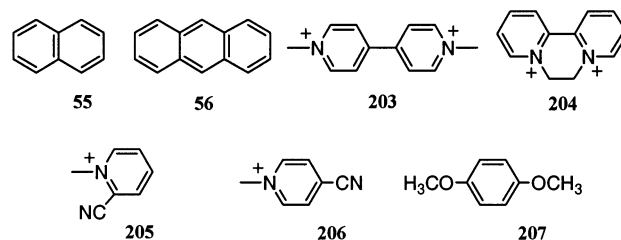
The decarboxylation of **201** in faujasite can be induced also by ET to excited methyl viologen, **203**²⁺; 308 nm-excitation of **203**²⁺ in NaY containing **201** generated **203**^{•+} and xanthyl radical, **47**[•].¹¹³ In these experiments, (**203**²⁺)^{*} and not NaY serves as electron acceptor; additional reactions with viologens as acceptors are discussed in the following section.

VII.C Viologens in Zeolites – Inert Media or Electron Acceptors

In this section, we discuss viologens in various assemblies intended for solar energy storage. Such devices can be efficient only if BET in the resulting radical ion pairs is slow. A continuing effort is devoted to develop molecular assemblies that might defeat BET and yield long-lived charge-separated species.⁴⁵⁶ Viologens are favorite electron acceptors in such assemblies because they can reduce H₂O to H₂.^{457,458} The generation of their radical cations has been studied (ESR, UV-Vis, Raman) in various media, including the external or internal surfaces of zeolites.

VII.C.1 ET between Aromatic Donors and Viologen Acceptors

Substituted pyridinium ions, including 2,2'- and 4,4'-bipyridinium dications, are strong electron acceptors in the ground state;⁴²⁷ their CT complexes with aromatic electron donors have broad absorption bands in the UV-Vis (300–700 nm; Figure 27; Table 14).⁴²⁷



The absorption maxima reflect the strength of the interaction and the redox potentials of the components. The photochemical conversion of CT complexes into geminate radical ion pairs in zeolites were reviewed in detail recently.⁴⁵⁹

Laser excitation (532 nm) of arene-viologen complexes inside zeolites Y or L, generated arene and viologen radical cations within picoseconds.⁴⁶⁰ Both species decay in picoseconds, apparently by BET. Additional long-lived residual may have lifetimes >1 ms, depending on the components, the zeolite structure, and its water content (Table 14). For comparison, geminate ion pairs formed from CT complexes in acetonitrile decay with second-order kinetics ($\tau < 30$ ps).

The increased pair lifetimes in zeolites were ascribed to Coulomb attraction between the negative zeolite framework and the radical cations, separating the pairs effectively (Scheme 24). The range of lifetimes was ascribed to interactions with different sites and by a range of distances between the ions. These systems might ultimately lead to long-lived radical cation pairs.⁴⁶⁰

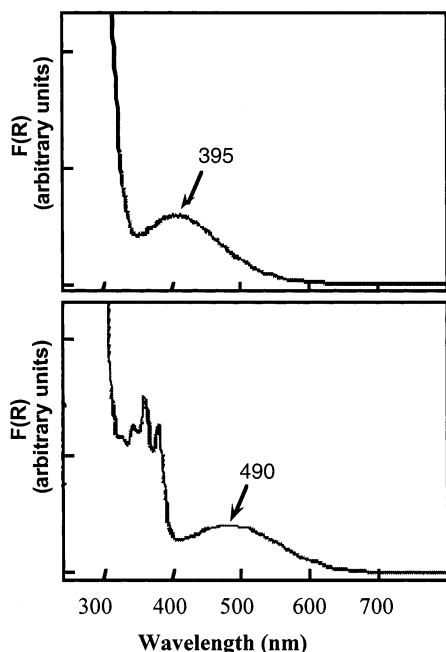


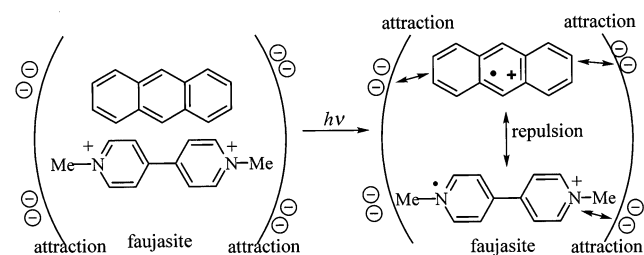
Figure 27. DR UV-Vis spectra [Kubelka-Munk, $F(R)$] of methyl viologen CT complexes with dimethoxybenzene (top) or anthracene (bottom) in zeolite NaY. M. Alvaro, B. Ferrer, H. Gardía, unpublished results; cf., ref 427.

Table 14. Redox Potentials of Aromatic Donors and Viologen Acceptors and Spectroscopic/Photophysical Properties of CT Complexes in Zeolite Y^a

CT complex	E_{ox} (V, vs SCE)	E_{red} (V, vs SCE)	$\lambda_{\text{max CT}}$ (nm)	k^b ($\times 10^9 \text{ s}^{-1}$)	residual ^c (%)
56/204	1.41	-0.25	505	4.7	9
56/203	1.41	-0.40	490	2.9	19
56/205	1.41	-0.62	450	1.4	5
56/206	1.41	-0.64	440	2.8	5
55/203	1.62	-0.40	390	1.0	50 ^d
55/206	1.62	-0.64	360	4.6	30 ^d
207/203	1.30	-0.40	395	8.7	0

^a Ref 427. ^b Decay rate constant of the radical ion pair (532 or 355 nm excitation). ^c Ratio between absorbances at 4 ns and 25 ps. ^d 2:1 complex.

Scheme 24



Aqueous slurries of zeolites loaded with arene-viologen CT complexes and powdered, hydrated, zeolites behaved differently.⁴⁶⁰ Slurries and powders generated the same transients, but slurries had nearly twice the picosecond decay rate, whereas larger fraction of residuals persisted beyond the millisecond range. This effect is unique for water, illustrating the importance of hydration on PET processes in zeolites. Their origin is not fully understood; water may block intrazeolite processes delaying encounters or enhance through-space electron tunneling.

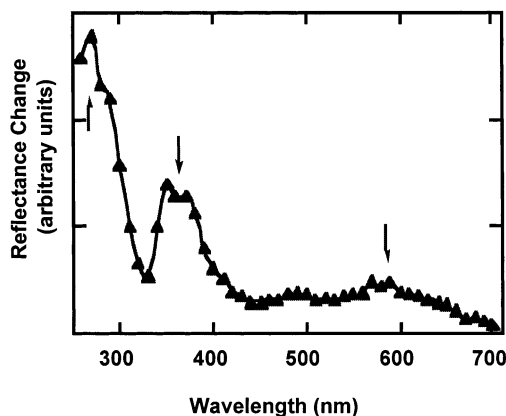


Figure 28. Transient DR spectrum (DJ/J_0) of $203^{2+}@LiNaY$ recorded 80 μs after 355 nm laser excitation. The arrows indicate the recovery of 203^{2+} ground state (270 nm) concurrent with the decay of 203^{2+} (370, 590 nm). Reprinted with permission from ref 461. Copyright 1997 American Chemical Society.

VII.C.2 ET from Zeolites to Viologen Acceptors

Oxygen centers in zeolite frameworks are basic sites and electron donors.⁴⁵⁹ The donor ability can be optimized by varying the framework Al content and the alkali counterions.⁴⁶¹ The basicity of zeolites increases with Al content and with decreasing charge density on the alkali ions. Completely Cs⁺-exchanged X zeolites should be most basic.^{76,462} A tight fit of the acceptor in the lattice may enhance the donor ability and stabilize the reduction product. Laser flash photolysis (266 or 355 nm) of 203^{2+} in alkali-exchanged zeolites generated 203^{2+} (390 nm, strong; 600 nm, broad; Figure 28). In zeolite Y, a dimer of 203^{2+} was also observed. The 203^{2+} signals decay very slowly ($> 100 \mu\text{s}$), regenerating the 270 nm band of 203^{2+} ; the residual absorption depend on the zeolite host.

Zeolites doped with metal atoms may be even more effective. Active Ag(0) clusters can be generated by NaBH_4 reduction of Ag⁺-exchanged Y zeolite ($\sim 1 \text{ Ag}^+$ per 10 supercages) followed by ion exchange with 203^{2+} . Excited Ag clusters formed by long-wavelength irradiation (absorption, λ_{max} 406 nm; emission, λ_{max} 495 nm), were quenched by 203^{2+} with formation of 203^{2+} .⁴⁶³ Interestingly, 203^{2+} was generated also by photolysis of zeolites containing titanium oxide clusters, prepared by hydrolysis of pre-exchanged titanyl dication.¹⁴² In this system, the zeolite serves as the electron donor.

The DR and emission spectra of 203^{2+} in alkali-exchanged zeolites of different crystal structures showed major shifts in λ_{max} and in the onset of bands, compatible with the formation of CT complexes between 203^{2+} and the zeolite as donor.^{428,461,464} 203^{2+} does not fluoresce in solution, but shows emission bands (340, 420 nm) in zeolites. The location of the guest inside zeolite L was derived by comparing a high-resolution X-ray diffraction pattern of a sample with 0.85 203^{2+} per unit cell with one calculated from a molecular model, applying the Rietveld refinement.⁴⁶⁵ The best fit was obtained for a weak interaction with 203^{2+} in contact with the channel walls at an angle of 27° to the main axis.⁴⁶⁵

Samples submitted to laser flash or low-intensity irradiation remain white or develop a light yellowish tint independent of the (acid/base) nature of the zeolite. However, samples of $\mathbf{203}^{2+}$ in RbNaY and CsNaY zeolites (the large radii of Rb^+ and Cs^+ prevent quantitative Na^+ exchange) turned blue upon lamp irradiation, due to $\mathbf{203}^{3+}$, which persisted for hours. At a loading of ~ 0.2 mmol/g of zeolite a conversion $> 30\%$ was estimated based on the absorptions of $\mathbf{203}^{2+}$ and $\mathbf{203}^{3+}$. Radical cation $\mathbf{203}^{3+}$ was observed visually upon lamp irradiation in NaZSM-5. This result reflects the geometry of the zeolite channel: although much less basic than faujasites, NaZSM-5 hosts $\mathbf{203}^{2+}$ more tightly than larger pore zeolites.⁴⁶¹

Combined, the results of laser flash photolysis and low-intensity irradiation indicate that enhanced basicity of the zeolite favors a CT complex between $\mathbf{203}^{2+}$ and the zeolite and stabilizes $\mathbf{203}^{3+}$ by retarding BET. The higher the basicity and electron density in the zeolite/electron donor, the slower is BET.

VII.C.3 Ruthenium Bipyridyl as Electron Donor

Zeolite Y containing an immobilized $\text{Ru}(\text{bpy})_3^{2+}$ complex inside a supercage can be prepared by ship-in-a-bottle synthesis (Section III);^{466,467} its size (~ 1.2 nm) ensures that it remains immobilized, yet can interact with molecules in adjacent cages through the 0.74 nm windows. The photophysical properties of encapsulated $\text{Ru}(\text{bpy})_3^{2+}$ vary with solvation effects⁴⁶⁸ or, at high $\text{Ru}(\text{bpy})_3^{2+}$ loadings, are affected by intermolecular through-space interactions.⁴⁶⁹

Once the $\text{Ru}(\text{bpy})_3^{2+}$ complex is formed, viologens with 2,2'- or 4,4'-bipyridinium structures are either introduced into the zeolite or placed in solution in contact with $\text{Ru}(\text{bpy})_3^{2+}$ @Y powder. Steady-state irradiation of tricomponent systems with the viologen size-excluded from the zeolite interior resulted in long-distance charge separation, building up significant concentrations of viologen radical cation in solution^{470–472}. A synthetic strategy to prepare a well organized assembly of two different ruthenium complexes, bis(2,2'-bipyridyl)(2,2'-bipyrazinyl)ruthenium (E° 1.50 V) and tris(5-methyl-2,2'-bipyridyl)ruthenium(II) (E° 1.18 V), in adjacent supercages resulted in significant improvement.^{472–474} This assembly offers a 4–5-fold enhanced efficiency for charge separation compared to a mechanical mixture of the two complexes in separate zeolite samples.^{472–474}

Transient Raman and DR UV–Vis spectra elucidated the role of zeolite structure affecting forward and return ET in the intra-zeolite $\text{Ru}(\text{bpy})_3^{2+}$ /viologen arrays.^{141,475} 532-nm laser excitation of $\text{Ru}(\text{bpy})_3^{2+}$, triggered ET on the nanosecond time scale; ($k_{\text{et}} > 10^7 \text{ s}^{-1}$). At high bipyridinium loadings, quantum yields, $0.44 < \Phi_{\text{ET}} < 0.59$, were achieved, depending on the redox potential of the bipyridinium dication. Intra-zeolite quenching of $\text{Ru}(\text{bpy})_3^{2+}$ by bipyridinium ions affects the initial intensity of the 370 nm (2,2'-bipyridine radical anion-like) band of $\text{Ru}(\text{bpy})_3^{2+}$, but not the lifetime of the surviving $\text{Ru}(\text{bpy})_3^{2+}$ triplets.⁴⁷⁵ This suggests that only $[\text{Ru}(\text{bpy})_3^{2+}]^*$ with bipyridinium in adjacent supercages is quenched. In contrast, $\text{Ru}(\text{bpy})_3^{2+}$ on the external surface of methyl

Table 15. Influence of the Bipyridinium Loading on the Decay Rate Constants in the $\text{Ru}(\text{bpy})_3^{2+}$ -Viologen/Zeolite Y System System^c

viologen	E_{red}^0 (V vs. NHE)	$k_{\text{b}} (\text{s}^{-1})$ (low loading) ^a	$k_{\text{b}} (\text{s}^{-1})$ (high loading) ^b	$k_{\text{hop}} (\text{s}^{-1})$
204	-0.37	4.0×10^4	2.5×10^5	2.5×10^5
203	-0.44	1.7×10^4	9.0×10^4	2.0×10^5
208	-0.55	1.1×10^4	1.8×10^5	2.3×10^5
209	-0.65	7.3×10^3	1.2×10^5	1.8×10^5

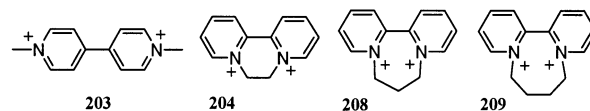
^a Approximately one bipyridinium molecule per 10 zeolite supercages. ^b Between 1.5 and 1.7 bipyridinium molecules per supercage. ^c From ref 475.

viologen-exchanged zeolite was quenched primarily by a dynamic mechanism, which affected the lifetime of $\text{Ru}(\text{bpy})_3^{2+}$.⁴⁷⁶

Photogenerated $\text{Ru}(\text{bpy})_3^{3+}$ /bipyridinium radical cation pairs regenerate the $\text{Ru}(\text{bpy})_3^{2+}$ /bipyridinium dication ground state, either in geminate pairs (fast) or after successive electron hoppings between bipyridinium radical cation and bipyridinium dication (slow).⁴⁷⁵ The extent of long-term charge separation increased with increasing bipyridinium loading (Table 15).

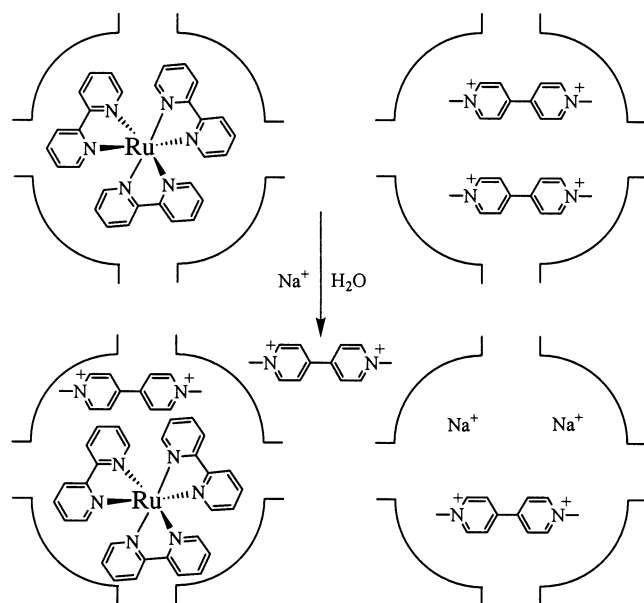
The rate constant of in-cage BET decreased with decreasing redox potential of the 2,2'-bipyridinium ions, i.e., with increasing driving force. The BET rates ($k \sim 10^4 \text{ s}^{-1}$) are remarkably slower than in solution ($k \sim 10^{10} \text{ s}^{-1}$; Table 15),⁴⁷⁷ suggesting that BET falls into the Marcus inverted region.⁴⁷⁵ These results demonstrate the significant stabilization of radical cations in zeolites, but the BET slow-down is not fully understood. Contributing factors include Coulomb interactions, changes in solvent reorganization energy and donor–acceptor orbital overlap, or steric constraints to spin inversion (which may require rotation). Clearly, more effort work seems necessary to fully clarify the origin and exploit the effect of the dramatic retardation of BET between $\text{Ru}(\text{bpy})_3^{2+}$ and bipyridiniums.

At high loadings (1.1–1.7 bipyridinium dications per supercage) the electron escape yield from the geminate pair was estimated as > 0.5 ; the rate constant for electron hopping, $k_{\text{hop}} \sim 10^5 \text{ s}^{-1}$, is comparable to that for BET (Table 15). Thus, for more than half of the geminate pairs the electron explores several supercages before being captured by $\text{Ru}(\text{bpy})_3^{3+}$.⁴⁷⁵



Intra-zeolite clusters of $\text{Ru}(\text{bpy})_3^{2+}$ / $\mathbf{203}^{2+}$ were studied in nanometric zeolite X crystals (250 nm aggregates of 13 ± 2.5 nm crystallites).⁴⁷⁸ Acidity causes extensive damage to the nanoparticles (loss of crys-

Scheme 25



tallinity $\geq 90\%$) and has to be carefully excluded during the “ship-in-a-bottle synthesis”. The charge separation efficiency for nanocrystalline X with intact crystal structure exceeds that of conventional micron-sized zeolite Y by a factor of 2 under comparable conditions.

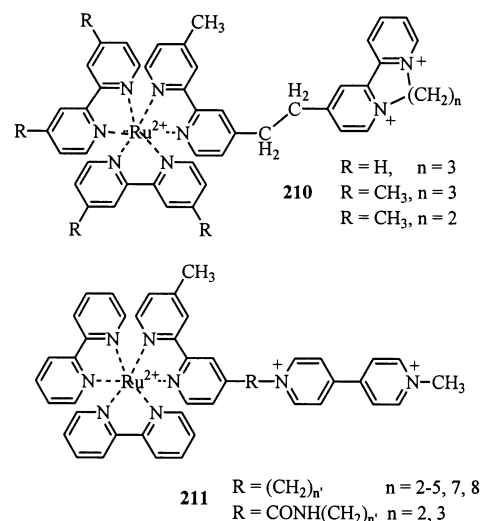
Potential interparticle reactions between $\text{Ru}(\text{bpy})_3^{2+}$ and $\mathbf{203}^{2+}$ were studied in aqueous suspensions of zeolite Y particles (Scheme 25).⁴⁷⁹ $\text{Ru}(\text{bpy})_3^{2+}$ can be trapped inside supercages or ionically bound on the surface. In aqueous suspensions of $\mathbf{203}^{2+}$ -exchanged Y zeolite interparticle diffusion can be followed by the decay of $\text{Ru}(\text{bpy})_3^{2+}$ luminescence. For $\text{Ru}(\text{bpy})_3^{2+}$ in zeolite supercages, the time constant for exchange of $\mathbf{203}^{2+}$ between particles ranges from 10^4 – 10^3 s at 0.1–3 mM Na^+ concentrations. Interparticle exchange is much slower (5.5×10^4 – 1.5×10^5 s) for internal $\mathbf{203}^{2+}$ with $\text{Ru}(\text{bpy})_3^{2+}$ on the external surface, possibly due to blockage of pore openings by external $\text{Ru}(\text{bpy})_3^{2+}$ units.

More elaborate systems have photoactive tris-(bipyridyl)ruthenium(II) units covalently linked to bipyridinium dications, adsorbed on the surface of a zeolite particle. Several supermolecules combining donor–sensitizer–acceptor subunits linked by appropriate spacers have been synthesized for solar energy storage. They contain all necessary components in conformationally rigid single molecules designed to optimize the quantum yield of charge-separation and increase the lifetimes of the charge-separated intermediates.⁴⁸⁰ Depending on the number of linked moieties they are called diads, triads, etc. The major drawback to this “molecular approach” is the major synthetic task of preparing the arrays. As a compromise between the molecular approach and the random incorporation of donor and acceptor components into zeolites, the synthesis of less demanding D–A diads or D–D–A triads and their inclusion in zeolites has been pursued.^{470,481}

Thus, covalently linked tris-(bipyridyl)ruthenium(II)-*N,N*-dialkyl-(2,2' or 4,4')-bipyridinium **210** and **211**, respectively, undergo intramolecular ET in

acetonitrile/water solutions on the nanosecond time scale (the $\text{Ru}(\text{bpy})_3^{2+}$ excited state is not observed). Small quantities of these diads can be ion-exchanged onto the external surface of zeolites Y, L, or mordenite at loadings ($\sim 2 \times 10^{-6}$ mol g^{-1}), corresponding to monolayer coverage. In an elegant ^{13}C NMR study, a diad with ^{13}C -labeled donor and acceptor moieties was exposed to an external paramagnetic probe, tris-(acetylacetonate)gadolinium(III), $[\text{Gd}(\text{acac})_3]$. The large tris-(bipyridyl)ruthenium moiety, size-excluded from the pores, was affected by the paramagnetic $\text{Gd}(\text{acac})_3$, while the smaller pendant bipyridinium unit, protected inside the pores, was not.⁴⁸¹

The forward ET of diad **211** on zeolites occurs within < 30 ns for an ethylene link, but is 10–100 times slower for longer spacers. ET in the half-in/half-out diad takes place on the zeolite surface, not in solution, decreasing approximately $1/e$ per spacer methylene group. The distance dependence is greater for monodirectional zeolites (L, mordenite) than for zeolite Y, probably reflecting some folding of the larger polymethylene links in the spacer zeolite Y.



Excitation of covalently linked diads on zeolite surface generated $\text{Ru}(\text{bpy})_3^{3+}$ and bipyridinium $^{+}$, which decay with identical, but complex, profiles (10–100 μs , vs < 10 ns in solution). A fast initial decay, assigned to intra-diad BET, is followed by a slower decay ($> 100 \mu\text{s}$; $\sim 10^5$ times slower than in solution). The longer-lived species are attributed to hopping of an electron out of a diad, leaving $\text{Ru}(\text{bpy})_3^{3+}$. The quantum yield for long-lived charge-separated species reached a maximum for the pentamethylene spacer and is higher (~ 0.07) for monodirectional zeolites (L, mordenite) than for zeolite Y (0.05) (Figure 29).

Further complexity was introduced by adding a size-excluded donor, D' , not covalently bound to the ruthenium cluster, in the aqueous suspension, forming a D– $\text{Ru}(\text{bpy})_3^{2+}$ –A triad. Here, A is a bipyridinium, occluded in the zeolite through ion-exchange, whereas $\text{Ru}(\text{bpy})_3^{2+}$, on the external zeolite surface, serves as the photoactive moiety (Scheme 26).⁴⁸¹ Depending on the nature of the second donor, D' , either the excited $[\text{Ru}(\text{bpy})_3^{2+}]^*$ or $\text{Ru}(\text{bpy})_3^{3+}$ serves as the acceptor.

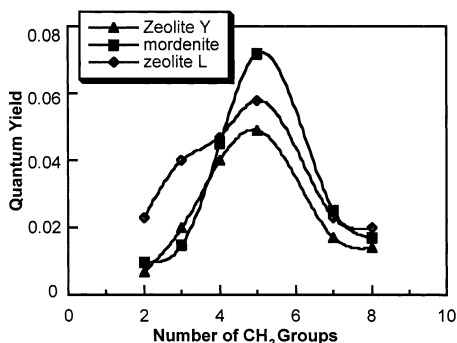
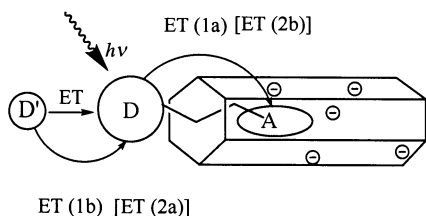
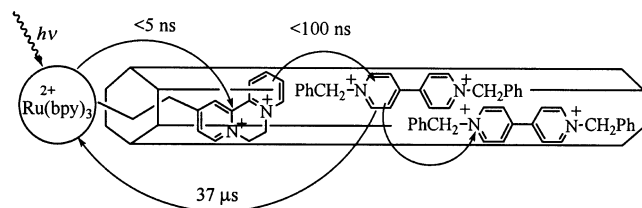


Figure 29. Efficiency of charge separation as a function of the number of CH₂ groups linking Ru(bpy)₃ to bipyridinium units for three zeolites. Reprinted with permission from ref 481. Copyright 1994 American Chemical Society.

Scheme 26



Scheme 27

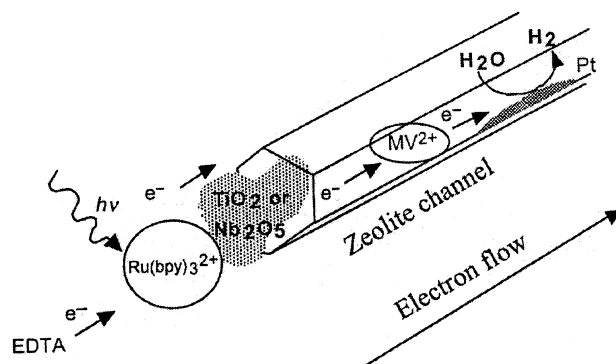


For example, promethazine cation ($E_0 = +0.94$ V vs SCE, CH₃CN) can reduce Ru(bpy)₃³⁺ ($E_0 = +1.23$ V), but not [Ru(bpy)₃²⁺]^{*} ($E_0 = 0.77$ V); the final charge-separated state is promethazine^{•++}-Ru(bpy)₃²⁺-bipyridinium radical cation (Scheme 26, ET1a, ET1b). The bipyridinium radical cation is formed within microseconds, while promethazine^{•++} radical dication is built up in microseconds concomitant with the decay of Ru(bpy)₃³⁺. This system decays via second-order kinetics over hundreds of microseconds. W(CN)₈⁴⁻ as co-donor instantaneously quenched [Ru(bpy)₃²⁺]^{*}, whereas the bipyridinium radical cation grew on the submicrosecond time scale (Scheme 26, ET2a, ET2b). The quantum yield of charge separation for the triad W(CN)₈⁴⁻-Ru(bpy)₃²⁺-bipyridinium dication (10%) was significantly higher than that for the diad Ru(bpy)₃²⁺-bipyridinium dication (2%).

A second acceptor, A', can also be added to diad **210**. With benzyl viologen, $E_0 = -0.59$ V, ionically exchanged in zeolite L or Y (Scheme 27), ET in the resulting D-A-A' triad is complete in < 100 ns, generating Ru(bpy)₃³⁺-A-A'^{•+} ($\Phi = 0.17\%$); the charge-separated state decays in 37 μs.⁴⁷⁰

Organized systems comprised of viologens in the micropores of zeolites allow water splitting with visible light. In essence, these systems function as light-driven pumps for vectorial ET from a sacrificial donor (amines, I₃⁻) to H₂O or H⁺. The process is most efficient if BET is minimized at every stage of the

Scheme 28



sequence. Effective systems use a monodirectional, large-pore zeolite (L) as host, combined with (i) size-excluded Ru(bpy)₃²⁺ outside the pores as (visible light) photosensitizer/initial electron donor; (ii) nano-sized particles of a semiconductor (TiO₂, Nb₂O₅) at the pore mouths, as efficient relay for external to internal electron flow; (iii) methyl viologen (**203**²⁺) inside the zeolite as initial electron acceptor; and (iv) Pt atom clusters highly dispersed within the zeolite in molecular contact with **203**²⁺ as catalytic sites for hydrogen production (Scheme 28).

One Ru(bpy)₃²⁺ ligand contains two carboxylic acid functions to ensure strong binding to the semiconductor particles. Excitation of Ru(bpy)₃²⁺-**203**²⁺ generated **203**^{•+} by ET to the Pt sites. ET to H⁺ restores **203**²⁺ from **203**^{•+}; the cycle is completed when a sacrificial electron donor reduces Ru(bpy)₃³⁺ back to Ru(bpy)₃²⁺. An analogous multicomponent photocatalytic assembly using zinc tetramethylpyridinium porphyrin as size-excluded photosensitizer located at the pore openings of zeolite Y, but lacking semiconductor oxide has been also reported.⁴⁸² These systems exemplify the versatility of zeolites for constructing multicomponent devices for generating charge-separated species.

VII.D. Oxygen as Electron Acceptor: Visible Light Irradiation of Hydrocarbon × O₂ CT Complexes inside Large-Pore Zeolites

Frei and co-workers have characterized CT complexes absorbing visible light; these are formed by incorporating hydrocarbon-oxygen gas mixtures into alkali or alkaline earth zeolite Y.^{22,23,196,483-490} An up-to-date review of the photochemistry of these CT complexes has appeared recently.⁴⁹¹ 2,3-Dimethyl-2-butene (**1**) was a favorite target; other small alkenes, alkylaromatics,⁴⁸⁷ or aliphatic hydrocarbons studied.⁴⁸¹ As expected for CT bands, increasing ionization potential of the alkene shifts the onset of the alkene×O₂ absorption to higher energies.

The alkene×O₂ CT complexes in the zeolite do not react in the dark at -50 °C over prolonged periods. However, irradiation with red light formed the corresponding hydroperoxide with high selectivity at high conversions. The excitation spectra for this conversion match the hydrocarbon×O₂ CT spectra in the zeolite (Figure 30). The growth of the hydroperoxide is consistent with a single-photon process. While hydroperoxides lacking an α-H are relatively

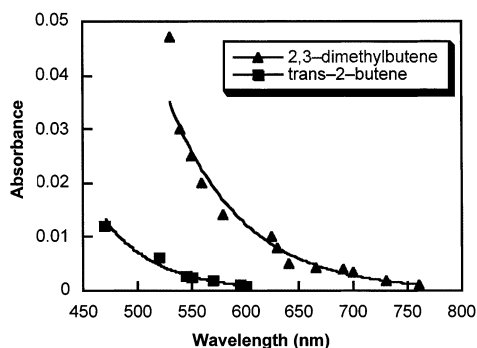
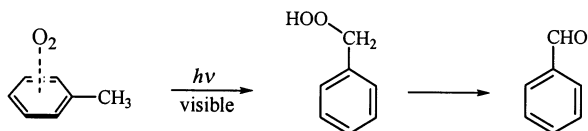


Figure 30. Photoresponse for hydroperoxide formation as a function of excitation wavelength for two alkenes inside CaY. The profiles coincide with the CT bands of the collisional alkene \times O₂ complexes in this zeolite. Reprinted with permission from ref 437. Copyright 1997 American Chemical Society.

stable, other primary hydroperoxides dehydrate spontaneously to aldehydes or ketones, products of major importance in the chemical industry.

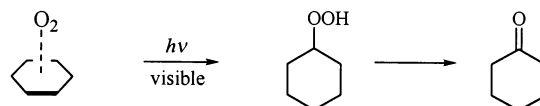
Alkene \times O₂ CT complexes are significantly stabilized in zeolites. In organic solvents, they absorb at 300–400 nm, with minor red shifts (≤ 10 nm) in polar solvents. In zeolites, the complexes show red shifts of ≥ 300 nm, attributed to stabilization of the CT complex excited states (~ 1.5 eV) by electrostatic interactions with the charge-balancing cations in the Y supercages. Cations in dehydrated zeolites are unshielded by framework oxygens; current models assign an atomic charge of +1 to Na⁺ in the supercage. While the ground state is weakly stabilized by ion-induced dipole interactions, the alkene⁺ \times O₂⁻ ion pair shows far stronger Coulomb interactions. This rationale is supported by the decreased stability of the complexes in silica faujasite (Si/Al ratio > 100; nonionic matrix without cations). Quantum chemical calculations might elucidate details of the interactions between CT complexes and zeolite.

The contact CT complex between toluene and oxygen in CaY or BaY absorbs in the visible; the photolysis thresholds, 590 for Ca²⁺, 500 nm for Ba²⁺, depend on the charge density on the cation.⁴⁸⁷ Irradiation ($\lambda > 390$ nm) produced benzaldehyde and water (FT-IR). Benzyl hydroperoxide is difficult to detect by in situ IR; its involvement was inferred from the thermal growth of benzaldehyde after photolysis. Long wavelength excitation avoids secondary photoreactions that would limit the selectivity.



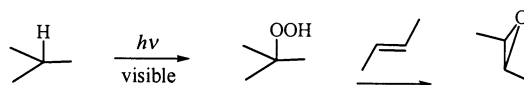
Even saturated hydrocarbons form CT complexes with O₂ in NaY zeolite with absorption edges in the visible region. The cyclohexane \times O₂ complex in NaY zeolite is shifted by ~ 2 eV,⁴⁸⁸ the isobutane \times O₂ complex in BaY by ~ 2.5 eV,⁴⁸⁵ reflecting once again significant stabilization by the high electrostatic fields inside zeolites. Irradiation of the cyclohexane \times O₂ complex formed cyclohexyl hydroperoxide and cyclohexanone. The hydroperoxide rearranges thermally

to cyclohexanone (complete selectivity at $\sim 40\%$ conversion).⁴⁸⁸

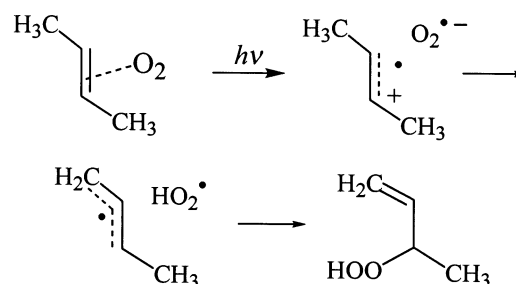


Current liquid-phase oxidations of cyclohexane yield cyclohexanone plus cyclohexanol in a combined selectivity of $\leq 70\%$ at only $\sim 9\%$ conversion. Thermal activation (≥ 80 °C) of the cyclohexane \times O₂ complex forms autoxidation products.⁴⁹² For faujasites with different cations, the rate of thermal oxygenation increases in the order NaY < BaY < SrY < CaY.⁴⁹²

Irradiation of the isobutane \times O₂ contact CT complex in zeolites caused the selective oxidation of tertiary alkyl C–H groups,⁴⁸⁵ forming *tert*-butyl hydroperoxide, which epoxidizes *cis*- and *trans*-2-butene with complete diastereospecificity.⁴⁸⁵

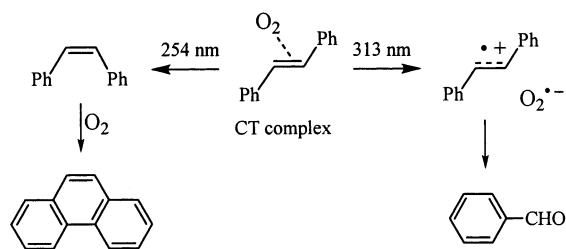


Photooxygenations inside zeolites proceed via contact radical ion pairs, which generate allyl radicals and hydroperoxyl radical, HO₂[•], by H⁺ transfer; in-cage recombination generates an allylic hydroperoxide. 2,3-Dimethyl-2-butene (**1**) formed acetone as a minor byproduct, most likely via a dioxetane, which is also involved in ET sensitized oxidations in solution.



Following irradiation of 2,3-dimethyl-2-butene \times O₂ in NaY at -100 °C product formation was complete within 320 ms¹⁴⁸ without evidence for hydroperoxide. This time limit, and an estimated diffusion coefficient (4×10^{-19} m² s⁻¹) for 2,3-dimethyl-3-hydroperoxy-1-butene, suggest that the hydroperoxide does not escape from a supercage during the laser pulse. Therefore, the lack of hydroperoxide growth rules out turnover at any specific site or supercage. This conclusion places a lower limit on the number of supercages participating in the reaction: it cannot be smaller than the number of product molecules generated during a the time needed to diffuse out of the parent cage. Accordingly, at least 1% of all NaY supercages participate in the photoreaction, a value 2–3 orders of magnitude higher than the highest estimate of Lewis acid, radical and/or defect sites in NaY. These sites cannot be significantly involved in the photooxygenation, leaving the high electrostatic fields around the cations in the Y supercages as the

Scheme 29



sole cause for the low-energy photochemical hydrocarbon oxidation.

Typical zeolite Y particles ($\sim 1 \mu\text{m}$) scatter visible light, giving them an opaque (“white”) appearance. For particles with grain sizes large compared to the probe wavelength, scattering coefficients are inversely proportional to the grain size;¹⁵⁰ thus, transparency in the visible improves with increasing particle size. NaY crystals of $\sim 40 \mu\text{m}$ form sufficiently transparent films to be studied by UV–Vis transmission spectroscopy.¹⁴⁸ Forty-micrometer NaY films transmit $\sim 70\%$ of the incident light at 700–250 nm; this compares well with the steadily decreasing transmittance of $1 \mu\text{m}$ NaY compressed pellets (31% at 700 nm, 12% at 300 nm, 1% at 250 nm).

The spectrum of the 2,3-dimethyl-2-butene- O_2 complex (by adsorbing alkene and O_2 vapors onto transparent NaY films) has an onset at ~ 700 nm and a flat maximum near 400–500 nm. Transmission and DR spectra are similar, except for the distorted absorbance in the latter; the wavelength dependent scattering coefficients for $1\text{-}\mu\text{m}$ NaY particles cause increasingly higher absorption coefficients toward shorter wavelengths. UV–Vis transmission spectroscopy of NaY crystals yielded more reliable values (~ 0.04), ~ 5 times smaller than estimates based on DR,^{23,483} for the quantum yield of ET-mediated photooxygenations.¹⁴⁸

The selectivity of terminal alkene oxidations (propene, 1-butene, 1-pentene) in Ba^{2+} -exchanged zeolites is lower than that of substituted alkenes, depending on excitation wavelength, temperature, and chain length.⁴⁹³ Brønsted acid-catalyzed reactions, double-bond migration, polymerization, and epoxide ring-opening, also take place, as well as reaction of the hydroperoxide with the parent alkene.⁴⁹³ Saturated aldehydes and ketones arise by thermal ring opening of epoxides or via dioxetanes. The yield of byproducts increases with decreasing excitation wavelength, increasing temperature, and increasing alkene chain length.

The photochemistry of stilbene (**54**, $n = 1$) in NaY in the presence of O_2 was wavelength-dependent (Scheme 29).⁴⁹⁴ Excitation at 313 nm yielded benzaldehyde, whereas 254-nm light caused cis–trans isomerization and led to phenanthrene. The 254 nm results are equivalent to the photoreaction in solution, whereas at 313 nm, excitation of the CT complex formed $54^{\bullet+}/\text{O}_2^{\bullet-}$.

Thiazine dyes (thionine, methylene blue) are poor ET sensitizers for stilbene oxidation in solution, efficient in Li^+ or Na^+ exchanged X and Y zeolites,⁴⁹⁵ but less efficient in Rb^+ and Cs^+ exchanged zeolites (Figure 31). The oxidation was formulated via ET

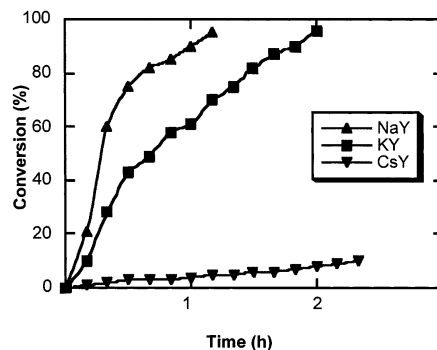
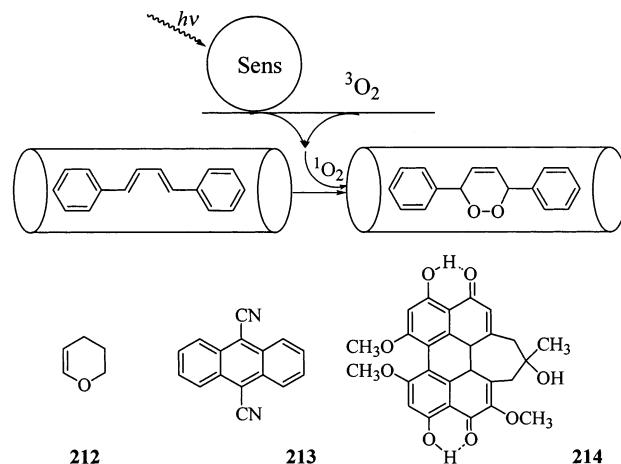


Figure 31. Conversion plot for the thionin photosensitized oxidation of 4,4'-dimethoxystilbene in three alkali metal ion exchanged Y zeolites. Reprinted with permission from ref 495. Copyright 1996 Elsevier Science.

Scheme 30



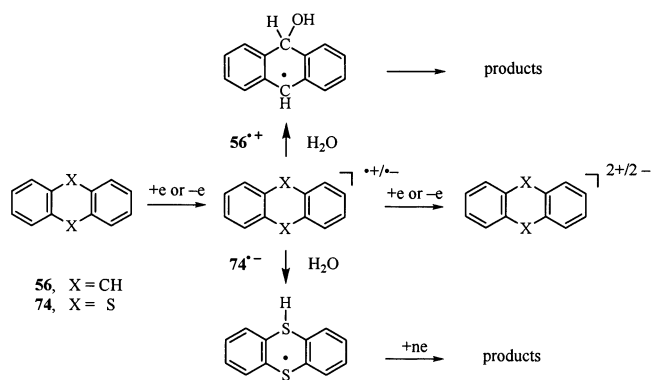
from stilbene to excited thiazine dye;⁴⁹⁵ it was suppressed by water and by efficient electron donors, viz., DABCO or *N,N*-dimethylaniline. PET oxidation in solution yields aldehydes while $^1\text{O}_2$ forms endoperoxides.

Incorporation into Na–ZSM-5 caused *trans*-stilbene, *trans,trans*-1,4-diphenyl-1,3-butadiene (**54**, $n = 1, 2$), or 2,3-dihydro- γ -pyran (**212**) to be selectively $^1\text{O}_2$ -oxygenated, avoiding ET pathways (e.g., Scheme 30).⁴⁹⁶ Bulky photosensitizers (9,10-dicyanoanthracene, **213**, hypocrellin A, **214**) and solvents (isooctane, pentaerythritol trimethyl ether) are size-excluded from medium pore ZSM-5; thus, acceptor–alkene encounter complexes, prerequisite for ET, are suppressed. In contrast, $^1\text{O}_2$ has a lifetime sufficient to diffuse into the zeolite and react with alkenes, even if generated in solution. For Al-rich ZSM-5 samples ($\text{Si}/\text{Al} < 25$) water affects the selectivity by moving the apolar alkenes to the external surface of the zeolite grains. Therefore, the reaction proceeded by competing $^1\text{O}_2$ and ET pathways as in solution and the selectivity observed for dry samples was lost.⁴⁹⁶

VIII. Electrochemical Generation of Radical Cations in Zeolites

Electrochemical oxidation, applying positive potentials on zeolite-modified electrodes containing organic compounds, is a general method to generate radical ions in zeolites.^{497,498} Because these experi-

Scheme 31



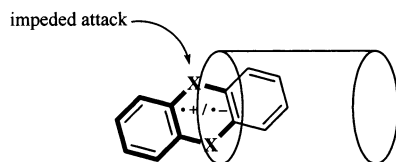
ments require diffusion of an electrolyte simultaneous with ET, and intracrystalline diffusion is slow relative to the measurement, it is widely accepted that electrochemical techniques only probe the external surface and a shallow layer of the zeolite grains.^{499,500} Are radical cations, that were electrochemically generated on an external surface or partially penetrating into a zeolite protected from nucleophilic attack?⁵⁰¹ Do they experience the dramatic stabilization of radical cations within zeolites?

Anthracene (**56**) and thianthrene (**74**) exhibit two reversible one-electron oxidation waves in anhydrous aprotic solvents, one due to radical cation formation, the second, at higher potentials, to conversion to dications (Scheme 31). Traces of water or other nucleophiles cause a single irreversible oxidation peak to occur, involving two or more electrons. Apparently, the radical cations form hydroxylated radicals and eventually oxides. The electro-reduction also has two reversible, one-electron waves, which again collapse to a single, irreversible multi-electron peak in the presence of water or protic solvents.

Adsorbed on the outside surface of mordenite or ZSM-5, **56** and **74** showed two separate oxidation or reduction waves under conditions where these are no longer seen in solution, showing that **56**^{•+} or **74**^{•+} are partially protected in the outermost layers of zeolite particles (Scheme 32); some oxides were formed. The redox potentials of **56** or **74** in zeolites were similar to values in polar solvents.

Zeolites containing **56** or **74** can be used as electrodes for the electrocatalytic reduction of nitrites in aqueous solution.⁵⁰² Nitrite ion, NO₂⁻, an important analyte in the assessment of drinking water quality, has a poor electrochemical response in aqueous solution because its redox reaction is slow on the time scale of the measurement. This problem was overcome by selective, zeolite modified electrodes containing **56** or **74**, which increased the analyte response. Radical cations on the electrode/zeolite surface readily form nitrite adducts,^{52,503} which are oxidized more rapidly than NO₂⁻ (electrocatalysis). Organic radical

Scheme 32



cation/zeolite electrodes can increase the electrochemical response by 2 orders of magnitude.⁵⁰² Similar effects underlie the use of zeolite modified electrodes containing 2,4,6-triphenylpyrylium ion (**165**⁺) to assay catecholamines in water.⁵⁰⁴

The electrochemistry of viologens within zeolites was studied in detail.^{505–507} Samples of Ag(0) clusters and methyl viologen (**203**²⁺) in zeolite Y had two reduction waves ($E_{1/2} = -0.49, -0.79$ V vs Ag/AgCl) due to reduction of **203**²⁺ (similar to values in solution)^{508,509} and an anodic wave (0.34 V vs Ag/AgCl) due to oxidation of Ag(0).⁴⁶³ Similarly, viologens were chemically reduced in various zeolites by alkali metals⁵¹⁰ and manganese polycarbonyls of different size with different counterions (eq 4).⁵¹¹ The redox potentials of **56** or **74** in zeolites were similar to values in polar solvents.



IX. Radical Anions within Zeolites

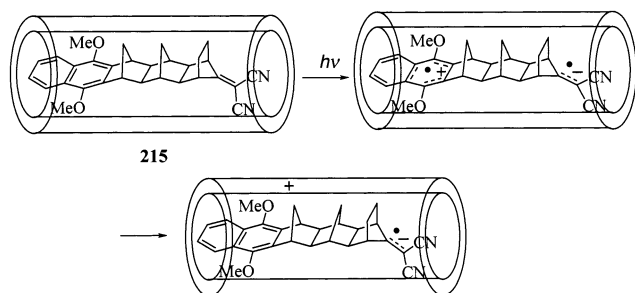
Although this review was conceived to deal first and foremost with the plethora of radical cations in zeolites, it may be useful to consider briefly the limited instances of radical anions in zeolites. Because zeolite lattices have overall a negative charge, determined by the Al content of the framework, they are well suited to stabilize positively charged species, viz., cations and radical cations. Negative ions, on the other hand, experience unfavorable Coulomb interactions with the zeolite framework, particularly in Al-rich zeolites; as a result, they are observed less frequently. To place this trend in perspective, we present a brief overview of radical anions formed inside zeolites.

Perhaps the most remarkable example of a persistent radical anion in zeolites is the semiprecious stone, lapis lazuli, known since ancient times and appreciated particularly as a pigment in ancient Egypt. The species imparting the blue hue is trisulfur radical anion, S₃^{•-}, accompanied by variable percentages of S₂^{•-}, which introduce a green tint. These sulfur radical anions are incarcerated inside sodalite cages, which immobilize and completely protect these otherwise highly reactive species from atmospheric attack or radical coupling. The composition and properties of related pigments, based on inorganic chalcogenide radical anions, e.g., Se₂^{•-},⁵¹² inside natural zeolites were reviewed recently.⁵¹³

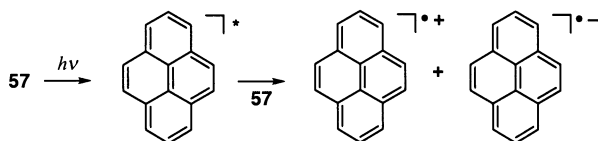
Superoxide radical anion, O₂^{•-}, was repeatedly observed inside zeolites or on their surface. O₂ frequently is the final electron acceptor when radical cations are photogenerated under aerobic conditions. Kochi and co-workers showed that diquat and paraquat radical cations react with molecular oxygen forming O₂^{•-} in zeolite Y as a “molecular pocket”.⁵¹⁴ In solution, the formation of O₂^{•-} had been invoked, without supporting spectroscopic evidence, to account for the reactivity of *N,N*-dialkylbipyridium radical cations. However, when encapsulated in a zeolite, O₂^{•-} can be characterized by conventional ESR spectroscopy.⁵¹⁴

[60]-Fullerene radical anion (C₆₀^{•-}) can be generated by inclusion into zeolites. C₆₀ is a strong electron

Scheme 33



Scheme 34



acceptor and the $C_{60}^{\bullet-}$ radical anion can be detected by ESR spectroscopy following C_{60} adsorption on the surface of NaX.⁵¹⁵ However, a more recent paper pointed out that the ESR spectra of $C_{60}^{\bullet+}$ and $C_{60}^{\bullet-}$ are very similar; identification of the observed spectrum as due to $C_{60}^{\bullet+}$ fits well with the common behavior of zeolites as single electron acceptors. An unambiguous characterization of the fullerene radical ion(s) appears desirable.¹³⁶

Conventional aluminosilicates containing electron donor sites spontaneously transfer an electron to tetracyanoethylene, generating its radical anion, $TCNE^{\bullet-}$. The radical anion was formed also upon incorporation of TCNE into Al/MCM-41; however, all-silica MCM-41 failed to generate $TCNE^{\bullet-}$.⁴⁰⁵

Photolysis ($\lambda < 310$ nm) of an Al/MCM-41 encapsulated diad containing 1,4-dimethoxynaphthalene covalently linked to a dicyanovinyl acceptor via a norbornane spacer (**215**) gave rise to a dicyanovinyl type radical anion (Scheme 33); the spectrum was remarkably persistent in the dark (≥ 1 d). The complementary radical cation of the dimethoxynaphthalene fragment was not detected, possibly due to ET from MCM-41 to the cationic site.⁴⁰⁵ No ESR signal was observed in (Al-free) MCM-41.

Examples of spontaneous ET from zeolites forming organic radical anions are rare; more typically, zeolites play a passive role as a polar environments for PET. For example, pyrene radical anion, $57^{\bullet-}$ (λ_{\max} 492 nm), was formed in NaX by PET between excited- and ground-state **57** (Scheme 34).⁵¹⁶ **57** fluorescence was quenched at increasing **57** concentration with a simultaneous rise of $57^{\bullet-}$ and $57^{\bullet+}$ absorptions. Similarly, the anthracene excimer (**56**...**56**)^{*} emission observed upon irradiation of **56** in faujasites was ascribed to fast BET in radical ion pairs.²⁵¹

Thomas and co-workers observed a different mechanism of $57^{\bullet-}$ formation in alkali metal exchanged zeolites. They recognized the relationship between the basicity of zeolites and their ability to donate electrons to excited organic molecules.^{517,518} Laser flash photolysis (337 nm) of **57** adsorbed on KY zeolite (1×10^{-6} mol g^{-1}) generated 357^* (λ_{\max} 410, 520 nm), $57^{\bullet+}$ (λ_{\max} 450 nm), and $57^{\bullet-}$ (λ_{\max} 490 nm; transient DR). $57^{\bullet-}$ was identified based on spectra

Table 16. Relative Yields of Pyrene Triplet (357^*), Radical Cation ($57^{\bullet+}$), and Radical Anion ($57^{\bullet-}$) in Alkali Metal Ion Exchanged Faujasites^a

zeolite ^b	357^*	$57^{\bullet+}$	$57^{\bullet-}$	$57^{\bullet-}/57^{\bullet+}$
LiX	0.082	0.150	0.085	0.57
KX	0.072	0.137	0.127	0.93
RbX	0.082	0.137	0.140	1.02
CsX	0.147	0.147	0.163	1.11
LiY	0.033	0.074	0.044	0.59
KY	0.030	0.075	0.077	1.03
RbY	0.040	0.076	0.088	1.16
CsY	0.111	0.086	0.101	1.17

^a From ref 402. Kubelka–Munk equation. ^bPyrene loading 2.8×10^{-6} mol g^{-1} .

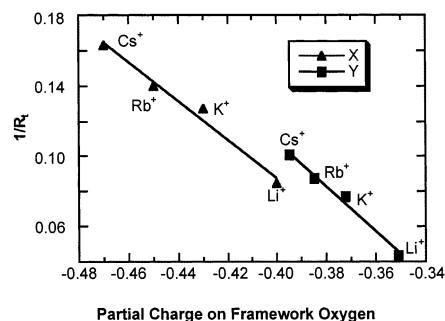
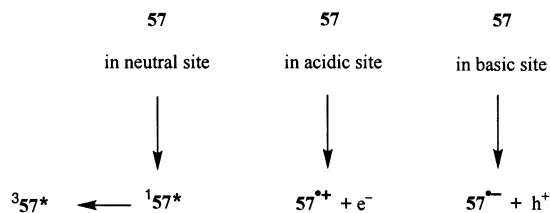


Figure 32. Pyrene radical anion yield ($57^{\bullet-}$) in alkali faujasites versus the calculated partial negative charge on the framework oxygens. Reprinted with permission from ref 518. Copyright 1994 American Chemical Society.

Scheme 35



observed by co-irradiation of **57** and *N,N*-dimethylaniline in zeolite KX; it was insensitive to NH_3 or *N,N*-dimethylaniline and scavenged by O_2 .⁵¹⁷ The linear increase of the yield of $57^{\bullet-}$ with laser power is compatible with a single-photon mechanism.

Consistent with the greater basicity of zeolite X the yield of $57^{\bullet-}$ was higher in zeolite X than in Y;⁴⁰² the yield also decreased in the sequence $Cs^+ > Rb^+ > K^+ > Li^+$ for both X and Y zeolites; the trend parallels the zeolite base strength (Table 16). Data for Na^+ are unclear because the bands of $57^{\bullet-}$ and the Na_4^{3+} cluster overlap. Finally, the yield of $57^{\bullet-}$ increased linearly with the partial negative charges on framework oxygens calculated from the mean Sanderson electronegativity of the alkali ion-exchanged X or Y zeolites (Figure 32).⁵¹⁸

Photolysis of **57** on the external surface of NaA (4 Å-pore size, Si/Al \sim 1:1, comparable to zeolite X) gave rise to 357^* and $57^{\bullet+}$, but failed to form $57^{\bullet-}$. This result supports the notion that $57^{\bullet-}$ is generated and stabilized only inside the supercages by interaction with the zeolite basic sites (Scheme 35).⁵¹⁸

The radical cations and anions decay independently with significantly different kinetics; direct ET from $57^{\bullet-}$ to $57^{\bullet+}$ can be ruled out. The lifetime of $57^{\bullet+}$

increases with increasing zeolite acidity, that of $57^{\cdot-}$ decreases with increasing basicity. Thus, the ratio $57^{\cdot-}/57^{\cdot+}$ depends on the zeolites basicity. The relative yield of 357^* was ascribed to a heavy atom effect. The quantum yield of 357^* in zeolites is lower than in solution (Table 16).⁵¹⁸

Hydration and different counterions affected the yields of 357^* , $57^{\cdot+}$, and $57^{\cdot-}$; the changes are complex; no clear trend was discernible. Contributing factors may include cation solvation, modification of the acid/basic strength of active sites, and weakening interactions between 57 and the active sites. Co-adsorbed water may replace alkali ion clusters as electron-traps.

Irradiation of 1,2,4,5-tetracyanobenzene (**216**) in NaY or partially exchanged Cs,NaY generated the radical anion, detected by time-resolved DR UV-Vis spectroscopy.²⁰³ Both singlet and triplet excited states can abstract an electron from the zeolite lattice. However, dealuminated Y zeolites, which are weaker electron donors than NaY or Cs, NaY, do not form radical anion **216**^{•-}.²⁰³

Irradiation of acetophenone (**183**) in the presence of aliphatic amines inside zeolite NaY (Section VII.A.3) generated amine dimer radical cations, however without any evidence for the radical anion **183**^{•-}. A few other carbonyl compounds gave rise to radical anions, although with an interesting dependence on loading. For example, triplet 1-azaxanthone is

quenched efficiently ($7.4 \times 10^8 \text{ M}^{-1} \text{ s}^{-1}$) by triethylamine in solution, generating the ketyl radical anion ($\lambda_{\text{max}} 670 \text{ nm}$).⁵¹⁹ In zeolite NaY, on the other hand, co-irradiation of triethylamine with 1-azaxanthone or benzophenone initially increased the triplet lifetimes; this effect was ascribed to the amine neutralizing NaY acid sites, which otherwise quench triplet states of aromatic ketones.⁵²⁰ Once the acid sites are neutralized, increased loadings of triethylamine (> 1.3 per supercage) begin to quench 1-azaxanthone and benzophenone triplets, generating radical anions.⁵²¹

These few examples show radical anions in zeolites to be an interesting area of research, though as yet of limited scope compared to the plethora of radical cations in zeolites. These limitations are not unexpected because of the unfavorable Coulomb interactions of anions with the overall negatively charged zeolite lattices. Still, additional anions or radical anions are expected to emerge in future research, particularly in Al-poor zeolites.

X. Organic Radical Cations Generated in Inorganic Solids Related to Zeolites

Although a comprehensive coverage of radical cations generated on the surface of solids other than zeolites goes beyond the scope of this review, many similarities in the chemical and photochemical behavior of organic molecules in zeolites and on related inorganic supports are apparent.^{434,522–526} In this context, we reiterate that the recent significant progress in organic radical cation chemistry in zeolites has its roots in the seminal studies of Rooney, Leftin, Hall, and others in the 1960s on amorphous silicas and aluminas.^{257,319–330,527–529} The adsorption of electron-rich arenes, alkenes, heterocycles, etc. on

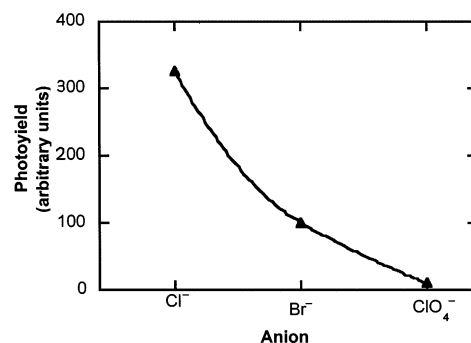


Figure 33. Effect of counteranion on the radical cation yield upon irradiation of methyl viologen adsorbed on porous silica gel. Reprinted with permission from ref 539. Copyright 1997 American Chemical Society.

acid solids spontaneously generated radical cations by ET from the organic substrate to the support. With the advent of synthetic zeolites (Barrer's faujasites), the pioneering studies were extended naturally to the newly synthesized aluminosilicates.

PET reactions of polycyclic aromatics on the surface of inorganic oxides (silica, alumina) or clays were studied thoroughly.^{434,523,524,530–531} Photolysis of pyrene (**57**) on silica or alumina generated 357^* and $57^{\cdot+}$,^{532–535} that of anthracene (**56**) on silica gel showed an interesting dependence on laser fluency; the formation of 356^* ($\lambda_{\text{max}} 420 \text{ nm}$) was monophotonic, whereas that of $56^{\cdot+}$ ($\lambda_{\text{max}} 715 \text{ nm}$) was bi- or multiphotonic.⁵³⁶ Similarly, distyrylbenzene triplet state and radical cation were generated on silica,⁵³⁷ and $57^{\cdot+}$ on the surface of silica gel.^{392,538}

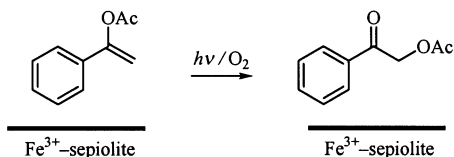
Irradiation (320 nm) of alkyl viologen chloride or bromide in porous silica gels caused ET from the halide anion to the viologen; the resulting radical cations were characterized by ESR and DR UV-Vis spectroscopy.⁵³⁹ In contrast to zeolites, silica gel is neutral; therefore, inclusion of *N*-alkyl viologen dications in silica requires co-inclusion of charge-balancing anions. The role of the counterions is born out by the effect of their redox potentials on the radical cation yields (Figure 33). Thus, irradiation of 203^{2+} diperchlorate failed to generate $203^{\cdot+}$, whereas the yield for Cl⁻ is higher than for Br⁻.

Including alkyl viologens during the sol-gel synthesis of the porous silica produced higher loadings (and higher radical cation yields) than impregnation after preparation. The viologen radical cation decays predominantly by BET; its yield in the steady-state irradiation is controlled by the radical cation stability, increasing with the pore dimensions, reaching a plateau at 6-nm pores. This is interpreted as reflecting the influence of the average distance between the viologen radical cation and the chlorine atoms on the BET rate.

Irradiation of pyrene (**57**) on Laponite, a synthetic layered clay, generated a strongly stabilized $57^{\cdot+}$ (half-life 75 h), identified by conventional UV-Vis spectroscopy.^{101,540} The quantum yield was estimated by determining the light absorbed from the difference of the light reflected/scattered by the samples with and without **57**, using the extinction coefficient of $57^{\cdot+}$ measured in solution ($6.0 \times 10^4 \text{ M}^{-1} \text{ s}^{-1}$ at 450 nm).¹⁴⁹ The system **57**/Laponite is used as standard

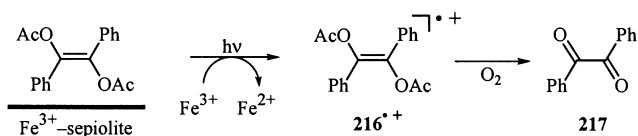
for measuring the quantum yield of $57^{+\bullet}$ in zeolites X and Y.⁵¹⁸

Sepiolite is a magnesium aluminosilicate clay of fiber structure. A fraction of Mg^{2+} ions located at the fiber edges can be exchanged for Na^+ by treatment with NaOH at 110 °C, and Na^+ can be replaced by metal ions (Fe^{3+} , Al^{3+} , Cr^{3+} , Cu^{2+} , etc.). Fe^{3+} ions in Fe^{3+} -exchanged Sepiolite (1.7 meq of $Fe^{3+} g^{-1}$) act as Lewis acid in thermal reactions or as photochemical electron acceptors.⁵⁴¹



Adsorption of perylene onto Fe^{3+} -sepiolite generated the radical cation, detected by ESR.⁵⁴² Photolysis of enol acetates on this material yielded α -acetoxy ketones, presumably via enol acetate radical cations. The mechanism was assigned by comparing the product distributions obtained with a Lewis acid catalyst (BF_3) and an ET photosensitizer (triphenylpyrylium, $165^+ BF_4^-$).⁵⁴¹

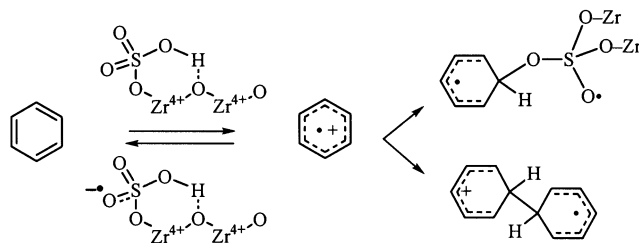
The photolysis of 4-acetoxychromene⁵⁴² or α,β -diacetoxystilbene (**216**)⁵⁴³ on the surface of Fe^{3+} -sepiolite yielded some products characteristic of ET sensitization by 165^+ (3-acetoxy-4-chromanone from 4-acetoxychromene; benzil, **217**, from **216**). Apparently, a fraction of the excited states generates radical cations by ET to Fe^{3+} ions.



N-Alkylphenothiazines are electron-rich heterocycles that easily generate the corresponding radical cation. Upon incorporation into MCM-type mesoporous silicates or microporous aluminophosphates their radical cations were detected by conventional spectroscopic techniques. Kevan and co-workers studied the influence of the alkyl chain and the chemical composition of the host on the photo yield of radical cations.^{544–546}

In contrast to acid zeolites, sulfated zirconia [ZrO_2 calcined with $(NH_4)_2SO_4$ or H_2SO_4]^{547–549} acts as a superacid, causing the skeletal isomerization of *n*-alkanes at room temperature.⁹ Interestingly, the activity of sulfated zirconia in isomerizing *n*-alkanes parallels its ability to oxidize benzene and alkylbenzenes.^{550–552}

Thus, reaction of benzene (**40**) on sulfated zirconia generated a complex mixture of biphenyl, alkylbenzenes, and phenol.^{551,553} Radical cation $40^{+\bullet}$ is the likely intermediate, reacting with or coupling to the solid support, forming phenyl sulfites or sulfates.⁵⁵¹ The reaction of adamantane over sulfated zirconia generated diadamantane, a product characteristic for free radical coupling; the adamantane radical cation may be the primary intermediate.⁵⁵²



Visible irradiation of benzene on sulfated zirconia leads to ionization.⁵⁵⁴ The presence of oxygen shifts the photoreaction red edge to longer wavelengths and appears to strengthen the acceptor sites.⁵⁵⁴ A qualitative correlation between the strength of acceptor sites and isomerization was noted.

Irradiation (370 nm) of *N, N, N', N'*-tetramethylbenzidine inside α -zirconium phosphate generated the radical cation (ESR, DR) in a monophotonic reaction;⁵⁵⁵ its half-life ($t_{1/2} \sim 10$ h) is an order of magnitude longer than that in micelles or on amorphous silica gel.

Finally, photolysis of organic guests on the surface of highly dispersed semiconductors generally induces redox reactions. TiO_2 and related semiconductors are not microporous solids; they can be prepared as colloids with particle sizes in the nanometer range. Smaller particles have greater external surface areas and adsorb larger quantities of organic molecules. Irradiation on semiconductor surfaces may selectively oxidize organic substrates but more often causes complete oxidative degradation. Organic radical cations are the likely primary intermediates; O_2 serves as the oxidizing agent. The effective wavelength for photooxidation is that absorbed by the semiconductor. Comprehensive reviews of the photoactivity of TiO_2 and other semiconductors have been published.^{229,556,557}

XI. Concluding Remarks and Perspective

The preceding review illustrates that zeolites are a large family of versatile, well-characterized acid catalysts, whose structure and properties are relatively well understood. The review focused especially on their ability to generate spontaneously organic radical cations or to serve as hosts in which these species can be stabilized after chemical, photochemical, or electrochemical generation.

Still, many intriguing questions remain, and new facets of zeolite chemistry are certain to attract the attention of future researchers. Among the topics that are expected to attract scrutiny, the following may be of special interest: (i) further insight into the nature of the electron acceptor sites and the fate of the captured/donated electron; (ii) control over the number of active sites and modulation of their oxidizing strength; (iii) theoretical approaches to better understand/explain the unique behavior of these microporous solids; (iv) attempts to promote electron transfer reactions on a preparative (gram to multigram) scale similar to chemical electron transfer reagents [tris(4-bromophenyl)amminium]; (v) attempts to generate additional radical anions within zeolites and to scope their relative stability; and (vi)

applications of indefinitely persistent organic radical cations inside zeolites in nanochemistry and material science.

Many new zeolites and microporous solids, such as the novel delaminated zeolites⁵⁵⁸ and periodic mesoporous organosilica hybrid materials,^{559–561} will be designed, synthesized, characterized, and applied. Of particular interest will be materials that would allow the slow evolution of primary radical ions and their controlled transformation into secondary species (radical ions, free radicals, ions), thereby making it possible to fully characterize the consecutive intermediates.

Further, zeolites appear well-suited as hosts to develop nanoscopic supramolecular systems for application in material science. Given the current emphasis on nanotechnology, one can envision functional molecular materials, perhaps even an array of molecular machines based on organic radical cations incorporated or synthesized within zeolite cavities, performing some light-powered action through the intermediacy of radical cations. Persistent organic radical cations might be isolated and, perhaps, ferromagnetic or antiferromagnetically coupled inside zeolites, although the task of orienting and handling the zeolite particles still awaits a solution. Recent reports describing films of oriented zeolite particles^{562–568} or the use of particles in the millimeter range may point the way to address this formidable task. In summary, there is no doubt that exciting research on sophisticated systems containing organic radical cations within zeolites will continue for the foreseeable future.

XII. Acknowledgments

We are indebted to many colleagues and co-workers who collaborated with us over the years, particularly Prof. Miguel A. Miranda who encouraged us to write this review. Iberdrola is acknowledged for awarding the 1997 Visiting Professor grant to H.D.R. The Generalitat Valenciana is also acknowledged for a fellowship to H.D.R. Financial support by CICYT (Spain) and NSF (USA) is gratefully acknowledged. H.G.G. thanks Dr. Emilio Palomares for his help in editing this manuscript.

XIII. References

- International Zeolite Conferences are held biennially. They are intended to report on current advances in zeolite synthesis and modification. Proceedings of these conferences are published as special volumes of the series *Studies in Surface Science and Catalysis*. The 12th meeting was held in Granada (Spain).
- Ocelli, M. L.; Robson, H. E., Eds.; *Zeolite Synthesis*; American Chemical Society: Washington, 1989; Vol. 398.
- Ocelli, M. L.; Robson, H., Eds.; *Molecular Sieves*; Van Nostrand Reinhold: New York, 1992; Vol. I: Synthesis of Microporous Materials.
- Chon, H.; Ihm, S.-K.; Sun Uh, Y., Eds.; *Progress in Zeolite and Microporous Materials*; Elsevier: Amsterdam, 1997; Vol. 105.
- Venuto, P. B.; Hamilton, L. A.; Landis, P. S.; Wise, J. J. *J. Catal.* **1966**, *5*, 81.
- Venuto, P. B. *Adv. Catal.* **1968**, *18*, 259.
- Hölderich, W. F. In *Heterogeneous Catalysis and Fine Chemistry*; Elsevier: Amsterdam, 1991; Vol. 59.
- Hölderich, W. F. *Stud. Surf. Sci. Catal.* **1993**, *75*, 127.
- Corma, A.; García, H. *Catal. Today* **1997**, *38*, 257.
- Wojciechowski, B. W.; Corma, A. *Catalytic Cracking, Catalysts Kinetics and Mechanisms*; Marcel Dekker: New York, 1984.
- Ocelli, M. L., Ed.; *Fluid Catalytic Cracking II. Concepts in Catalyst Design*; American Chemical Society: Washington, 1991; Vol. 452.
- Ocelli, M. L.; O'Connor, P., Eds.; *Fluid Catalytic Cracking III. Materials and Processes*; American Chemical Society: Washington, 1994; Vol. 571.
- Barrer, R. M. *Zeolites and Clay Minerals as Sorbents and Molecular Sieves*; Academic Press: London, 1978.
- van Bekkum, H.; Flanigen, E. M.; Jansen, J. C., Eds.; *Introduction to Zeolite Science and Practice*; Elsevier: Amsterdam, 1991.
- Guidelines for Mastering the Properties of Molecular Sieves. Relationship Between the Physicochemical Properties of Zeolitic Systems and their Low Dimensionality*; Barthomeuf, D.; Derouane, E. G.; Hölderich, W., Eds.; Plenum Press: New York, 1990.
- Zeolite Microporous Solids: Synthesis, Structure and Reactivity*; Derouane, E. G.; Lemos, F.; Naccache, C.; Ramoa Ribeiro, F., Eds.; Kluwer Academic: Dordrecht, 1992; Vol. 352.
- Breck, D. W. *Zeolite Molecular Sieves: Structure, Chemistry and Use*; John Wiley and Sons: New York, 1974.
- McDaniel, C. V.; Maher, P. K. In *ACS Monograph*; Rabo, J. A., Ed.; American Chemical Society: Washington, DC, 1976; Vol. 171.
- Rabo, J. A.; Angell, C. L.; Kasai, P. H.; Schomaker, V. *Discuss. Faraday Soc.* **1966**, *41*, 328.
- Dempsey, E. *J. Phys. Chem.* **1969**, *73*, 3660.
- Jousse, F.; Cohen de Lara, E. *J. Phys. Chem.* **1996**, *100*, 233.
- Blatter, F.; Frei, H. *J. Am. Chem. Soc.* **1993**, *115*, 7501.
- Blatter, F.; Frei, H. *J. Am. Chem. Soc.* **1994**, *116*, 1812.
- Cambor, M. A.; Corma, A.; Valencia, S. *Chem. Commun.* **1996**, 2265.
- Cambor, M. A.; Corma, A.; Mifsud, A.; Pérez-Pariente, J.; Valencia, S. *Stud. Surf. Sci. Catal.* **1997**, *105*, 341.
- Dessau, R. M. *ACS Symp. Ser.* **1980**, *135*, Chapter 6.
- Argauer, R. J.; Landolt, G. R. U. S. Patent 1982, 3702886.
- Cambor, M. A.; Mifsud, A.; Pérez-Pariente, J. *Zeolites* **1991**, *11*, 792.
- Davis, M. E. *Acc. Chem. Res.* **1993**, *26*, 111.
- Meier, W. M.; Olson, D. H. *Atlas of Zeolite Structure Types*; Butterworth: London, 1992.
- Meier, W. M.; Olson, D. H.; Baerlocher, C. *Zeolites* **1996**, *17*, 1.
- Kärger, J.; Ruthven, D. M. *Diffusion in Zeolites and Other Microporous Solids*; John Wiley and Sons: New York, 1992.
- Turro, N. J. *Pure Appl. Chem.* **1986**, *58*, 1219.
- Yoon, K. B.; Kochi, J. K. *J. Am. Chem. Soc.* **1988**, *110*, 6586.
- Cohen, M. D.; Schmidt, G. M. J. *J. Chem. Soc.* **1964**, 1996.
- Cohen, M. D.; Schmidt, M. J. G. *Proc. Inter. Symp. Reactivity Solids, 4th*; Amsterdam, 1961, 556.
- Weiss, R. G.; Ramamurthy, V.; Hammond, G. S. *Acc. Chem. Res.* **1993**, *26*, 530.
- Brunauer, S.; Emmett, P. H.; Teller, E. *J. Am. Chem. Soc.* **1938**, *60*, 309.
- Terasaki, O.; Yamazaki, K.; Thomas, J. M.; Ohsuna, T.; Watanabe, D.; Sanders, J. V.; Barry, J. C. *J. Solid State Chem.* **1988**, *77*, 72.
- Terasaki, O. *J. Electron Microsc.* **1994**, *43*, 337–346.
- Zandbergen, H. W.; van Dick, D. Proc. XIth Int. Congress on Electron Microscopy, Kyoto, 1986.
- Niemantsverdriet, J. W. *Spectroscopy in Catalysis*; VCH: Weinheim, 1993.
- Schrader, B. *Infrared and Raman Spectroscopy (Methods and Applications)*; VCH Publishers Inc: Weinheim, 1995.
- Klinowski, J. *Prog. NMR Spectrosc.* **1984**, *16*, 237.
- Engelhardt, G.; Michel, D. *High-Resolution Solid-State NMR of Silicates and Zeolites*; John Wiley & Sons: Norwich (U.K.), 1987.
- Ertl, G.; Küppers, J. *Low Energy Electrons and Surface Chemistry*; VCH: Weinheim, 1985.
- Jacobs, P. A.; Beyer, H. K. *J. Phys. Chem.* **1979**, *83*, 1174.
- Rocha, J.; Carr, S. W.; Klinowski, J. *Chem. Phys. Lett.* **1991**, *187*, 401.
- Harvey, G.; Prins, R.; Crockett, R.; Roduner, E. *J. Chem. Soc., Faraday Trans.* **1996**, *92*, 2027.
- Scherzer, J.; Gruia, A. J. *Hydrocracking Science and Technology*; Marcel Dekker: New York, 1996.
- Ozin, G. A.; Godber, J. *J. Phys. Chem.* **1989**, *93*, 878.
- Bard, A. J.; Ledwith, A.; Shine, H. J. In *Adv. Phys. Org. Chem.*; Academic Press: London, 1976; Vol. 12.
- Zholobenko, V. L.; Kustov, L. M.; Kazanskii, V. B. *Kinet. Catal.* **1989**, *30*, 792.
- Kucherov, A. V.; Slinkin, A. A.; Kharson, M.; Bondarenko, T. N.; Minachev, K. M. *Kinet. Catal.* **1989**, *30*, 193.
- Ichikawa, T.; Yamaguchi, M.; Yoshida, H. *Chem. Lett.* **1989**, 1472.
- Goldfarb, D.; Strohmaier, K. G.; Vaughan, D. E. W.; Thomann, H.; Poluektov, O. G.; Schmidt, J. *J. Am. Chem. Soc.* **1996**, *118*, 4665.
- Goldfarb, D.; Bernardo, M.; Strohmaier, K. G.; Vaughan, D. E. W.; Thomann, H. *J. Am. Chem. Soc.* **1994**, *116*, 6344.
- Loktev, M. I.; Slinkin, A. A. *Usp. Khim.* **1976**, *45*, 1594.
- Weisz, P. B. *Annu. Rev. Phys. Chem.* **1970**, *21*, 175.
- Rabo, J. A.; Poutsma, M. L. *Molecular Sieve II*; American Chemical Society: Washington, 1971.

- (61) Vedrine, J. C.; Abou-Kas, A.; Massardier, J.; Dalmai-Imelik, G. *J. Chem. Soc., Faraday Trans.* **1974**, *70*, 1039.
- (62) Krzyzanowski, S. *Bull. Acad. Pol. Sci.* **1976**, *24*, 915.
- (63) Kucherov, A. V.; Slinkin, A. A.; Kondratyev, D. A.; Bondarenko, T. N.; Rubinstein, A. M.; Minachev, K. M. *J. Mol. Catal.* **1986**, *37*, 107.
- (64) Khadzhiev, S. N.; Yaralov, N. G.; Shumorski, Y. V. *React. Kinet. Catal. Lett.* **1984**, *24*, 297.
- (65) Slinkin, A. A.; Emberson, S. C.; Derouane, E. G. *Kinet. Catal.* **1994**, *35*, 102.
- (66) Cano, M. L.; Corma, A.; Fornés, V.; García, H. *J. Phys. Chem.* **1995**, *99*, 4241.
- (67) Corma, A.; Fornés, V.; García, H.; Martí, V.; Miranda, M. A. *Chem. Mater.* **1995**, *7*, 2136.
- (68) Sommer, J.; Hachoumy, M.; Garin, F. *J. Am. Chem. Soc.* **1994**, *116*, 5491.
- (69) Corma, A. *Chem. Rev.* **1995**, *95*, 559.
- (70) Rooney, J. J.; Pink, R. C. *Proc. Chem. Soc.* **1960**, 70.
- (71) Flockhart, B. D.; McLoughlin, L.; Pink, R. C. *J. Catal.* **1972**, *25*, 305.
- (72) Ward, J. W.; Hansford, R. C. *J. Catal.* **1964**, *13*, 364.
- (73) Rabo, J. A.; Gajda, G. *J. Catal. Rev. Sci. Eng.* **1989**, *31*, 385.
- (74) Corma, A.; García, H.; Primo, J. *J. Chem. Res. (S)* **1988**, 40.
- (75) Mortier, W. J. *J. Catal.* **1978**, *55*, 138.
- (76) Barthomeuf, D. In *NATO ASI Series C*; Fraissard, J., Petrakis, L., Eds.; Kluwer Academic: Dordrecht, 1994; Vol. 444.
- (77) Pine, L. A.; Maher, P. J.; Wachter, W. A. *J. Catal.* **1984**, *85*, 446.
- (78) Zicovich-Wilson, C.; Planelles, J. H.; Jaskolski, W. *Int. J. Quantum Chem.* **1994**, *50*, 429.
- (79) Zicovich-Wilson, C. M.; Corma, A.; Viruela, P. *J. Phys. Chem.* **1994**, *98*, 10863.
- (80) Sastre, G.; Viruela, P. M.; Corma, A. *Chem. Phys. Lett.* **1997**, *264*, 565.
- (81) Corma, A.; García, H.; Sastre, G.; Viruela, P. M. *J. Phys. Chem. B* **1997**, *101*, 4575.
- (82) Marquez, F.; García, H.; Palomares, E.; Fernandez, L.; Corma, A. *J. Am. Chem. Soc.* **2000**, *122*, 6520.
- (83) Marquez, F.; Zicovich-Wilson, C.; Corma, A.; Palomares, E.; García, H. *J. Phys. Chem. B* **2001**, *105*, 9973.
- (84) Arribas, J.; Corma, A.; Fornés, V. *J. Catal.* **1984**, *88*, 374.
- (85) Emeis, C. A. *J. Catal.* **1993**, *141*, 347.
- (86) Corma, A.; Fornés, V.; Forni, L.; Marquez, F.; Martínez-Triguero, J.; Moschetti, D. *J. Catal.* **1998**, *179*, 451.
- (87) Shih, S. *J. Catal.* **1983**, *79*, 390.
- (88) Chen, F. R.; Fripiat, J. J. *J. Phys. Chem.* **1992**, *96*, 819.
- (89) Yudanov, I. V.; Zakharov, I. I.; Zhidomirov, G. M. *React. Kinet. Catal. Lett.* **1992**, *48*, 411.
- (90) Harvey, G.; Prins, R.; Crockett, R.; Roduner, E. *J. Chem. Soc., Faraday Trans.* **1996**, *92*, 2027.
- (91) Shih, S. *J. Catal.* **1983**, *79*, 390.
- (92) Folgado, J. V.; García, H.; Martí, V.; Esplá, M. *Tetrahedron* **1997**, *53*, 4947.
- (93) Ramamurthy, V.; Caspar, J. V.; Corbin, D. R. *J. Am. Chem. Soc.* **1991**, *113*, 594.
- (94) Caldararu, H.; Carageorghopol, A.; Russu, R. *Colloids Surf. A* **1993**, *72*, 37.
- (95) Vedrine, J. C.; Auroux, A.; Bolis, V.; Dejaifve, P.; Naccache, C.; Wierzchowski, P.; Derouane, E. G.; Nagy, J. B.; Gilson, J.-P.; van Hooff, J. H. C.; van der Berg, J. P.; Wolthuizen, J. *J. Catal.* **1979**, *59*, 248.
- (96) Kucherov, A. V.; Slinkin, A. A. *Kinet. Katal.* **1982**, *23*, 1172.
- (97) Kucherov, A. V.; Slinkin, A. A. *Kinet. Katal.* **1983**, *24*, 955.
- (98) Lange, J. P.; Gutsze, A.; Karge, H. G. *J. Catal.* **1988**, *114*, 136.
- (99) Chen, F. R.; Guo, X. X. *J. Chem. Soc., Faraday Trans.* **1992**, *88*, 511.
- (100) Wierzchowski, P.; Garbowski, E.; Vedrine, J. C. *J. Chem. Phys.* **1981**, *78*, 41.
- (101) Iu, K. K.; Thomas, J. K. *J. Phys. Chem.* **1991**, *95*, 506.
- (102) Iu, K. K.; Thomas, J. K. *Colloids Surf.* **1992**, *63*, 39.
- (103) Iu, K. K.; Liu, X. S.; Thomas, J. K. *J. Photochem. Photobiol. A* **1994**, *79*, 103.
- (104) Rabo, J. A. P.; P. E.; Stamires, D. N.; Boyle, J. E. Molecular sieve catalysts in hydrocarbon reactions. *Actes Congr. Intern. Catalyse, 2e, Paris, 1960* **1961**, *2*, 2055.
- (105) Park, Y. S.; Lee, Y. S.; Yoon, K. B. *J. Am. Chem. Soc.* **1993**, *115*, 12220.
- (106) Edwards, P. P.; Andreson, P. A.; Thomas, J. M. *Acc. Chem. Res.* **1996**, *29*, 23.
- (107) Dollish, F. R.; Hall, W. K. *J. Phys. Chem.* **1967**, *71*, 1005.
- (108) Tokunaga, H. J.; Ono, Y.; Keii, T. *Bull. Chem. Soc. Jpn.* **1973**, *46*, 3569.
- (109) Shine, H. J.; Piette, L. *J. Am. Chem. Soc.* **1962**, *84*, 4798.
- (110) Aalsbersberg, W. J.; Hoijtink, G. J.; Mackor, E. L.; Weijland, W. P. *J. Chem. Soc.* **1959**, 3049.
- (111) Ronlan, A.; Parker, V. D. *J. Chem. Soc., Chem. Commun.* **1974**, 33.
- (112) Volodin, A. M.; Bolshov, V. A.; Panov, G. I. *J. Phys. Chem.* **1994**, *98*, 7548.
- (113) Cozens, F. L.; Cano, M. L.; García, H.; Schepp, N. P. *J. Am. Chem. Soc.* **1998**, *120*, 5667.
- (114) Goupil, J.-M.; Hemidy, J.-F.; Cornet, D. *J. Chim. Phys.* **1976**, *73*, 431–435.
- (115) Muha, G. M. *J. Phys. Chem.* **1970**, *74*, 2939.
- (116) Beyer, H. K.; Belenykaja, I. M. *Stud. Surf. Sci. Catal.* **1980**, *5*, 203.
- (117) Lucken, E. A. C. *J. Chem. Soc.* **1962**, 4963.
- (118) Fava, A.; Sogo, P. B.; Calvin, M. *J. Am. Chem. Soc.* **1957**, *79*, 1078.
- (119) Jones, G., II; Huang, B.; Griffin, S. F. *J. Org. Chem.* **1993**, *58*, 2035.
- (120) Boduszek, B.; Shine, H. J. *J. Org. Chem.* **1988**, *53*, 5142.
- (121) Lakkaraju, P. S.; Zhou, D.; Roth, H. D. *J. Chem. Soc., Perkin Trans. 2* **1998**, 1119.
- (122) Radwglia, R.; Engelhardt, G. *Chem. Phys. Lett.* **1985**, *114*, 28.
- (123) Auerbach, S. M.; Henson, N. J.; Cheetham, A. K.; Metiu, H. I. *J. Phys. Chem.* **1995**, *99*, 10600.
- (124) Nowak, A. K.; Den Ouden, C. J. J.; Pickett, S. D.; Smit, B.; Cheetham, A. K.; Post, M. F. M.; Thomas, J. M. *J. Phys. Chem.* **1991**, *95*, 848.
- (125) Nowak, A. K.; Cheetham, A. K. *Stud. Surf. Sci. Catal.* **1986**, *28*, 475.
- (126) Pickett, S. D.; Nowak, A. K.; Thomas, J. M.; Cheetham, A. K. *Zeolites* **1989**, *9*, 123.
- (127) Mellot, C. F.; Cheetham, A. K.; Harms, S.; Savitz, S.; Gorte, R. J.; Myers, A. L. *J. Am. Chem. Soc.* **1998**, *120*, 5788.
- (128) Grey, C. P.; Poshni, F. I.; Gualtieri, A. F.; Norby, P.; Hanson, J. C.; Corbin, D. R. *J. Am. Chem. Soc.* **1997**, *119*, 1981.
- (129) Lim, K. H.; Grey, C. P. *J. Am. Chem. Soc.* **2000**, *122*, 9768.
- (130) Eckert, J.; Draznieks, C. M.; Cheetham, A. K. *J. Am. Chem. Soc.* **2002**, *124*, 170.
- (131) Turro, N. J.; Lei, X.; Cheng, C.-C. *J. Am. Chem. Soc.* **1985**, *107*, 5824.
- (132) Baldovi, M. V.; Cozens, F. L.; Fornés, V.; García, H.; Scaiano, J. C. *Chem. Mater.* **1996**, *8*, 152.
- (133) Sastre, G.; Cano, M. L.; Corma, A.; Nicolopoulos, S.; González-Calbet, J. M.; Vallet-Regí, M.; García, H. *J. Phys. Chem. B* **1997**, *101*, 10184.
- (134) Steele, M. R.; Macdonald, P. M.; Ozin, G. A. *J. Am. Chem. Soc.* **1993**, *115*, 7285.
- (135) Kim, Y. I.; Keller, S. W.; Krueger, J. S.; Yonemoto, E. H.; Saupe, G. B.; Mallouk, T. E. *J. Phys. Chem. B* **1997**, *101*, 2491.
- (136) Fukuzumi, S.; Suenobu, T.; Urano, T.; Tanaka, K. *Chem. Lett.* **1997**, 875.
- (137) Herron, N.; Stucky, G. D.; Tolman, C. A. *J. Chem. Soc., Chem. Commun.* **1986**, 1521.
- (138) Herron, N. *Inorg. Chem.* **1986**, *25*, 4714.
- (139) Balkus, K. J.; Gabrielov, A. G. *J. Incl. Phenom. Mol. Recognit. Chem.* **1995**, *21*, 159.
- (140) Quayle, W. H.; Lunsford, J. H. *Inorg. Chem.* **1982**, *21*, 97.
- (141) Dutta, P. K.; Turbeville, W. *J. Phys. Chem.* **1992**, *96*, 9410.
- (142) Liu, X. S.; Lu, K. K.; Thomas, J. K. *J. Chem. Soc., Faraday Trans.* **1993**, *89*, 1861.
- (143) Yamashita, H.; Ichihashi, Y.; Anpo, M.; Hashimoto, M.; Louis, C.; Che, M. *J. Phys. Chem.* **1996**, *100*, 16041.
- (144) Anpo, M.; Yamashita, H.; Ichihashi, Y.; Fujii, Y.; Honda, M. *J. Phys. Chem. B* **1997**, *101*, 2632.
- (145) Corrent, S.; Cosa, G.; Scaiano, J. C.; Galletero, M. S.; Alvaro, M.; García, H. *Chem. Mater.* **2001**, *13*, 715.
- (146) Bossmann, S. H.; Turro, C.; Schnabel, C.; Pokhrel, M. R.; Payawan, L. M., Jr; Baumeister, J. B.; Wörner, M. *J. Phys. Chem. B* **2001**, *105*, 5374.
- (147) Engel, S.; Kynast, U.; Unger, K. K.; Schüth, F. *Stud. Surf. Sci. Catal.* **1994**, *84*, 477.
- (148) Vasenkov, S.; Frei, H. *J. Phys. Chem. B* **1997**, *101*, 4539.
- (149) Shida, T. *Electronic Absorption Spectra of Radical Ions*; Verlag Chemie: New York, 1988.
- (150) Kortum, G. *Reflectance Spectroscopy*; Springer: Berlin, 1969.
- (151) Kubelka, P.; Munk, F. *Z. Tech. Phys.* **1931**, *12*, 593.
- (152) Hashimoto, S. In *Molecular and Supramolecular Photochemistry*; Ramamurthy, V., Schanze, K. S., Eds.; Marcel Dekker: New York, 2000; Vol. 5.
- (153) Wilkinson, F.; Kelly, G. In *Handbook of Organic Photochemistry*; Scaiano, J. C., Ed.; CRC Press: Boca Raton, FL, 1989; Vol. 1.
- (154) Bohne, C.; Redmond, R. W.; Scaiano, J. C. In *Photochemistry in Organized and Constrained Media*; Ramamurthy, V., Ed.; VCH: New York, 1991.
- (155) Lakowicz, J. R. *Principles of Fluorescence Spectroscopy*; Plenum Press: New York and London, 1983.
- (156) Makarova, M. A.; Dwyer, J. *J. Phys. Chem.* **1993**, *97*, 6337.
- (157) Misono, Y.; Shibasaki, K.; Yamasawa, N.; Mineo, Y.; Itoh, K. *J. Phys. Chem.* **1993**, *97*, 6054.
- (158) Carrington, A.; Moss, R. E.; Todd, P. F. *Mol. Phys.* **1967**, *12*, 95.
- (159) Wertz, J. E.; Bolton, J. R. *Electron Spin Resonance; Elementary Theory and Practical Applications*, McGraw-Hill: New York, 1972.
- (160) McLauchlan, K. A.; Stevens, D. G. *J. Chem. Phys.* **1987**, *87*, 4399.
- (161) Fessenden, R. W.; Schuler, R. H. *J. Chem. Phys.* **1963**, *39*, 2147.

- (162) McLauchlan, K. A.; Stevens, D. G. *Chem. Phys. Lett.* **1985**, *115*, 108.
- (163) Buckley, C. D.; McLauchlan, K. A. *Mol. Phys.* **1985**, *54*, 1.
- (164) McLauchlan, K. A.; Stevens, D. G. *Mol. Phys.* **1986**, *57*, 223.
- (165) Basu, S.; McLauchlan, K. A. *J. Magn. Reson.* **1983**, *51*, 335.
- (166) Smaller, B.; Remko, J. R.; Avery, E. C. *Chem. Phys.* **1968**, *48*, 5174.
- (167) Trifunac, A. D.; Norris, J. R. *Chem. Phys. Lett.* **1978**, *59*, 140.
- (168) Trifunac, A. D.; Norris, J. R.; Lawler, R. G. *J. Chem. Phys.* **1979**, *71*, 4380.
- (169) El Sayed, M. *MTP Intern. Rev. Science, Spectrosc.* **1972**, *119*, 1972.
- (170) Frankevich, E. L.; Pristupa, A. I.; Lesin, V. I. *Chem. Phys. Lett.* **1977**, *47*, 304.
- (171) Anisimov, O. A.; Grigoryants, V. M.; Molchanov, V. K.; Molin, Y. N. *Phys. Chem.* **1979**, *248*, 380.
- (172) Trifunac, A. D.; Smith, J. P. *Chem. Phys. Lett.* **1980**, *73*, 94.
- (173) Werst, D. W.; Trifunac, A. D. *J. Phys. Chem.* **1991**, *95*, 3466.
- (174) Corma, A. *Chem. Rev.* **1997**, *97*, 2373.
- (175) Hölderich, W. F.; Hesse, M.; Näumann, F. *Angew. Chem., Int. Ed. Engl.* **1988**, *27*, 226.
- (176) Hölderich, W. F. *Stud. Surf. Sci. Catal.* **1993**, *75*, 127.
- (177) Venuto, P. B. *Microporous Mater.* **1994**, *2*, 297.
- (178) Vishnetskaya, M. V.; Romanovskii, B. V. *Zh. Fiz. Khim.* **1993**, *67*, 1740.
- (179) Vishnetskaya, M. V.; Romanovskii, B. V.; Lipovich, V. G. *Petroleum Chem.* **1997**, *37*, 195.
- (180) Choukroun, H.; Brunel, D.; Germain, A. *J. Chem. Soc., Chem. Commun.* **1986**, 6.
- (181) Chen, F. R.; Guo, X. X. *J. Chem. Soc., Faraday Trans.* **1992**, *88*, 511.
- (182) Pardillos, J.; Brunel, D.; Coq, B.; Massiani, P.; Ménorval, L. C.; Figueras, F. *J. Am. Chem. Soc.* **1990**, *112*, 1313.
- (183) Becker, L.; Forster, H. *Appl. Catal. A* **1997**, *153*, 31.
- (184) Pollack, S. S.; Sprecher, R. F.; Frommell, E. A. *J. Mol. Catal.* **1991**, *66*, 195.
- (185) Rhodes, C. J. *J. Am. Chem. Soc.* **1988**, *110*, 4446.
- (186) Rhodes, C. J. *J. Chem. Soc., Chem. Commun.* **1991**, 900.
- (187) Rhodes, C. J. *J. Chem. Soc., Faraday Trans.* **1991**, *87*, 3179.
- (188) Rhodes, C. J.; Standing, M. *J. Chem. Soc., Perkin Trans 2* **1992**, 1455.
- (189) Rhodes, C. J. *Colloids Surf. A* **1993**, *72*, 111.
- (190) Roduner, E.; Crockett, R. *J. Phys. Chem.* **1993**, *97*, 11853.
- (191) Crockett, R.; Roduner, E. *J. Chem. Soc., Perkin Trans 2* **1993**, 1503.
- (192) Baciocchi, E.; Del Giacco, T.; Elisei, F. *J. Am. Chem. Soc.* **1993**, *115*, 12290.
- (193) Brunel, D.; Nagy, J. B.; Daelen, G.; Derouane, E. G.; Geneste, P.; Vanderveken, D. *J. Appl. Catal. A* **1993**, *99*, 9.
- (194) Chen, F. R.; Fripiat, J. J. *J. Phys. Chem.* **1993**, *97*, 5796.
- (195) Belevskii, V. N.; Shchapin, I. Y. *Acta Chem. Scand.* **1997**, *51*, 1085.
- (196) Blatter, F.; Sun, H.; Vasenkov, S.; Frei, H. *Catal. Today* **1998**, *41*, 297.
- (197) Feldman, V. I. *Acta Chem. Scand.* **1997**, *51*, 181.
- (198) Roth, H. D.; Weng, H. X.; Zhou, D. H.; Lakkaraju, P. S. *Acta Chem. Scand.* **1997**, *51*, 626.
- (199) Werst, D. W.; Han, P. *Catal. Lett.* **1997**, *45*, 253.
- (200) Werst, D. W.; Han, P.; Trifunac, A. D. *Chem. Phys. Lett.* **1997**, *269*, 333.
- (201) Werst, D. W.; Han, P.; Trifunac, A. D. *Radiat. Phys. Chem.* **1998**, *51*, 255.
- (202) Werst, D. W.; Trifunac, A. D. *Acc. Chem. Res.* **1998**, *31*, 651.
- (203) Hashimoto, S. *J. Chem. Soc., Faraday Trans.* **1997**, *93*, 4401.
- (204) Corio, P. L.; Shih, S. *J. Phys. Chem.* **1971**, *75*, 3475.
- (205) Ichikawa, T.; Yamaguchi, M.; Yoshida, H. *J. Phys. Chem.* **1987**, *91*, 6400.
- (206) Roduner, E.; Wu, L. M.; Crockett, R.; Rhodes, C. J. *Catal. Lett.* **1992**, *14*, 373.
- (207) Roduner, E.; Crockett, R.; Wu, L. M. *J. Chem. Soc., Faraday Trans.* **1993**, *89*, 2101.
- (208) Ichikawa, T.; Hosokawa, H.; Yoshida, H. *Bull. Chem. Soc. Jpn.* **1994**, *67*, 1544.
- (209) Shih, S. *J. Phys. Chem.* **1975**, *79*, 2201.
- (210) Courtneidge, J. L.; Davies, A. G.; Tollerfield, S. M.; Rideout, J.; Symons, M. C. R. *J. Chem. Soc., Chem. Commun.* **1985**, 1092.
- (211) Courtneidge, J. L.; Davies, A. G. *Acc. Chem. Res.* **1987**, *20*, 90.
- (212) Shiotani, M.; Yano, A.; Ohta, N.; Ichikawa, T. *Chem. Phys. Lett.* **1988**, *147*, 38.
- (213) Fox, M. A.; Campbell, K. A.; Hünig, S.; Berneth, H.; Maier, G.; Schneider, K. A.; Malsch, K. D. *J. Org. Chem.* **1982**, *47*, 3408.
- (214) Shiotani, M.; Lund, A. In *Radical Ionic Systems*; Lund, A., Shiotani, M., Eds.; Kluwer Academic: Dordrecht, 1991; p 151.
- (215) Roduner, E.; Crockett, R. *J. Phys. Chem.* **1993**, *97*, 11853.
- (216) Chachaty, C. *J. Chim. Phys.* **1967**, *64*, 614.
- (217) Shida, T.; Egawa, Y.; Kubodera, H. *J. Chem. Phys.* **1980**, *73*, 5963.
- (218) Veselov, A. V.; Melekhov, V. I.; Anisimov, O. A.; Molin, Y. N.; Ushida, K.; Shida, T. *Chem. Phys. Lett.* **1987**, *133*, 478.
- (219) van der Waal, J. C.; van Bekkum, H.; Vital, J. M. *J. Mol. Catal.* **1996**, *97*, 185.
- (220) Crockett, R.; Roduner, E. *J. Chem. Soc., Perkin Trans 2* **1994**, 347.
- (221) Bolshov, V. A.; Volodin, A. M.; Zhidomirov, G. M.; Shubin, A. A.; Bedilo, A. F. *J. Phys. Chem.* **1994**, *98*, 7551.
- (222) Erickson, R.; Lindgren, M.; Lund, A.; Sjöqvist, L. *Colloids Surf. A* **1993**, *72*, 207.
- (223) Bolshov, V. A.; Toktarev, A. V.; Volodin, A. M. *Mendeleev Commun.* **1994**, 212.
- (224) Germain, A.; Akouz, T.; Figueras, F. *J. Catal.* **1994**, *147*, 163.
- (225) Germain, A.; Akouz, T.; Figueras, F. *Appl. Catal.: A* **1996**, *136*, 57.
- (226) Kurita, Y.; Sonoda, T.; Sato, M. *J. Catal.* **1970**, *19*, 82.
- (227) Erickson, R.; Lund, A.; Lindgren, M. *Chem. Phys.* **1995**, *193*, 89.
- (228) Carter, M. K.; Vincow, G. *J. Chem. Phys.* **1967**, *47*, 292.
- (229) *Photoinduced Electron Transfer, Part C*; Fox, M. A., Chanon, M., Eds.; Elsevier: Amsterdam, 1988.
- (230) Zhang, X.; Bordwell, F. G. *J. Org. Chem.* **1992**, *57*, 4163.
- (231) Amyes, T. L.; Richard, J. P.; Novack, M. *J. Am. Chem. Soc.* **1992**, *114*, 8032.
- (232) McClelland, R. A.; Mathivanan, N.; Steenken, S. *J. Am. Chem. Soc.* **1990**, *112*, 4857.
- (233) Soma, Y.; Soma, M.; Harada, I. *J. Phys. Chem.* **1985**, *89*, 738.
- (234) Soma, Y.; Soma, M.; Harada, I. *Chem. Phys. Lett.* **1983**, *94*, 475.
- (235) Ernstbrunner, E.; Girling, R. B.; Grossman, W. E. L.; Hester, R. E. *J. Chem. Soc., Perkin Trans. 2* **1978**, 177.
- (236) Fenn, D. B.; Mortland, M. M.; Pinnavaia, T. J. *Clays Clay Miner.* **1973**, *21*, 315.
- (237) Pinnavaia, T. J.; Mortland, M. M. *J. Phys. Chem.* **1971**, *75*, 3957.
- (238) Soma, Y.; Soma, M.; Harada, I. *Chem. Phys. Lett.* **1983**, *99*, 153.
- (239) Soma, Y.; Soma, M.; Harada, I. *J. Phys. Chem.* **1984**, *88*, 3034.
- (240) Soma, Y.; Soma, M.; Furukawa, Y.; Harada, I. *Clays Clay Miner.* **1987**, *35*, 53.
- (241) Arnold, A.; Gerson, F. *J. Am. Chem. Soc.* **1990**, *112*, 2027.
- (242) Lakkaraju, P. S.; Zhou, D.; Roth, H. D. *J. Chem. Soc. Chem. Commun.* **1996**, 2605.
- (243) Roth, H. D.; Weng, H.; Zhou, D.; Lakkaraju, P. S. *Acta Chem. Scand.* **1997**, *51*, 626.
- (244) Goetz, M.; Eckert, G. *J. Am. Chem. Soc.* **1996**, *118*, 140.
- (245) Eckert, G.; Goetz, M. *J. Am. Chem. Soc.* **1994**, *116*, 11999.
- (246) Lakkaraju, P. S.; Zhou, D. H.; Roth, H. D. *J. Chem. Soc., Chem. Commun.* **1996**, 2605.
- (247) Ramamurthy, V. *Chimia* **1992**, *46*, 359.
- (248) Ramamurthy, V.; Eaton, D. F.; Caspar, J. V. *Acc. Chem. Res.* **1992**, *25*, 299.
- (249) Gessner, F.; Olea, A.; Lobaugh, J. H.; Johnston, L. J.; Scaiano, J. C. *J. Org. Chem.* **1989**, *54*, 259.
- (250) Hashimoto, S.; Mutoh, T.; Fukumura, H.; Masuhara, H. *J. Chem. Soc., Faraday Trans.* **1996**, *92*, 3653.
- (251) Hashimoto, S.; Fukazawa, N.; Fukumura, H.; Masuhara, H. *Chem. Phys. Lett.* **1994**, *219*, 445.
- (252) Liu, X.; Iu, K.-K.; Thomas, J. K.; He, H.; Klinowski, J. *J. Am. Chem. Soc.* **1994**, *116*, 11811.
- (253) Khulbe, K. C.; Mann, R. S. *React. Kinet. Catal. Lett.* **1995**, *56*, 63.
- (254) Borkowski, R. P.; Doetschman, D. C.; Fox, J. D.; Gargossian, C. *Solid Stat. Ion.* **1997**, *100*, 95.
- (255) Doetschman, D. C.; Thomas, G. D. *Chem. Phys.* **1998**, *228*, 103.
- (256) García, H.; Martí, V.; Casades, I.; Fornés, V.; Roth, H. *Phys. Chem. Chem. Phys.* **2001**, *3*, 2955.
- (257) Flockhart, B. D.; Scott, J. A. N.; Pink, R. C. *Trans. Faraday Soc.* **1966**, *62*, 730.
- (258) Griffith, O. H.; Cornell, D. W.; McConnell, H. M. *J. Chem. Phys.* **1965**, *43*, 2909.
- (259) Martí, V.; Fornés, V.; García, H.; Roth, H. D. *Eur. J. Org. Chem.* **2000**, 3, 473.
- (260) Corma, A.; García, H.; Iborra, S.; Martí, V.; Miranda, M. A.; Primo, J. *J. Am. Chem. Soc.* **1993**, *115*, 2177.
- (261) Stamiros, D. N.; Turkevich, J. *J. Am. Chem. Soc.* **1964**, *86*, 749.
- (262) Vanderveken, D. J.; Baudoux, G.; Durant, F.; Vercauteren, D. *J. J. Chem. Phys.* **1992**, *88*, 2497.
- (263) Khulbe, K. C.; Mann, R. S. *React. Kinet. Catal. Lett.* **1998**, *65*, 87.
- (264) Edlund, O.; Lund, A.; Nilsson, A. *J. Chem. Phys.* **1968**, *49*, 749.
- (265) Wan, J. K. S. *Ber. Bunsen-Ges. Phys. Chem.* **1968**, *72*, 245.
- (266) Smith, P.; Stevens, R. D.; Kaba, R. A. *J. Phys. Chem.* **1971**, *75*, 2048.
- (267) Nelsen, S. F.; Blackstock, S. C.; Yumibe, N. P.; Frigo, T. B.; Carpenter, J. E.; Weinhold, F. *J. Am. Chem. Soc.* **1985**, *107*, 143.
- (268) Fantechi, R.; Helcké, G. A. *J. Chem. Soc. Faraday Trans. 2* **1972**, *68*, 924.
- (269) Oyaizu, K.; Iwasaki, N.; Yamamoto, K.; Nishide, H.; Tsuchida, E. *Bull. Chem. Soc. Jpn.* **1994**, *67*, 1456.
- (270) Yamamoto, K.; Oyaizu, K.; Tsuchida, E. *Macromol. Chem. Phys.* **1994**, *195*, 3087.
- (271) Yamamoto, K.; Tsuchida, E.; Nishide, H.; Yoshida, S.; Park, Y. S. *J. Electrochem. Soc.* **1992**, *139*, 2401.

- (272) Martí, V.; Fernández, L.; Fornés, V.; García, H.; Roth, H. D. *J. Chem. Soc., Perkin Trans. 2* **1999**, 145.
- (273) Lakkaraju, P. S.; Shen, K.; Roth, H. D.; García, H. *J. Phys. Chem. A* **1999**, *103*, 7381.
- (274) Roth, H. D.; Shen, K.; Lakkaraju, P. S.; Fernández, L. *Chem. Commun.* **1998**, 2447.
- (275) Bock, H.; Stein, U. *Angew. Chem., Int. Ed. Engl.* **1980**, *19*, 834.
- (276) Bock, H.; Stein, U.; Semkow, A. *Chem. Ber.* **1980**, *113*, 3208.
- (277) Gourcy, J.-G.; Jeminet, G.; Simonet, J. *J. Chem. Soc., Chem. Commun.* **1974**, 634.
- (278) Hwang, B.; Chon, H. *Zeolites* **1990**, *10*, 101.
- (279) Enzel, P.; Bein, T. *J. Chem. Soc., Chem. Commun.* **1989**, 1326.
- (280) Enzel, P.; Bein, T. *Synth. Met.* **1993**, *55*, 1238.
- (281) Enzel, P.; Bein, T. *Synth. Met.* **1993**, *55*, 1238.
- (282) Ponti, A.; Oliva, C.; Forni, L. *J. Chem. Soc., Faraday Trans.* **1991**, *87*, 3151.
- (283) Caspar, J. V.; Ramamurthy, V.; Corbin, D. R. *J. Am. Chem. Soc.* **1991**, *113*, 600.
- (284) Kanatzidis, M. G.; Tonge, L. M.; Marks, T. J.; Marcy, H. O.; Kannewurf, C. R. *J. Am. Chem. Soc.* **1987**, *109*, 3797.
- (285) Kanatzidis, M. G.; Hubbard, M.; Tonge, L. M.; Marks, T. J.; Marcy, H. O.; Kannewurf, C. R. *Synth. Met.* **1989**, *28*, C89.
- (286) Brandt, P.; Fischer, R. D.; Martinez, E. S.; Calleja, R. D. *Angew. Chem., Int. Ed. Engl.* **1989**, *28*, 1265.
- (287) Pinnavaia, T. J.; Hall, P. L.; Cady, S. S.; Mortland, M. M. *J. Phys. Chem.* **1974**, *78*, 994.
- (288) Cloos, P.; Poel, D. V.; Camerlynck, J. P. *Nature* **1973**, *243*, 54.
- (289) Bein, T. in *Studies in Surface Science and Catalysis*; Chon, H., Woo, S. I., Park, S.-E., Eds.; Elsevier: Amsterdam, 1996; Vol. 102.
- (290) Ruiz-Hitzky, E.; Aranda, P. A. *Quim., Int. Ed.* **1997**, *93*, 197.
- (291) Tajima, K.; Aida, T. *Chem. Commun.* **2000**, 2399.
- (292) Chao, T. H.; Erf, H. A. *J. Catal.* **1986**, *100*, 492.
- (293) Bein, T.; Enzel, P. *Synth. Met.* **1989**, *29*, 163.
- (294) Bein, T.; Enzel, P.; Beuneeu, F.; Zuppiroli, L. *Adv. Chem.* **1990**, *226*, 433.
- (295) Bein, T.; Enzel, P. *Mol. Cryst. Liq. Cryst.* **1990**, *181*, 315.
- (296) Hwang, B.; Chon, H. *Zeolites* **1990**, *10*, 101.
- (297) Dutta, P. K.; Puri, M. *J. Catal.* **1988**, *111*, 453.
- (298) Millar, G. J.; Lewis, A. R.; Bowmaker, G. A.; Cooney, R. P. *J. Mater. Chem.* **1993**, *3*, 867.
- (299) Lewis, A. R.; Millar, G. J.; Cooney, R. P.; Bowmaker, G. A. *Chem. Mater.* **1993**, *5*, 1509.
- (300) Bordiga, S.; Ricchiardi, G.; Spoto, G.; Scarano, D.; Carnelli, L.; Zecchina, A.; Areat, C. O. *J. Chem. Soc., Faraday Trans.* **1993**, *89*, 1843.
- (301) Cox, S. D.; Stucky, G. D. *J. Phys. Chem.* **1991**, *95*, 710.
- (302) Pereira, C.; Kokotailo, G. T.; Gorte, R. J. *J. Phys. Chem.* **1991**, *95*, 705.
- (303) Lay, A. K.; Cardin, D. J.; Gilbert, A.; Constantine, S.; Alvaro, M.; García, H.; Galletero, M. S.; Márquez, F. *J. Am. Chem. Soc.* **2001**, *123*, 3141.
- (304) Alvaro, M.; Ferrer, B.; García, H.; Lay, A.; Trinidad, F.; Valenciano, J. *Chem. Phys. Lett.* **2002**, *356*, 577.
- (305) Galletero, M. S.; Alvaro, M.; García, H.; Gómez-García, C. J.; Lay, A. K. *Phys. Chem. Chem. Phys.* **2002**, *4*, 115.
- (306) Hirsch, A. *The Chemistry of Fullerenes*; Thieme Verlag: New York, 1994.
- (307) Bourdelande, J. L.; Galletero, M. S.; García, H. *Chem. Phys. Lett.*, in press.
- (308) Poutsma, M. L. in *Zeolite Chemistry and Catalysis*; Rabo, J. A., Ed.; American Chemical Society: Washington, DC, 1976.
- (309) Ward, J. W. in *Zeolite Chemistry and Catalysis*; Rabo, J. A., Ed.; American Chemical Society: Washington, DC, 1976.
- (310) Liu, X. S.; Iu, K. K.; Thomas, J. K.; He, H. Y.; Klinowski, J. *J. Am. Chem. Soc.* **1994**, *116*, 11811.
- (311) Liu, X. S.; Zhang, G. H.; Thomas, J. K. *J. Phys. Chem. B* **1997**, *101*, 2182.
- (312) Pitchumani, K.; Joy, A.; Prevost, N.; Ramamurthy, V. *J. Chem. Soc., Chem. Commun.* **1997**, 127.
- (313) Ward, J. W. *J. Phys. Chem.* **1968**, *72*, 4211.
- (314) Uytterhoeven, J. B.; Schoonheydt, R.; Liengme, B. V.; Hall, W. K. *J. Catal.* **1969**, *13*, 425.
- (315) Kao, H. M.; Grey, C. P.; Pitchumani, K.; Lakshminarasimhan, P. H.; Ramamurthy, V. *J. Phys. Chem. A* **1998**, *102*, 5627.
- (316) Kojima, M.; Takeya, H.; Kuriyama, Y.; Oishi, S. *Chem. Lett.* **1997**, 997-998.
- (317) Pitchumani, K.; Corbin, D. R.; Ramamurthy, V. *J. Am. Chem. Soc.* **1996**, *118*, 8152.
- (318) Pitchumani, K.; Lakshminarasimhan, P. H.; Prevost, N.; Corbin, D. R.; Ramamurthy, V. *Chem. Commun.* **1997**, 181.
- (319) Rooney, J. J.; Pink, R. C. *Trans. Faraday Soc.* **1962**, *58*, 1632.
- (320) Leftin, H. P. *J. Phys. Chem.* **1960**, *64*, 1714.
- (321) Leftin, H. P.; Hall, W. K. *J. Phys. Chem.* **1960**, *64*, 382.
- (322) Leftin, H. P.; Hobson, M. C.; Leigh, J. S. *J. Phys. Chem.* **1962**, *66*, 1214.
- (323) Leftin, H. P.; Hall, W. K. *J. Phys. Chem.* **1962**, *66*, 1457.
- (324) Leftin, H. P.; Hobson, M. C. *J. Adv. Catal.* **1963**, *14*, 115.
- (325) Hall, W. K. *J. Catal.* **1962**, *1*, 53.
- (326) Terenin, A. *Adv. Catal.* **1964**, *15*, 227.
- (327) Hirschler, A. E. *J. Catal.* **1963**, *2*, 428.
- (328) Hirschler, A. E.; Hudson, J. O. *J. Catal.* **1964**, *3*, 239.
- (329) Hirschler, A. E. *J. Catal.* **1966**, *5*, 196.
- (330) Flockhart, B. D.; Pink, R. C. *J. Catal.* **1965**, *4*, 90.
- (331) Rooney, J. J.; Hathaway, B. J. *J. Catal.* **1964**, *3*, 447.
- (332) Fornés, V.; García, H.; Jovanovic, S.; Martí, V. *Tetrahedron* **1997**, *53*, 4715.
- (333) Evans, A. G.; Jones, N.; Thomas, J. H. *J. Chem. Soc.* **1955**, 1824.
- (334) Evans, A. G.; Jones, N.; Jones, P. M. S.; Thomas, J. H. *J. Chem. Soc.* **1956**, 2757.
- (335) Evans, A. G.; Jones, P. M. S.; Thomas, J. H. *J. Chem. Soc.* **1957**, 104.
- (336) Grace, J. A.; Symons, M. C. R. *J. Chem. Soc.* **1959**, 958.
- (337) Schmidt, J.; Bös, J.; Mai, H.; Decker, U.; Halbig, M. *Radiat. Phys. Chem.* **1985**, *26*, 543.
- (338) Schmidt, J.; Decker, U.; Teplý, J.; Bös, J.; Mai, H. *Radiat. Phys. Chem. Part C* **1990**, *36*, 715.
- (339) Lakshminarasimhan, P.; Thomas, K. J.; Brancalione, L.; Wood, P. D.; Johnston, L. J.; Ramamurthy, V. *J. Phys. Chem. B* **1999**, *103*, 9247.
- (340) Turner, G.; Bakker, M. G.; Ramamurthy, V., unpublished work.
- (341) Corma, A.; García, H. *J. Chem. Soc., Dalton Trans.* **2000**, 1381.
- (342) Rooney, J. J. In *Elementary Reaction Steps in Heterogeneous Catalysis*; Joyner, R. W., van Santen, R. A., Eds.; Kluwer Academic Publishers: Amsterdam, 1993; Vol. 398.
- (343) Pollack, S. S.; Sprecher, R. F.; Frommell, E. A. *J. Mol. Catal.* **1991**, *66*, 195.
- (344) Cozens, F. L.; Bogdanova, R.; Régimbald, M.; García, H.; Martí, V.; Scaiano, J. C. *J. Phys. Chem. B* **1997**, *101*, 6921.
- (345) Fornés, V.; García, H.; Martí, V.; Fernández, L. *Tetrahedron* **1998**, *54*, 3837.
- (346) Fernández, L.; García, H.; Martí, V. *Phys. Chem. Chem. Phys.* **1999**, *2*, 3689.
- (347) Jayathirtha Rao, V.; Prevost, N.; Ramamurthy, V.; Jayathirtha Rao, V.; Kojima, M.; Johnston, L. *J. Chem. Commun.* **1997**, *22*, 2209.
- (348) Roth, H. D.; Herberzt, T.; Lakkaraju, P. S.; Sluggett, G.; Turro, N. J. *J. Phys. Chem. A* **1999**, *103*, 11350.
- (349) Cozens, F. L.; O'Neill, M.; Schepp, N. P. *J. Am. Chem. Soc.* **1997**, *119*, 7583-7584.
- (350) Roth, H. D.; Shen, K.; Lakkaraju, P. S.; Fernández, L. *Chem. Commun.* **1998**, 2447.
- (351) Trifunac, A. D.; Qin, X.-Z. *Appl. Magn. Reson.* **1990**, *1*, 29.
- (352) Lakkaraju, P. S.; Zhang, J.; Roth, H. D. *J. Chem. Soc., Perkin Trans. 2* **1993**, 2319.
- (353) Lakkaraju, P. S.; Zhang, J.; Roth, H. D. *J. Phys. Chem.* **1994**, *98*, 2722.
- (354) Stone, T. J.; Waters, W. A. *J. Chem. Soc.* **1965**, 1488.
- (355) Stone, T. J.; Waters, W. A. *J. Chem. Soc.* **1964**, 4302.
- (356) Stone, T. J.; Waters, W. A. *J. Chem. Soc.* **1964**, 213.
- (357) Stone, T. J.; Waters, W. A. *Proc. Chem. Soc.* **1962**, 253.
- (358) Hewgill, F. R.; Stone, T. J.; Waters, W. A. *J. Chem. Soc.* **1964**, 408.
- (359) Roth, H. D.; Schilling, M. L. M. *J. Am. Chem. Soc.* **1980**, *102*, 7956.
- (360) Herberzt, T.; Lakkaraju, P. S.; Blume, F.; Blume, M.; Roth, H. D. *Eur. J. Org. Chem.* **2000**, 467.
- (361) A. Berndt cited in R. A. Forrester, K. I., Kothe, G., Nelsen, S. F., Ohya-Nishiguchi, H., Watanabe, K., Wilker, W. "Organic Cation Radicals and Polyradicals" in Landolt Börnstein Numerical Data and Functional Relationships in Science and Technology: Springer-Verlag, Heidelberg, 1980; Vol. 9, part d2.
- (362) Toriyama, K.; Nunome, K.; M. Iwasaki, M. *J. Am. Chem. Soc.* **1981**, *103*, 3591.
- (363) Toriyama, K.; Nunome, K.; M. Iwasaki, M. *J. Am. Chem. Soc.* **1987**, *109*, 4496.
- (364) Barnabas, M. V.; Werst, D. W.; Trifunac, A. D. *Chem. Phys. Lett.* **1993**, *204*, 435.
- (365) Werst, D. W.; Picos, E. A.; Tartakovsky, E. E.; Trifunac, A. D. *Chem. Phys. Lett.* **1994**, *229*, 421.
- (366) Lotais, B. C.; Jonah, C. D. *Radiat. Phys. Chem.* **1989**, *33*, 505.
- (367) Sauer, M. C. J.; Schmidt, K. H. *Radiat. Phys. Chem.* **1988**, *32*, 281.
- (368) Melekhov, V. I.; Anisimov, O. A.; Sjoquist, L.; Lund, A. *Chem. Phys. Lett.* **1990**, *174*, 95.
- (369) Barnabas, M. V.; Trifunac, A. D. *Chem. Phys. Lett.* **1991**, *187*, 565.
- (370) Qin, X. Z.; Trifunac, A. D. *J. Phys. Chem.* **1990**, *94*, 4751.
- (371) Qin, X.-Z.; Snow, L. D. *J. Am. Chem. Soc.* **1984**, *106*, 7640.
- (372) Ushida, K.; Shida, T.; Shimokoshi, K. *J. Phys. Chem.* **1989**, *93*, 5388.
- (373) Williams, F.; Guo, Q.-X.; Nelsen, S. F. *J. Am. Chem. Soc.* **1988**, *110*.
- (374) Roth, H. D.; Lakkaraju, P. S.; Zhang, J. *J. Chem. Soc., Chem. Commun.* **1994**, 1969.
- (375) Raghavachari, K.; Haddon, R. C.; Roth, H. D. *J. Am. Chem. Soc.* **1983**, *105*, 3110.

- (376) Barnabas, M. V.; Trifunac, A. D. *Chem. Phys. Lett.* **1992**, *193*, 298.
- (377) Werst, D. W.; Tartakovsky, E. E.; Picos, E. A.; Trifunac, A. D. *J. Phys. Chem.* **1994**, *98*, 10249.
- (378) Picos, E. A.; Han, P.; Werst, D. W. *J. Phys. Chem.* **1996**, *100*, 7191.
- (379) Shida, T.; Egawa, Y.; Kubodera, H.; Kato, T. *J. Phys. Chem.* **1980**, *73*, 5963.
- (380) Desrosiers, M. F.; Trifunac, A. D. *Chem. Phys. Lett.* **1985**, *118*, 441.
- (381) Qin, X. Z.; Trifunac, A. D. *J. Phys. Chem.* **1991**, *95*, 6466.
- (382) Barnabas, M. V.; Trifunac, A. D. *J. Chem. Soc., Chem. Commun.* **1993**, 813.
- (383) Gerson, F.; Qin, X.-Z. *Helv. Chim. Acta* **1989**, *72*, 383.
- (384) Toriyama, K.; Nunome, K.; Iwasaki, M. *J. Chem. Soc., Chem. Commun.* **1983**, 1346.
- (385) Bauld, N. L.; Bellville, D. J.; Pabon, R.; Chelsky, R.; Green, G. *J. Am. Chem. Soc.* **1983**, *105*, 2378.
- (386) Cromack, K. R.; Werst, D. W.; Barnabas, M. V.; Trifunac, A. D. *Chem. Phys. Lett.* **1994**, *218*, 485.
- (387) Bach, R. D.; Schilke, I. L.; Schlegel, H. B. *J. Org. Chem.* **1996**, *61*, 4845.
- (388) Ishiguro, K.; Khudyakov, I. V.; McGarry, P. F.; Turro, N. J.; Roth, H. D. *J. Am. Chem. Soc.* **1994**, *116*, 6933.
- (389) Erickson, R.; Benetis, N. P.; Lund, A.; Lindgren, M. *J. Phys. Chem. A* **1997**, *101*, 2390.
- (390) Hashimoto, S. *Chem. Phys. Lett.* **1996**, *262*, 292.
- (391) Park, J.; Kang, W. K.; Ryoo, R.; Jung, K. H.; Jang, D. J. *J. Photochem. Photobiol. A* **1994**, *80*, 333.
- (392) Mao, Y.; Iu, K. K.; Thomas, J. K. *Langmuir* **1994**, *10*, 709.
- (393) Chanon, M. *Bull. Soc. Chim. Fr.* **1985**, 209.
- (394) Chanon, M.; Julliard, M.; Santamaria, J.; F., C. *New J. Chem.* **1992**, *16*, 171.
- (395) Kavarnos, G. J.; Turro, N. J. *Chem. Rev.* **1986**, *86*, 401.
- (396) Ebersson, L. *Electron-Transfer Reactions in Organic Chemistry*; Springer-Verlag: Berlin, 1987.
- (397) Ramamurthy, V. *Photochemistry in Organized and Constrained Media*; VCH: New York, 1991.
- (398) Scaiano, J. C. *J. Am. Chem. Soc.* **1980**, *102*, 7747.
- (399) Casal, H. L.; Scaiano, J. C. *Can. J. Chem.* **1985**, *63*, 1308.
- (400) Ramamurthy, V.; Sanderson, D. R.; Eaton, D. F. *Photochem. Photobiol.* **1992**, *56*, 297.
- (401) Uppili, S.; Thomas, K. L.; Crompton, E. M.; Ramamurthy, V. *Langmuir* **2000**, *16*, 265.
- (402) Barthomeuf, D. *J. Phys. Chem.* **1984**, *88*, 43.
- (403) Zhang, Z.; Turro, N. J.; Johnston, L.; Ramamurthy, V. *Tetrahedron Lett.* **1996**, *37*, 4861.
- (404) Sankararaman, S.; Yoon, K. B.; Yabe, T.; Kochi, J. K. *J. Am. Chem. Soc.* **1991**, *113*, 1419.
- (405) Kuchi, V.; Oliver, A. M.; Paddon-Row, M. N.; Howe, R. F. *Chem. Commun.* **1999**, 1149.
- (406) Berkhout, S., <http://orgwww.chem.uva.nl/~stijnzb/zeolites>.
- (407) Ramamurthy, V.; Lakshminarasimhan, P.; Grey, C. P.; Johnston, L. *J. Chem. Commun.* **1998**, 2411.
- (408) Scaiano, J. C.; García, H. *Acc. Chem. Res.* **1999**, *32*.
- (409) Müller, F.; Mattay, J. *Chem. Rev.* **1993**, *93*, 99.
- (410) Miranda, M. A.; García, H. *Chem. Rev.* **1994**, *94*, 1063.
- (411) Corma, A.; Fornés, V.; García, H.; Miranda, M. A.; Primo, J.; Sabater, M. J. *J. Am. Chem. Soc.* **1994**, *116*, 2276.
- (412) Fornés, V.; García, H.; Miranda, M. A.; Mojarrad, F.; Sabater, M.-J.; Suliman, N. N. E. *Tetrahedron* **1996**, *52*, 7755.
- (413) Corma, A.; Fornés, V.; García, H.; Miranda, M. A.; Sabater, M. J. *J. Am. Chem. Soc.* **1994**, *116*, 9767.
- (414) Sanjuán, A.; Alvaro, M.; Aguirre, G.; García, H.; Scaiano, J. C. *J. Am. Chem. Soc.* **1998**, *120*, 7351.
- (415) Sanjuán, A.; Aguirre, G.; Alvaro, M.; García, H. *Appl. Catal. B* **1998**, *15*, 247.
- (416) Sanjuán, A.; Guillermo, A.; Alvaro, M.; García, H. *Water Res.* **2000**, *34*, 320.
- (417) Sanjuán, A.; Aguirre, G.; Alvaro, M.; García, H.; Scaiano, J. C. *Appl. Catal. B* **2000**, *25*, 257.
- (418) Sanjuán, A.; Alvaro, M.; García, H.; Scaiano, J. C. *Photochem. Photobiol. Sci.*, in press.
- (419) Blasco, T.; Cambor, M. A.; Corma, A.; Esteve, P.; Guil, J. M.; Martínez, A.; Perdigón-Melón, J. A.; Valencia, S. *J. Phys. Chem. B* **1998**, *102*, 75.
- (420) Adam, W.; García, H.; Mitchell, C. M.; Saha-Möller, C. R.; Weichold, O. *Chem. Commun.* **1998**, 2609.
- (421) Sanjuán, A.; Alvaro, M.; Corma, A.; García, H. *Chem. Commun.* **1999**, 1641.
- (422) Adam, W.; Corma, A.; Miranda, M. A.; Sabaterpicot, M. J.; Sahin, C. *J. Am. Chem. Soc.* **1996**, *118*, 2380.
- (423) Brancalion, L.; Brousmiche, D.; Rao, V. J.; Johnston, L. J.; Ramamurthy, V. *J. Am. Chem. Soc.* **1998**, *120*, 4926.
- (424) Cano, M. L.; Corma, A.; Fornés, V.; García, H.; Miranda, M.; Baerlocher, C.; Lengauer, C. *J. Am. Chem. Soc.* **1996**, *118*, 11006.
- (425) Scaiano, J. C.; García, S.; García, H. *Tetrahedron Lett.* **1997**, *38*, 5929.
- (426) Scaiano, J. C.; Stewart, L. C.; Liviant, P.; Majors, A. W. *Can. J. Chem.* **1984**, *62*, 1339.
- (427) Yoon, K. B. *Chem. Rev.* **1993**, *93*, 321.
- (428) Alvaro, M.; García, H.; García, S.; Fernández, L. *Tetrahedron Lett.* **1996**, *37*, 2873.
- (429) Liu, X.; Iu, K. K.; Thomas, J. K. *J. Phys. Chem.* **1989**, *93*, 4120.
- (430) Iu, K. K.; Thomas, J. K. *Langmuir* **1990**, *6*, 471.
- (431) Cozens, F. L.; Régimbald, M.; García, H.; Scaiano, J. C. *J. Phys. Chem.* **1996**, *100*, 18173.
- (432) Gessner, F.; Scaiano, J. C. *J. Photochem. Photobiol. A* **1992**, *67*, 91.
- (433) Gener, I.; Buntinx, G.; Brémard, C. *Angew. Chem., Int. Ed. Engl.* **1999**, *38*, 1819.
- (434) Thomas, J. K. *Chem. Rev.* **1993**, *93*, 301.
- (435) Liu, X.; Iu, K.-K.; Thomas, J. K. *J. Phys. Chem.* **1994**, *98*, 13720.
- (436) Brancalion, L.; Brousmiche, D.; Johnston, L. J. *Can. J. Chem.* **1999**, *77*, 787.
- (437) Sung-Suh, H. M.; Luan, Z.; Kevan, L. *J. Phys. Chem. B* **1997**, *101*, 10455.
- (438) Law, K.-Y. *Chem. Rev.* **1993**, *93*, 449.
- (439) Cano, M. L.; Cozens, F. L.; Esteves, M. A.; Marquez, F.; Garcia, H. *J. Org. Chem.* **1997**, *62*, 7121.
- (440) Das, S.; Thomas, K. G.; George, M. V.; Kamat, P. V. *J. Chem. Soc., Faraday Trans.* **1992**, *88*, 3419.
- (441) Das, S.; Thomas, G.; Thomas, K. J.; Kamat, P. V.; George, M. V. *J. Phys. Chem.* **1994**, *98*, 9291.
- (442) Johnston, L. J.; Schepp, N. P. *J. Am. Chem. Soc.* **1993**, *115*, 6564.
- (443) Schepp, N. P.; Johnston, L. J. *J. Am. Chem. Soc.* **1994**, *116*, 10330.
- (444) Schepp, N. P.; Johnston, L. J. *J. Am. Chem. Soc.* **1994**, *116*, 6895.
- (445) Schepp, N. P.; Johnston, L. J. *J. Am. Chem. Soc.* **1996**, *118*, 2872.
- (446) Rao, V. J.; Prevost, N.; Ramamurthy, V.; Kojima, M.; Johnston, L. J. *Chem. Commun.* **1997**, 2209.
- (447) Matsubara, C.; Kojima, M. *Tetrahedron Lett.* **1999**, *40*, 3439.
- (448) Ghosh, S.; Bauld, N. L. *J. Catal.* **1985**, *95*, 300.
- (449) Lorenz, K.; Bauld, N. L. *J. Catal.* **1985**, *95*, 616.
- (450) Miyashi, T.; Ikeda, H.; Konno, A.; Okitsu, O.; Takahashi, Y. *Pure Appl. Chem.* **1990**, *62*, 1531.
- (451) Ikeda, H.; Minegishi, T.; Abe, H.; Konno, A.; Goodman, J. L.; Miyashi, T. *J. Am. Chem. Soc.* **1998**, *120*, 87.
- (452) Miyashi, T.; Konno, A.; Takahashi, Y. *J. Am. Chem. Soc.* **1988**, *110*, 3676.
- (453) Lednev, I. K.; Mathivanan, N.; Johnston, L. J. *J. Phys. Chem.* **1994**, *98*, 11444.
- (454) Maslak, P.; Chapman, W. H. *J. Chem. Soc., Chem. Commun.* **1989**, 1809.
- (455) Cozens, F. L.; Ortiz, W.; Schepp, N. P. *J. Am. Chem. Soc.* **1998**, *120*, 13543.
- (456) Bard, A. J.; Fox, M. A. *Acc. Chem. Res.* **1995**, *28*, 141.
- (457) Kalyansundaram, K. *Photochemistry in Microheterogeneous Systems*; Academic: Orlando, 1987.
- (458) Grätzel, M. *Heterogeneous Photoinduced Electron Transfer*; Boca Raton, 1989.
- (459) Yoon, K. B. In *Solid State and Surface Photochemistry*; Ramamurthy, V., Schanze, K. S., Eds.; Marcel Dekker: New York, 2000; Vol. 8.
- (460) Yoon, K. B.; Hubig, S. M.; Kochi, J. K. *J. Phys. Chem.* **1994**, *98*, 3865.
- (461) Alvaro, M.; Garcia, H.; Garcia, S.; Marquez, F.; Scaiano, J. C. *J. Phys. Chem. B* **1997**, *101*, 3043.
- (462) Corma, A.; Fornés, V.; Martín-Aranda, R. M.; García, H.; Primo, J. *Appl. Catal.* **1990**, *59*, 237.
- (463) Szulbinski, W. S. *Inorg. Chem. Acta* **1998**, *269*, 253.
- (464) Park, Y. S.; Um, S. Y.; Yoon, K. B. *J. Am. Chem. Soc.* **1999**, *121*, 3193.
- (465) Hennessy, B.; Megelski, S.; Marcollu, C.; Shklover, V.; Bärocher, C.; Calzaferrri, G. *J. Phys. Chem. B* **1999**, *103*, 3340.
- (466) Dutta, P. K.; Ledney, M. *Prog. Inorg. Chem.* **1997**, *44*, 209.
- (467) De Wilde, W.; Peeters, G.; Lunsford, J. H. *J. Phys. Chem.* **1980**, *84*, 2306.
- (468) Coutant, M. A.; Le, T.; Castagnola, N.; Dutta, P. K. *J. Phys. Chem. B* **2000**, *104*, 10783.
- (469) Sykora, M.; Kincaid, J. R.; Dutta, P. K.; Castagnola, N. *J. Phys. Chem. B* **1999**, *103*, 309.
- (470) Krüger, J. S.; Mayer, J. E.; Mallouk, T. E. *J. Am. Chem. Soc.* **1988**, *110*, 8232.
- (471) Borja, M.; Dutta, P. K. *Nature* **1993**, *362*, 43.
- (472) Sykora, M.; Kincaid, J. R. *Nature* **1997**, *387*, 162.
- (473) Sykora, M.; Maruszewski, K.; Treffert-Ziemelis, S. M.; Kincaid, J. R. *J. Am. Chem. Soc.* **1998**, *120*, 3490.
- (474) Kincaid, J. R. *Chem. Eur. J.* **2000**, *6*, 4055.
- (475) Vitale, M.; Castagnola, N. B.; Ortins, N. J.; Brooke, J. A.; Vaidyalingam, Dutta, P. K. *J. Phys. Chem. B* **1999**, *103*, 2408.
- (476) Kim, Y. L.; Mallouk, T. E. *J. Phys. Chem.* **1992**, *96*, 2879.
- (477) Hoffman, M. Z. *J. Phys. Chem.* **1988**, *92*, 3458.
- (478) Castagnola, N.; Dutta, P. K. *J. Phys. Chem. B* **1998**, *102*, 1696.
- (479) Brigham, E. S.; Snowden, P. T.; Kim, Y. I.; Mallouk, T. E. *J. Phys. Chem.* **1993**, *97*, 8650.

- (480) Gust, D.; Moore, T. A.; Liddell, P. A.; Nemeth, G. A.; Makings, L. R.; Moore, A. L.; Barrett, D.; Pessiki, P. J.; Bensasson, R. V.; Rougee, M.; Chachaty, C.; DeSchryver, F. C.; van der Auweraer, M.; Holzwarth, A. R.; Connolly, J. S. *J. Am. Chem. Soc.* **1987**, *109*, 846.
- (481) Yonemoto, E. H.; Kim, Y. I.; Schmehl, R. H.; Wallin, J. O.; Shoulders, B. A.; Richardson, B. R.; Haw, J. F.; Mallouk, T. E. *J. Am. Chem. Soc.* **1994**, *116*, 10557.
- (482) Persaud, L.; Bard, A. J.; Champion, A.; Fox, M. A.; Mallouk, T. E.; Webber, S. E.; White, J. M. *J. Am. Chem. Soc.* **1987**, *109*, 7309.
- (483) Blatter, F.; Moreau, F.; Frei, H. *J. Phys. Chem.* **1994**, *98*, 13403.
- (484) Blatter, F.; Sun, H.; Frei, H. *Catal. Lett.* **1995**, *35*, 1.
- (485) Blatter, F.; Sun, H.; Frei, H. *Chem. Eur. J.* **1996**, *2*, 385.
- (486) Blatter, F.; Sun, H.; Frei, H. *Angew. Chem., Int. Ed. Engl.* **1996**, *35*, 5.
- (487) Sun, H.; Blatter, F.; Frei, H. *J. Am. Chem. Soc.* **1994**, *116*, 7951.
- (488) Sun, H.; Blatter, F.; Frei, H. *J. Am. Chem. Soc.* **1996**, *118*, 6873.
- (489) Sun, H.; Blatter, F.; Frei, H. In *ACS Symp. Ser.*; Oyama, S. T., Warren, B. K., Eds.; American Chemical Society: Washington DC, 1996; Vol. 638.
- (490) Vasenkov, S.; Frei, H. *Mol. Supramol. Photochem.* **2000**, *5*, 295.
- (491) Vasenkov, S.; Frei, H. In *Molecular and Supramolecular Photochemistry*; Ramamurthy, V., Schanze, K. S., Eds.; Marcel Dekker: New York, 2000; Vol. 5.
- (492) Vanoppen, D. L.; Devos, D. E.; Jacobs, P. A. *Stud. Surf. Sci. Catal.* **1997**, *105*, 1045.
- (493) Xiang, Y.; Larsen, S. C.; Grassian, V. H. *J. Am. Chem. Soc.* **1999**, *121*, 5063.
- (494) Takeya, H.; Kuriyama, Y.; Kojima, M. *Tetrahedron Lett.* **1998**, *39*, 5967.
- (495) Li, X.; Ramamurthy, V. *Tetrahedron Lett.* **1996**, *37*, 5235.
- (496) Tung, C. C.; Wang, H.; Ying, Y. M. *J. Am. Chem. Soc.* **1998**, *120*, 5179.
- (497) Rolison, D. R. *Chem. Rev.* **1990**, *90*, 867.
- (498) Rolison, D. R. *Stud. Surf. Sci. Catal.* **1994**, *85*, 543.
- (499) Bedoui, Balkus, J. *Phys. Chem.* **1996**, *100*.
- (500) Bessel, C. A.; Rolison, D. R. *J. Phys. Chem. B* **1997**, *101*, 1148.
- (501) Doménech, A.; Casades, I.; García, H. *J. Org. Chem.* **1999**, *64*, 3731.
- (502) Doménech, A.; García, H.; Doménech-Carbó, M. T.; Gallerto, M. S. *Anal. Chem.* **2002**, *74*, 562.
- (503) Hammerich, O.; Parker, V. D. In *Adv. Phys. Org. Chem.*; Academic Press: London, 1984; Vol. 20.
- (504) Doménech, A.; Doménech-Carbó, M. T.; García, H.; Galletero, M. S. *Chem. Commun.* **1999**, 2173.
- (505) Li, J.; Calzaferri, G. *J. Electroanal. Chem.* **1994**, *377*, 163.
- (506) Li, J.; Pfanner, K.; Calzaferri, G. *J. Phys. Chem.* **1995**, *99*, 2119.
- (507) Calzaferri, G.; Lanz, M.; Li, J. *J. Chem. Soc., Chem. Commun.* **1995**, 1313.
- (508) Gemborys, H. A.; Shaw, B. R. *J. Electroanal. Chem.* **1986**, *208*, 95.
- (509) Li, Z.; Wang, C. M.; Persaud, L.; Mallouk, T. E. *J. Phys. Chem.* **1988**, *92*, 2592.
- (510) Park, Y. S.; Lee, K.; Lee, C.; Yoon, K. B. *Langmuir* **2000**, *16*, 4470–4477.
- (511) Yoon, K. B.; Park, Y. S.; Kochi, J. K. *J. Am. Chem. Soc.* **1996**, *118*, 12710.
- (512) Goldbach, A.; Iton, L.; Grimsditch, M.; Saboungi, M. L. *J. Am. Chem. Soc.* **1996**, *118*, 2004.
- (513) Reimen, D.; Lindner, G.-G. *Chem. Soc. Rev.* **1999**, *28*, 75.
- (514) Yoon, K. B.; Kochi, J. K. *J. Am. Chem. Soc.* **1988**, *110*, 6586.
- (515) Keizer, P. N.; Morton, J. R.; Preston, K. F.; Sugden, A. K. *J. Phys. Chem.* **1991**, *95*, 7117.
- (516) Hashimoto, S. *Chem. Phys. Lett.* **1996**, *252*, 236.
- (517) Liu, X. S.; Iu, K. K.; Thomas, J. K. *Chem. Phys. Lett.* **1993**, *204*, 163.
- (518) Liu, X. S.; Iu, K. K.; Thomas, J. K. *J. Phys. Chem.* **1994**, *98*, 7877.
- (519) Martínez, L. J.; Scaiano, J. C. *J. Phys. Chem. B* **1998**, *103*, 203.
- (520) Scaiano, J. C.; Kaila, M.; Corrent, S. *J. Phys. Chem. B* **1997**, *101*, 8564.
- (521) Corrent, S.; Martínez, L. J.; Scaiano, J. C.; García, H.; Fornés, V. *J. Phys. Chem. B* **1999**, *103*, 8097.
- (522) For selected reviews on the photochemistry of organic compounds adsorbed in silica, oxides or clays, see the following references.
- (523) Johnston, L. J. In *Photochemistry in Organized and Constrained Media*; Ramamurthy, V., Ed.; VCH: New York, 1991.
- (524) Jones, W. In *Photochemistry in Organized and Constrained Media*; Ramamurthy, V., Ed.; VCH: New York, 1991.
- (525) Dabestani, R.; Sigman, M. E. In *Molecular and Supramolecular Photochemistry*; Ramamurthy, V., Schanze, K. S., Eds.; Marcel Dekker: New York, 2000; Vol. 5.
- (526) Takagi, K.; Shichi, T. In *Molecular and Supramolecular Photochemistry*; Ramamurthy, V., Schanze, K. S., Eds.; Marcel Dekker: New York, 2000; Vol. 5.
- (527) Hall, W. K.; Dolish, F. R. *Colloid Interface Sci.* **1968**, *26*, 261.
- (528) Dollish, F. R.; Hall, W. K. *J. Phys. Chem.* **1965**, *69*, 4402.
- (529) Hodgson, R. L.; Raley, J. H. *J. Catal.* **1965**, *4*, 6.
- (530) Worrall, D. R.; Williams, S. L.; Wilkinson, F.; Crossley, J. E.; Bouas-Laurent, H.; Desvergne, J.-P. *J. Phys. Chem. B* **1999**, *103*, 9255.
- (531) Ruetten, S. A. *J. Phys. Chem. B* **1999**, *103*, 9285.
- (532) Bauer, R. K.; Borenstein, R.; De Mayo, P.; Okada, K.; Rafalska, M.; Ware, W. R.; Wu, K. C. *J. Am. Chem. Soc.* **1982**, *104*, 4635.
- (533) Pankasem, S.; Thomas, J. K. *J. Phys. Chem.* **1991**, *95*, 6990.
- (534) Pankasem, S.; Thomas, J. K. *J. Phys. Chem.* **1991**, *95*, 7385.
- (535) Marro, M. A. T.; Thomas, J. K. *J. Photochem. Photobiol. A* **1993**, *72*, 251.
- (536) Wilkinson, F.; Worrall, D. R.; Williams, S. L. *J. Phys. Chem.* **1995**, *99*, 6689.
- (537) Oelkrug, D.; Reich, S.; Wilkinson, F.; Leicester, P. A. *J. Phys. Chem.* **1991**, *95*, 269.
- (538) Mao, Y.; Thomas, J. K. *Chem. Phys. Lett.* **1994**, *226*, 127.
- (539) Xiang, B. S.; Kevan, L. *J. Phys. Chem.* **1994**, *98*, 5120.
- (540) Liu, X.; Iu, K. K.; Thomas, J. K. *Langmuir* **1992**, *8*, 539.
- (541) Baldovi, V.; Corma, A.; García, H.; Iborra, S.; Miranda, M. A.; Primo, J. *Recl. Trav. Chim. Pays-Bas* **1992**, *111*, 126.
- (542) Climent, M. J.; Corma, A.; García, H.; Miranda, M. A.; Primo, J. *J. Photochem. Photobiol. A: Chem.* **1991**, *59*, 379.
- (543) Baldovi, M. V.; García, H.; Miranda, M. A.; Primo, J.; Soto, J.; Vargas, F. *Tetrahedron* **1995**, *51*, 8113.
- (544) Krishna, R. M.; Prakash, A. M.; Kevan, L. *J. Phys. Chem. B* **2000**, *104*, 1796.
- (545) Chang, Z.; Koodali, R.; Krishna, R. M.; Kevan, L. *J. Phys. Chem. B* **2000**, *104*, 5579.
- (546) Bae, J. Y.; Ranjit, K. T.; Luan, Z.; Krishna, R. M.; Kevan, L. *J. Phys. Chem. B* **2000**, *104*, 9661.
- (547) Corma, A.; Juanrajadell, M. I.; Lopeznieto, J. M.; Martínez, A.; Martínez, C. *Appl. Catal. A* **1994**, *111*, 175.
- (548) Corma, A.; Fornés, V.; Juanrajadell, M. I.; Lópeznieto, J. M. *Appl. Catal. A* **1994**, *116*, 151.
- (549) Song, X. M.; Sayari, A. *Catal. Rev.* **1996**, *38*, 329.
- (550) Bedilo, A. F.; Volodin, A. M.; Zenkovets, G. A.; Timoshok, G. V. *React. Kinet. Catal. Lett.* **1995**, *55*, 183.
- (551) Ghenciu, A.; Farcasiu, D. *J. Chem. Soc., Chem. Commun.* **1996**, 169.
- (552) Farcasiu, D.; Ghenciu, A.; Li, J. Q. *J. Catal.* **1996**, *158*, 116.
- (553) Timoshok, A. V.; Bedilo, A. F.; Volodin, A. M. *React. Kinet. Catal. Lett.* **1996**, *59*, 165–171.
- (554) Bedilo, A. F.; Kim, V. I.; Volodin, A. M. *J. Catal.* **1998**, *176*, 294–304.
- (555) Krishna, R. M.; Kevan, L. *Micropor. Mesopor. Mater.* **1999**, *32*, 169–174.
- (556) Fox, M. A.; Dulay, M. T. *Chem. Rev.* **1993**, *93*, 341–357.
- (557) Legrini, O.; Oliveros, E.; Braun, A. M. *Chem. Rev.* **1993**, *93*, 671–698.
- (558) Corma, A.; Fornés, V.; Pergher, S. B.; Maesen, T. L. M.; Buglass, J. G. *Nature* **1998**, *396*, 353–356.
- (559) Asefa, T.; MacLachlan, M. J.; Coombs, N.; Ozin, G. A. *Nature* **1999**, *402*, 867–871.
- (560) Asefa, T.; MacLachlan, M. J.; Grondey, H.; Coombs, N.; Ozin, G. A. *Angew. Chem., Int. Ed. Engl.* **2000**, *39*, 1808–1811.
- (561) MacLachlan, M. J.; Asefa, T.; Ozin, G. A. *Chem. Eur. J.* **2000**, *6*, 2507–2511.
- (562) Ha, K.; Lee, Y.-J.; Lee, H. J.; Yoon, K. B. *Adv. Mater.* **2000**, *12*, 1114–1117.
- (563) Ha, K.; Lee, Y.-J.; Jung, D.-Y.; Lee, J. H.; Yoon, K. B. *Adv. Mater.* **2000**, *12*, 1614–1617.
- (564) Ha, K.; Lee, Y.-J.; Chun, Y. S.; Park, Y. S.; Lee, G. S.; Yoon, K. B. *Adv. Mater.* **2001**, *13*, 594–596.
- (565) Kulak, A.; Park, Y. S.; Lee, Y.-J.; Chun, Y. S.; Ha, K.; Yoon, K. B. *J. Am. Chem. Soc.* **2000**, *122*, 9308–9309.
- (566) Kulak, A.; Lee, Y.-J.; Park, Y. S.; Yoon, K. B. *Angew. Chem., Int. Ed. Engl.* **2000**, *39*, 950–953.
- (567) Lee, G. S.; Lee, Y.-J.; Ha, K.; Yoon, K. B. *Tetrahedron* **2000**, *56*, 6965–6968.
- (568) Lee, G. S.; Lee, Y.-J.; Choi, S. Y.; Park, Y. S.; Yoon, K. B. *J. Am. Chem. Soc.* **2000**, *122*, 12151–12157.

